ISSN 1434-8454

ISRN DLR-FB--2008-15

ISRN DLR-FB--2008-15

F. Holzäpfel (Ed.)

Forschungsbericht 2008-15

The DLR Project Wirbelschleppe

Detecting, Characterizing, Controlling, Attenuating, Understanding, and Predicting Aircraft Wake Vortices

Frank Holzäpfel (Editor)
Thomas Gerz (Project Manager)

Deutsches Zentrum für Luft- und Raumfahrt
Oberpfaffenhofen, Berlin, Braunschweig
und Göttingen

DLR Deutsches Zentrum für Luft- und Raumfahrt e.V.
in der Helmholtz-Gemeinschaft

aircraft wake vortices, detection, characterization, control, attenuation, prediction

The DLR Project Wake Vortex – Detecting, Characterizing, Controlling, Attenuating, Understanding, and Predicting Aircraft Wake Vortices

Research Centers Oberpfaffenhofen, Berlin, Braunschweig, and Göttingen
Frank Holzäpfel (Editor), Thomas Gerz (Project Manager)

DLR-Forschungsbericht 2008-15, 2008, 134 pages, 89 figures, 14 tables, 289 references, 49,00 €

This collection of reports presents an excerpt of the investigations that were performed in the framework of the DLR Projekt Wirbelschleppe. A similar sample of reports was presented as part of three dedicated wake vortex sessions accomplished at the 1st European Air and Space Conference (CEAS 2007) and Deutscher Luft- und Raumfahrtkongress 2007 in Berlin. The Projekt Wirbelschleppe was conducted in two phases in the time frame from 1999 to 2007 with the five contributing DLR Institutes Institute of Atmospheric Physics, Institute of Aerodynamics und Flow Technology, Institute of Flight Systems, Institute of Flight Guidance, Institute of Robotics und Mechatronics and the Institute of Aeronautics and Astronautics of the University of Technology Berlin. The project unified a multitude of different aspects and disciplines of wake vortex research which can be characterized by four main themes:

- Minimization of wake vortices by measures at the aircraft
- Development and demonstration of a system for wake vortex prediction and observation
- Airborne wake vortex detection and active control
- Integration of systems into air traffic control

The Projekt Wirbelschleppe greatly benefited from the European projects AWIATOR, ATC-Wake, Credos, C-Wake, Eurowake, FAR-Wake, FLYSAFE, I-Wake, S-Wake, WakeNet, WakeNet2-Europe, WakeNet3-Europe, and Wavenc. DLR's wake vortex activities will be continued in the Projekt Wetter & Fliegen (2008-2011). Because the current compilation represents only a limited extract of the accomplished work, it is completed by a list of references emerging from the project.

Flugzeug Wirbelschleppen, Detektion, Charakterisierung, Kontrolle, Abschwächung, Vorhersage

Das DLR Projekt Wirbelschleppe – Detektion, Charakterisierung, Kontrolle, Abschwächung, Verständnis und Vorhersage von Flugzeug Wirbelschleppen

Forschungszentren Oberpfaffenhofen, Berlin, Braunschweig und Göttingen
Frank Holzäpfel (Editor), Thomas Gerz (Projektleiter)

DLR-Forschungsbericht 2008-15, 2008, 134 Seiten, 89 Bilder, 14 Tabellen, 289 Referenzen, 49,00 €

Die vorliegende Sammlung von Berichten repräsentiert einen Auszug von Forschungsarbeiten, die im Rahmen des DLR Projektes Wirbelschleppe durchgeführt wurden. Eine ähnliche Auswahl von Manuskripten wurde bereits in drei Wirbelschleppen Sitzungen der 1st European Air and Space Conference (CEAS 2007) und des Deutschen Luft- und Raumfahrtkongresses 2007 in Berlin präsentiert. Das Projekt Wirbelschleppe erstreckte sich in zwei Etappen über den Zeitraum von 1999 bis 2007. Beteiligte DLR Institute waren das Institut für Physik der Atmosphäre, das Institut für Aerodynamik und Strömungstechnik, das Institut für Flugsystemtechnik, das Institut für Flugführung, das Institut für Robotik und Mechatronik, sowie das Institut für Luft- und Raumfahrt der Technischen Universität Berlin. Das Projekt umfasste vielfältige Aspekte und Disziplinen der Wirbelschleppenforschung, die durch vier Hauptthemen charakterisiert werden können:

- Minimierung von Wirbelschleppen am Flugzeug
- Entwicklung und Demonstration des Systems zur Wirbelschleppenvorhersage und -beobachtung
- Bordautonome Erkennung von Wirbelschleppen und aktive Steuerungskonzepte
- Einbindung der Maßnahmen in Verfahren der Luftverkehrskontrolle

Das Projekt Wirbelschleppe profitierte maßgeblich durch die EU-Projekte AWIATOR, ATC-Wake, Credos, C-Wake, Eurowake, FAR-Wake, FLYSAFE, I-Wake, S-Wake, WakeNet, WakeNet2-Europe, WakeNet3-Europe und Wavenc. Die Wirbelschleppenforschung des DLR wird im Projekt Wetter & Fliegen (2008-2011) fortgeführt. Da die vorliegende Auswahl nur einen kleinen Teil der im Projekt Wirbelschleppe durchgeführten Arbeiten repräsentieren kann, ist eine vollständige Liste der aus dem Projekt hervorgegangenen Veröffentlichungen angefügt.

Forschungsbericht 2008-15

The DLR Project Wirbelschleppe

Detecting, Characterizing, Controlling, Attenuating, Understanding, and Predicting Aircraft Wake Vortices

Frank Holzäpfel (Editor)
Thomas Gerz (Project Manager)

Deutsches Zentrum für Luft- und Raumfahrt
Oberpfaffenhofen, Berlin, Braunschweig
und Göttingen

121 Seiten
77 Bilder
4 Tabellen
108 Literaturstellen

DLR **Deutsches Zentrum für Luft- und Raumfahrt** e.V.
in der Helmholtz-Gemeinschaft

Forschungsbericht 2008-15

The DLR Project Wake Vortex

Detecting, Characterizing, Controlling, Attenuating,
Understanding, and Predicting Aircraft Wake Vortices

Collection of Reports

Das DLR Projekt Wirbelschleppe

Detektion, Charakterisierung, Kontrolle, Abschwächung,
Verständnis und Vorhersage von Flugzeug Wirbelschleppen

Sammlung von Berichten

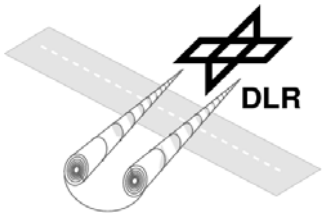

Editor
F. Holzäpfel

Project Manager
T. Gerz

DLR **Deutsches Zentrum für Luft- und Raumfahrt** e.V.
in der Helmholtz-Gemeinschaft

aircraft wake vortices, detection, characterization, control, attenuation, prediction

The DLR Project Wake Vortex

This collection of reports presents an excerpt of the investigations that were performed in the framework of the DLR Projekt Wirbelschleppe. A similar sample of reports was presented as part of three dedicated wake vortex sessions accomplished at the 1st European Air and Space Conference (CEAS 2007) and Deutscher Luft- und Raumfahrtkongress 2007 in Berlin. The Projekt Wirbelschleppe was conducted in two phases in the time frame from 1999 to 2007 with the five contributing DLR Institutes Institute of Atmospheric Physics, Institute of Aerodynamics und Flow Technology, Institute of Flight Systems, Institute of Flight Guidance, Institute of Robotics und Mechatronics and the Institute of Aeronautics and Astronautics of the University of Technology Berlin. The project unified a multitude of different aspects and disciplines of wake vortex research which can be characterized by four main themes:

- Minimization of wake vortices by measures at the aircraft
- Development and demonstration of a system for wake vortex prediction and observation
- Airborne wake vortex detection and active control
- Integration of systems into air traffic control

The Projekt Wirbelschleppe greatly benefited from the European projects AWIATOR, ATC-Wake, Credos, C-Wake, Eurowake, FAR-Wake, FLYSAFE, I-Wake, S-Wake, WakeNet, WakeNet2-Europe, WakeNet3-Europe, and Wavenc. DLR's wake vortex activities will be continued in the Projekt Wetter & Fliegen (2008-2011). Because the current compilation represents only a limited extract of the accomplished work, it is completed by a list of references emerging from the project.

Flugzeug Wirbelschleppen, Detektion, Charakterisierung, Kontrolle, Abschwächung, Vorhersage

Das DLR Projekt Wirbelschleppe

Die vorliegende Sammlung von Berichten repräsentiert einen Auszug von Forschungsarbeiten, die im Rahmen des DLR Projektes Wirbelschleppe durchgeführt wurden. Eine ähnliche Auswahl von Manuskripten wurde bereits in drei Wirbelschleppen Sessions der 1st European Air and Space Conference (CEAS 2007) und des Deutschen Luft- und Raumfahrtkongresses 2007 in Berlin präsentiert. Das Projekt Wirbelschleppe erstreckte sich in zwei Etappen über den Zeitraum von 1999 bis 2007. Beteiligte DLR Institute waren das Institut für Physik der Atmosphäre, das Institut für Aerodynamik und Strömungstechnik, das Institut für Flugsystemtechnik, das Institut für Flugführung, das Institut für Robotik und Mechatronik, sowie das Institut für Luft- und Raumfahrt der Technischen Universität Berlin. Das Projekt umfasste vielfältige Aspekte und Disziplinen der Wirbelschleppenforschung, die durch vier Hauptthemen charakterisiert werden können:

- Minimierung von Wirbelschleppen am Flugzeug
- Entwicklung und Demonstration des Systems zur Vorhersage und Beobachtung von Wirbelschleppen
- Bordautonome Erkennung von Wirbelschleppen und aktive Steuerungskonzepte
- Einbindung der Maßnahmen in Verfahren der Luftverkehrskontrolle

Das Projekt Wirbelschleppe profitierte maßgeblich durch die EU-Projekte AWIATOR, ATC-Wake, Credos, C-Wake, Eurowake, FAR-Wake, FLYSAFE, I-Wake, S-Wake, WakeNet, WakeNet2-Europe, WakeNet3-Europe und Wavenc. Die Wirbelschleppenforschung des DLR wird im Projekt Wetter & Fliegen (2008-2011) fortgeführt. Da die vorliegende Auswahl nur einen kleinen Teil der im Projekt Wirbelschleppe durchgeführten Arbeiten repräsentieren kann, ist eine vollständige Liste der im Projekt erstellten Veröffentlichungen angefügt.

Table of Contents

Wake vortex alleviation by differential and oscillating flap settings: a numerical and experimental study

G. Voß, E. Stumpf, R. Konrath, C. v. Carmer, C. P. Krückeberg, H. Meyer

Deutsches Zentrum für Luft- und Raumfahrt e.V. in der Helmholtz-Gemeinschaft
Institut für Aerodynamik und Strömungstechnik, Lilienthalplatz 7, 38108 Braunschweig
Bunsenstraße 10, 37073 Göttingen

1. ABSTRACT

In this article the results of numerical simulations and experimental investigations on wake vortex alleviation using Differential Flap Setting (DFS) and Oscillating Flap Setting (OFS) by means of a principle model with rectangular wing as a vortex generator are presented. The numerical investigation was made using Euler computations with the DLR flow solver TAU, the experiment was performed in a water towing tank at DLR Göttingen. The comparison of different configurations according to flap setting, trigger frequency and influence of Horizontal Tail Plane (HTP) vortex is conducted in this paper. Both the numerical and the experimental investigations show that it is possible to influence the wake vortex development using configurative applications on aircraft wings.

2. INTRODUCTION

An aircraft generates a wake flow which is called wake vortex, trailing vortex or wake turbulence. It results from the difference of pressure between bottom side and up side of a wing or in general of lift generating units. Due to that pressure difference a flow at the tip of lift units occurs which generates a vortex system. Depending on the load distribution along the wing small vortices are shedding from the trailing edge. During roll-up phase the small co-rotating vortices are merging to large vortex systems which are stable dependent of atmospheric conditions. This is potentially hazardous for following aircraft that encounter strong wake vortices.

Since the strength of the wake vortices increases with increasing lift (respectively weight) of the aircraft, this problem is serious for high capacity airliners, in particular during take off and landing. Presently, the growth of air traffic has led to the construction of very large aircraft which produce very strong wake vortices. Increase of separation distances might compensate the advantage of larger transport capacity. Hence, it is necessary to develop new methods to accurately predict the vortex evolution in order to avoid encounters or to adjust the effect on aircraft behaviour during the encounter.

Another approach to optimize the separation standards is wake vortex alleviation by configurative methods at aircraft lift devices. Wake vortex control has become one challenging task in civil aviation which aims at increasing flight safety and airport efficiency. The objective of the investigations conducted in this work is the excitation of vortex instabilities of the vortex system behind a lifting body.

3. THEORY

3.1. Vortex parameters

The wake of an aircraft is basically a vortex-dominated flow. Within the wake one can find vortex layers shed from the trailing edges and single vortices which separate from the side edges of the lift devices. Within a distance of about ten spans behind the aircraft the complex wake topology is reduced to a system of few counter-rotating vortices.

Some important vortex parameters should be characterized as follows. In common a vortex is defined by a rotational motion of particles around a single focus. The trajectories of the particles do not need to be circular and in the case of spatial vortices are not necessarily closed.

The vortex motion of the particles can be described by a distribution of either the velocity vector $\vec{v}$ or the vorticity vector $\vec{\omega}$. Vorticity is here defined as the rotation of the velocity in a point in space:

(1) $$\vec{\omega} = \nabla \times \vec{v}$$

In the special case of a planar vortex field the vortex flow is two-dimensional. The vorticity vector in yz-plane (see Fig. 1) is reduced to the axial component of $\vec{\omega}$.

(2) $$\omega_x = \frac{\partial v}{\partial z} - \frac{\partial w}{\partial y}$$

The integration of the axial vorticity ω_x is a measure for the strength of a vortex, called circulation. The circulation Γ_0 in the yz-plane is defined as:

(3) $$\Gamma_0 = \int_{-\infty}^{\infty}\int_{-\infty}^{\infty} \omega_x \, dy dz$$

Fig. 1 shows a sketch of a counter-rotating 4-vortex system. The main parameters to describe a 4-vortex system are the ratio of spacing b_1/b_0 and the ratio of circulation Γ_1/Γ_0 of both vortex pairs. The behaviour of a 4-vortex system depends on the value of these vortex parameters. With the Donaldson-Bilanin diagram (Fig. 2) one can classify the motion of the vortices. The solid line separates vortex parameters where primary and secondary vortices separate and where secondary vortices orbit around the descending primary vortices.

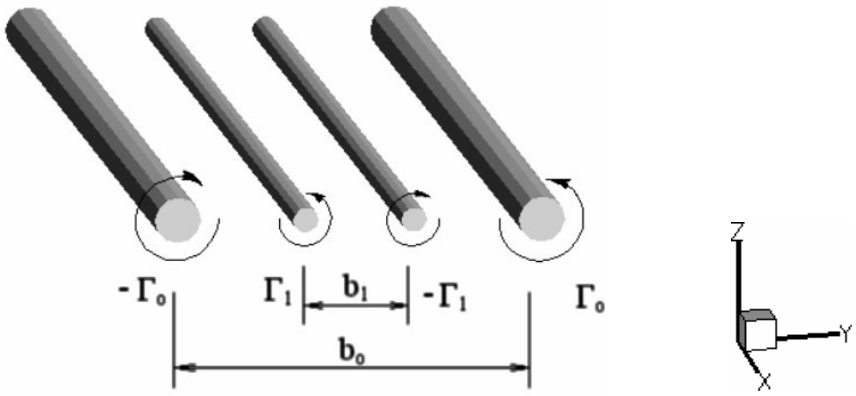

Fig. 1: Counter-rotating 4-vortex-system with spacings b_0 and b_1 and Circulations Γ_0 and Γ_1

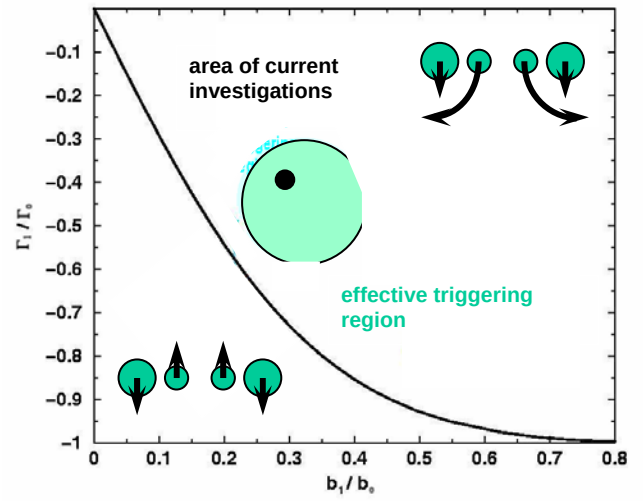

Fig. 2: Donaldson-Bilanin-diagram

3.2. Vortex instabilities

The natural vortex decay is based on vortex instabilities. One can differentiate between centrifugal and cooperative instabilities.

Vortex pairs may exhibit an instability which is based on interactions between vortex systems over the symmetry plane. Due to that fact these instabilities are called cooperative instabilities. The requirement for that kind of instabilitity is a radial deformation field induced by a neighbour vortex and a three-dimensional initialization disturbance. The main mechanism is the resonance between the deformation field and the disturbance.

The occurrence of cooperative instabilities depends on the existance of initial perturbances. This means normally a sinusoidal amplitude which results from the superposition of two Kelvin waves *A* and *B*, if the Kelvin waves are reversed ($m_A = -m_B$), helix-shaped ($|m_A| = |m_B| = 1$), steady-state ($\omega_A - \omega_B = 0$) and if they have the same wave-number ($k_A - k_B = 0$). Kelvin waves are defined as

(4) $$(u', v_r', v_\theta', p') = (u, v_r, v_\theta, p)e^{i(kx+m\theta-\tilde{\omega}t)}$$

If induced by atmospheric or aircraft boundary layer turbulence an amplitude of two parallel vortices occurs and if the decomposition of the perturbance into a finite number of Kelvin-waves includes two Kelvin-waves with the conditions denoted above a cooperative instability can develop in the plane with maximum dilation. It was shown that this kind of parameter combinations for specified wave-numbers exist [1]. In the case of existance of other pairs of Kelvin-waves with wave-numbers different from k_A more cooperative instabilities may appear in parallel. Water towing tank experiments have shown that long-wavelength and short-wavelength instabilities can exist in parallel [1].

In aircraft wakes mostly long-wavelength instabilities (Crow instabilitiy) can be observed by watching the condensation trail. The Crow instability exhibits only small growth rates and has in common wavelengths of about $5 < \lambda_{Crow}/b < 10$. It develops in planes with maximum deformation, i.e. the vortex amplitude grows in planes which are inclined by $\pm\pi/4$ against the horizontal plane. A projection of Crow instability into the xy-plane displays a symmetric and sinusoidal amplitude of the vortex axis, the projection into the xz-plane shows an in-phase amplitude.

4. NUMERICAL STUDIES

4.1. The TAU code

The numerical flow solver TAU is an unstructured finite volume method based on 3-dimensional Euler- or Navier-Stokes-equations. The calculation of a flow state in discrete points of an calculating domain requires for each point the definition of a capable control volume. Over the control volume the basic equations are integrated. Assuming constant flow values in each control volume the integration equation can be transferred into a simple sum equation.

Thus, the change of the vector $\vec{W}$ of the dependent variable of a cell is equal to the flux $\vec{Q}$ through the cell side-faces reduced by a dissipation part to stabilize the method.

(5) $$\frac{\Delta\vec{W}}{\Delta t} = -\frac{1}{V}\sum_{k=1}^{n}(\vec{Q}_k - \vec{D}_k)$$

V is the volume of the cell, n the number of the cell faces. The dissipation part is scaled with two constants $k^{(2)}$ and $k^{(4)}$. $k^{(2)}$ affects stability in regions in which shocks occur. $k^{(4)}$ makes sure that a global damping is available. Hence, in subsonic areas this is the important parameter. Based on an arbitrary initial solution the discretized equations are integrated in discrete timesteps with an explicit multi-stage Runge-Kutta method over time until a steady flow field has developed.

This ansatz goes back to the work of Jameson, Schmidt and Turkel [4]. To initialize the calculation at all points of the grid, pressure, density and velocity of free stream is set.

In this work all calculations had inviscid boundary conditions since former investigations have shown that there are no significant differences of viscid and inviscid calculations but one can save a lot of grid points in the primary grid if no prism layers for resolving the boundary layer have to be performed [1].

4.2. TAU calculations

The standard grid which was used for the numerical examinations has a size of 14 Mill. whereas the grid size of the finest comparison grid is about 40 Mill. The integration volume is 24 spans in all directions. The unsteady calculations are made with six periods to achieve convergence. The number of timesteps to resolve the periodic movement is 180. Per timestep 100 inner iterations are performed. All unsteady calculations are carried out as a restart from a steady solution which are made with 12000 timesteps. Due to the crash of unsteady calculations with second order central spatial discretization a second order upwind method was used. The time discretization in the numerical investigations was the Runge Kutta method.

5. EXPERIMENTAL STUDIES

5.1. The F13 model

The DLR F13 model (see Figs. 3 and 4) serves as a vortex generator which produces a specific two- or four-vortex system. In the current case the four-vortex-system is a counter-rotating four-vortex system.

The main wing of the F13 model has a span of b = 0,3 m and a chord length of c = 0,05 m. Thus the aspect ratio A_R is 6 and the angle of attack α is 10°. The profile is a Wortmann FX63-137B-PT. This is a Low-Reynolds-Number-profile which was modified in Princeton-University. The horizontal tail wing (HTP) has the same profile parameters as the main wing but the chord length is c = 0,035 m and the span b = 0,09 m. To produce a counter-rotating 4-vortex system the Angle of Attack is set to -6°. In case of the calculations with HTP the span ratio is b_1/b_2 = 0,3 and the circulation ratio is Γ_1/Γ_2 = -0,4. The Reynolds-number Re based on chord length of wing is ~100000. These values are used both in numerical and experimental studies.

The model is equiped with six rectangular flaps which can be moved independently. The periodical control of the flaps is done via a frequency generator which drives servo motors from aircraft modeling.

Fig. 3: F13 model with movable flaps, flaps are deflected, no HTP mounted

5.2. The water towing tank

The water towing tank has the advantage of providing an incoming flow with very low disturbance levels due to the fact that the model is towed through still water. The towing tank consists of a water tank and a trolley supporting the model with its controlling

instruments. The water tank has a total length of 18 m with a square cross section of 1,1 m x 1,1 m. It has ten pairs of glass windows allowing easy illumination for flow visualization and Particle Image Velocimetry (PIV) measurements.

The measurement in the water towing tank are made in an Eulerian frame, i.e. the measurement plane remained fixed in the observation plane while the model is passing. Several magnetic switches are placed beside the rails for triggering instruments as well as for switching off and braking the trolley.

After the water in the tank has calmed down a free-stream turbulence close to zero can be assumed. The F13 model was towed through the quiet water just as an aeroplane wing moving through quiescent atmosphere might do. The trolley was towed at a speed of 2 m/s, for which the chord based Reynolds number is 100,000.

5.3. StereoPIV setup

A moving StereoPIV measurement system [16] was employed in order to obtain time-resolved cross-sectional flow fields of the descending wake vortex system. A laser light sheet, powered by a dual cavity Nd:YAG laser (max. pulse energy of 400 mJ at 532 nm with 5 ns pulses), stretched over the full flow depth perpendicular to the tank axis. The water volume was seeded with hollow glass spheres with a mean diameter of 11 microns and a density of 1.1 g/cm^3. Two high-resolution PIV cameras (CCD chip size of 1600 px x 1200 px, dynamic range 14 bit gray-scale) acquired double-frame images of the illuminated seeding particles from both sides of the measurement plane (dual-side, forward-scattering, 45° off-axis arrangement). The cameras were attached to a carrier beam that was traversed downwards at a pre-set speed to follow the descending vortices in the developing wake. Large glass windows in the side walls and in the bottom of the tank allowed for convenient optical access. Using lenses of f = 35 mm and f# 2.8, Scheimpflug adapters and air-glass-water transition prisms resulted in a field-of-view of 364,8 mm by 235,2 mm. A programmable sequencer synchronized the cameras with the pulsed laser light sheet and with the traversing system. Controlled by the sequencer, also the time delay between the laser double pulses was increased during a measurement run in order to account for the decreasing axial and azimuthal velocities in the evolving wake vortex system. The StereoPIV system was operated at a capturing frequency of 10 Hz over a duration of up to 30 s.

5.4. PIV evaluation of camera images

For calibration and stereo reconstruction, stereo images of a calibration grid in different positions were employed. In order to de-warp and map the stereo image recordings to reconstructed images onto a Cartesian grid, a ratio of first order polynomials was used as projection equation, and the necessary coefficients were evaluated. As to compensate for a possible slight misalignment between the plane of the calibration grid and the plane of the light sheet, a disparity correction has been performed on a set of particle images obtained from illumination with an especially thin light sheet.

The state-of-the-art PIV displacement algorithms employed a multi-pass multi-grid interrogation method with window deformation (e.g. [17]), a multiple (Hart) correlation method, sub-pixel image shifting (image deformation) involving cubic B-splines, and peak detection based on Whittaker reconstruction. The multi-grid interrogation was performed by de-sampling of the images due to binning of neighboring pixels ([17], [19]). The size of the final correlation window was 32px x 32px and 50% overlap, and

resulted in time-resolved flow fields with more than 10,000 vectors. For outlier detection normalized median filtering [18] and replacement by lower-order peaks was employed.

6. WING CONFIGURATIONS

Different wing configurations were used for numerical calculations. Configuration 00 denotes the baseline configuration without moving flap, the other configurations establish outboard loadings to trigger long wavelength instabilities like the Crow instability.

The free stream velocity of calculations is set to 30 m/s (Ma = 0,0874). This is nearly the minimum velocity which can be handled by TAU to give good results. In both cases incompressible boundary conditions can be assumed. The change to compressible flow conditions can be set to about Ma 0,2 which is not reached in these investigations. In contrast to the very small difference between Reynolds-numbers in water and air flow conditions is the large difference between Mach-numbers. The Mach-numer in the air flow conditions is by factor 70 larger than the Mach-number in water flow environment. However, for comparability this will be negligible.

The frequencies which were chosen for flap motion in the towing tank are 0,8 and 1,0 Hz. Over the generalized reduced frequency

(6) $$f_{red} = \frac{2\pi f * l_{chord}}{v_{\infty}}$$

one can determine the respective frequency for air environment which amount to 12 and 15 Hz respectively.

TAB. 1 gives a list of chosen configurations, Fig. 5 and Fig. 6 show schematically the flap deflection of the F13 model for several configurations. The oscillations of the different flap sections are generally out of phase which allows keeping the total lift approximately constant.

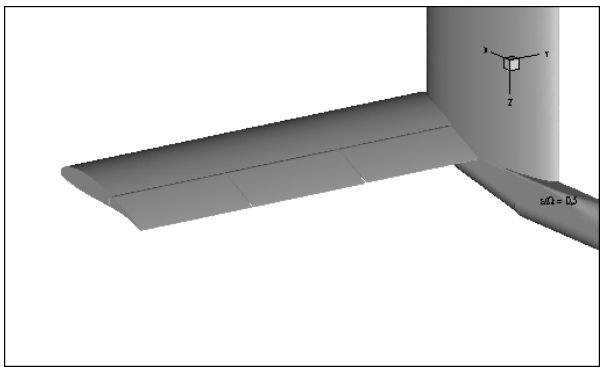

Fig. 4: Numerical F13 model, flaps in baseline configuration 00

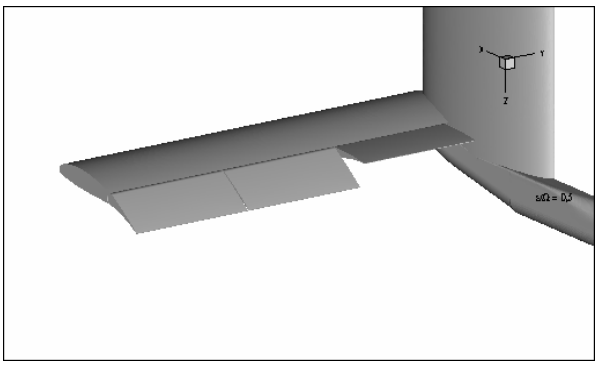

Fig. 5: Flap deflection for configurations 04 and 05

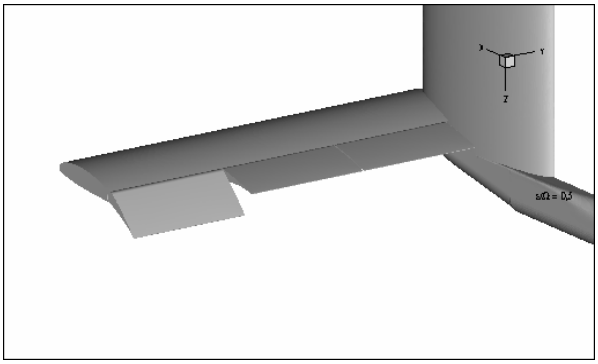

Fig. 6: Flap deflection for configurations 01, 02, 03 and 06

Config.	i/b flap (°)	m/b flap (°)	o/b flap (°)	freq. (Hz) (num.)	freq. (Hz) (exp.)	HTP	farfield grid refinement
00	0	0	0	--	--	no/yes	coarse
01	0 to -10	0 to -10	0 to 20	--	--	no	coarse
02	0 to -10	0 to -10	0 to 20	12	0,8	no	coarse
03	0 to -10	0 to -10	0 to 20	12	0,8	yes	coarse
04	0 to -20	0 to 10	0 to 10	12	0,8	yes	coarse
05	0 to -20	0 to 10	0 to 10	15	1,0	yes	coarse
06	0 to -10	0 to -10	0 to 20	12		yes	fine

TAB. 1: Configurations of flap deflections and oscillation frequencies

7. RESULTS

7.1. Numerical results

7.1.1. Baseline configuration

Two different configurations without flap deflection are considered. Fig. 7 shows the iso-surfaces $s/\omega = 0{,}5$ where s denotes the shear tensor and ω is the vorticity vector [21]. Thus, s/ω filters small-scale vorticity and means the ratio of strain flow and vortex flow, see [15]. The smaller co-rotating vorticity tubes between main vortex and fuselage are shed from the flap gaps. Studies of calculations without flap gaps have shown that these weak vortices have no influence on the development of main vortex and HTP vortex.

7.1.2. Grid dependency

All calculations of F13 configurations reveal an effect of periodical flap oscillations on the development of wake vortices. But first it is necessary to clarify if grid refinement has some influence on vortex decay. In the cases (00 – 06) the fine grid regions which are essential for resolving wake vortex formation are extending only to a distance of one span behind the principle aircraft model due to limited computational ressources.

In the transition from the fine grid parts to the coarser grid parts the numerical dissipation is becoming very strong, which could cause some some feedback on the fine resolved part of the domain, e.g. end effects. To except this effect one computation of outboard loading with HTP with pre-refined grid from the nearfield up to the very end of the farfield was performed. In Tab. 1 this configuration is denoted as 06 which is compared to configuration 05 as the reference case. Fig. 8 gives an impression of the position of pre-refined grid areas used to resolve wake vortex tubes and vortex bursting.

Fig. 9 shows a full period of oscillations in the nearfield areas with lower grid resolution compared to the large grid case. The spatial distribution of vorticity fragments is similar in both cases. End effects caused by the rapidly changing grid resolution in the farfield areas are obviously not the reason for the occurence of vortex bursting. After bursting of vortices as a result of periodical flap moving a re-organisation of the vortex structure with a larger vortex diameter is taking place. This structure exhibits a small loop which possibly may trigger the long-wavelength Crow-instability.

7.1.3. Differential Flap Setting

Compared to the baseline case (conf. 00) the case with the deflected flaps (conf. 01) yields results with more decay of the main vortex than in baseline case. The vortex pipe is considerably wider and within the boundary area the vortex is more frayed out (see Fig. 10). ,

7.1.4. Oscillating Flap Setting

In Figs. 11-13 some screenshots from animations are shown which are generated from the results of unsteady calculations. In each case the second picture from the top shows the fully deflected flap configuration whereas the bottom pictures indicate the non-deflected flap configuration. The images on the top and at the third position correspond to half-deflected flaps.

The perturbation which is generated by the oscillatory movement of flaps is transported downstream immediately after shedding from the lift device. Thereby either a strong frayed vortex structure can be obtained or the vortex diameter is increased according to the configuration of flap deflection. In addition to that there are helical structures which are very pronounced when the flap angle is approximately half of its maximum level. This could be an indication that the triggered instability is a helical instability. Further investigations are necessary to verify this.

The direct comparison of undisturbed and oscillating disturbance as well as the comparison of steady deflected and oscillated moved flaps are shown in Fig. 11 and Fig. 12, respectively. It is obvious that the disturbance of vortex tubes is accelerated when the configurative methods (i.e periodically moving flaps) are applied to the model. This matter of fact was the base to chose the configuration for experimental studies which are performed in water towing tank at DLR Goettingen.

The results of calculations with HTP and periodically driven flaps indicate that there is an influence on vortex behaviour which depends obviously on the triggering frequency. Fig. 13 shows the difference of vortex development between frequencies of f = 12 Hz and f = 15 Hz.

Due to limited hardware resources for the unsteady calculations a compromise had to be found for choosing the best grid refinement. It would have taken at least 25 to 30 Mill. grid points to come to a sufficient refinement. The change in vorticity distribution which appears may come from something like end effects or side effects. This has its reason in a larger gradient in pressure and density with the consequence of more dissipation. Further studies with focal point on grid dependency have to be done to clarify this issue.

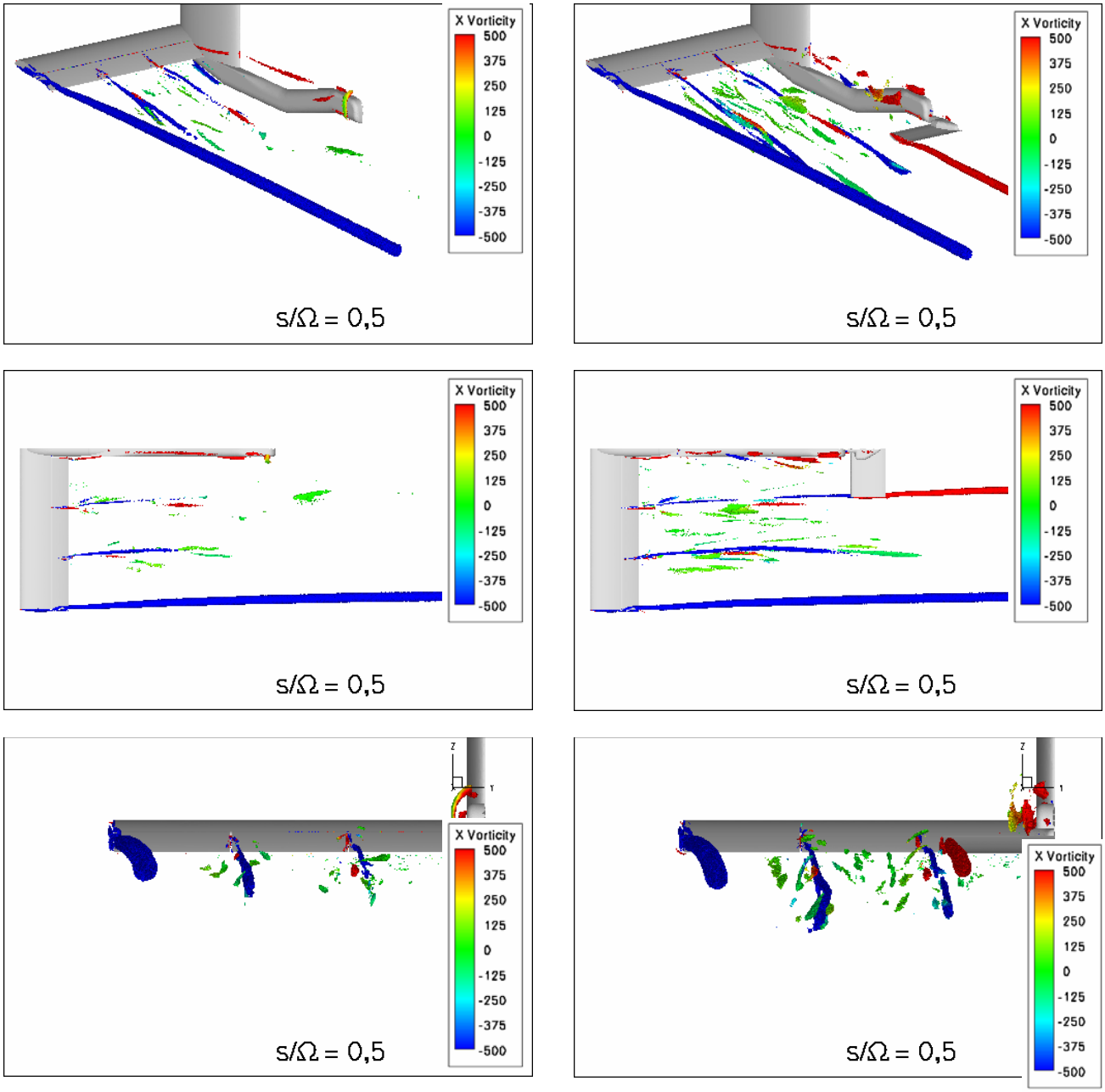

Fig. 7: Comparison Configuration baseline without HTP vs. baseline with HTP, colored vorticity from -500 1/s to 500 1/s

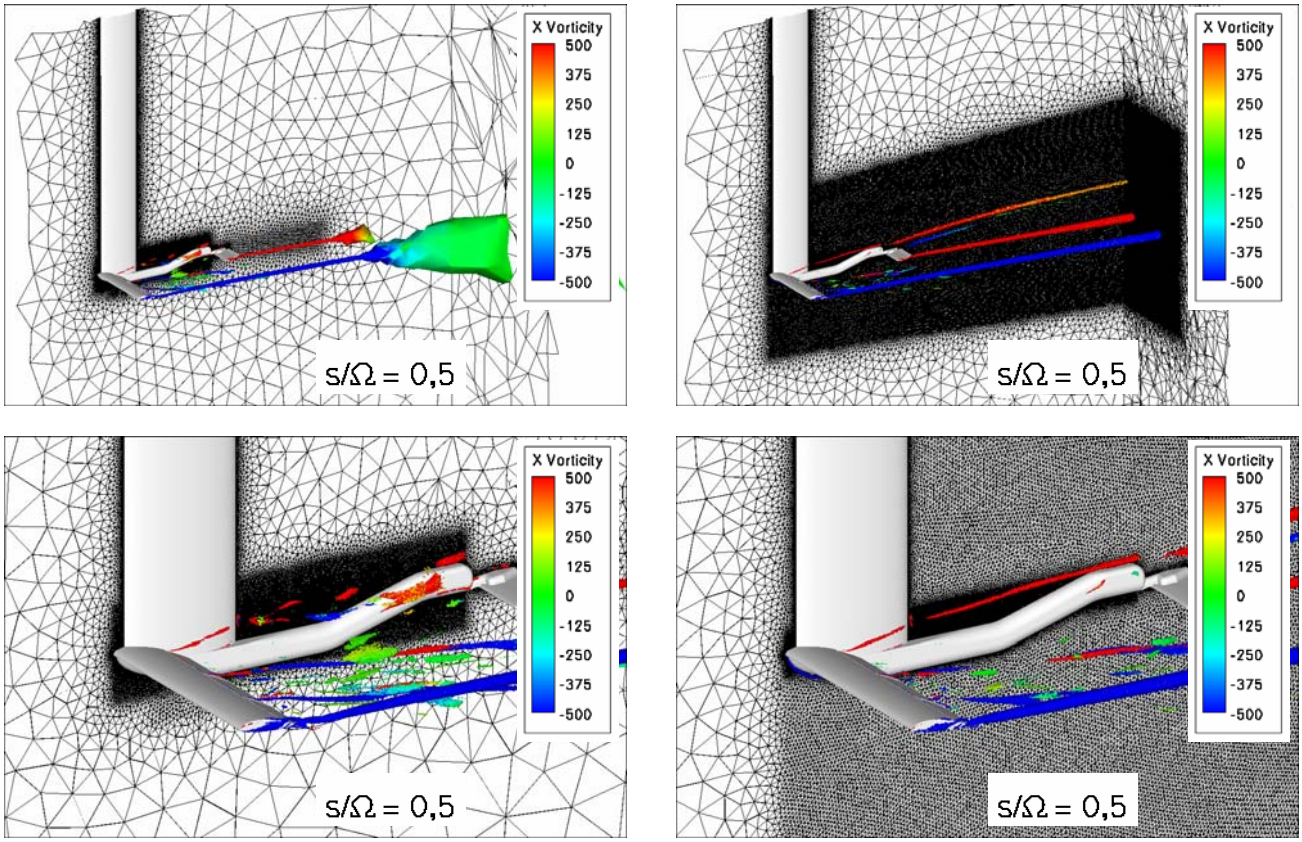

Fig. 8: Comparison Configuration 03 left (reference grid size) vs. 06 right (large grid size)

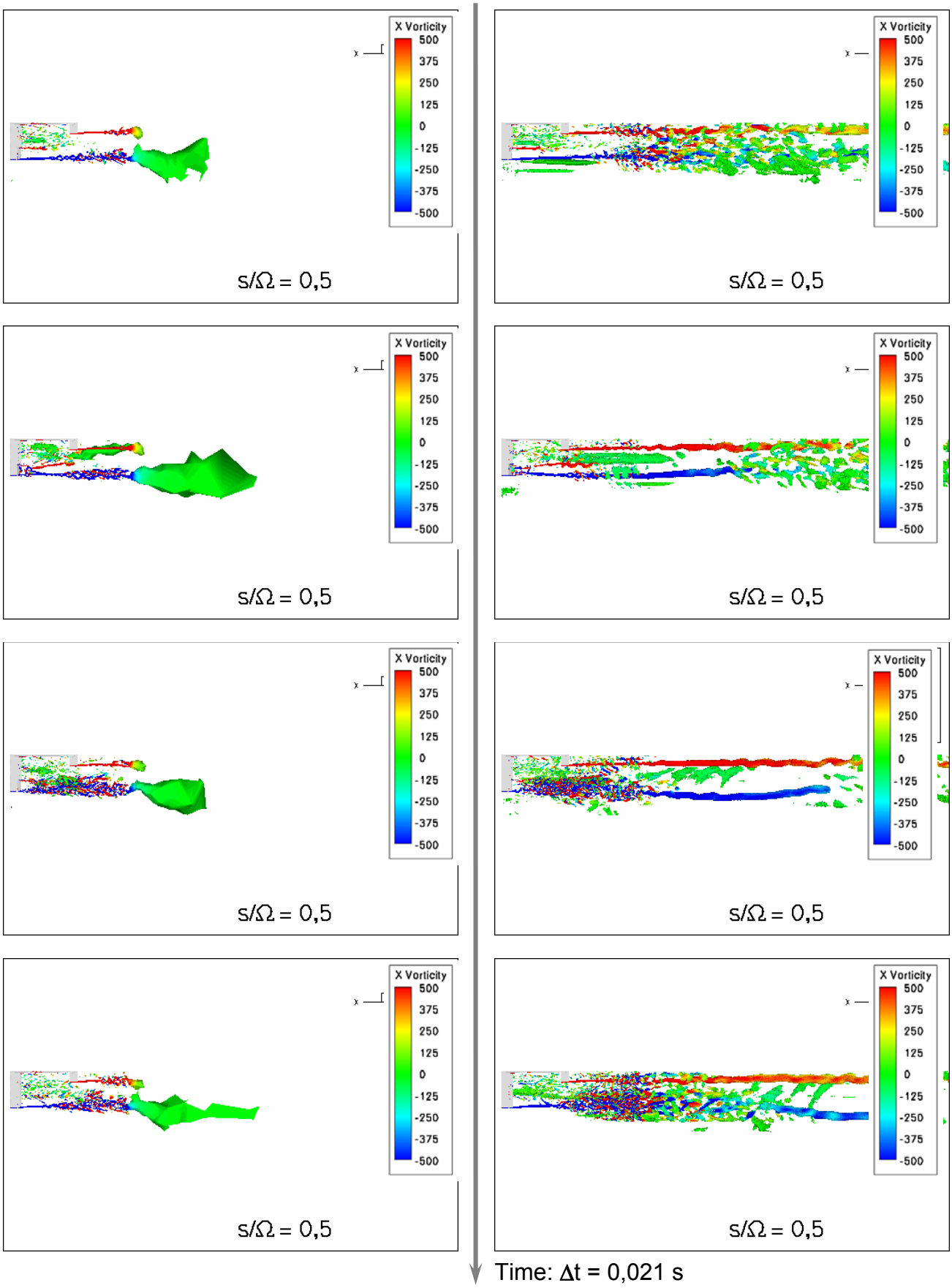

Fig. 9: Full period of flap oscillation. Comparison Configuration 06 (reference grid size) vs. 07 (large grid size), colored by vorticity from -500 1/s to 500 1/s

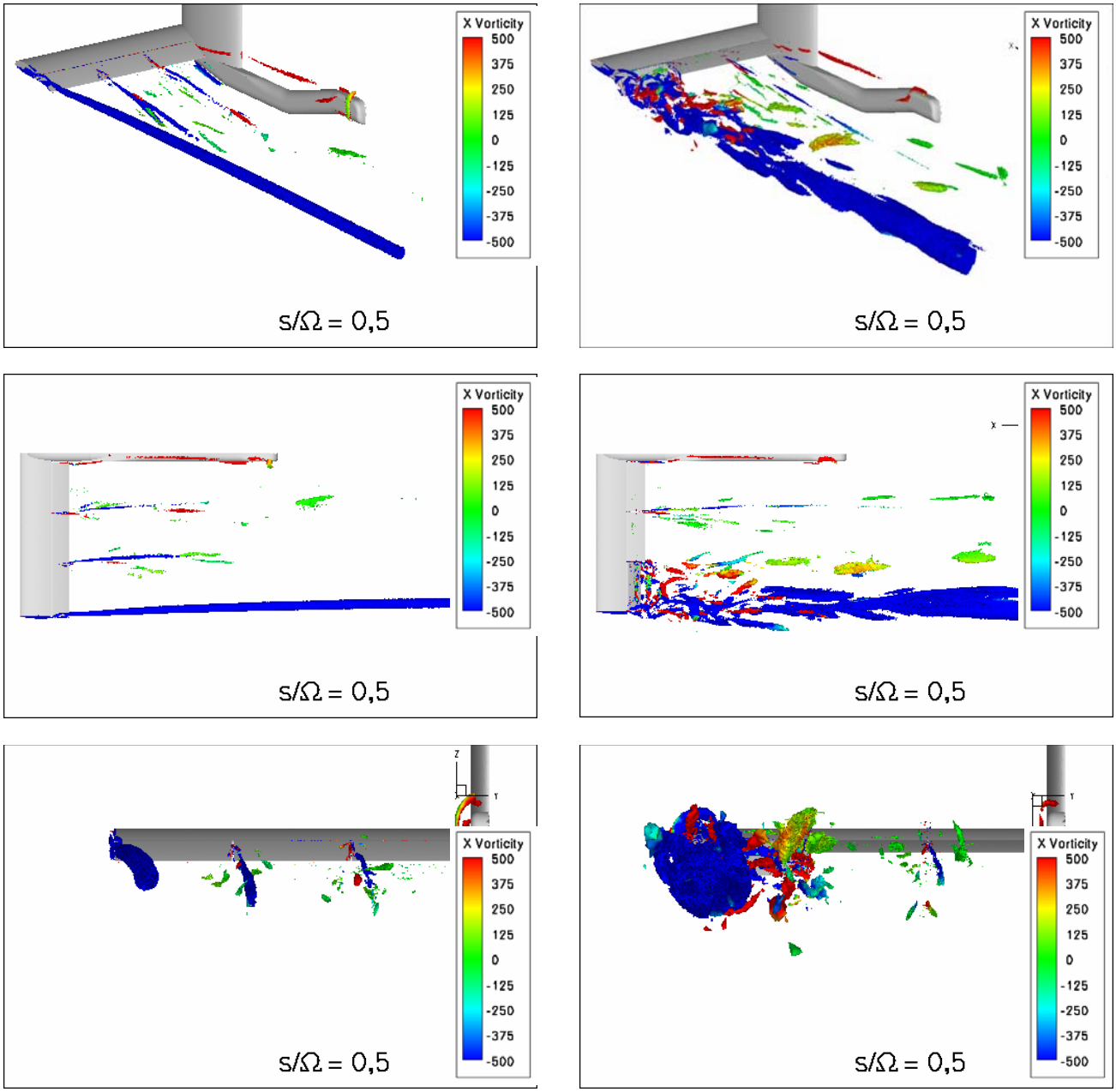

Fig. 10: Full period of flap oscillation. Comparison Configuration baseline vs. DFS, colored by vorticity from -500 1/s to 500 1/s

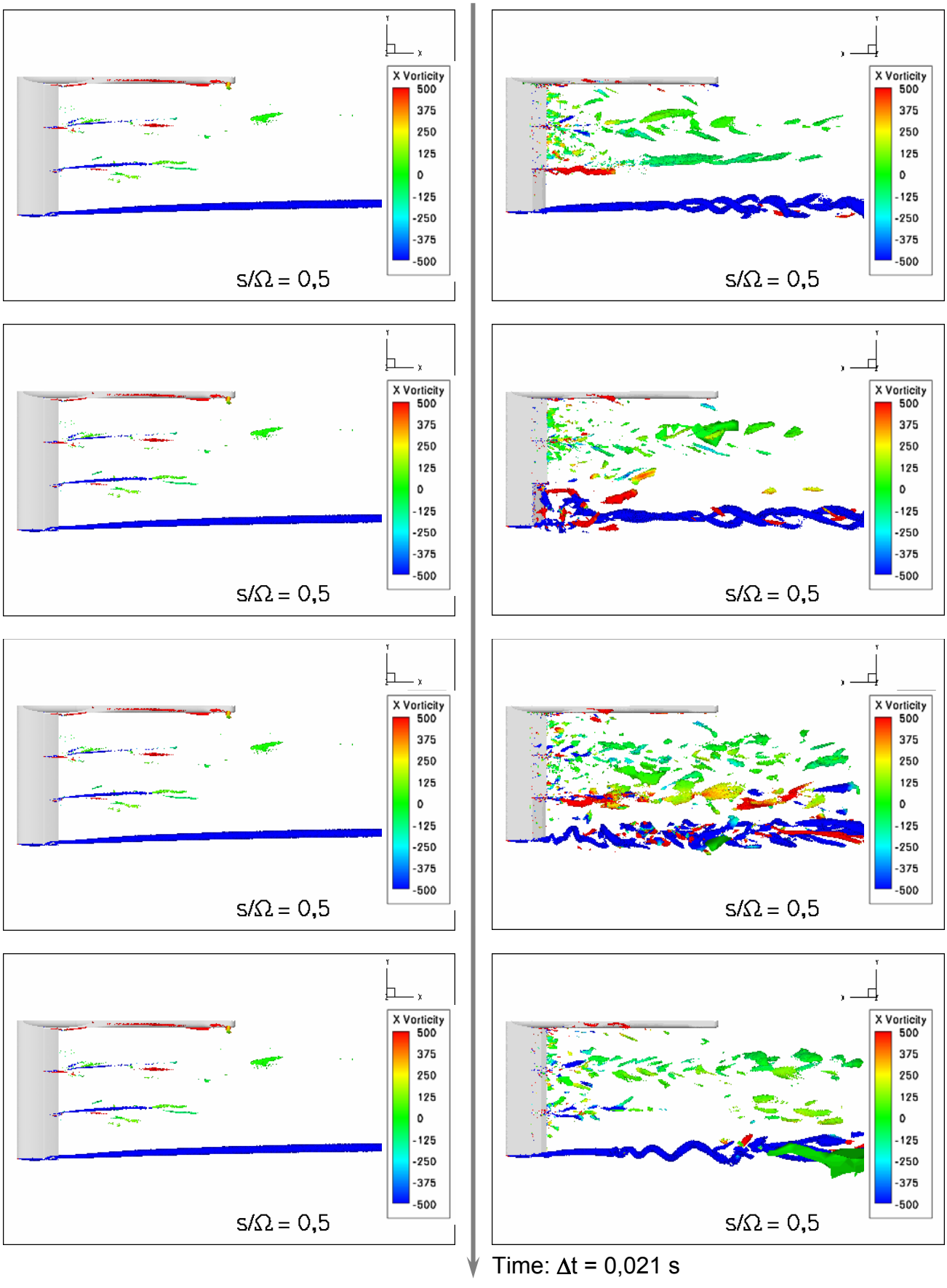

Fig. 11: Full period of flap oscillation. Comparison Configuration baseline without HTP vs. OFS without HTP, colored by vorticity from -500 1/s to 500 1/s

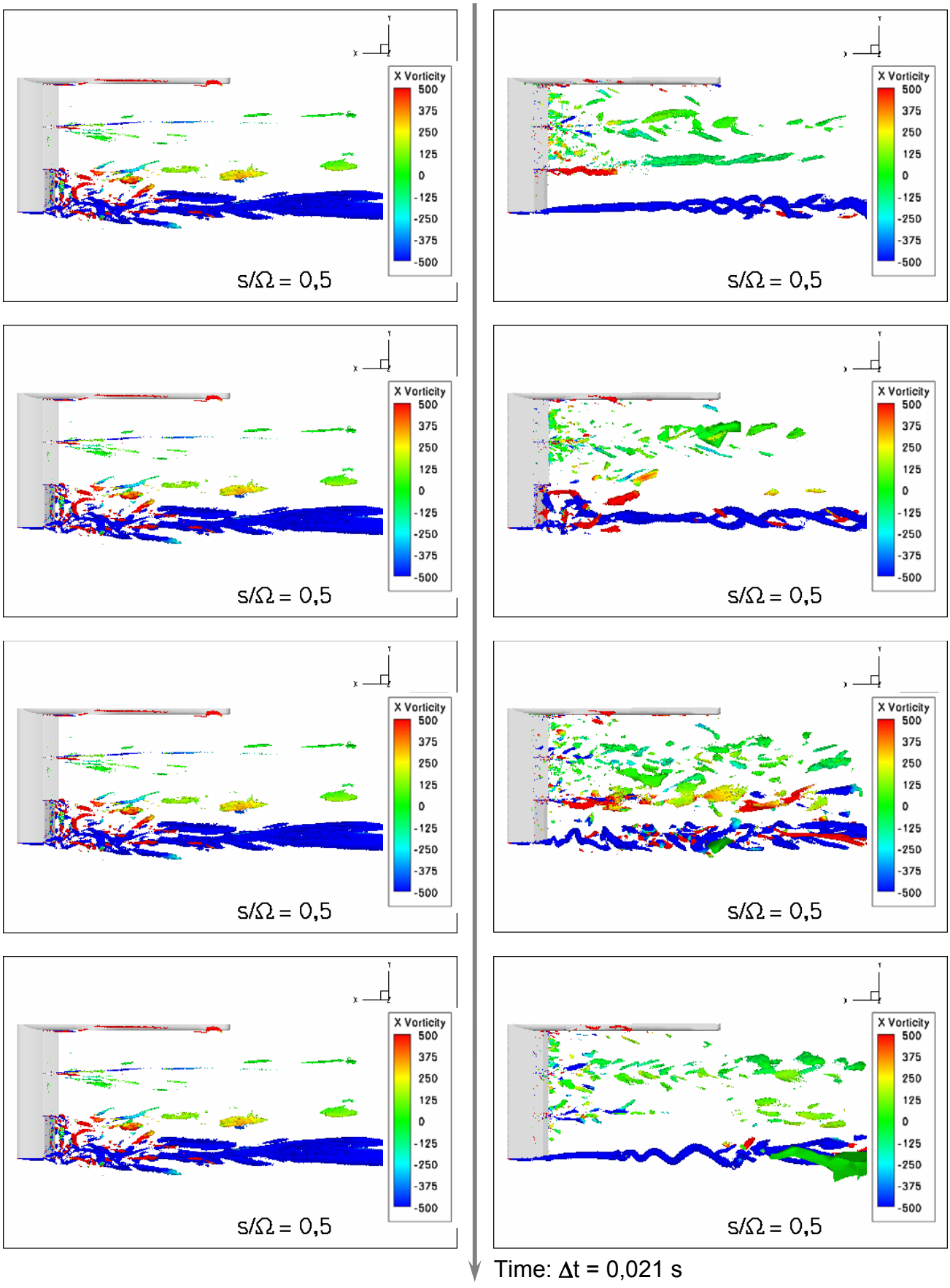

Fig. 12: Full period of flap oscillation. Comparison Configuration 01 (DFS) vs. 02 (OFS), colored by vorticity from 500 1/s to 500 1/s

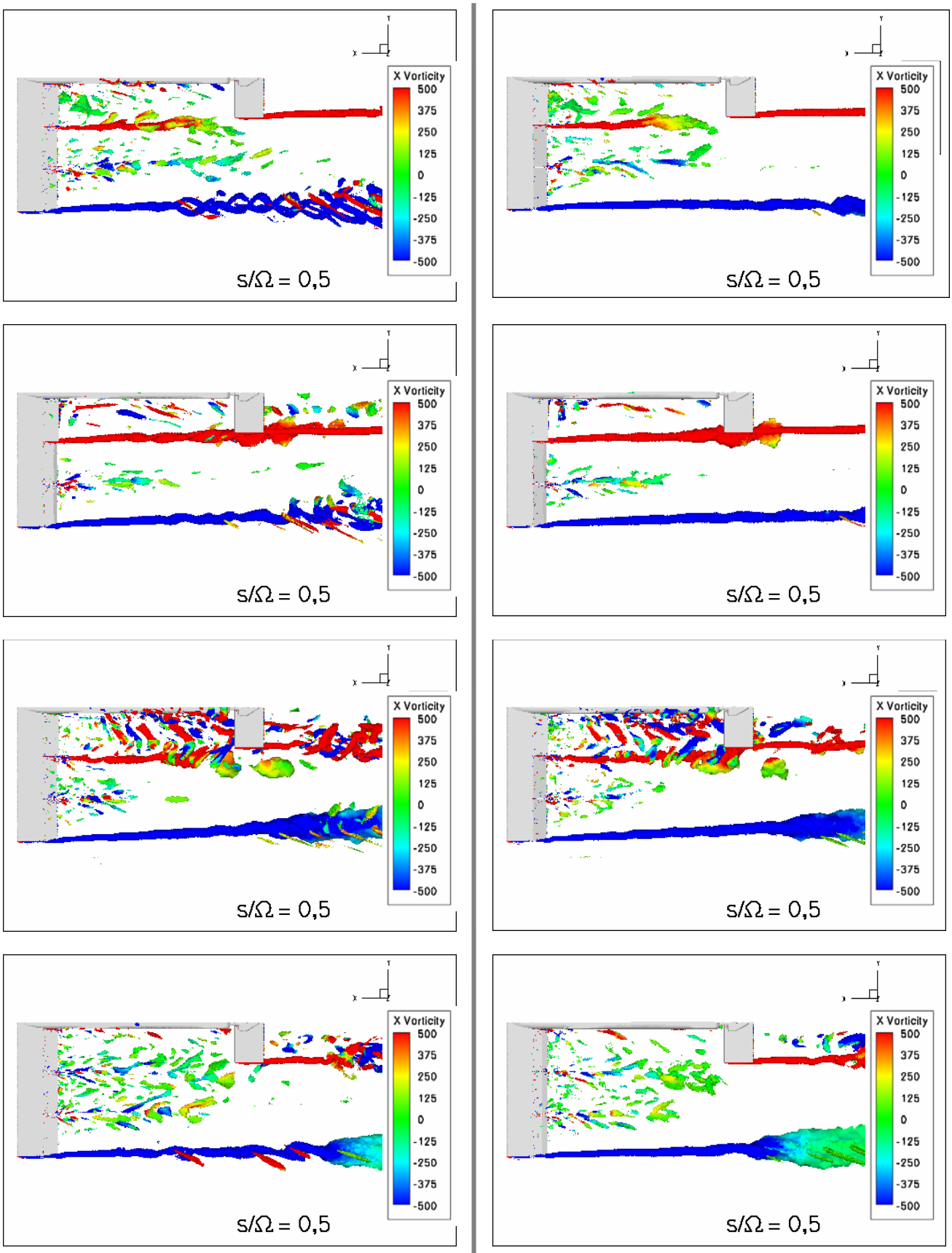

Time: Δt = 0,021 s

Time: Δt = 0,0168 s

Fig. 13: Full period of flap oscillation. Comparison Configuration 04 vs. 05 (dependency of frequency), colored by vorticity from -500 1/s to 500 1/s

7.2 Experimental results

For the analysis of the experimental investigations data sets accordingly to the CFD observations were taken. The list of configurations can be found in TAB.1.

The comparison between baseline configuration with HTP (00) and oscillating flap configuration (03, outboard flap +20°, midboard and inboard flap -10° maximum deflection) in Fig. 14 shows obviously, that vorticity is reduced earlier if the counter-rotating vortices which are shed from the outboard flap, are interacting. After vortex collapse there is nearly no rest vorticity. Due to the over-all circulation the vortex from HTP is moving downwards leaving the measurement field. In the baseline case the HTP vortex rotates around the main vortex. Finally both vortices are merging. The widening of vorticity is slower than in the OFS case.

A similar view results from comparison of baseline configuration without HTP and DFS configuration (01) in Fig. 16. In this case there is also an interaction of the counter-rotating vortices from the fully deflected outboard flap, which provides an accelerated expansion of both vortices. The undisturbed vorticity widening of the main vortex obtained in baseline configuration is taken place much slower than in DFS case.

The direct comparison between DFS and OFS configuration in Fig. 17 results in a faster widening of vorticity, if the flaps are moved periodically. Here not only the change in the lift distribution obviously plays a role, but actually the incitation of a vortex instability. It is a priori not recognizable which kind of instability works here.

The next item deals with the direct comparison between an outboard and an inboard configuration as shown in Fig. 18. Outboard configuration means the full-deflected outboard flap (+20°) and according to that the half deflected midboard and inboard flap with -10° deflection angle whereas the inboard configuration denotes the half-deflected outboard and midboard flap (+10°) and the full-deflected inboard flap (-20°). It is obvious here that an outboard configuation is more effective than an inboard configuration. The periodical shift of lift distribution in outboard direction and the accompanying accelerated vortex widening indicates strongly that the Crow instability was triggered in this case. This corresponds partly with the results of a flight test which was conducted in framework of AWIATOR project in 2003 ([20]).

Finally the dependence of vortex widening from the triggering frequency shall be discussed. Fig. 19 shows that it is necessary to choose a capable frequency to ensure resonance with the eigenfrequency of a vortex instability. In the special case of comparison of two triggering frequencies (0,8 Hz vs. 1,0 Hz) it is obvious, that the frequency 0,8 Hz is clearly more efficient.

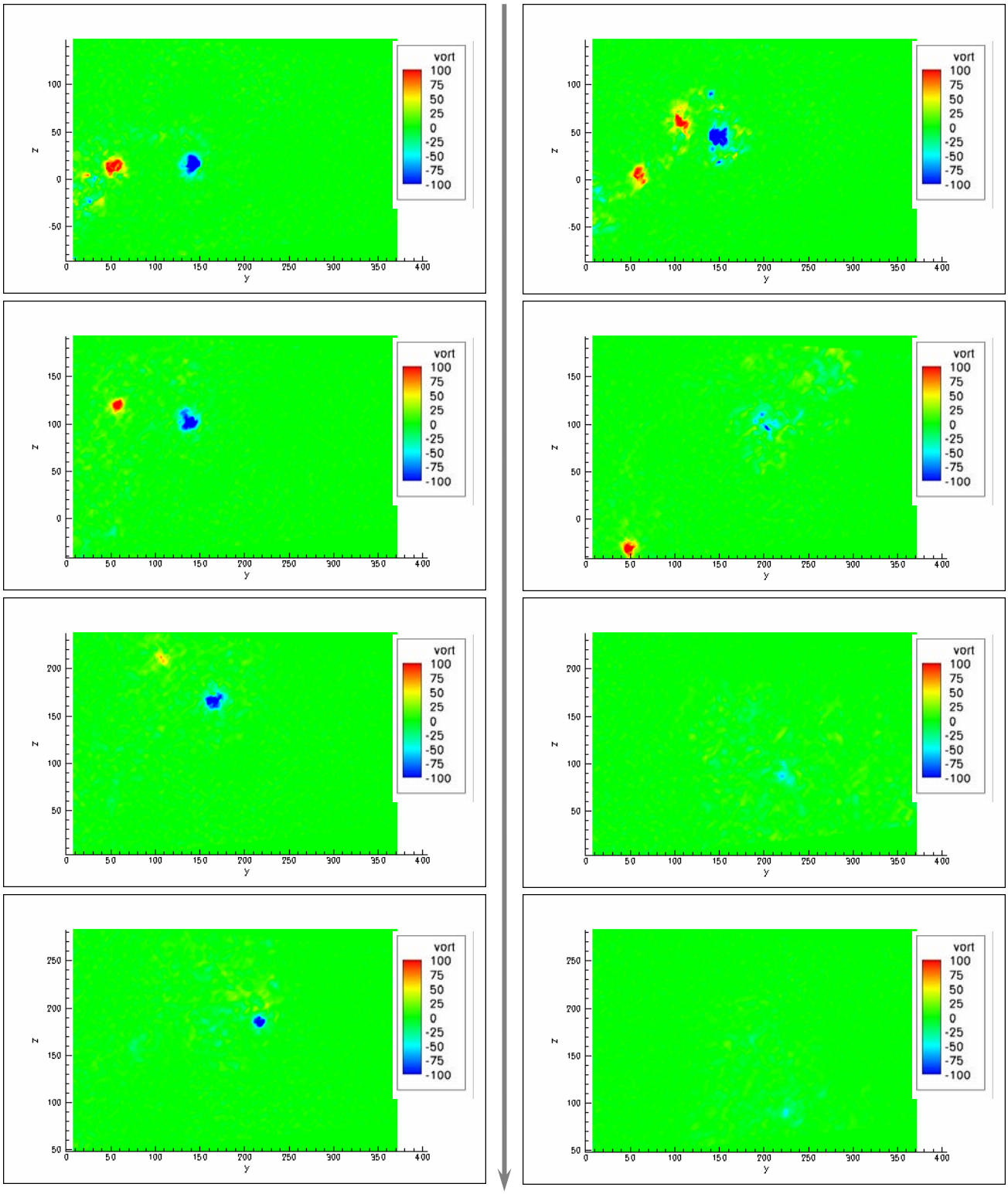

Time: $\Delta t \approx 1{,}5$ s

Time: $\Delta t \approx 1{,}5$ s

Fig. 14: Full period of flap oscillation. Comparison Configuration 00 vs. 03 (baseline vs. OFS with HTP), colored by vorticity from -100 1/s to 100 1/s

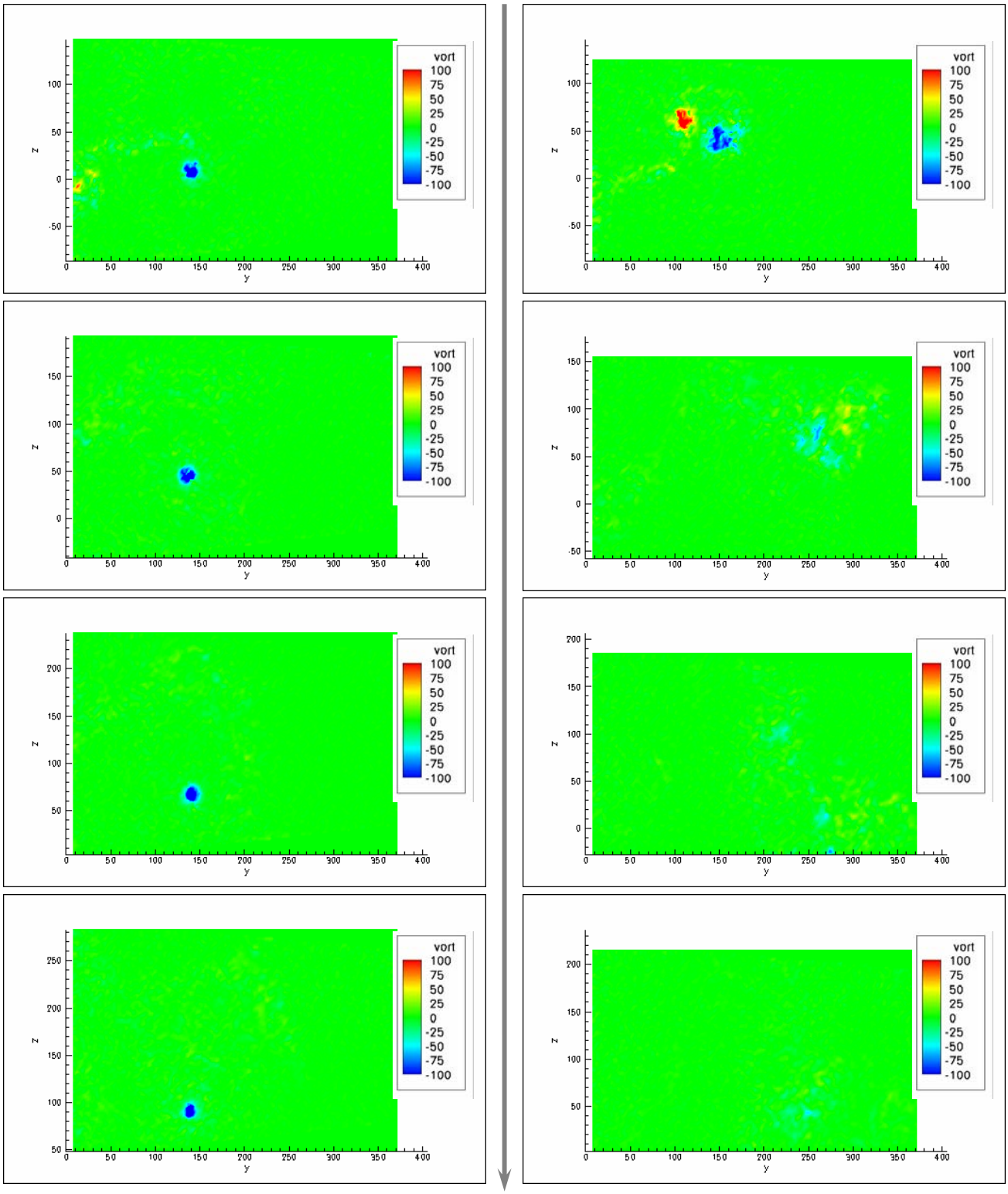

Time: $\Delta t \approx 1{,}5$ s

Time: $\Delta t \approx 1{,}5$ s

Fig. 15: Full period of flap oscillation. Comparison Configuration 00 vs. 02 (baseline vs. OFS without HTP), colored by vorticity from -100 1/s to 100 1/s

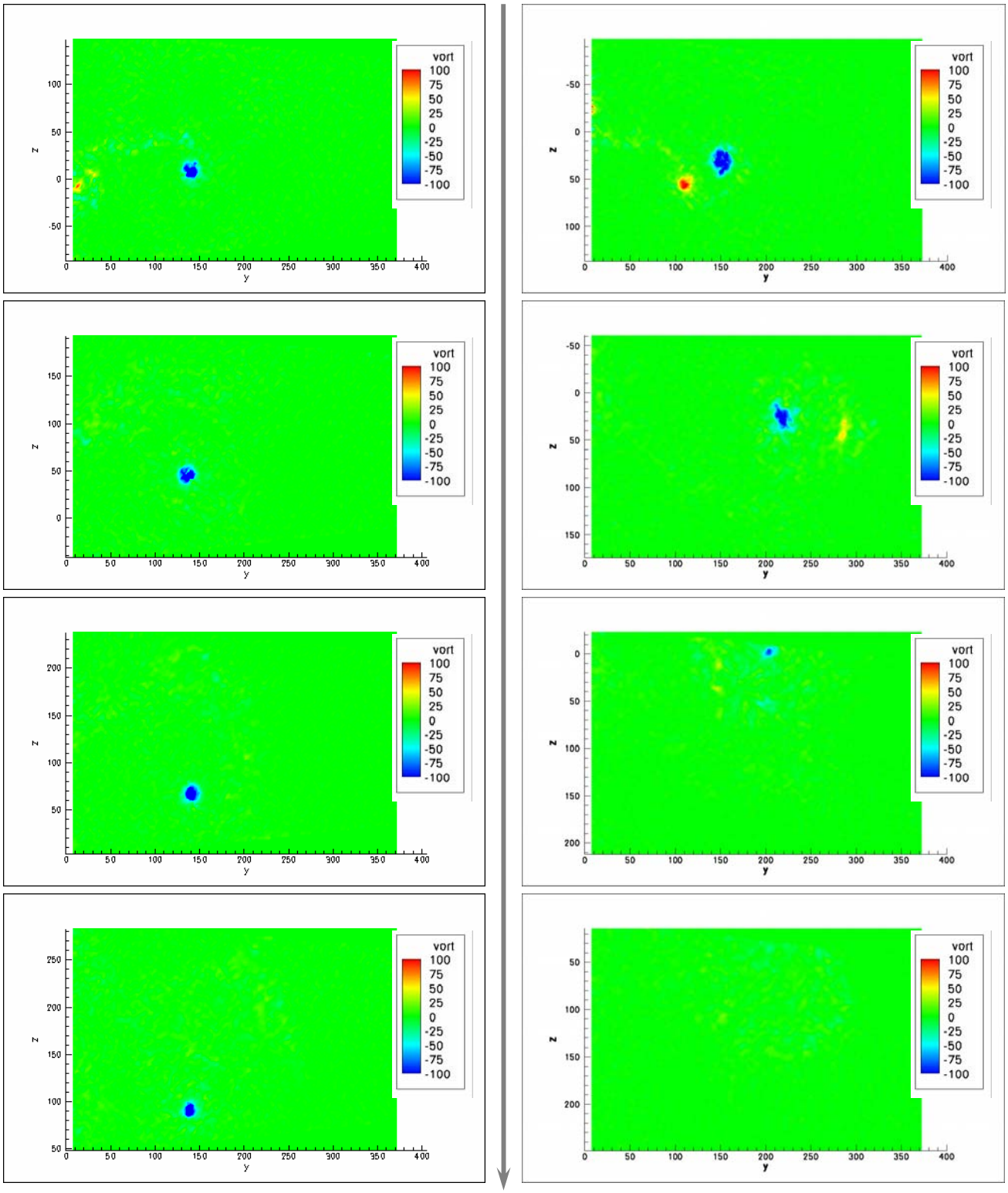

Time: $\Delta t \approx 1{,}5$ s

Time: $\Delta t \approx 1{,}5$ s

Fig. 16: Full period of flap oscillation. Comparison Configuration 00 vs. 01 (baseline vs. DFS), colored by vorticity from -100 1/s to 100 1/s

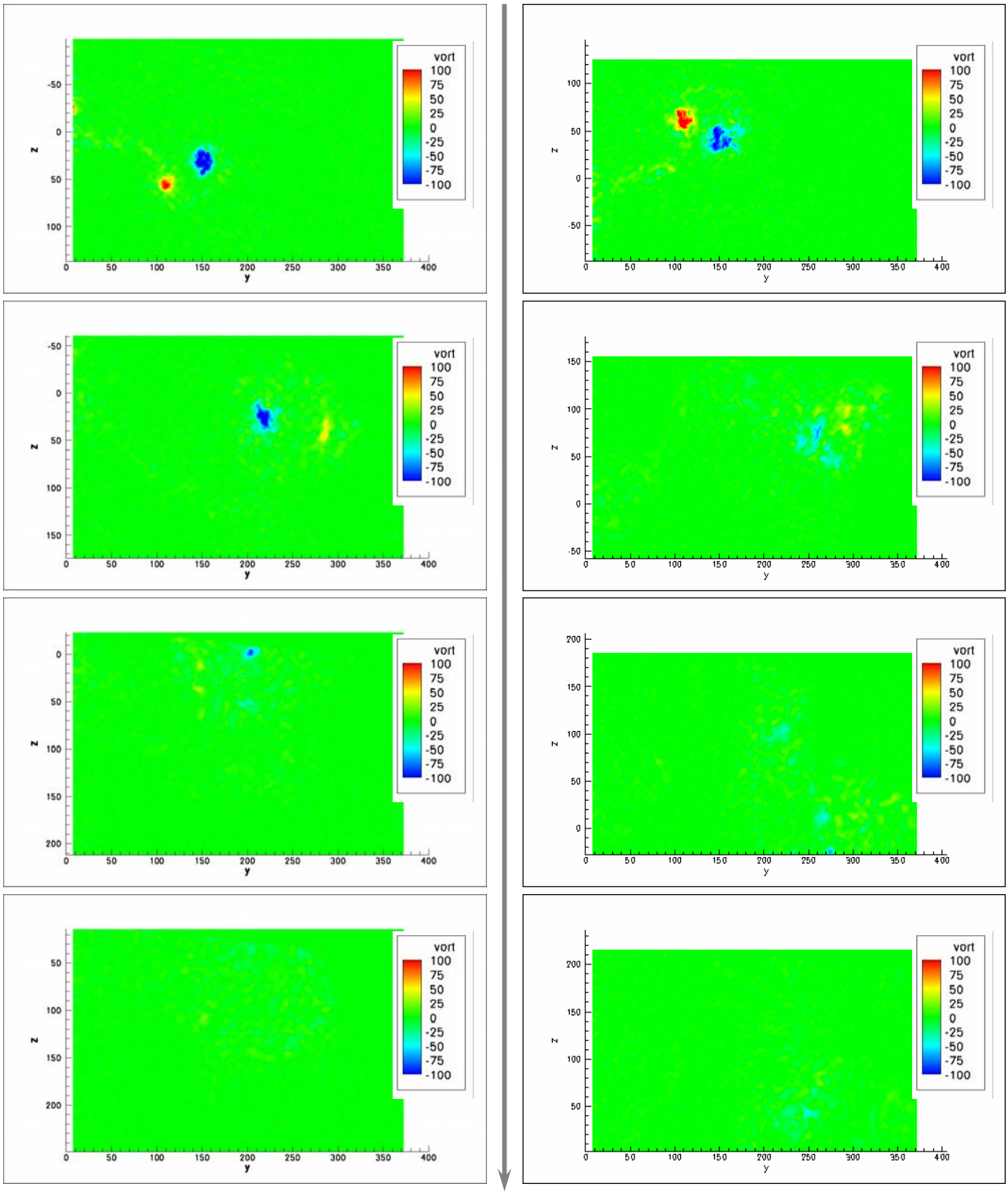

Time: $\Delta t \approx 1{,}5$ s

Time: $\Delta t \approx 1{,}5$ s

Fig. 17: Full period of flap oscillation. Comparison Configuration 01 vs. 02 (DFS vs. OFS), colored by vorticity from -100 1/s to 100 1/s

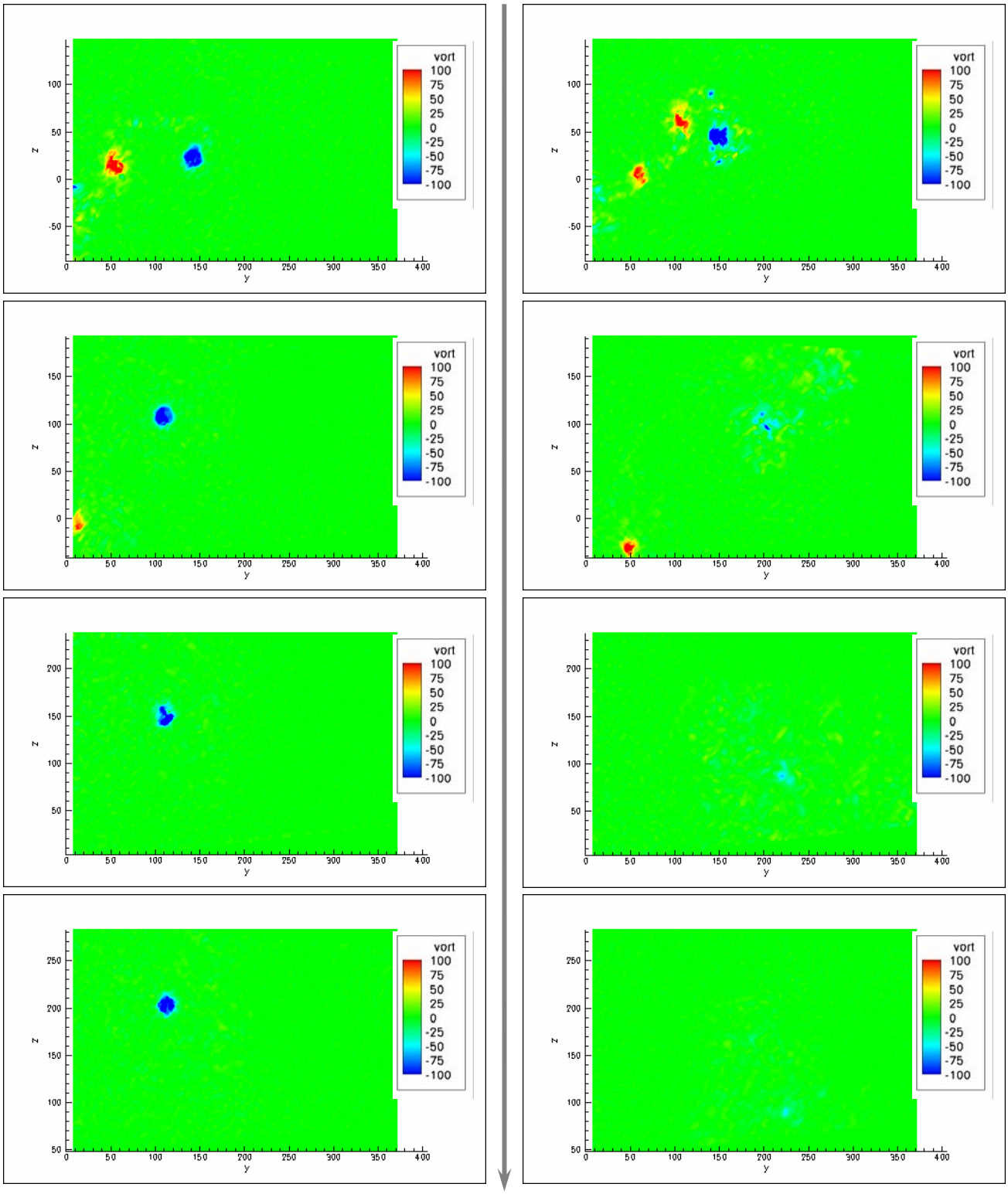

Time: $\Delta t \approx 1{,}67$ s

Time: $\Delta t \approx 1{,}67$ s

Fig. 18: Full period of flap oscillation. Comparison Configuration 04 vs. 03 (inboard loading vs. outboard loading), colored by vorticity from -100 1/s to 100 1/s

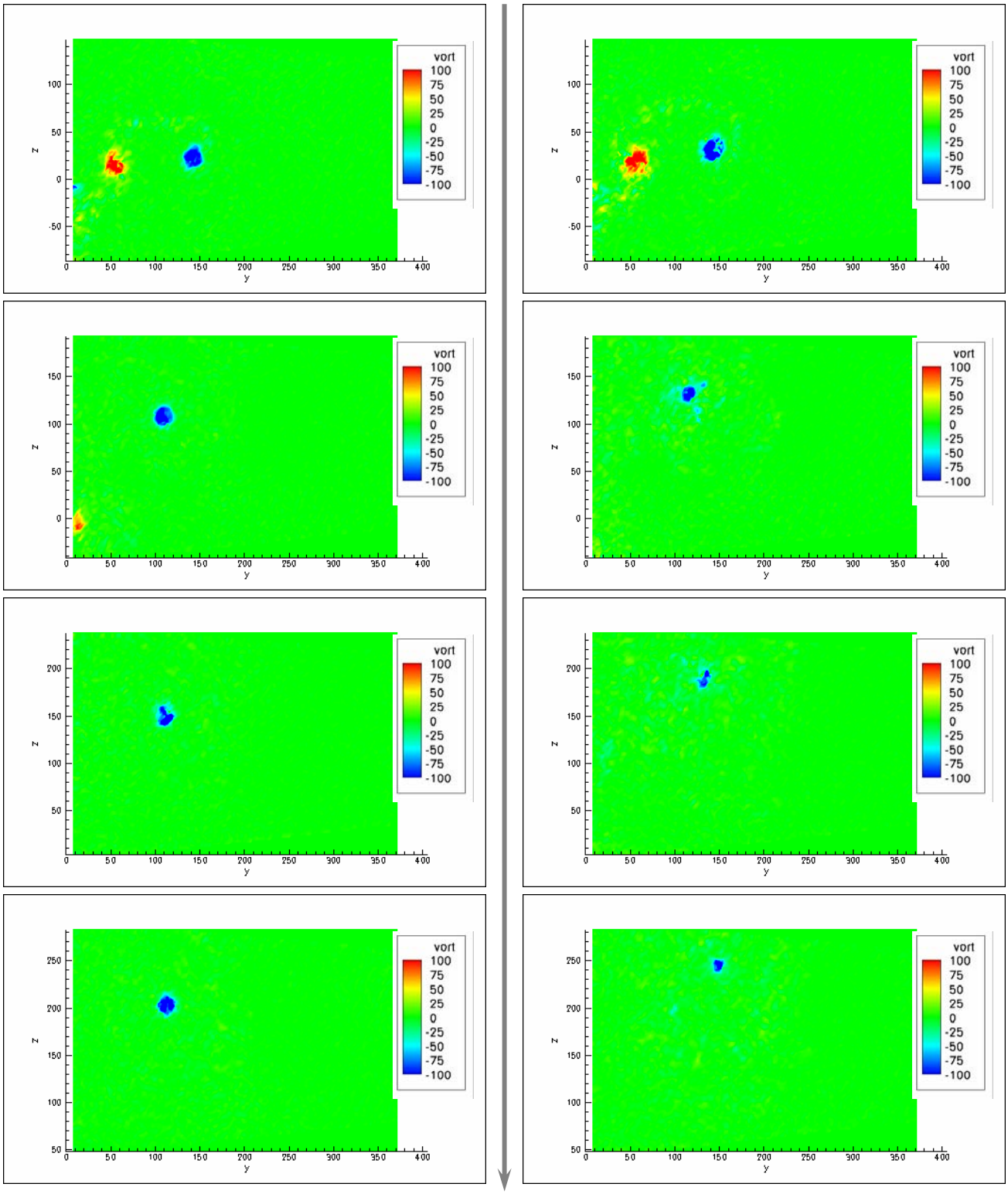

Time: $\Delta t \approx 1{,}67$ s

Time: $\Delta t \approx 1{,}336$ s

Fig. 19: Full period of flap oscillation. Comparison Configuration 04 vs. 05 (dependency of frequency), colored by vorticity from -100 1/s to 100 1/s

8. CONCLUSIONS

Numerical simulations of wake vortex generation by a generic wing configuration have shown that configurative modifications of lift devices constitute a promising way to achieve premature vortex decay. A grid study was conducted to show if vortex bursting is based on some kind of end effect which is caused by too much dissipation in the adjacent coarse grid regions. The grid study demonstrates that grid refinement is only to a minor degree responsible for the observed helical instabilities respective vortex breakdown phenomena. Independent of this it is obvious that the magnitude of vortex breakdown depends also on the triggering frequency of the oscillating flaps. Possibly, the resulting long wave oscillation of the primary vortex may effectively trigger the long-wavelength instability. However, evidence of this effect can be only achieved in the far field where the typical sinusoidal oscillations and subsequent ring formation develop. At this time there are not enough hardware resources available for unsteady computations on fine grids up to distances of 100 spans.

Experimental studies have shown that there is a quite pronounced effect on the vorticity distribution if flaps are deflected or in periodic motion. The effect seems to be somewhat stronger if flaps are in oscillating mode.

Acknowledgement

The work in this publication was done in the framework of Wirbelschleppe II project, which was funded by DLR.

REFERENCES

[1] E. Stumpf, Investigations of 4-Vortex Systems for an Alleviation of Vortex Wakes and its Realization with Transport Aircraft, Doctoral Thesis RWTH Aachen, 2004

[2] M. Galle, Ein Verfahren zur numerischen Simulation kompressibler, reibungsbehafteter Strömungen auf hybriden Netzen, Doctoral Thesis, DLR-FB 99-04, 1999

[3] T. Gerhold, O.Friedrich, J. Evans, Calculations of Complex Three-dimensional Configurations Employing the DLR-□-code, AIAA 97-0167, Reno, 1997

[4] A. Jameson, W. Schmidt, E. Turkel, Numerical Solutions of the Euler Equations by Finite Volume Methods Using Runge-Kutta Time Stepping Schemes, AIAA 81-1259, Palo Alto, 1981

[5] A. Jameson, Transonic Flow Calculations, MAE Report 1651, Princeton Unerversity, 1983

[6] T. Gerz, F. Holzäpfel, D. Darracq, Commercial aircraft wake vortices, Progress in Aerospace Science 38, 181-208, 2002

[7] L. Jacquin, D. Fabre, D. Sipp, V. Theofilis, H. Vollmers, Instability and unsteadiness of aircraft wake vortices, Aerospace Science and Technology 7, 577-593, 2003

[8] F. Bao, H. Vollmers, H. Mattner, Experimental Study on Controlling Wake Vortex in Water Towing Tank, ICIASF03, Göttingen, 2003

[9] E. Stumpf, Effect of Flap Strakes with regard to vortex wake alleviation, ECCOMAS2000, Barcelona, 2000

[10] E. Stumpf, R. Rudnik, A. Ronzheimer, Euler computations of the nearfield wake vortex of an aircraft in take-off configuration, Aerospace Science and Technology 4, 535-543, 2000

[11] E. Stumpf, J. Wild, A. A. Dafa´Alla, E. A. Meese, Numerical Simulations of the Wake Vortex Near Field of High Lift Configurations, ECCOMAS2004, Jyväskylä, 2004

[12] G. Voß, S. Melber-Wilkending, R. Rudnik, Premature Decay of Wake Vortices with Differential and Oscillating Flap Setting, ECCOMAS2006, Egmond aan Zee, 2006

[13] S. Haverkamp, G.Neuwerth, D. Jacob, Active and Passive Vortex Wake Mitigation using Control Surfaces, Aerospace Science and Technology 9, 5-18, 2005
[14] S. Haverkamp, G.Neuwerth, D. Jacob, Studies on the Influence of Outboard Flaps on the Vortex Wake of a rectangular Wing, Aerospace Science and Technology 7, 331-339, 2003
[15] S. Melber, Wirbelkorrektur für Ein- und Zweigleichungs-Turbulenzmodelle und Implementation für das Spalart-Almaras Turbulenzmodell in den Strömungslöser DLR-TAU, IB 124 – 2002/17, 2002
[16] F. Bao , and H. Vollmers. Alleviation of end-effect in facilities for far wake investigations. 43rd AIAA Aerospace Sciences Meeting & Exhibit, Reno, NV, AIAA 2005-0907, 2005
[17] M. Raffel, C. E. Willert, and J. Kompenhans. Particle image velocimetry. A practical guide. Springer, Berlin Heidelberg New York, 1998
[18] J. Westerweel and F. Scarano. Universal outlier detection for PIV data. Exp Fluids, V39(6):1096-1100, Dec. 2005
[19] C. Willert, Stereoscopic digital particle image velocimetry for application in wind tunnel flows. Meas Sci Technol, 8:1465-1479, 1997
[20] Eike Stumpf et al., ATTAS Smoke Try Out Test, AWIATOR Technical Report 1.1.3-31
[21] Stefan Melber, Wirbelkorrektur für Ein- und Zweigleichungs-Turbulenzmodelle und Implementation für das Spalart-Almaras-Turbulenzmodell in den Strömungslöser DLR-TAU, IB 124-2002/17

EXPERIMENTAL INVESTIGATIONS OF THE INFLUENCE OF AXIAL JETS ON 2- AND 4-VORTEX SYSTEMS

Robert Konrath[1], Carl F. v. Carmer[1], Heinrich Vollmers[1], Huang Shuoqiao[2]
[1] Institute of Aerodynamics and Flow Technology,
German Aerospace Center (DLR),
37073 Göttingen, Bunsenstr. 10, Germany.
[2] Fluid Mechanic Institute,
Beijing University of Aeronautics and Astronautics,
100083 Beijing, Xueyuan road 37, China

OVERVIEW

The effects of jets on wake vortices were investigated experimentally in a towing tank. Considered are two cases of 4-vortex systems consisting of two counter-rotating vortex pairs. As reference the corresponding 2-vortex system is also considered. The used vortex generator consisting of one or two rectangular wings was equipped with two pressurized water jet nozzles. Two different jet strengths were employed, resulting in parameter values of *R* (ratio between jet thrust and vortex strength) of 0.2 and 0.74. Cross-plane velocity fields were determined by means of Stereo-Particle Image Velocimetry (PIV). The jet/vortex interactions are discussed, as well as the influence of the jets on the occurrence of an interaction between inner and outer vortices in the near far field, which is presumed to lead to a more rapid decay of the wing vortices.

1. INTRODUCTION

Vortex sheets shed off the wings of an aircraft, roll up and organize into a pair of counter-rotating vortices of equal-strength in the aircraft wake. Such large-scale vortical structures are usually quite stable and energetic, and pose a potential hazard to following aircraft. As a consequence, regulatory separation distances have to be met during takeoff and landing, which thereby reduce the airport capacity. The alleviation of wake vortices remains an important issue in commercial aviation (Gerz et al. 2002, 2005; Spalart 1998). In order to develop effective strategies for an early decay of the large-scale structures in wake vortex systems, the development and possible forcing of their cooperative instabilities have been studied analytically and numerically (Bristol et al. 2004; Crouch 1997, 2005; Jacquin et al. 2003, 2005; Rennich and Lele 1999; Winckelmans et al. 2005).

Vortices introduced, for instance, by inboard edges of the flaps or the horizontal tail wing can lead to the formation of a 4-vortex system in the far wake, consisting of two unequal-strength counter-rotating vortex pairs. The inner vortices trigger instabilities of the outer tip vortices which may lead to a more rapid disintegration of the complete vortex system. Therefore, the generation of such a 4-vortex system could be an efficient way of promoting the decay of the wing tip vortices.

As part of DLR's Project *Wirbelschleppe*, Bao and Vollmers (2003) performed experiments on 4-vortex systems in the towing tank in Göttingen (WSG). Velocity fields in a cross plane were measured by means of PIV in order to be able to examine which parameters influence most strongly the interaction between the inner and the outer tip vortices. During this interaction process the tip vortices are strongly disturbed and the inner vortices vanish. The results of Vollmers and Bao are shown in **Figure 1,** within

which the circulation ratio Γ_1/Γ_0 is plotted against the span width ratio b_1/b_0 of the wings generating the 4-vortex system – the subscripts 0 and 1 refer to the outer and inner vortex pair respectively (s. **Fig. 2**). The symbols in the figure correspond to the investigated cases, which range from Γ_1/Γ_0 = -0.3 to -0.8 for b_1/b_0 = 0.2, 0.3, 0.4 and 0.5. The cases for which an efficient interaction between the inner and outer vortices could be observed are indicated by the shaded area. If the span width ratio is too large; viz. $b_1/b_0 \geq 0.4$, the interaction occurs too early and the disturbances of the tip vortices are not as strong. For $b_1/b_0 \leq 0.2$ the inner vortices are initially too close together so that both cancel each other out. Another requirement is that the inner vortices descend together with the outer vortices. This is the case above the solid line in the diagram which is determined theoretically using Biot-Savart's law. For cases lying below this line the inner vortices diverge with respect to the outer vortices, whereas for points above the line the inner vortices start to orbit around the outer vortices so that both can interact in the near far field.

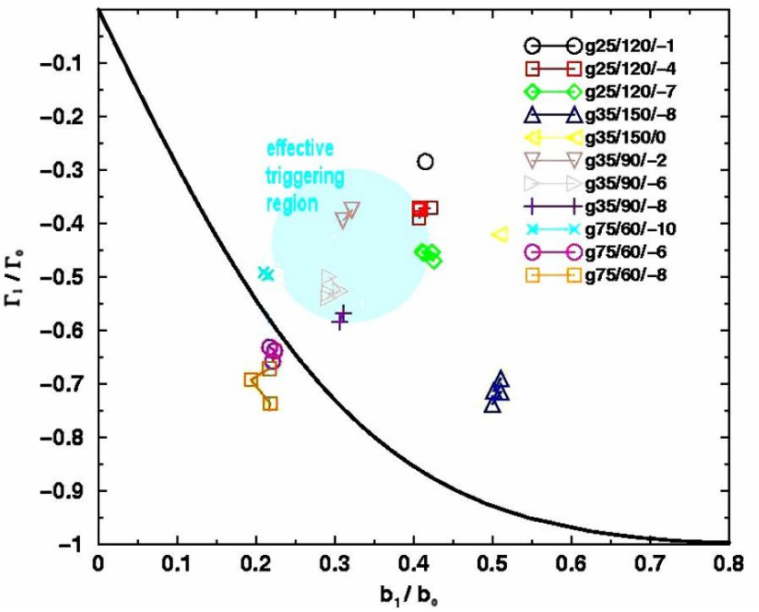

Fig. 1: Measured 4-vortex systems and region of effective vortex interaction according to Bao and Vollmers (2003).

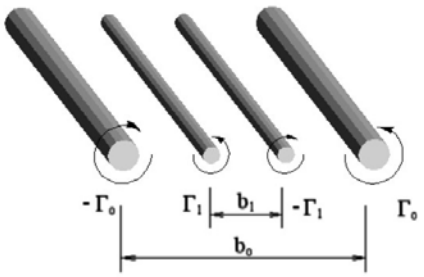

Fig. 2: Sketch of 4-vortex system.

An analysis of the vortex parameters (Carmer and Konrath, 2006) reveals that the circulation of the inner vortices is transferred to that of the opposite signed circulation of the tip vortices; i.e. the circulation strength of the tip vortices is reduced. Flow visualizations of Ortega et al. (2003) show how the inner vortices first execute sinusoidal deflections which lead to the formation of omega-shaped vortex structures around the tip vortices and finally break up into vortex rings.

The current investigations were carried out within the Project *Wirbelschleppe 2* of DLR. The objective was to verify the robustness of the 4-vortex system method for alleviation of wake vortices. For this the vortex generator (F13 model) was equipped with two water jet engines (see **Fig. 3**). The jets' impact on the vortex trajectories and decay of the 2- and 4-vortex systems is discussed for two different jet strengths.

2. EXPERIMENTAL SETUP

2.1. Towing tank facility

The experiments were carried out in the water tow tank at Göttingen (WSG) which has a total length of 18 m and a cross section size of 1.1 m x 1.1 m. The tank is equipped with several glass windows on the side and the bottom walls providing good optical access. At the top of the tank a carriage to which models can be attached is moving along two tracks. The maximum tow speed is 5 m/s. For triggering purposes several magnetic sensors are arranged nearby the tracks. To ensure quiescent ambient conditions a waiting period of 20 minutes between each run was applied allowing the water to settle down.

2.2. Generic wing model with jet engines

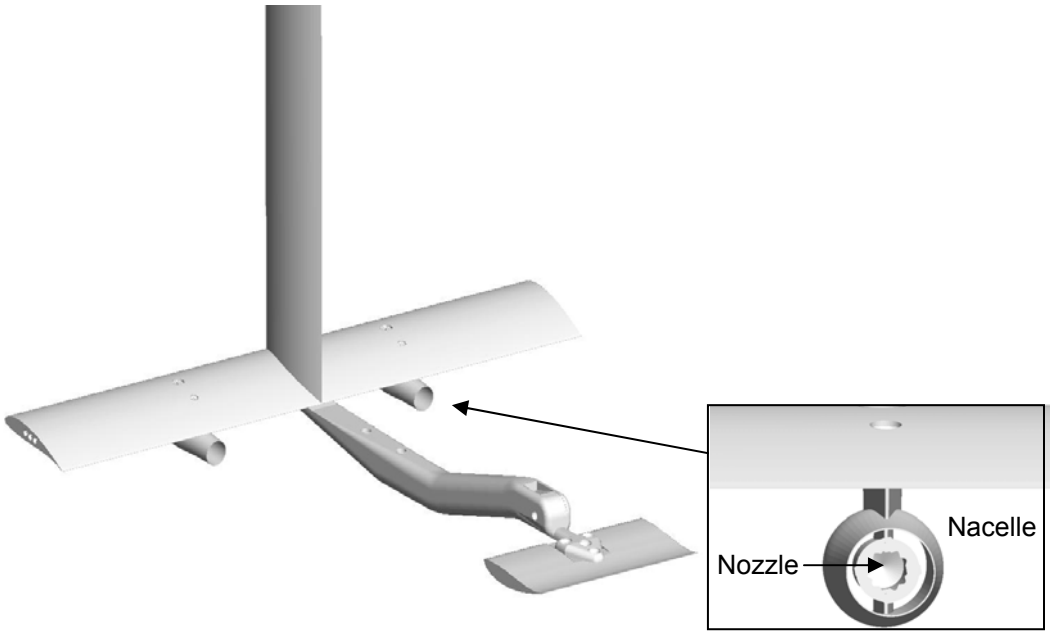

Fig. 3: F13 model with main wing and horizontal tail wing for the generation of two counter-rotating vortex pairs and the arrangement of two jet nozzles.

A special version of the F13 wing model was constructed to generate well-defined 2- and 4-vortex systems and to allow the attachment of two nozzles for the generation of water jets (**Fig. 3**). It consists of a horizontal rectangular main wing with fixed incidence angle to produce a pair of symmetric counter-rotating vortices. The wing is attached to the carriage of the tow tank via a profiled strut which ends in the centre of the wing. To produce another inner co- or counter-rotating vortex pair an additional rectangular wing

F13 model	Wing span, mm	Chord length, mm	Incidence	Aspect ratio
Main wing	$b = b_0 = 300$	50	$\alpha = 10°$	6
Horz. tip wings	$b_1 = 60; 90; 120; 150$	25; 35; 50; 75	$\varepsilon = -16° – +4°$	

Table 1: Dimensions and parameters of generic wing model F13.

(horizontal tail wing) can be mounted using a thin fuselage. Several horizontal tail wings with different span widths and chord lengths are available (**Table 1**). A Wortmann profile, which had been modified by Princeton University FX63-137B-PT and was especially designed for low Reynolds numbers, was used for the main wing as well as for the horizontal tail wings. Together with an adjustable inclination angle of the horizontal tail wing, the circulation and span width ratio between inner and outer vortex pairs can be varied within a wide range.

The jets were simulated using a pair of nozzles supplied with water. The L-shaped nozzles are streamlined and are enclosed by through-flow nacelles which are attached to the pressure side of the main wing via pylons. The internal diameters of the nozzles at the exits are 5.5 mm and the diameters of the nacelles' outlets are 10.8 mm. Their spanwise separation is 0.4 *b* (**Fig. 4a**) and the nozzle axes are inclined by 4° in a vertical direction with respect to the free stream (**Fig. 4b**), which pertains to take-off cases of real aircraft. The strut as well as the main wing incorporates small pipes which connect the two nozzles to a pressurized water reservoir that is fixed on the carriage of the tow tank. The jet velocities at the nozzles can be changed by adjusting different pressure levels of up to 6 bar within the water reservoir (**Fig 4c**).

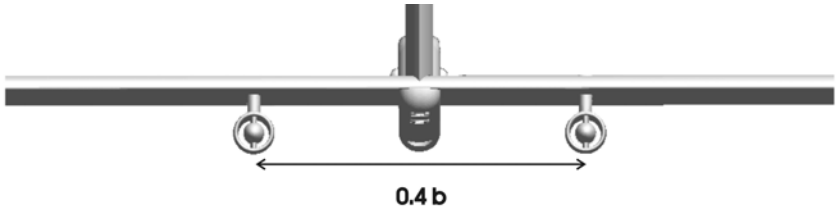

(a) Spanwise locations of nozzles.

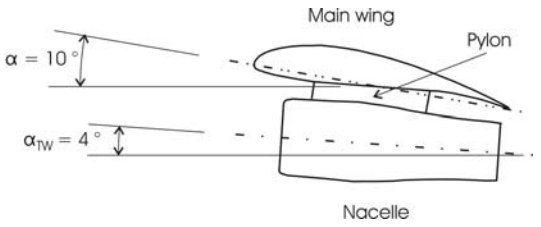

(b) Inclination of nacelles and nozzles and attachment beneath the main wing.

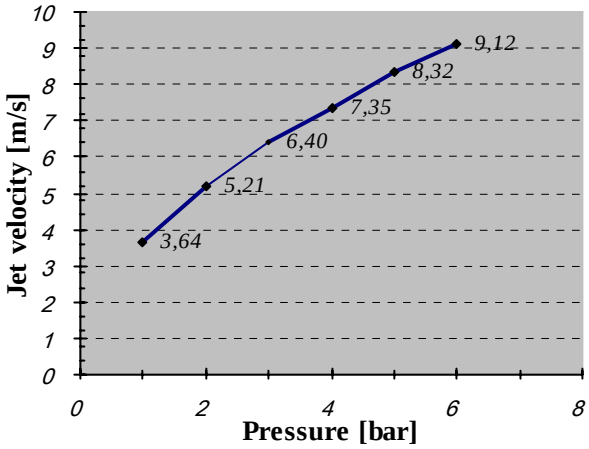

(c) Jet velocities for different water tank pressures.

Fig. 4: Arrangement of nozzles and jet parameters.

2.3. Stereo-PIV system

A Stereo-PIV measurement system was employed in order to obtain time-dependent cross-sectional flow velocity fields of the descending wake vortex system of the port side of the wings. The tank was seeded with hollow glass spheres with a mean diameter of 11 microns and a density of 1.1 g/cm^3.

The laser light sheet produced by a dual cavity Nd:YAG laser emitting two pulses of 190 mJ pulse energy with a repetition rate of 10 Hz, illuminated a cross plane through a side window of the water tank. The two PIV cameras were positioned at the opposite side of the tank with viewing angles of about ±45° with respect to the light sheet. The high-resolution cameras (PCO-1600, 1600 x 1200 px) are able to acquire double-frame images with a maximum recording rate of 15 Hz. Two glass prisms filled with water were arranged in front of the cameras such that the air/water interface was aligned perpendicular to the axis of the lens (with focal length 21 mm) axis in order to avoid image aberrations. The cameras were attached to vertical translation stages which allow the camera systems to follow the descent of the vortex system. A programmable sequencer synchronized the triggering of cameras, the translation stages and the laser.

3. RESULTS

3.1. Test parameters

In all cases the model was towed with a constant velocity of U = 1.5 m/s. The measurement parameters of the 2-vortex system are summarized in **Table 2**. Three different vortex configurations are investigated (**Table 3**), i.e. a 2-vortex system (Configuration I) without attached horizontal tail wing for reference and two cases of 4-vortex systems (Configuration II & III). The circulation values and ratios are estimated from PIV data obtained one span downstream of the trailing edge of the main wing using the line integral:

$$\Gamma = \oint \vec{v} \cdot d\vec{s} \qquad (1)$$

The integration is performed on circles with an origin close to the vortex centers. Using different circle radii, the resulting maximum magnitude of circulation was chosen as the final result for a specific vortex.

U	1.5 m/s	Model velocity
Re	74 250	Chord based Reynolds number, Re = U c / ν
Re$_\Gamma$	46 800	Circulation based Reynolds number, Re$_\Gamma$ = Γ_0 / ν
ν	$1.01 \cdot 10^{-6}$ m^2/s	Kinematic viscosity
c_L	0.99	Lift coefficient of main wing
Γ_0	0.0473 m^2/s	Circulation of tip vortices.

Table 2: Test parameters of the 2-vortex system.

Configuration	Γ_1/Γ_0	b_1/b_0	Incidence of tail plane	
I	na	na	na	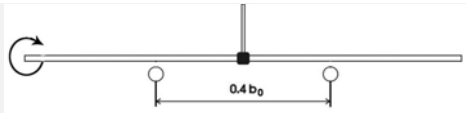
II	-0.38	0.3	ε = -3°	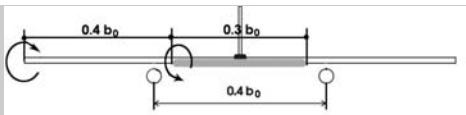
III	-0.48	0.4	ε = -4°	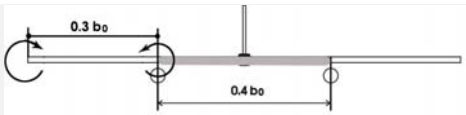

Table 3: Vortex configurations with circulation (Γ_1/Γ_0) and span width (b_1/b_0) ratios.

The tests were carried with and without water jets. Two different jet strengths were used, corresponding to *R* parameter values of 0.2 and 0.74. The *R* parameter is defined as the ratio of the jet thrust to the vortex strength:

$$R = \frac{\rho_j U_j \left(U_j - U\right) A_j}{\rho \Gamma_0^2} \qquad (2)$$

where ρ_j is the jet density, U_j the mean jet velocity and A_j the jet area (2.376e-5 m^2). The jet parameters are summarized in **Table 4** for both settings. In order to calculate the *R* parameters with reasonable accuracy, the mean jet velocities and the vortex circulations have to be determined precisely. The vortex circulation in equation (1) is calculated from PIV measurements (s. Tab. 3) with no attached horizontal tail wing and without water jets. The mean jet velocity U_j is determined from flow rate measurements.

Pressure	Flowrate	U_j	Thrust	R, (eq. (2))	$R_D = \frac{U_j D_j}{\nu}$
2 bar	0.12 liter/s	5.2 m/s	0.46 N	0.2	28 400
6 bar	0.22 liter/s	9.1 m/s	1.64 N	0.74	49 600

Table 4: Jet parameters for two pressure settings and a model velocity of U = 1.5 m/s.

Margaris et al. (2008) estimated *R*-values for two airplanes (A330, B737) in cruise and take-off configurations. For cruise conditions the estimated *R* parameters are found to be in the order of one. Significantly higher *R*-values came out for take-off conditions which, however, are subject to larger uncertainties in their estimation.

In the following the non-dimensional time t* is used, which is defined as:

$$t^* = \frac{t \cdot U}{b_0}. \qquad (3)$$

3.2. Jet / vortex interactions of the 2-vortex system

Figure 5 shows a comparison of the tip vortex trajectories of configuration I for the following three cases: no jet (*R* = 0), *R* = 0.2 and 0.74. The trajectories are very similar. Differences can be seen only in the descent rate of the vortices, which increases with increasing jet strength. This can be explained by the positive inclination angle of the jets of 4°, introducing a downward directed momentum to the flow.

Velocity field distributions are plotted in **Figure 6** from t* = 1 to 8.5 for the strong jet with *R* = 0.74. The colour distributions are related to the out-off-plane velocity of the jet flow. The tip vortex, which can be clearly indentified by the in-plane velocity vectors moving downward, seems not to be strongly disturbed by the turbulent jet flow. The out-off plane velocity distributions show how the jet region enlarges in time and starts to be deformed by the vortex in the time region from t* = 1 to 3.5. Due to the vortex induced flow the descent of the jet is slightly greater than that of the tip vortex. Fluid of the jet is stretched and forms spiral-shaped structures while it is entrained by the vortex which can be seen at t* = 6.5 and 8.5. Now the out-off-plane velocity magnitudes of the jet are greatly reduced.

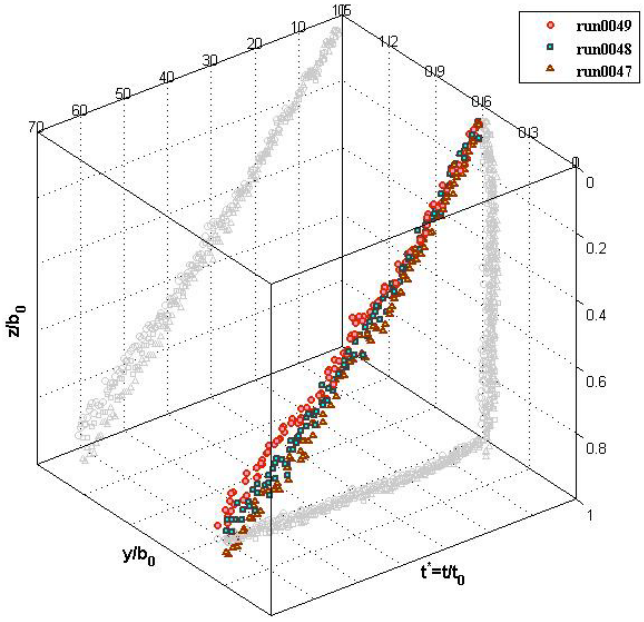

Figure 5: Vortex trajectories of configuration I (2-vortex system) without water jet (Run 0049) and for a jet with *R* = 0.2 and 0.74 (Runs 0048 and 0047 respectively).

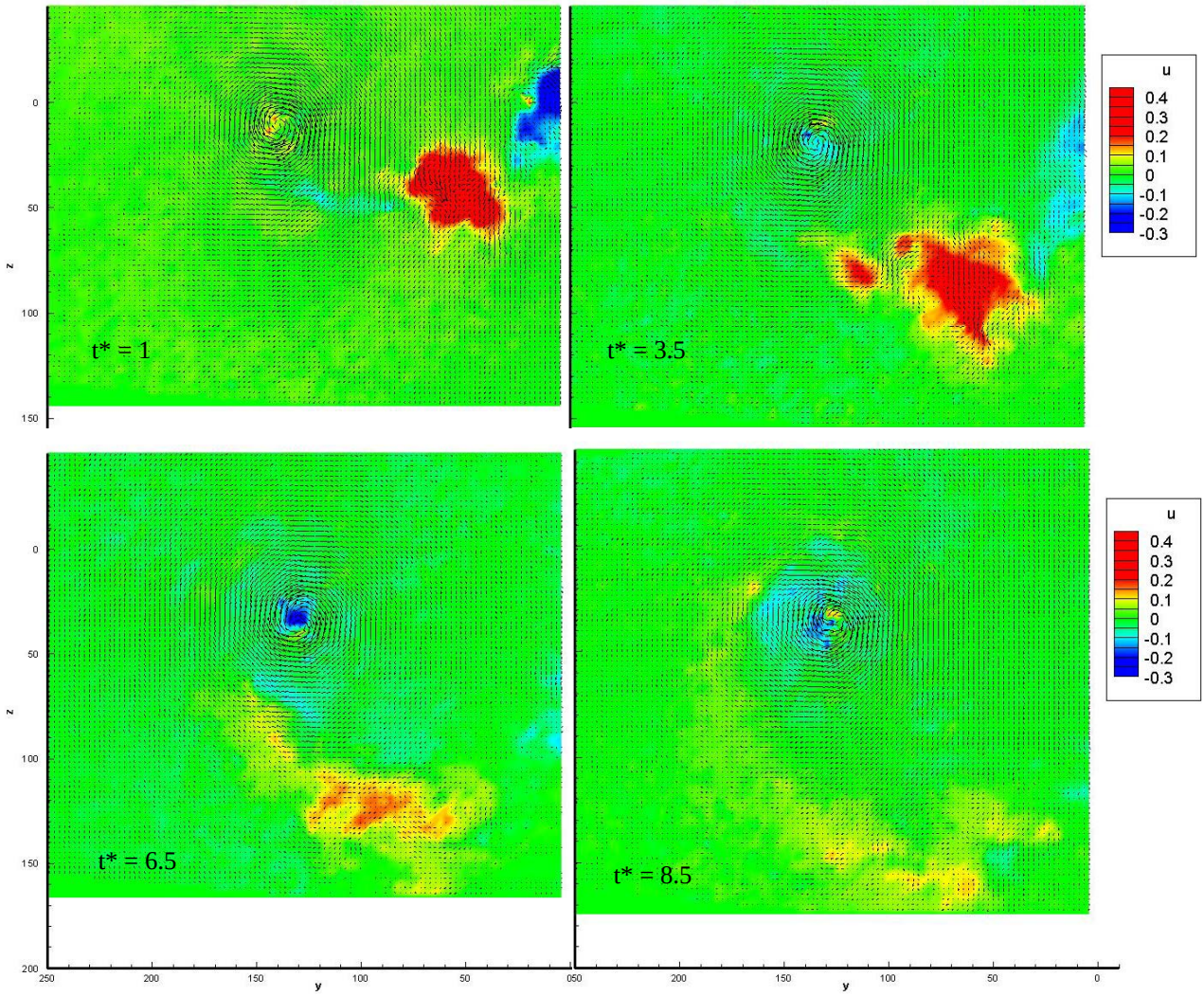

Figure 6: Flow velocity distributions of configuration I (2-vortex system) with jets with R = 0.74.

3.3. Jet / vortex interaction of 4-vortex systems

For reference **Figure 7** shows the velocity and vorticity distributions of configuration III (Γ_1/Γ_0 = -0.48, b_1/b_0 = 0.4) without water jets. The outer wing tip vortex (negative vorticity) and the inner counter-rotating vortex (positive vorticity) can be clearly identified: the inner vortex orbits around the outer tip vortex and at t* = 17 is located directly beneath the tip vortex. At t* = 28.5 the expected vortex interaction has taken place; i.e. the inner vortex has vanished and the tip vortex has significantly lower vorticity peak values inside the core region. This vortex interaction consists of a 3D merging process from which we observe only 2D slices.

The velocity and vorticity distributions for the same case, however, now with water jets (R = 0.74), are plotted in **Figure 8**. In this case the jets are located exactly beneath the inner vortices. The vorticity distributions show how the inner vortex is deformed by the turbulent jet flow just after its generation at a time from t* = 1 to 2. At t* = 2.5 an inner vortex with increased size and lowered peak vorticity can be observed, which then van-

ishes in the vorticity distributions at t* = 5. In **Figure 9** the out-off-plane velocity distributions are shown for the same case. These distributions show how the fluid of the jet is pushed by the inner vortex into a counter-clockwise direction (t* = 1 to 5). The movement of the inner vortex seems not to be affected by the jet. The resulting decreased descent of the fluid of the jet leads obviously to a stronger entrainment by the outer tip vortex (see t* = 10.5 to 16.5), when seen in comparison with the 2-vortex system (see Figure 6). The wake flow in the main vortex is now very pronounced.

For the same vortex configuration (III, Γ_1/Γ_0 = -0.48, b_1/b_0 = 0.4) with the weaker jet case of *R* = 0.2, the inner vortex is not disturbed by the jet, showing very similar vorticity distributions (not shown here) to the case without water jets (see Fig. 7). The fluid of the jet is distributed similar to the case of the stronger jet (*R* = 0.74), where, however, the jet dissipates very quickly (not shown here).

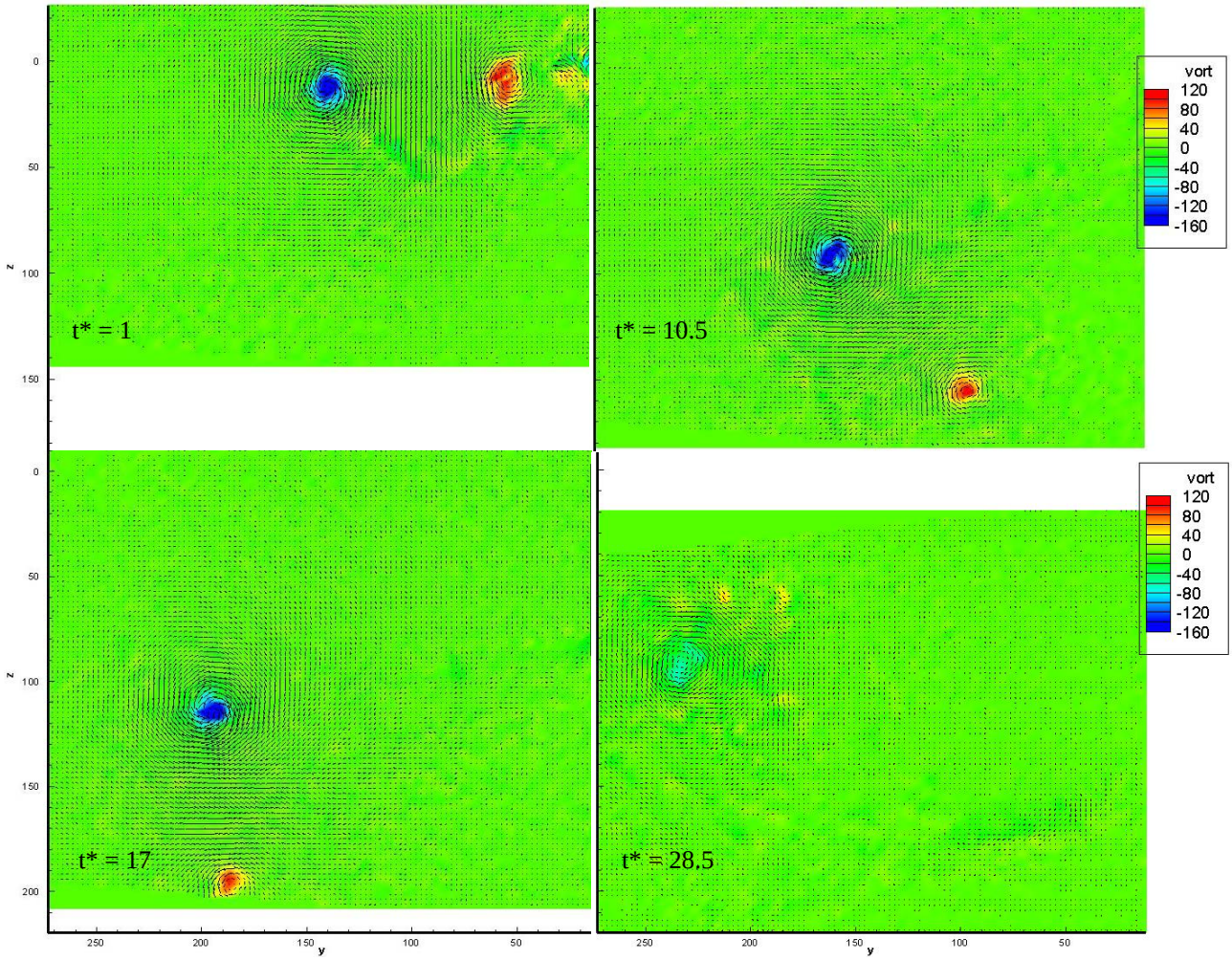

Figure 7: Flow velocity and vorticity distributions of configuration III (4-vortex system, Γ_1/Γ_0 = -0.48, b_1/b_0 = 0.4) with no blowing jets.

The weaker inner vortex for the configuration II (Γ_1/Γ_0 = -0.38, b_1/b_0 = 0.3) is slightly disturbed by the weaker jet of *R* = 0.2 resulting in lower peak values and increased size (not shown here). Its trajectory again is very similar to the case without water jets. However, in this case the inner vortex is initially located at a further inboard location. The fluid of the jet is now pushed in a downward direction (not shown here). For the strong

jet case (R = 0.74) the inner vortex vanishes quickly (t* = 1 to 3, not shown here), although the fluid of the jet is also distributed by the inner vortices.

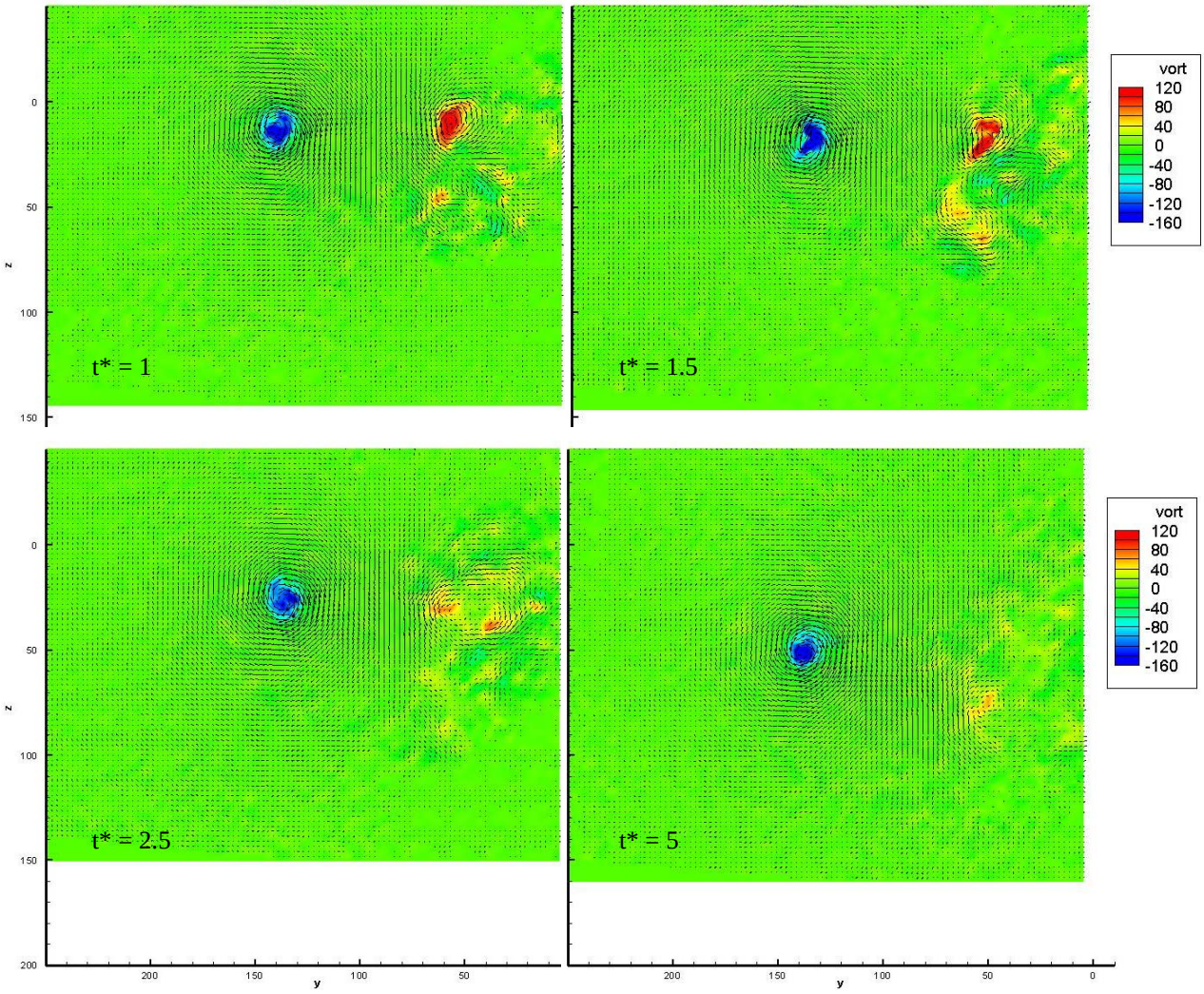

Figure 8: Flow velocity and vorticity distributions of configuration III (4-vortex system, Γ_1/Γ_0 = -0.48, b_1/b_0 = 0.4) with jets with R = 0.74.

3.4. Interaction between outer tip vortices and inner tail wing vortices in the far field with and without jets

The following discussion of the results focuses on the interaction between the outer wing tip vortex and the inner horizontal tail wing vortex in the near far field. This interaction results in a two vortex system where the oppositely signed circulation of the inner vortex is transferred to the outer tip vortex. After their reorganisation the strongly disturbed outer vortices have an increased core size with lower vorticity peak values (see Fig. 7).

As described in the former section the structure of the inner vortices is affected by the jet, dependent on the *R* parameter and the circulation ratio. **Figure 10** shows the tip vortex trajectories for both 4-vortex configurations as a function of the strength of the jets. At the beginning all trajectories are very similar. However, with no water jets, the trajectories show a hump between t* = 45 and 60 for configuration II (Γ_1/Γ_0 = -0.38, b_1/b_0 = 0.3), which is even more pronounced for configuration III (Γ_1/Γ_0 = -0.48, b_1/b_0 = 0.4) between t* = 20 and 50. This hump can be interpreted as interaction of inner and outer vortices which occurs earlier in the case of configuration III because of the lower separation distance between the counter-rotating vortices. With water jets this hump is less distinctive and cannot be seen in the result of configuration II with strong jet of *R* = 0.74. This is in accordance with the observation that the inner vortex is strongly disturbed by the jet in this case and vanishes quickly in the PIV results. **Figure 11** shows the spatial-temporal evolution of the vorticity distributions from t* = 1 to t* = 30 for configuration III. The plots show that the peak vorticity of the inner vortex reduces faster with increasing jet strength. However, the peak vorticity evolution for the tip vortex is similar for all cases. This applies also to the abrupt drop of the peak vorticity at t* = 30, which indicates the occurrence of the desired vortex interaction.

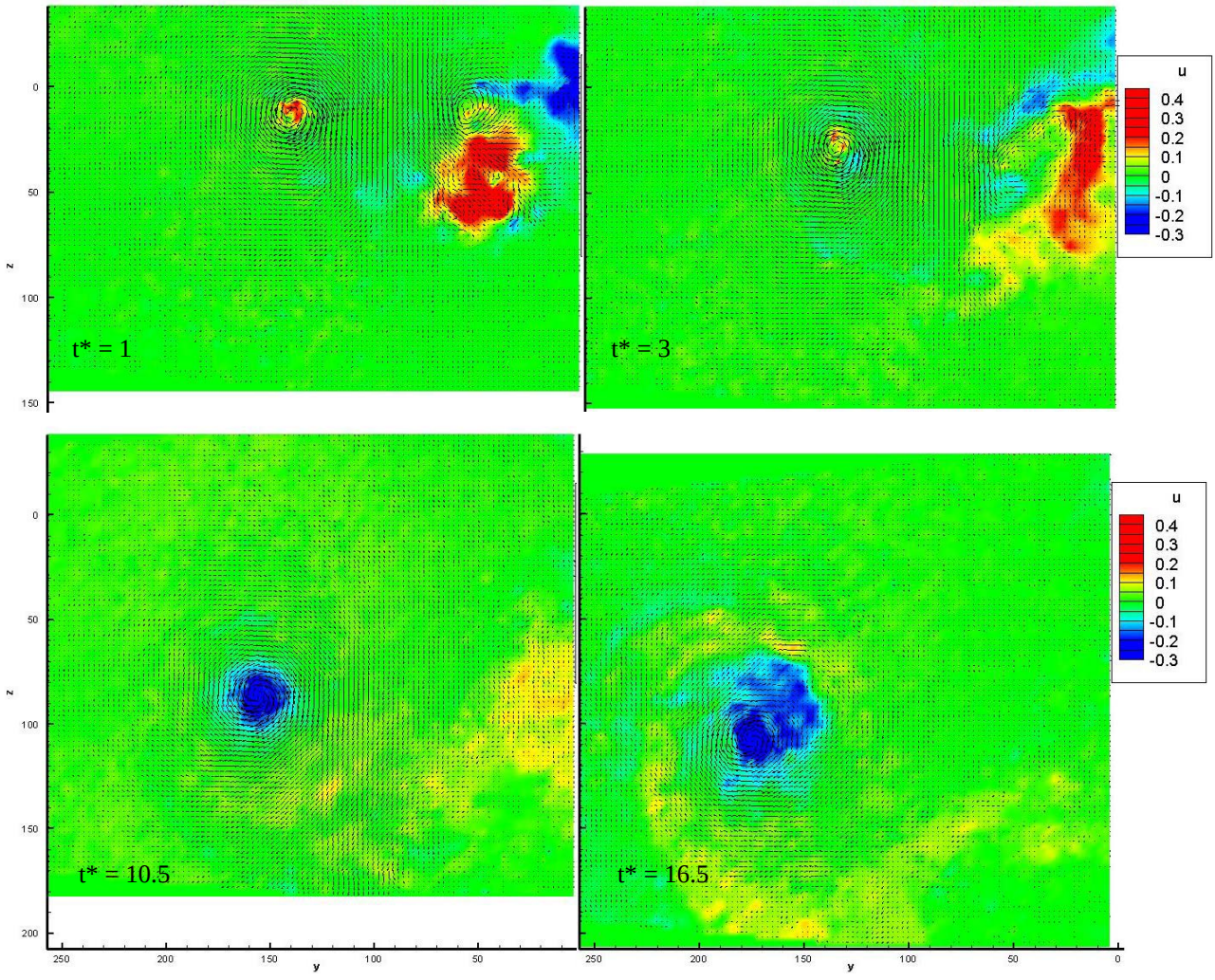

Figure 9: Flow velocity distributions of configuration III (4-vortex system, Γ_1/Γ_0 = -0.48, b_1/b_0 = 0.4) with jets with *R* = 0.74.

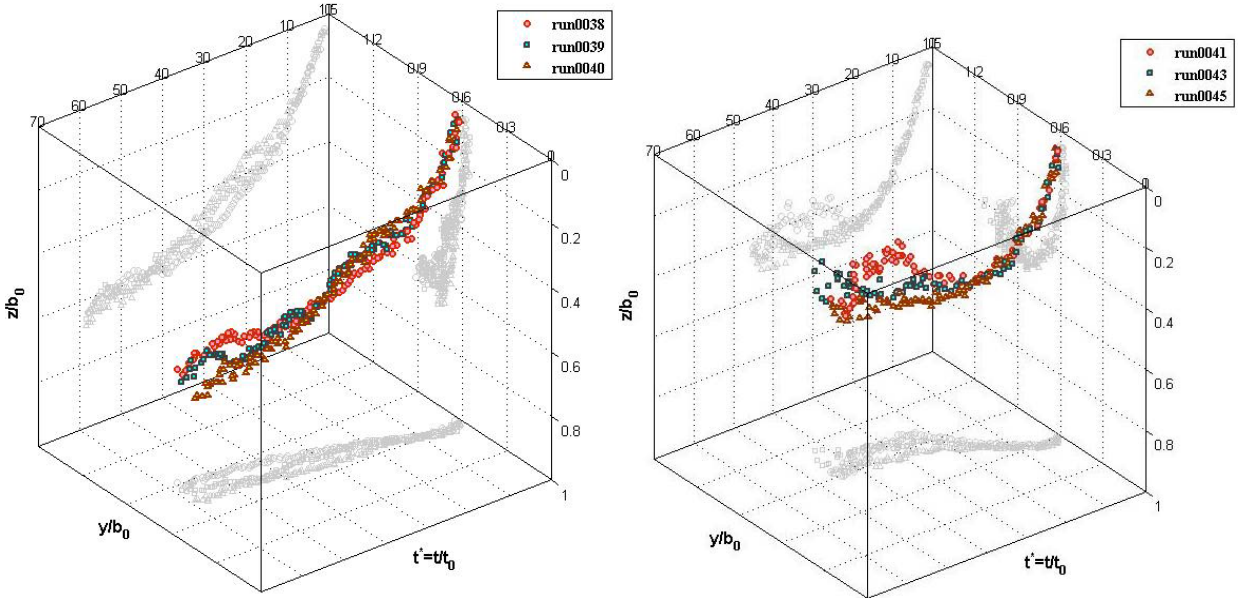

Figure 10: Tip vortex trajectories of 4-vortex systems of configuration II (left) and configuration III (right) as a function of the jet strength; no blowing jet (Runs 0038 and 0041), with water jets with R = 0.2 (Runs 0039 and 0043) and with R = 0.74 (Runs 0040 and 0045).

4. CONCLUSIONS

To investigate the effects of jets on wake vortices, Stereo-PIV measurements were performed in a towing tank using a wing model to which two jet engines separated by 0.4 wings spans b_0 are attached. Considered were two cases of counter-rotating 4-vortex systems with circulation ratio Γ_1/Γ_0 = -0.48 and span ratio b_1/b_0 = 0.4 and Γ_1/Γ_0 = -0.38, b_1/b_0 = 0.3. For comparison the corresponding 2-vortex system is also considered. Two different jet strengths were used, with values of the parameter R (ratio between jet thrust and tip vortex strength) of 0.2 and 0.74.

The influence of the jets on the 2-vortex configuration was found to be negligible. Only the descent rate of the vortices is slightly higher with increasing jet speeds, which results from the positive inclination angle of the jets of 4°.

For the case of the 4-vortex system the inner vortices are located above the jets. The degree of jet-induced disturbances of the inner vortices depends on the R parameter and circulation ratio. The inner vortex of Γ_1/Γ_0 = -0.48 is not disturbed for the weaker jet of R = 0.2. Slightly disturbed are the inner vortices for Γ_1/Γ_0 = -0.48 and R = 0.74 as well as for Γ_1/Γ_0 = -0.38 and R = 0.2. The inner vortex is destroyed by the jet flow for Γ_1/Γ_0 = -0.38 and R = 0.74. However, in all cases the vortex trajectories are not strongly influenced by the jet. On the other hand the inner vortices distribute the fluid of the jets. For the vortex system of b_1/b_0 = 0.4; i.e. with an inner vortex located exactly above the jet, the inner vortex distributes the jet fluid in a counter-clockwise direction, which reduces the downward motion of the jet. For b_1/b_0 = 0.3 the jet is located between both vortices and, therefore, the jet fluid is pushed downward. The location of the inner vortices with respect to the jets affects the jet fluid entrainment by the tip vortices.

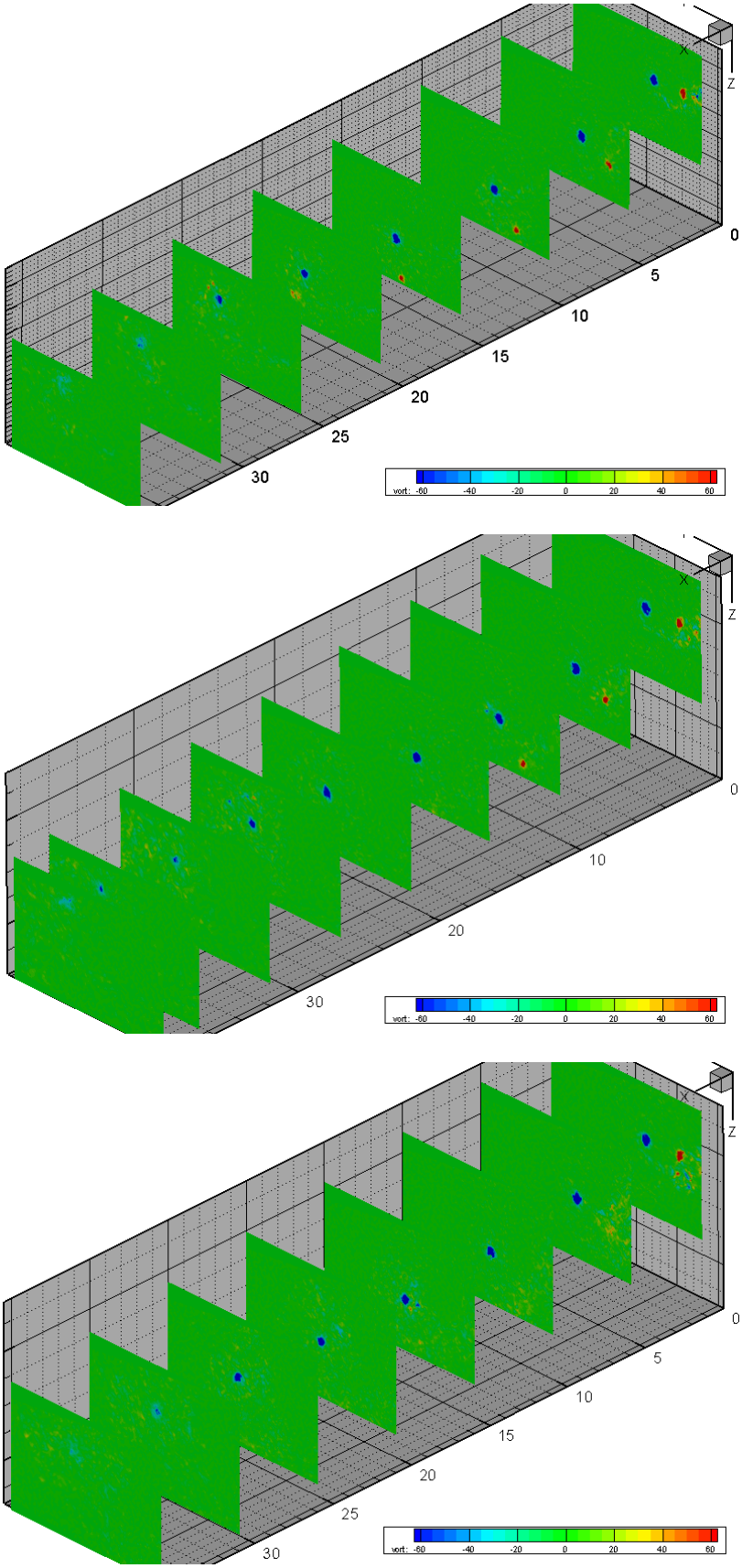

Figure 11: Spatial-temporal vorticity distributions of configuration III for no blowing jets (top) and blowing jets with R = 0.2 (mid) and R = 0.74 (bottom).

The occurrence of the desired interaction between inner tail wing vortex and outer tip wing vortex could be seen for all jet settings and Γ_1/Γ_0 = -0.48, although the inner vortex is located directly above the jet. For the lower circulation ratio of Γ_1/Γ_0 = -0.38 the inner vortex is too weak and changes in the tip vortex characteristics are not significant enough. Lower circulation ratios are desirable for applications to real aircraft. Then, the location of the vortex generators has to be chosen carefully in order to influence the tip vortices efficiently.

REFERENCES

[1] F. Bao, H. Vollmers, H. Mattner. Experimental study on controlling wake vortex in water towing tank. Proc. of *ICIASF'03*, August 25-29, Göttingen, Germany, 2003.

[2] R.L. Bristol, J.M. Ortega, P.S. Marcus, O. Savas. On cooperative instabilities of parallel vortex pairs. *J. Fluid Mech.* 517:331–358, 2004.

[3] C.F.v. Carmer, R. Konrath, A. Schröder, J.-C. Monnier. Identification of vortex pairs in aircraft wakes from sectional velocity data, *Exp. Fluids* 44: 367-380, 2008.

[4] C.F.v. Carmer, A. Heider, A. Schröder, R. Konrath, J. Agocs, A. Gilliot, J.C. Monnier. Evaluation of large-scale wing vortex wakes from multi-camera PIV measurements in free-flight laboratory. In: Schröder A, Willert CE (eds) Particle Image Velocimetry: New Developments and Recent Applications, *Topics Appl. Physics,* vol. 112, Springer, Berlin, pp. 379–396., 2007.

[5] C.F.v. Carmer, R. Konrath. Influence of Reynolds number on generation and decay of aircraft wakes: experimental investigation using generic models, F13 and F13X. Tech. Rep. *DLR-IB 224-2006 A 29*, German Aerospace Center (DLR), 2006.

[6] J.D. Crouch. Airplane trailing vortices and their control. *C. R. Phys.* 6(4–5):487–499, 2005.

[7] J.D. Crouch. Instability and transient growth for two trailing vortex pairs. *J. Fluid Mech.* 350:311–330, 1997.

[8] T. Gerz, F. Holzäpfel, D. Darracq. Commercial aircraft wake vortices. *Prog. Aerosp. Sci.* 38(3):181–208, 2002.

[9] T. Gerz, F. Holzäpfel, W. Bryant, F. Köpp, M. Frech, A. Tafferner, G. Winckelmans. Research towards a wake-vortex advisory system for optimal aircraft spacing. *C. R. Phys.* 6(4–5):501–523, 2005.

[10] L. Jacquin, D. Fabre, D. Sipp, E. Coustols. Unsteadiness, instability and turbulence in trailing vortices. *C. R. Phys.* 6(4–5):399–414, 2005.

[11] L. Jacquin, D. Fabre, D. Sipp, V. Theofilis, H. Vollmers. Instability and unsteadiness of aircraft wake vortices. *Aerosp. Sci. Technol.* 7(8):577–593, 2003.

[12] P. Margaris, D. Marles, I. Gursul. Experiments on jet/vortex interaction. *Exp. Fluids* 44: 261-278, 2008.

[13] J.M. Ortega, R.L. Bristol, O. Savas. Experimental study of the instability of unequal strength counter rotating vortex pairs. *J. Fluid Mech.* 474:35–84, 2003.

[14] S.C. Rennich, S. K. Lele. Method for accelerating the destruction of aircraft wake vortices. *J. Aircraft* 36(2):398–404, 1999.

[15] P.R. Spalart. Airplane trailing vortices. *Annual Rev. Fluid Mech.* 30(1):107–138, 1998.

[16] G. Winckelmans, R. Cocle, L. Dufresne, R.Capart. Vortex methods and their application to trailing wake vortex simulations. *C. R. Phys.* 6(4–5):467–486, 2005.

GROUND-BASED AND AIR-BORNE LIDAR FOR WAKE VORTEX DETECTION AND CHARACTERISATION

A. Wiegele, S. Rahm, I. Smalikho
Institut für Physik der Atmosphäre
Deutsches Zentrum für Luft- und Raumfahrt (DLR),
Oberpfaffenhofen, D-82234 Wessling, Germany

OVERVIEW

In the last two years several ground based and airborne wake vortex campaigns have been performed with the DLR coherent Doppler Lidar. The objectives of those campaigns were (i) measurements for comparison with the wake vortex prediction and monitoring system WSVBS, (ii) the measurement and description of wakes generated by the new Airbus A380 aircraft and a reference aircraft for the ICAO aircraft separation, and (iii) the observation of the influence of different aircraft configurations on the vortex life time in the project AWIATOR.

1. INTRODUCTION

As a consequence of lift, aircraft produce a downdraft beneath the wings air. Because of the shear between the subsiding and the unaffected air wake vortices are rolled up. The behaviour of that wake vortices is a major issue in aeronautical research. Besides other topics in this context (contrails, fuel consumption), wake vortices are a matter of safety and risk management because following aircraft may be endangered.

Trailing wake vortices can be measured by Doppler radar [1], continuous wave (CW) Lidar [2] and coherent Doppler lidar. To measure with coherent Doppler lidar is rather new [3, 4, 5], but the method has been proven to be successful in a number of studies [6, 7, 8].

This paper gives a brief overview about the coherent Doppler lidar instrument that is used by DLR, the measurement technique, some campaigns as examples, and correlated results.

2. MEASUREMENT REQUIREMENTS AND INFLUENCE OF METEROLOGIC CONDITIONS

In the atmospheric boundary layer the measurements can be performed with a ground based lidar. In the typical configuration, the lidar performs an elevation scan with the line of sight (LOS) perpendicular to the vortex axis (Fig. 1, left) [9]. A low scanning speed of 2° or less per second is sufficient because the vortex is moving relatively slow in the lidar coordinate system. The advantage of this setup is also a generally high aerosol load and humidity in the atmospheric boundary layer, leading to a high backscatter coefficient and high quality vortex measurements. The disadvantage however is the property of the boundary layer itself. The atmosphere near the ground is either layered at calm wind conditions and low turbulence or it is well mixed and very turbulent. Both atmospheric conditions have a significant influence on the behavior of wake vortices. In addition, the topology and surface roughness have an impact that is difficult to predict if a vortex is generated in proximity to the surface.

In the free atmosphere the conditions are generally more homogeneous, compared to the boundary layer, and close to neutral stratification. However, the main drawback here is mostly the lack of aerosol particles resulting in a pretty poor signal to noise ratio mak-

ing good lidar measurements impossible. This restriction can be overcome by (i) using smoke generators at the generating aircraft or by flying (ii) under contrail generating conditions or (iii) in a hazy atmospheric layer. Here limiting factors are either the finite time of smoke generation or the prediction of these rare conditions. For wake vortex observations in the free troposphere, the Doppler Lidar is installed in the DLR research aircraft Falcon F20 in a downward looking configuration (Figure 1b) [8]. Then, the Falcon is flying 600 to 1000 m (1800 to 3000 ft) higher than the generating aircraft and along the wake track. In this case the geometry for the vortex measurement is better suited because both vortices are separated according to the LOS of the lidar. The scanning speed needs to be higher due to the virtually high relative movement of the vortex in the lidar coordinate system.

3. LIDAR SYSTEM AND MEASUREMENT GEOMETRY

The DLR lidar system consists of a wind tracer transceiver from Lockheed Martin Coherent Technologies. It is operating at approximately 2.02 micron wavelength with 1.5 mJ energy and a repetition rate of 500 Hz.

The DLR custom build scanner in front of the transceiver consists of two Silicon wedges that can be turned independently by two stepper motors. Thus it is possible to address each LOS direction inside a cone with +/- 30° opening angle. Such a scanner is compact and - compared to a mirror scanner - insensitive to vibration.

The data system follows the strategy of early digitizing, which means the heterodyning signal is directly digitized together with a timestamp. All other housekeeping parameters are also stored in their original data format together with a timestamp in a separate computer. This computer also controls the scanner. This strategy offers maximal flexibility during the offline data processing especially for the correction of time and frequency jitter of the transmitted pulse, or the suppression of pulses where the seeding was not optimal. The correction of any offsets or systematic errors of housekeeping parameters is also easily possible. Thus at wake vortex measurements with a maximum range of 2 km the data rate is roughly 250 MByte per minute that can be handled by a regular commercial computer with SCSI hard disk. During the measurements preliminary results with reduced resolution (called quick-looks, e. g. see Fig. 4) can be investigated.

3.1. Ground based measurements

For ground based wake vortex measurements, the lidar is ideally placed in 1000 m distance normal to the flight path of the wake vortex generating aircraft. This distance is a trade-off between high resolution and good signal to noise ratio requiring a close range and high volume covered at a higher range. The elevation angles are adapted to the altitude of the aircraft and range from 0° to 50°. Therefore, wake measurements Out-Of-Ground-Effect (OGE) as well as In-Ground-Effect (IGE) are possible.

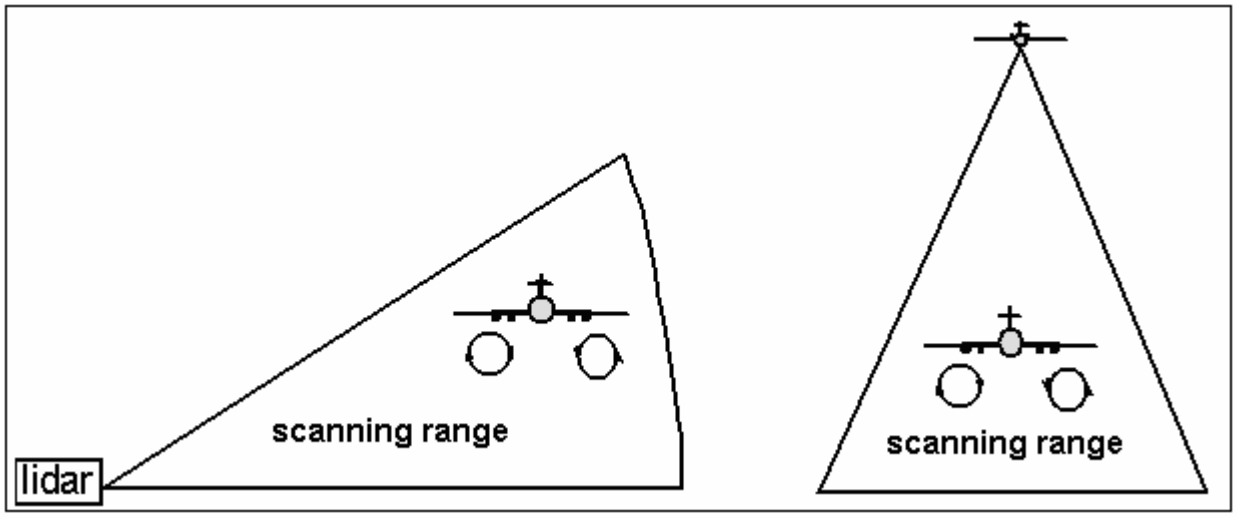

FIG 1. Scan pattern for ground based (left) and airborne (right) wake vortex measurements.

3.2. Airborne measurements

As mentioned above the Falcon F20 aircraft is used as platform for airborne wake vortex measurements in a downward looking configuration [10] and is flying 600 to 1000 m above the flight track of the wake generating aircraft. This distance turns out to be the optimal compromise between resolution and width of the scanned cross section. The higher flight level also relaxes safety issues for the operating of several planes close together. The accuracy of navigation is critical. At a 1000 m range the measuring aircraft (Falcon F20) has to be right above the vortex pair with an accuracy of better than +/-400 m laterally. These high requirements for aircraft navigation are difficult to meet due to the advection of the vortices by crosswind, the low visibility of an older vortex (even if seeded by smoke or marked by contrail) and the aircraft velocity of 100 - 200 m/s.

In case the vortex of the generating aircraft is seeded by smoke to improve the SNR, the time of the smoke generator is limited to a total of 10 to 20 minutes. Depending on the velocity of the generating aircraft, the required vortex ages, the velocity range of the chasing aircraft with the lidar, and the clearance of the flight control several approaches are possible to optimize measurements during the limited time of smoke generation. Where possible the generating aircraft is flying along the local wind direction to minimize the drifting of the vortex beside the trajectory. The Falcon can fly either the opposite direction if the measurements need to cover a wide range of vortex ages, or it can fly in the same direction with a different speed for a higher density of measurements per vortex age.

4. DATA PROCESSING

Data processing is performed offline in a four stage processing procedure. For high quality results of the circulation strength the homogeneity of the backscatter coefficient has to be monitored closely. Therefore, automated handling is not advisable. The final products of the processing are the position of the centre of each vortex and its circulation strength.

The measured signal consists of the monitor signal and the backscatter signal for each single shot. The monitor signal provides the exact time and frequency of the outgoing pulse that is necessary to analyze the backscatter signal correctly. The four stages of

processing consist of the estimation of (i) the Doppler spectra (spectra of the power of coherently detected backscatter signals), (ii) the radial velocity spectra and velocity envelopes, (iii) both vortex core positions, and (iv) both vortex circulation values [9].

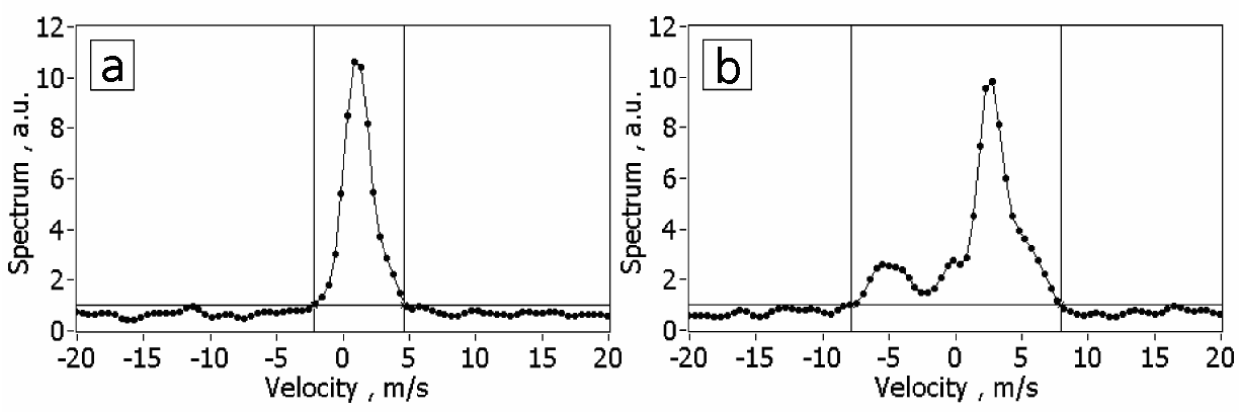

FIG 2. Examples for spectra of ambient turbulence (a) and with the spectral contribution of a wake vortex (b). This contribution here originates from the part of a vortex that rotates towards the instrument, because negative velocities point towards the lidar. Here arbitrary units (a.u.) denote a relative frequency of occurrence of the corresponding velocities.

At step (ii) the spectra obtained in step (i) are analyzed to achieve both, the radial background velocity and the contributions that are caused by wake vortices (see Fig. 2). The latter become apparent by side peaks or broadening of the mean peaks that have to be above a threshold to avoid noise peaks. Here, the mean peaks are caused by the spectrum of background velocities and the threshold is chosen corresponding to the noise value. The horizontal bars in Fig. 2 denote the threshold while the vertical bars indicate the respective positive and negative envelopes of velocities.

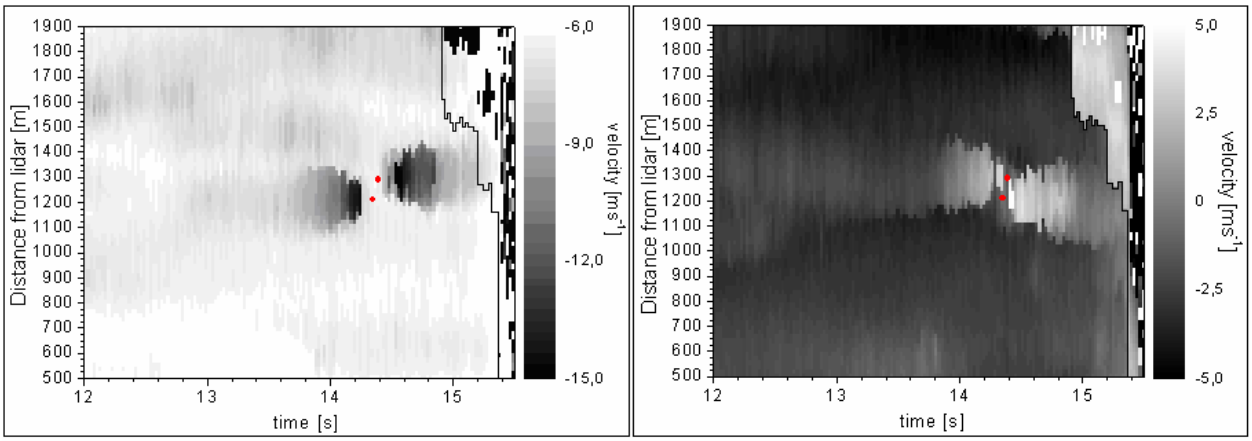

FIG 3. Positive velocity envelopes (right) and negative velocity envelopes (left) obtained from spectral analysis plotted versus distance to the lidar and time. The red dots denote the positions of both vortex cores between the maxima of positive envelopes velocity and the minima of negative velocity envelopes.

In the next step the vortex core position can be derived from the envelopes (see Fig. 3).The values of the positive and negative envelope velocities are plotted versus distance to the lidar and time. The scan has been performed like it is shown in Fig. 1 (left)

from top to bottom. The area to the right of the black line is partly influenced by hard target measurements close to the surface or the surface itself.

Both figures show two velocity minima or maxima, respectively. Both pairs of minimum and maximum velocity are caused by one of both vortices. In between each pair the position of the vortex cores can be found, in Fig. 3 these are marked with red dots.

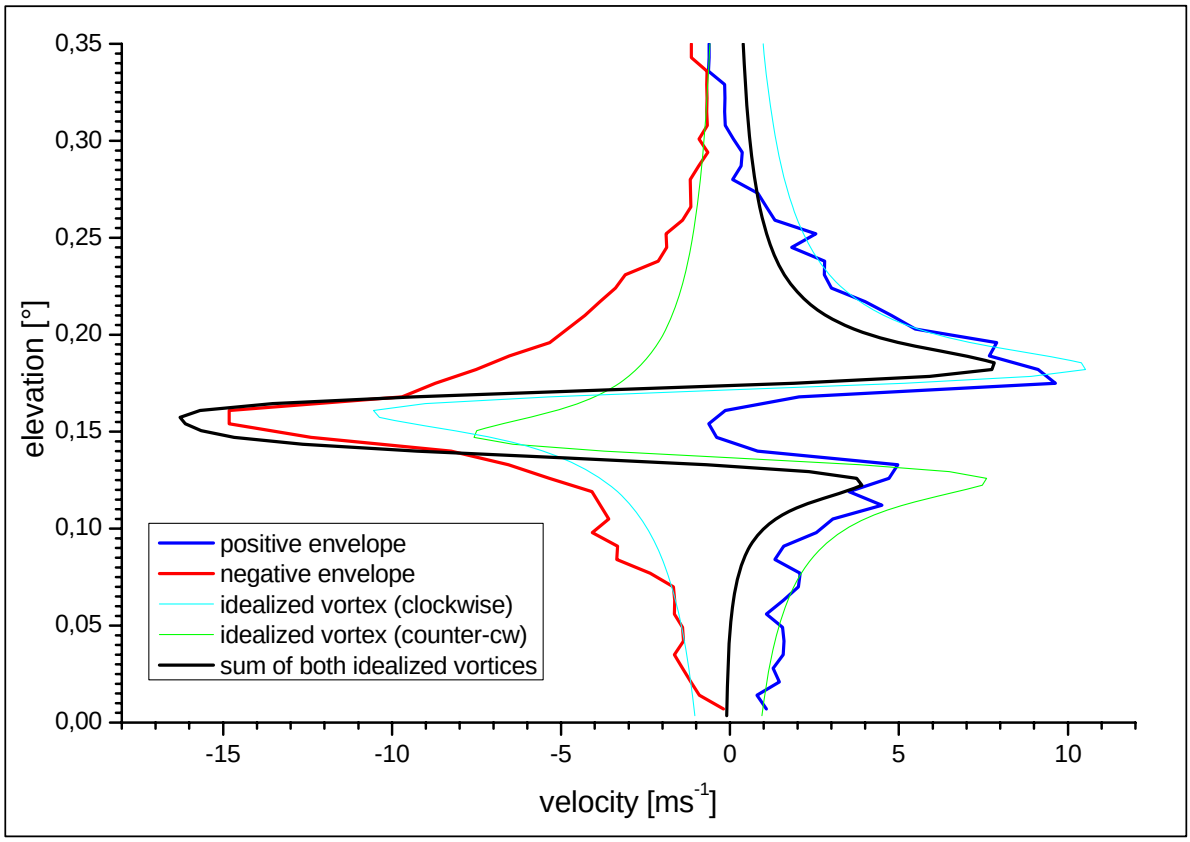

FIG 4. Velocities induced by a vortex pair. Shown are positive and negative envelope velocities at vortex core distance versus altitude and velocities of idealized synthetic vortices to illustrate the contribution of both vortices to the measured envelopes.

The vicinity of the vortex core position can be used to find the circulation value (velocity times the vortex radius integrated between 5 m and 15 m from vortex centre). The envelope velocities at vortex core distance above and below the core (see Fig. 4) are used for the integration where the contribution of the background velocities mutually are cancelled out between both sides of the vortex [11, 12]. In Fig. 4 the discrepancy between the positive envelope and the idealized vortex at lowest levels is caused by the contribution of the other vortex.

5. WAKE VORTEX MONITORING

At Frankfurt Airport (Germany) a high number of measurements have been performed with the focus on wake vortex displacement in the context of WSVBS [13, 14, 15] (*Wir-*

belschleppen-Vorhersage- und -Beobachtungssystem, German for Wake Vortex Prediction and Monitoring System). Therefore, wake vortex transport has been tracked for the monitoring of the predictions of a probabilistic vortex model [16] that are used for dynamical adjustment of aircraft separations.

These measurements between December 2006 and February 2007 covered a variety of meteorological and ambient conditions with a real traffic mixture. The lidar site was situated laterally to the glide slope of the runways 25R and 25L and close to the touch-down zone (see Fig. 6). Three different azimuth directions have been chosen to cover the last nautical mile before the touch-down zone. This corresponds to the most critical area because there wake vortices can not descend significantly below the flight corridor. Consequentially, most encounters occur at heights below 100m [17, 18]. The elevation angles have been reduced to a range from 0° to 6° (up to 8° for the outermost azimuth direction) to obtain a high temporal resolution for the landing aircraft. Approximately vortices of 1100 heavy aircraft have been monitored.

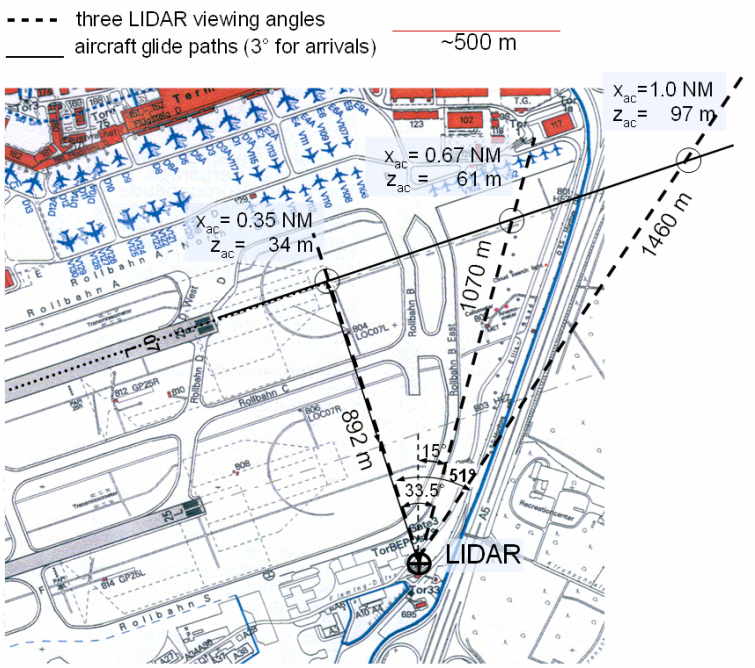

FIG 5. Measurement scheme at Frankfurt airport, Germany. x_{ac}, z_{ac} denote the distance to touch-down zone and the height of landing aircraft in the three vertical scan planes of the LIDAR (dashed lines); The local operation center of DWD (German weather service) and the meteorological profiler were situated between both extended runway centrelines. Map reprinted by courtesy of Fraport AG.

Figure 6 shows three results of vortex core position displacements obtained during this campaign as an example. Each pair of vortices was generated by the same aircraft at different distances to the touch-down zone corresponding to different initial altitudes. It is obvious, that the right vortices first subsided and then rebounded while the left ones remained in lower altitudes. At the time of measurement a weak crosswind to the right side has been present, which is responsible for the asymmetric vortex rebound.

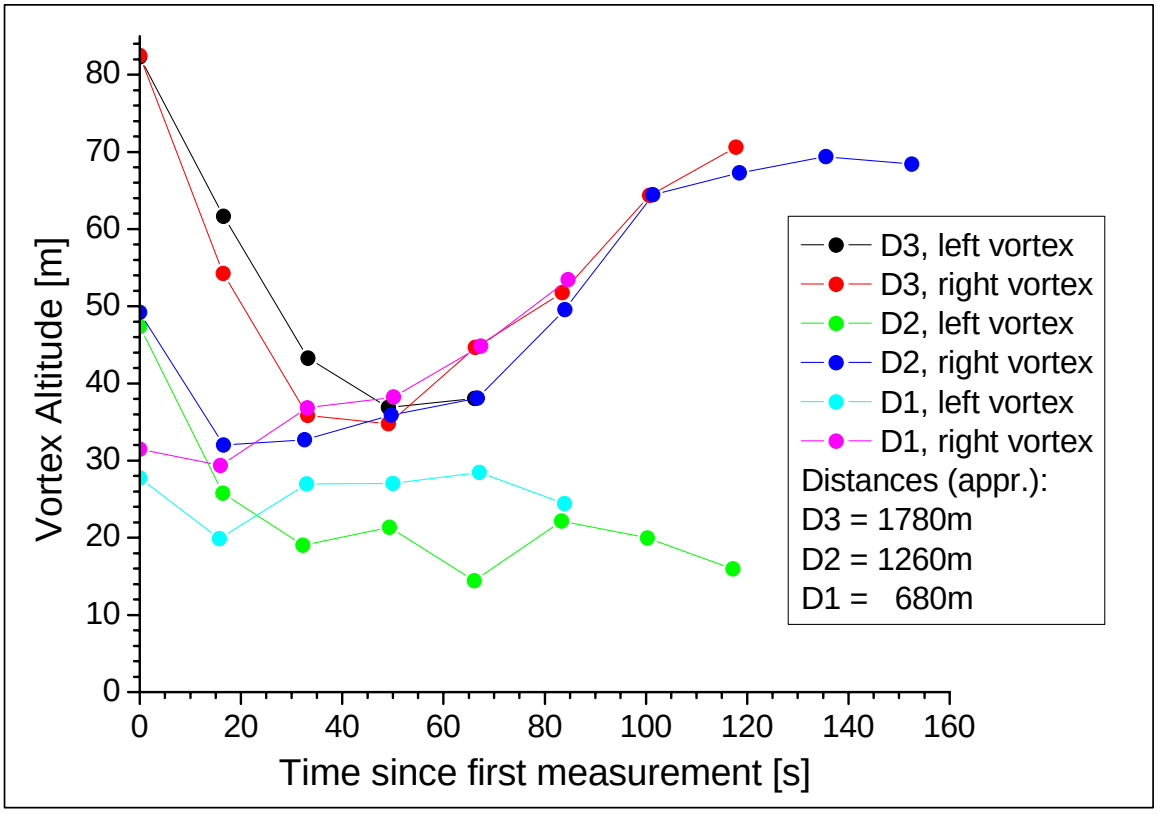

FIG 6. Altitude of vortex cores over time at different distances (D1-D3) to the touch-down zone for a single aircraft on Jan 30th, 2007, Frankfurt, Germany.

6. EFFECTS OF AIRCRAFT CONFIGURATIONS

Another interesting topic is whether static or dynamic settings of flaps can have an influence on the vortex strength or lifetime. One idea is that instabilities are introduced in the wake vortex that cause early rapid decay [19]. Experiments with a model in a towing tank are limited by Re number effects and the size of the tank. Again, the Doppler lidar is currently the only instrument that can probe high-accuracy wake vortex characteristics in the atmosphere generated by a real aircraft.

For such investigations, the influence of the atmosphere on the wake vortices has to be as small as possible. Consequently, those measurements took place above the atmospheric boundary layer. An A340-300 from Airbus with smoke generators mounted below both wings was used as vortex generator. It was flying above the atmospheric boundary layer at approximately 3000 m altitude where the temperature is still high enough to allow the operation of smoke generators. The lidar was installed on the DLR Falcon F20 looking downward. Four sets of flights were performed in total on two days.

Airborne wake vortex measurements basically imply that the scanning plane is not perpendicular to the vortex axes because of the movement of the lidar flying with the aircraft, i.e. the different scans are cutting the vortices in a zigzag pattern.

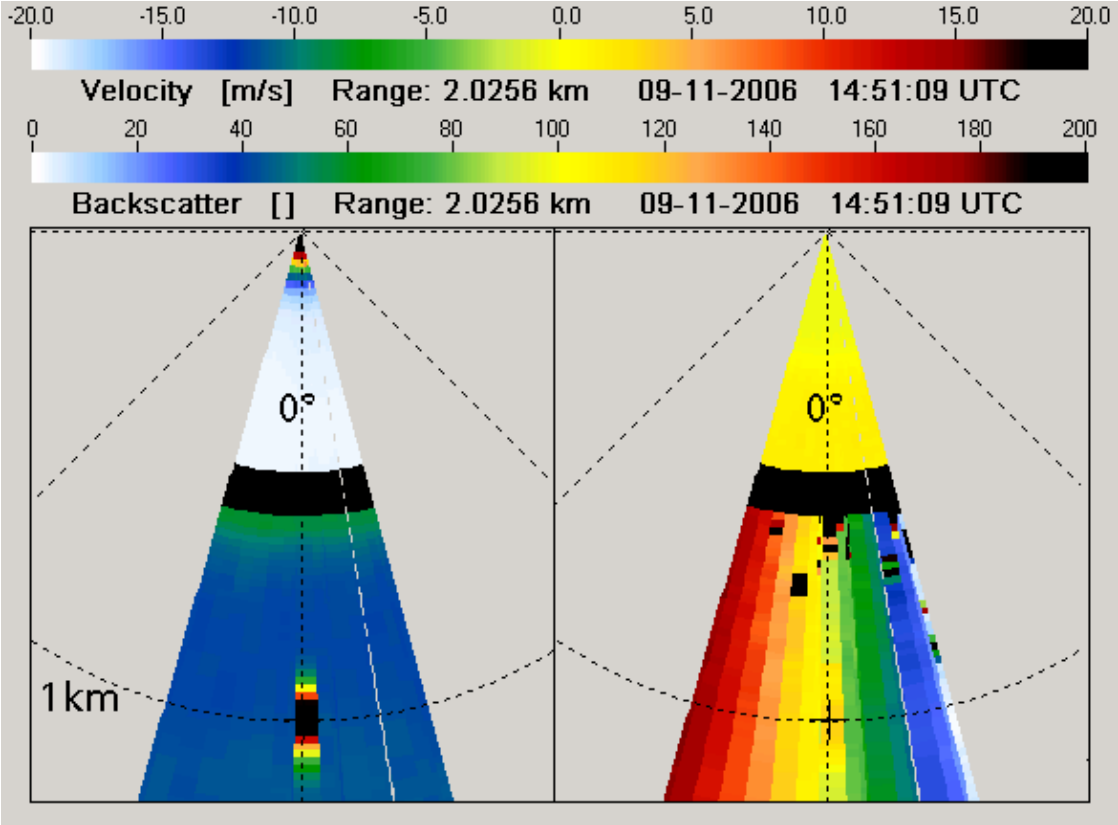

FIG 7. Quick-looks (preliminary figures obtained during the measurements) of backscatter (left) and velocity (right) for a single scan during the AWIATOR campaign, see corresponding colour codes above.

In order to measure nonetheless perpendicular to the vortex axis the double wedge scanner control has been modified such that the LOS points forward at the beginning of a scan and backward at the end. This strategy compensates the the aircraft flight speed such that the laser beam cuts the wake vortices effectively perpendicular to the flight direction. This mode has been operated during the AWIATOR measurements for the first time. A drawback of this method can be seen in Figure 7. The backscatter (left) shows the vortex clearly, because of its seeding with smoke, while the vortex signature inside the rainbow-like velocity plot (right) is hidden because of the alternating contributions of the flight speed to the measured velocities.

Three different wing configurations have been tested against one standard setting (baseline). At those flights the A340 and the Falcon with the lidar were flying in opposite direction. At a flight level below the A340 a Fairchild Metro II from NLR, equipped with video cameras, was flying in the same direction and straight below the Falcon aircraft. This way a correlation of the vortex parameters obtained from the lidar measurement with the optical appearance of the smoke seeded wake vortex pair is possible.

The video of the vortices seeded by smoke taken from NLR have been “stitched” to an image shown in Fig. 8 (Courtesy of A. de Bruin). Clearly visible are the different stages of vortex deformation, linking, and ring formation. The effluence of smoke indicates vortex bursting phenomena occurring at various locations along the vortices, corresponding to different vortex ages.

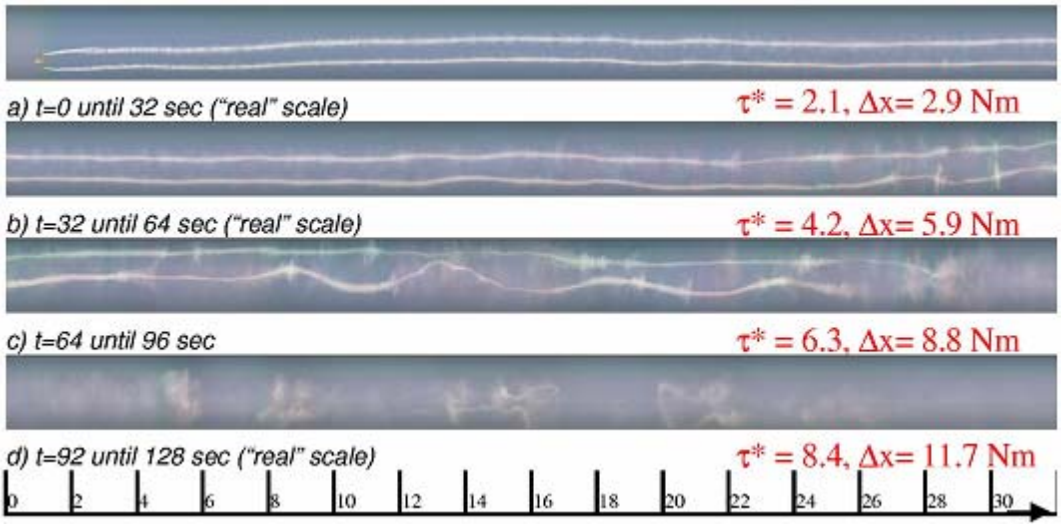

FIG 8. “Stitched”- video image of smoke traces taken from NLR aircraft flying below the Airbus. Timescales are given in seconds and normalised age of vortex τ^*.

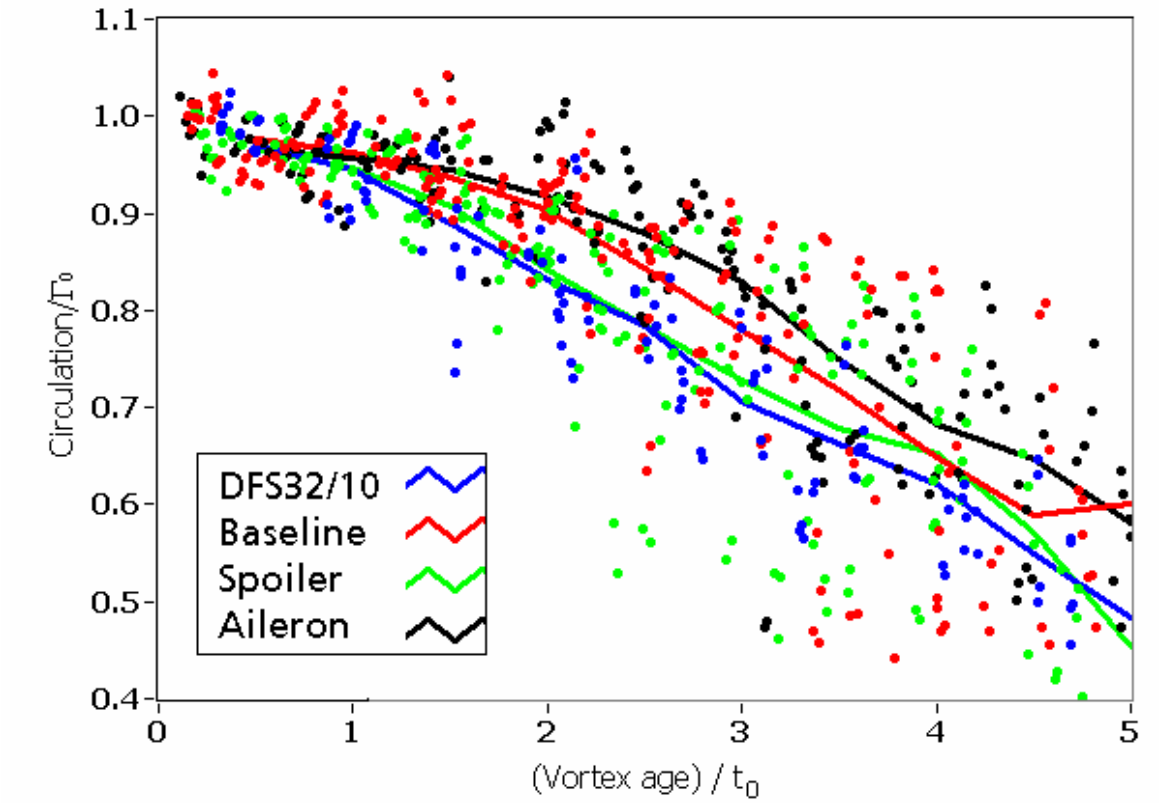

FIG 9. Normalized circulation against vortex age for four different wing configurations. Red colours denote the baseline configuration.

Figure 9 shows the evolution of the circulation strength as a function of vortex age for the four different configurations. Shown are the single data points as well as mean curves derived from all eight single measurements for each configuration. Detailed information about the different configurations can be found in reference [19]. Consideration of the respective meteorological conditions allows to adapt the circulation evolutions to nominal identical atmospheric conditions which in turn enables to identify the most promising aircraft configuration [20].

7. AIRBUS A380 VORTEX MEASUREMENTS

The DLR Doppler lidar system has been used to assess the wake vortices of the new Airbus A380. In that context DLR acted as a subcontractor for Airbus.

The measurements for the A380 started in April 2005 at the airport Blagnac during the normal flight test program with only a few landings a week. This set of measurements confirmed the value of Doppler lidar measurements for the characterization of wake vortices. In consequence, a regular measurement series started with measurements in different altitudes above ground in order to study the wake vortices IGE as well as OGE. Sodar and RASS wind profiler were used to probe the atmosphere in terms of wind, temperature, and eddy dissipation rate (EDR). To get a comparison with existing aircraft, most of the measurements were done alternatingly with passes of other heavy aircraft in order to obtain comparable results under similar atmospheric conditions concerning turbulence, temperature stratification, and cross wind. Those measurements were observed by a member of Eurocontrol and/or the FAA.

The behaviour of a wake vortex pair generated by an aircraft at cruising altitude is also a point of consideration. Because smoke generators do not work reliably at cruising altitudes, meteorological conditions with persistent contrails had to be searched. Therefore, airborne measurements took place, where the A380 and the heavy reference aircraft were flying during appropriate conditions at cruising altitude in parallel so that the wake vortices could be measured simultaneously and the results could be compared against each other. The vortices of both generating aircraft were measured starting directly behind the aircraft up to a distance of 25 nm, which corresponds to a vortex age of roughly 4 minutes. Some additional ground based measurements have been performed with the focus on measurements in a very calm atmosphere.

The result of these measurements is reflected in the present update of the ICAO guidance regarding A380 wake turbulence separations [21].

8. CONCLUSIONS

Doppler lidar is the leading instrument for measuring wake vortices of real aircraft because of its long range and high accuracy. The manuscript describes capabilities of the DLR Doppler lidar focusing on the possibility of fast scanning at different ranges and the usage on different platforms (airborne and ground based) and different measuring geometries.

In particular it demonstrates that:

- The DLR Doppler lidar is an instrument that is able to characterise wake vortices from ground proximity up to the free atmosphere.
- Wake vortex transport can be monitored within the critical height range of up to 100m of the final approach to an airport. Thus, lidar is well suited to monitor wake

vortex predictions of a wake vortex advisory system that aims to increase the capacity of congested airports.

- Lidar is capable to estimate the effects of modifications at the aircraft wings provided that the impact of ambient conditions on vortex decay can be neglected or considered appropriately.
- Very detailed investigations of wake vortices of single aircraft (A380) are possible with DLR Doppler lidar. Air traffic control can benefit due to the categorization of typical circulation strengths for different aircraft types.

In future it is intended to automate the lidar and the processing of the wake vortex algorithm to receive the locations and circulation strengths of wake vortices close to real time.

ACKNOWLEDGEMENTS

The measurements in Frankfurt 2006/2007 were funded by the DLR project Wirbelschleppe. The wake vortex measurements on the Airbus A380 were performed under Airbus contract. The A340-300 measurements were funded by the European Union AWIATOR program contract no. G4RD.CD200200836.

REFERENCES

[1] Marshall, R.E., and Myers, T.J., 1996: Wingtip generated wake vortices as radar target, *Aerospace and Electronic Systems Magazine*, *IEEE*, Volume 11, Issue 12, Page(s):27 – 30, doi10.1109/62.544796.

[2] Köpp, F., Schwiesow, R.L., and Werner, C., 1984: Remote Measurements of Boundary-Layer Wind Profiles Using a CW Doppler Lidar. J. Appl. Meteor., 23, 148–154.

[3] Hannon, S. M., and Thomson, J. A., 1994: Aircraft Wake Vortex Detection and Measurement with Pulsed Solid-State Coherent Laser Radar, *Journal of Modern Optics,* Vol. 41, pp. 2175-2196.

[4] Köpp, F., 1994: Doppler Lidar Investigation of Wake Vortex Transport Between Closely Spaced Runways, *AIAA Journal,* Vol. 32. , pp. 805-810.

[5] Constant, G., Foord, R., Forrester, P. A., and Vaughan, J. M., 1994: Coherent Laser Radar and the Problem of Aircraft Wake Vortices, *Journal of Modern Optics,* Vol. 41, 2153-2173.

[6] Harris, M., Vaughan, J. M., Huenecke, K., and Huenecke, C., 2000: Aircraft Wake Vortices: a Comparison of Wind-Tunnel Data with Field-Trial Measurements by Laser Radar, *Aerospace Science and Technology,* Vol. 4, pp. 363-370.

[7] Harris, M., Young, R. I., Köpp, F., Dolfi, A., and Cariou, J.-P., 2002: Wake Vortex Detection and Monitoring, *Aerospace Science and Technology,* Vol. 6, pp. 325-331.

[8] Köpp, F., Smalikho, I., Rahm, S., Dolfi, A., Cariou, J.-P., Harris, M., Young, R. I., Weekes, K., and Gordon, N., 2003: Characterisation of Aircraft Wake Vortices by Multiple-Lidar Triangulation, *AIAA Journal,* Vol. 41, pp. 1081-1088.

[9] Köpp, F., 1999: Wake-Vortex Characteristics of Military-Type Aircraft Measured at Airport Oberpfaffenhofen Using the DLR Laser Doppler Anemometer, *Aerospace Science and Technology,* Vol. 3, pp. 191-199. *Oceanic Technology*, Vol. 21, 2004, pp 194-206.

[10] Rahm, S., Smalikho, I., Köpp, F., 2007: Characterization of Aircraft Wake Vortices by Airborne Coherent Doppler Lidar, *Journal of Aircraft,* Vol. 44 (be published soon).

[11] Köpp, F., Rahm, S., and Smalikho, I., 2004: Characterization of Aircraft Wake Vortices by 2-μm Pulsed Doppler Lidar, *Journal of Atmospheric and Oceanic Technology*, Vol. 21, pp 194-206.
[12] Holzäpfel, F., Gerz, T., Köpp, F., Stumpf, E., Harris, M., Young, R. I., and Dolfi, A., 2003: Strategies for Circulation Evaluation of Aircraft Wake Vortices Measured by Lidar, *Journal of Atmospheric and Oceanic Technology,* Vol. 20, pp. 1183-1195.
[13] Gerz T., Holzäpfel F., Bryant W., Köpp F., Frech M., Tafferner A. and Winckelmans G., 2005: Research towards a wake-vortex advisory system for optimal aircraft spacing, *Comptes Rendus Physique*, Académie des Sciences, Paris, 6, No. 4-5, 501-523.
[14] Holzäpfel, F., Gerz, T., Frech, M., Tafferner, A., Köpp, F., Smalikho, I., Rahm, S., Hahn, K.-U. Schwarz, C., 2007: The Wake Vortex Prediction and Monitoring System WSVBS – Part I: Design, CEAS-2007-Proceedings, Berlin.
[15] Gerz, T. ,Holzäpfel, F., Gerling, W., Scharnweber, A., Frech, M., Wiegele, A., Kober, K., Dengler, K., Rahm, S., 2007: The Wake Vortex Prediction and Monitoring System WSVBS – Part II: Performance and ATC integration at Frankfurt airport, CEAS-2007-Proceedings, Berlin.
[16] Holzäpfel F., 2003: A Probabilistic Two-Phase Wake Vortex Decay and Transport Model, Journal of Aircraft, Vol. 40, No. 2, pp. 323-331.
[17] Critchley, J., Foot, P., 1991: UK CAA Wake Vortex Database: Analysis of Incidents Reported Between 1982 and 1990, Civil Aviation Authority, CAA Paper 91.
[18] Holzäpfel, F., Steen, M., 2007: Aircraft Wake-Vortex Evaluation in Ground Proximity: Analysis and Parameterization, *AIAA Journal*, Vol. 45, pp. 218-227.
[19] de Bruin, A. C., Schrauf G., 2007: Wake vortex results from the AWIATOR project, CEAS-2007-Proceedings, Berlin.
[20] Leweke, T., Le Dizès, S., 2007: Analysis of F/T-1 and F/T-2 LIDAR measurements and smoke visualisations, AWIATOR Technical Report.
[21] ICAO, 2006: Guidance On A380-800 Wake Vortex Aspects, http://www.icao.int/icao/en/ro/apac/2006/RASMAG6/ip02.pdf

Acoustic Properties of Aircraft Wake Vortices

P. Böhning[1], U. Michel[2] and R. Baumann[3]
[1] Rolls-Royce Deutschland Ltd & Co KG, Dahlewitz, Eschenweg 11,
D-15827 Blankenfelde-Mahlow, Germany
[2] Deutsches Zentrum für Luft- und Raumfahrt (DLR), Institute of Propulsion Technology,
Müller-Breslau-Str. 8, D-10623 Berlin, Germany
[3] Deutsches Zentrum für Luft- und Raumfahrt (DLR), Institut für Physik der Atmosphäre,
Oberpfaffenhofen, D-82234 Wessling, Germany

ABSTRACT

The noise generation by aircraft wake vortices has been studied numerically and experimentally. The numerical study revealed a relation between the circulation Γ, the vortex core size r_c and the frequency f_a of the peak level in the vortex noise spectra, $f_a \approx \Gamma/(2\pi r_c)^2$. The experimental data were obtained in measurements at airports applying phased microphone arrays. It has been revealed that sound sources are closely located to the vortex cores. The focused noise spectra of the wake vortices of all measured aircraft types are dominated by two maxima. The second maximum at f = 100 Hz is clearly caused by wake vortices. The origin of the first at 12 Hz has not been identified. Wake vortices were acoustically detected in 80 percent of the flyovers. Lowest detection rates were observed for the newer aircraft types Airbus 319, 320 and Boeing 737-800. A comparison of the wake trajectories obtained by phased microphone arrays and LIDAR revealed that the detection capability of the latter is superior.

1. INTRODUCTION

Aircraft wake vortices represent a major constraint for the separation of consecutive aircraft en-route and in terminal areas. The current aircraft separation rules for landing and take-off defined by the *International Civil Aviation Organisation (ICAO)* in 1971 [1], already represent an important capacity limiting factor at congested airports. The rules categorize aircraft into four maximum take-off weight classes, *light*, *medium*, *heavy* and a recently introduced class for the Airbus A380. The minimal separation distance depends only on the combination of the weight classes of the leading and following aircraft ignoring the actual wake vortex behaviour which varies between different aircraft types and depends strongly on the actual meteorological conditions as demonstrated in several studies conducted in the recent years [2].

The expected increase in air traffic makes a reduction of the aircraft separation without negative effects on the safety level highly desirable. This in turn demands precise knowledge of the wake vortex structure and its evolution under different meteorological conditions. To gain this knowledge an intense research effort has been undertaken in the *European Union (EU)* and in the *United States (US)* to develop reliable wake vortex prediction methods and detection technologies in recent years. A number of flyover measurement campaigns were conducted in which LIDAR has become the standard technique for measuring the wake vortex parameters in field tests. A complimentary detection technology has attracted researchers' interest after the observation that wake vortices emit a faint noise which varies with the aircraft type generating the vortices. The wake vortex noise is therefore expected to provide additional information about wake vortex characteristics in flyover test.

The *German Aerospace Center (DLR)* proposed the application of a phased microphone array for the investigation of wake vortex noise. In contrast to a single microphone a phased microphone array allows to distinguish between noise originating from the wake vortex, the aircraft and from other sources on the ground. The capability of phased microphone arrays to localize the noise sources of wake vortices was first demonstrated in a test at Berlin's *Airport Schönefeld* in 2000 [3]. In a second test, conducted in Tarbes, France, in 2002, phased microphone arrays were applied to study the wake vortex noise of an Airbus 340 which was flown in different configurations and with different engine settings [4]. Both tests were conducted in the framework of the European research project *C-Wake*.

At the same time, similar activities took place in the *US* as part of a research project. Its objective was the development and evaluation of alternative wake detection technologies such as *phased microphone arrays*, *opto-acoustic microphones*, *Continuous LIDAR* and *Pulsed LIDAR*. These technologies were evaluated in a field test at the *Denver International Airport* organized by the *NASA Langley Research Center* and the *Volpe Center, Department of Transportation (DoT)* in 2003, [5]-[8]. *DLR* participated applying a phased microphone array.

Currently, studies on wake vortex noise concentrate on identifying the dominant noise generating mechanisms in the vortices and on finding a governing relation between aerodynamic wake parameters such as circulation and core size and the spectral and temporal characteristics of the vortex noise using experimental and numerical data.

2. WAKE VORTEX LIFE CYCLE AND SOUND GENERATING MECHANISMS

The life cycle of an aircraft wake vortex consists of a roll-up, diffusion and a rapid decay phase [9]. The roll-up phase comprises the shedding of concentrated and distributed vorticity by the aircraft, an intense vorticity interaction and the final roll up to two strong counter-rotating vortices. This process is finished within $x < 10$ B, where B refers to the aircraft's wing span. The acceleration of vorticity is expected to be the main source of sound in this early state of vortex life.

During the diffusion phase the counter-rotating vortices remain stable and move slowly downwards due to the mutually induced velocity. The generation of noise by wake vortices in this phase surprises as it is well-known that slowly moving potential vortices do not emit any sound. However, there are two potential noise generating mechanisms. First, a spinning Kirchhoff-vortex, having an elliptical core of uniform vorticity does emit a tone at a frequency equal to the double of the vortex rotation frequency. So, it can be expected that any perturbation of a homogeneous vorticity distribution in one of the two rotating vortex cores is a potential source of sound. The noise produced should be in the same frequency range as the rotation frequency of the vortex cores [10]. Second, the likely more important mechanism is the interaction of secondary vorticity structures (SVS) with the two main vortices which are referred to as primary vorticity structures (PVS). This interaction is also believed to be the main decaying mechanism in aircraft wake vortices [11]. SVS are turbulent eddies from the atmospheric turbulence or engine exhaust jets which interact with the swirling mean flow field of the PVS. These eddies are getting stretched and tilted in the mean flow [11],[12] and accelerated as they are getting closer to the cores of the main vortices. Accelerated vorticity is an effective sound source.

The rapid decay phase is predominated by instability effects that cause the wake vortex to rapidly break up. Responsible instability effects must provoke sufficiently large

amplitudes of perturbation. Mechanisms providing only small perturbation amplitudes may provoke local vortex busting. These instabilities are often recognised as sharp whipping noise. Instability mechanisms which provoke displacements of the vortex cores in the range of the vortex spacing cause linking of the two primary vortices and a formation of vortex rings.

3. NUMERICAL STUDY

The generation of sound by the interaction of SVS with PVS was studied on a four-vortex system as shown in **FIG 1**. This configuration may be used as a simplified model for the vortices shed from wing tips and outer flap edges, which quickly merge into a strong outer vortex pair, and the counter-rotating vortices shed from the inner flap edges forming a second, weaker vortex pair. The behaviour of such a system, i.e. weak or strong interaction of the vortex filaments, is described by the Donaldson-Bilanin diagram [13]. It depends on the ratio of the initial circulation of the outer (1) and inner (2) vortex filaments Γ_2/Γ_1 and the ratio of their initial spacing b_2/b_1. The ratio of the initial circulation was set to Γ_2/Γ_1 = -0.3 (Γ_1=1) and of the initial vortex spacing b_2/b_1 = 0.3. The negative sign of the circulation ratio indicates that the outer and inner vortex filaments are counter-rotating. The weaker vortex filaments are expected to strongly interact with the corresponding main vortices. An initial disturbance consisting of a sinusoidal displacement of the vortex cores with an amplitude of a_0=0.0001 b_1 and wave length λ = 0.98 b_1 along their axis was applied to trigger the development of instabilities. The 3D-LES was performed by *DLR Institute of Atmospheric Physics* using its in-house incompressible *LESTUF* code [14]. The original LES was performed in the framework of the European research project *AWIATOR*.

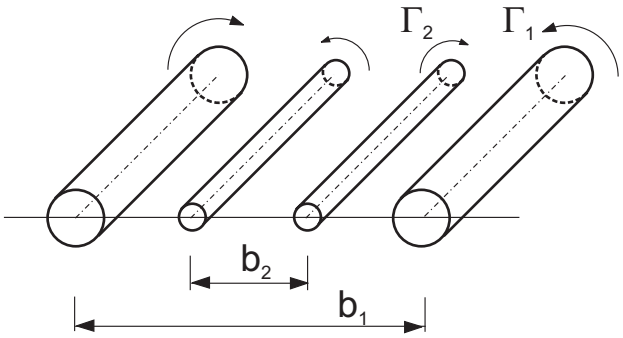

FIG 1: Four-vortex system used for study of wake vortex noise

The LES was carried out in two steps. First, the simulation was run for a long time interval but with a low time resolution to identify the main flow features. Second, a smaller interval interesting for the noise study was re-calculated with a higher time resolution. The second calculation was initialised with the flow field obtained in the first simulation. A domain size of $L_x \times L_y \times L_z$ = 4.8 $b_1 \times$ 0.98 $b_1 \times$ 8 b_1 with a grid spacing of $\Delta y/b_1$ = 0.01536 in the direction of flight and $\Delta x/b_1 = \Delta z/b_1$ = 0.0125 in the spanwise x and the vertical direction z was chosen. The vortex core radii are r_{c1} = 0.075 b_1 and r_{c2} = 0.05 b_1. The time resolution of the first simulation was $\Delta t^* = \Delta t/t_0 = 3.18*10^{-4}$, with $t_0 = 2\pi\, b_1^2/\Gamma_1$.

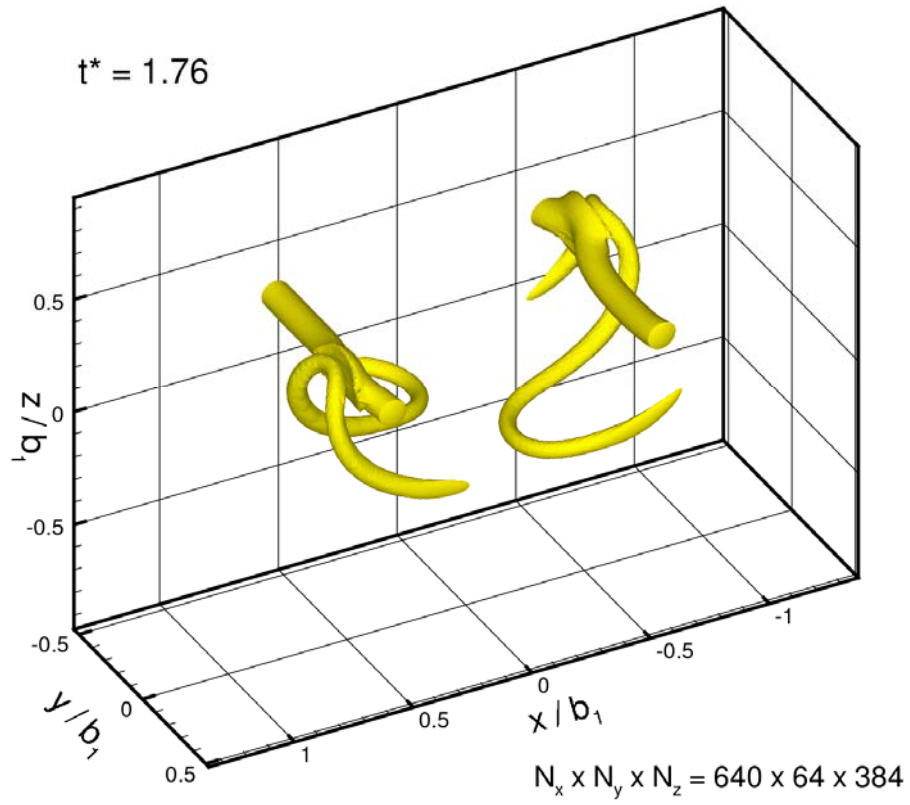

FIG 2: Normalized λ_2*-surfaces of the simulated four-vortex system at normalized time t* = 1.76

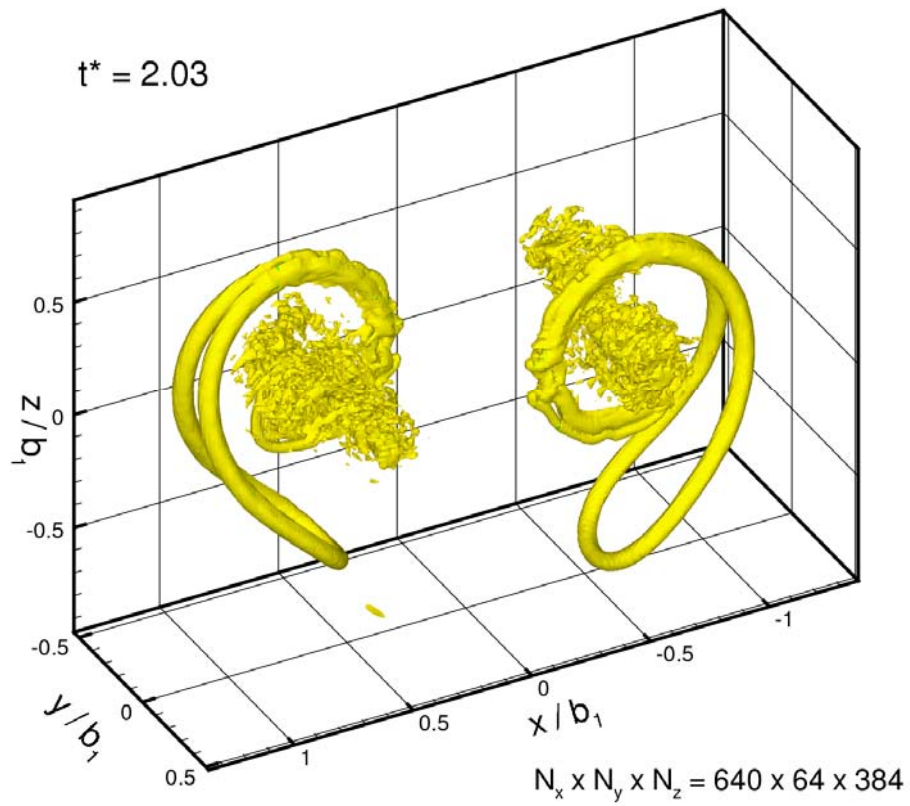

FIG 3: Normalized λ_2*-surfaces of the simulated four-vortex system at normalized time t* = 2.03

FIG 2 and **FIG 3** show the normalized λ_2*-surfaces [15] of the four-vortex system at two instants of normalized time, t* = 1.76 and t* = 2.03. At the beginning of the simulation the weaker vortex starts to slowly rotate around its corresponding primary vortex. Due to the initial displacement of the vortex cores the weaker filaments experience varying acceleration along their axes and become consequently deformed. As long as the spacing between stronger and weaker vortices is large, the weaker rotate slowly around the stronger filaments. At t* = 1.76, however, a short segment of the weaker filament touches the core of the stronger vortex and starts to rotate at a much higher speed $v_\theta = v_\theta(r \approx r_{c1})$ around the mean vortex. The resulting in-homogenous vorticity distribution close to the core of the main vortex is expected to produce sound at frequencies close to the rotation frequency of the core f_r.

A few rotations later finer scale turbulence produced by the strong interaction is found to be distributed around the surviving outer filaments. This fine-scale turbulence is believed to produce sound at frequencies above the rotation frequency of the main vortex cores.

The flow field was de-normalised with the parameters of a landing Bombardier CRJ200 aircraft at t* = 1.69. The parameters are aircraft weight m = 19100 kg, wing span B = 21.2 m and landing speed v = 80m/s. Assuming an elliptical lift distribution the vortex spacing is $b_1 = \pi/4 = 16.7$ m and the initial vortex sink rate $w_0 = b_1 / t_0 = 1.28$ m/s. The resulting distributions of the vorticity ω_y and the velocity v_z along a line across the vortex cores at t* = 1.69 are plotted in **FIG 4**. v_z is asymmetric since the profile is offset by the sink speed of the vortex system. The core radius is estimated from the distance between the turning points in the velocity profile to be of $r_c \approx 0.1\ b_1$. The maximal tangential velocity is $v_\theta\ (r = r_{c1}) \approx 12$ m/s. A rotation frequency of $f_r = 1.1$ Hz results.

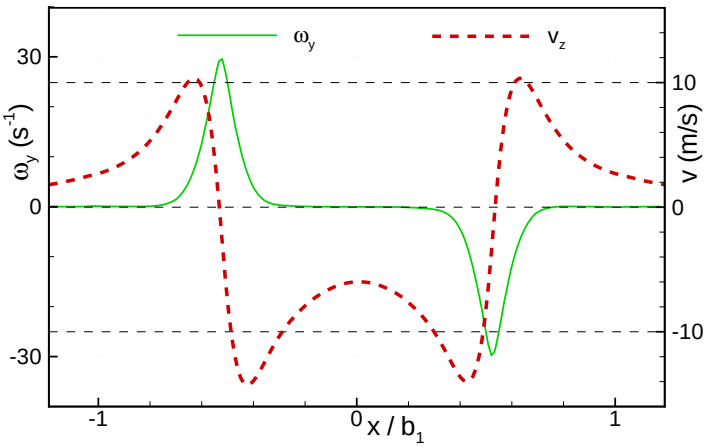

FIG 4: Vorticity ω_y and velocity v_z distribution along a line crossing the vortex cores

The generation of vortex sound in flows with small Mach numbers M « 1 and large Reynolds numbers Re » 1 is described by equation (1). This far-field solution of *Lighthill's* equation was first derived by *Powell* [17] and later studied in more detail by *Howe* [18]. x refers to the observer position, *v* to the local flow velocity and ρ_0 to the mean flow density. The term in brackets is evaluated at retarded time $t_r \approx t - |\vec{x} - \vec{y}| / c_0$. Equation (1) states that only accelerated vorticity ω generates sound. Vorticity at rest is silent. The term in the integral together with the LES solution suggests that the dominant sound sources are located where the SVS touches the PVS and experience their highest accelerations.

$$p(\vec{x},t) = \frac{-\rho_0 x_i}{4\pi c_0 |\vec{x}|^2} \frac{\partial}{\partial t} \int \left[(\vec{\omega} \times \vec{v}) \right]_i d^3\vec{y} \qquad (1)$$

A significant advantage of this formulation over the far-field solution based on the *Lighthill*-Tensor is that the volume integral is limited to a relative small region where strong vorticity ω is found. A second far-field solution, equation (2), was derived by *Möhring* [19] by the assumption that the sound source is acoustically compact. This formulation has been applied for the calculation of the far-field wake vortex noise in the present study.

$$p(\vec{x},t) = \frac{-\rho_0 x_i x_j}{12\pi c_0^2 |\vec{x}|^3} \frac{\partial^3}{\partial t^3} \int y_i \left(\vec{y} \times \vec{\omega} \right)_j (\vec{y}, t - |\vec{x}| / c_0) d^3\vec{y} \qquad (2)$$

The integral is evaluated at an approximated retarded time $t_r \approx t - |\vec{x}|/c_0$. *Möhring's* far-field solution is valid for small Mach numbers M « 1 and large Reynolds numbers Re » 1. A significant disadvantage of this formulation is the numerical noise produced by the third derivative with respect to the time *t*. The LES dedicated to the noise study was run with a higher time resolution of $\Delta t^* = 3.18 \cdot 10^{-5}$ in the interval $t^* = 1.69 \ldots 2.07$. Only a reduced domain containing significant vorticity of size $L_x \times L_y \times L_z = 2.5\ b_1 \times 0.98\ b_1 \times 1.75\ b_1$ has been evaluated.

FIG 5 shows the calculated power spectral density. It is dominated by a hump at f ≈ 0.9 Hz which is very close to the estimated rotation frequency of the core f ≈ 1.1 Hz. In experiments the peak levels are found at much higher frequencies, $f_1 \approx 10$ Hz and $f_2 \approx 100$ Hz. The origin of the peak in experimental data at f_2 is certainly the wake vortex although the source of the first peak is still in question. The discrepancy between the peak frequencies found in the numerical study and the experimental results is probably caused by the core radii used in the simulation. Unfortunately, the minimal feasible core radii in the simulation were limited by computational restrictions. Smaller core radii would require a higher spatial resolution which in turn means a longer calculation time. Smaller core radii, however, would let the SVS rotate around the outer filaments at higher speed. As a consequence, the hump in the spectra would appear at higher frequencies.

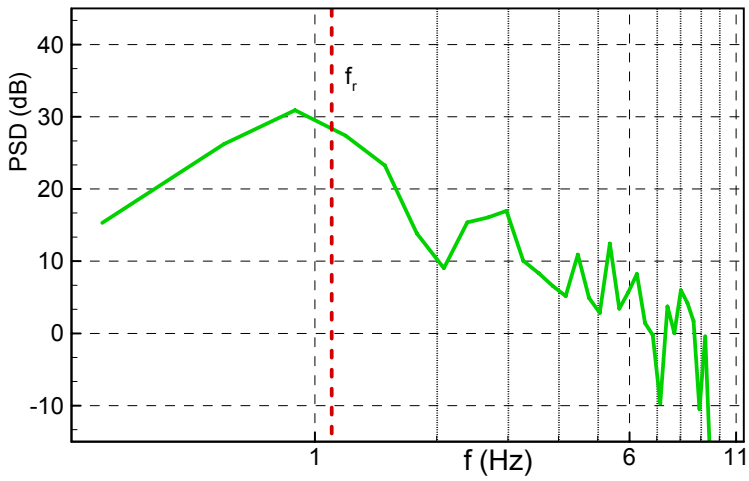

FIG 5: Wake vortex noise spectrum average over an interval of length Δt=3.2sec

The measurement of vortex core radii in fly-over test is still difficult and depends on the vortex model used for the data fit. Recent measurements, however, indicate much smaller core radii of $r_c \approx 0.01 \ldots 0.02$ B [16] than used in the LES. As the rotation frequency of a vortex is proportional to $1/r^2$, a core radius of $r_c = 0.013\ b_1$, corresponding to $r_c \approx 0.01$B assuming an elliptical lift distribution, would move the hump to f ≈ 53 Hz. This frequency is in the frequency range where peak levels were found in the experiments.

The numerically predicted level at the peak frequency is L = 28 dB. A normalization on the vortex length would give a correction of $\Delta L = -10\ log(L_y\ b_1\ /\ 1m) = -12\ dB$. The numerically predicted level L = 16 dB and L = 10 ... 20 dB observed in measurements are in surprisingly good agreement, especially when recalling that the circulation ratio of $\Gamma_2/\Gamma_1 = -0.3$ used in the LES is much higher than expected in real wake vortices.

4. EXPERIMENTAL SET-UP AND DATA REDUCTION

The *DLR (German Aerospace Center)* participated in several flyover measurements applying phased microphone arrays for the localization and the characterization of aircraft wake vortices. The experimental results obtained with two complimentary arrays, in the following called T- and X-array, are discussed in the next section. The first consisted of 128 low-cost microphones pre-installed on 4 boards each of size 1.2 x 1.7 m. The second consisted of 64 microphones equally spaced on the two arms of a cross each of D = 40 m length.

The microphone signals of the T-array were processed by the *classical beamforming* algorithm in the time domain providing the noise source distributions of the wake vortex in 1/3-octave bands. An X-array offers some practical advantages concerning the installation and good sidelobe suppression between the two axes. Unfortunately, high sidelobes emerge along the axes which, however, can be suppressed by a modified algorithm. This modified method was developed for the processing in the frequency domain [19] and later adopted to the time domain [21]. The underlying idea is to remove these elements from the cross-spectral matrix which were calculated from the signal of microphones belonging to the same arm of the cross-array. In the time domain this reads, first, the *classical beamforming* is performed for the microphones of each arm separately. Second, the two focused time signals $b_A(y,t)$ and $b_B(y,t)$ are cross-correlated, equation (3a), which results in a single value $s(y, \tau = 0)$ describing the broadband sound energy content originating from the focus point. A spectral estimation requires (i) filtering of the two focused time signals $b_A(y,t)$ and $b_B(y,t)$ or (ii) calculating the Fourier transformed $B_A(y,\omega)$ and $B_B(y,\omega)$ before cross-correlating. The latter provides a narrow band spectrum of the sound energy radiated from the focus point.

$$s(\vec{y}, \tau = 0) = \sum_{n=1}^{N} b_A(\vec{y}, t_n) b_B(\vec{y}, t_n) \tag{3a}$$

$$or: \qquad S(\vec{y}) = B_A^*(\vec{y}, \omega)\, B_B(\vec{y}, \omega) \tag{3b}$$

The cross-correlation matrix may not remain *positive-definite* after the modification which could result in negative radiated energy for certain focus positions. It can be assumed that if negative energy occurs at a focus point then no dominant source is located at this position. Hence, a simple maximum condition was introduced setting negative values to zero.

(4a)

$$s^{\mathrm{mod}}(\vec{y}) = \max\{s(\vec{y}),0\}$$

$$or: \quad S^{\mathrm{mod}}(\vec{y}) = \max\{S(\vec{y});0\} \tag{4b}$$

This means that no information was obtained for these focus points. Taking the absolute values as energy content would lead to wrong results.

5. DISCUSSION OF THE EXPERIMENTAL RESULTS

The experimental results presented below are based on the microphone array data measured by *DLR* in a field test at the *Denver International Airport* organized by the *NASA* and the *DoT* in 2003 [5]-[8]. LIDAR and weather data were provided by *NASA, DoT* and *Flight Safety Technologies Inc. (FSTI)*. In the discussion below the ICAO aircraft types codes are used which are summarized in TAB 2 of the appendix.

5.1. Source distribution in horizontal plane

FIG 6 and **FIG 7** show the evolution of the sound source distribution in the wake vortex behind an aircraft of type B733 in the 1/3-octave bands f = 160 Hz and f = 80 Hz respectively. The four time intervals evaluated are centred at t = 4.7, 7.9, 11.1 and 14.2 sec after the aircraft flyover. Each interval has a length Δt = 1.57 sec. The aircraft crossed the microphone array in x-direction at an altitude of h = 200 m and a speed of v = 80 m/s. The scan altitude was adjusted to the current wake vortex altitude which was derived from LIDAR measurements.

The source distributions in **FIG 6** reveal a concentration of noise sources with varying intensity along two parallel lines in flight direction. These lines are associated with the position of the cores of the two main vortices. It was concluded that the noise sources are located close to or at the main vortex cores. This in turn allows the two vortices of an aircraft wake vortex to be localised and tracked separately. It also meets the expectations from the numerical study where the vorticity in the vicinity of the core was identified as potential sound source.

The variation of source intensity along the lines was also observed in other measurements where different microphone arrays and processing techniques were applied. Therefore, the variation of the source intensity is believed to be an inherent property of wake vortices. At lower frequencies (**FIG 7**) the source intensity variations are less emphasised since a larger beam width of the microphone array causes the source distribution to be spatially averaged.

By changing the averaging time of the calculation varying source distributions were found which means that the source distribution is highly unsteady. It was concluded that the coherence time length is smaller than 1 sec for all frequency bands.

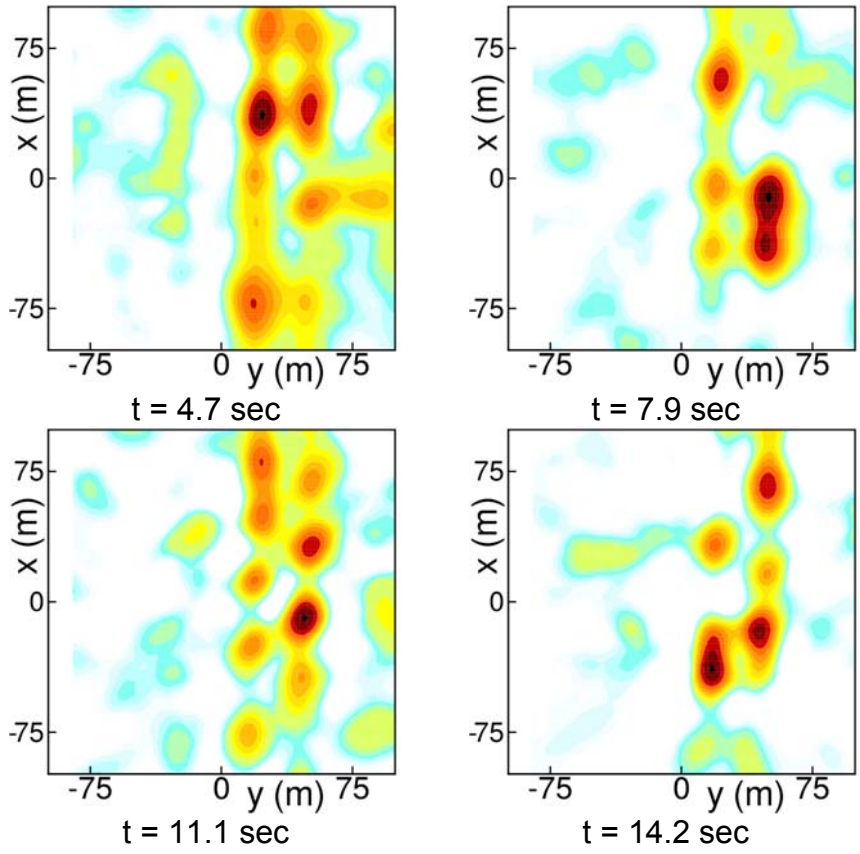

FIG 6: Source distribution in a 1/3-octave band f = 160 Hz in the wake vortex of an aircraft of type B733 at different times after fly-over

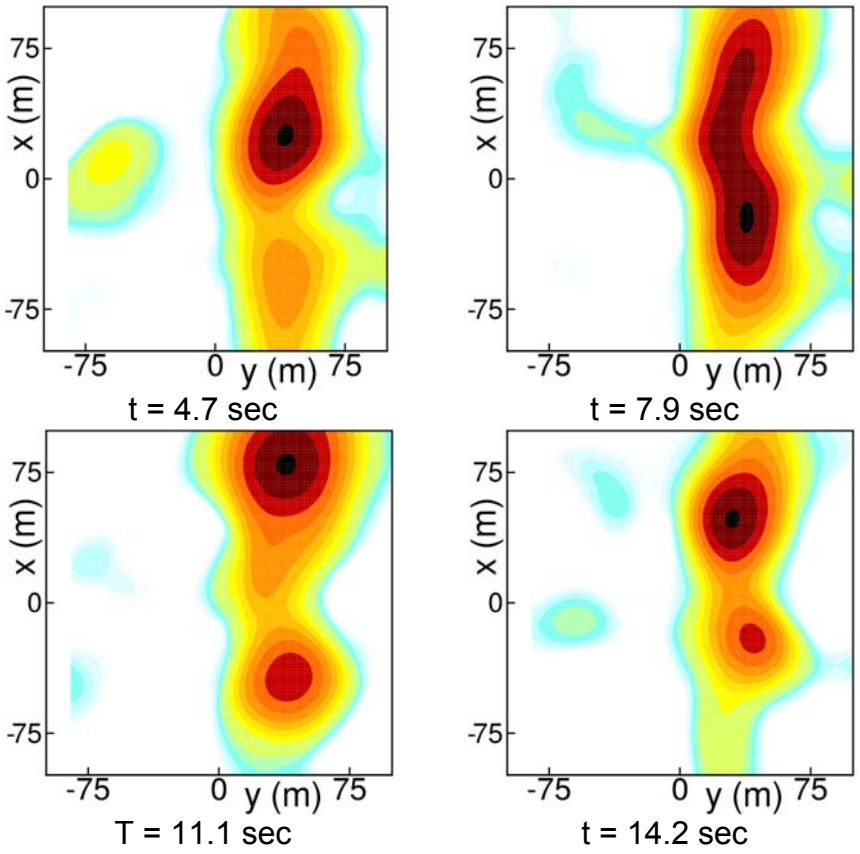

FIG 7: Source distribution in the 1/3-octave band f = 80 Hz the in the wake vortex of an aircraft of type B733 at different times after fly-over

5.2. Source distribution in vertical plane

As it was found that the sound sources are located close to the vortex cores a scan for sources in a vertical plane, the y-z plane, might allow the vortex altitude to be determined. Unfortunately the spatial resolution of a two-dimensional array in a direction perpendicular to the ground is very pour. An example of a scanned source distribution in the y-z plane for the wake vortex behind an aircraft of type B733 is given in

FIG 8. The flyover altitude was h = 180 m, marked in the plots by a dashed line, and the aircraft speed was v = 80 m/s. The vortex positions derived from simultaneously conducted LIDAR measurements are indicated in the plots by blue circles. The distributions are based on the data obtained by the X-array.

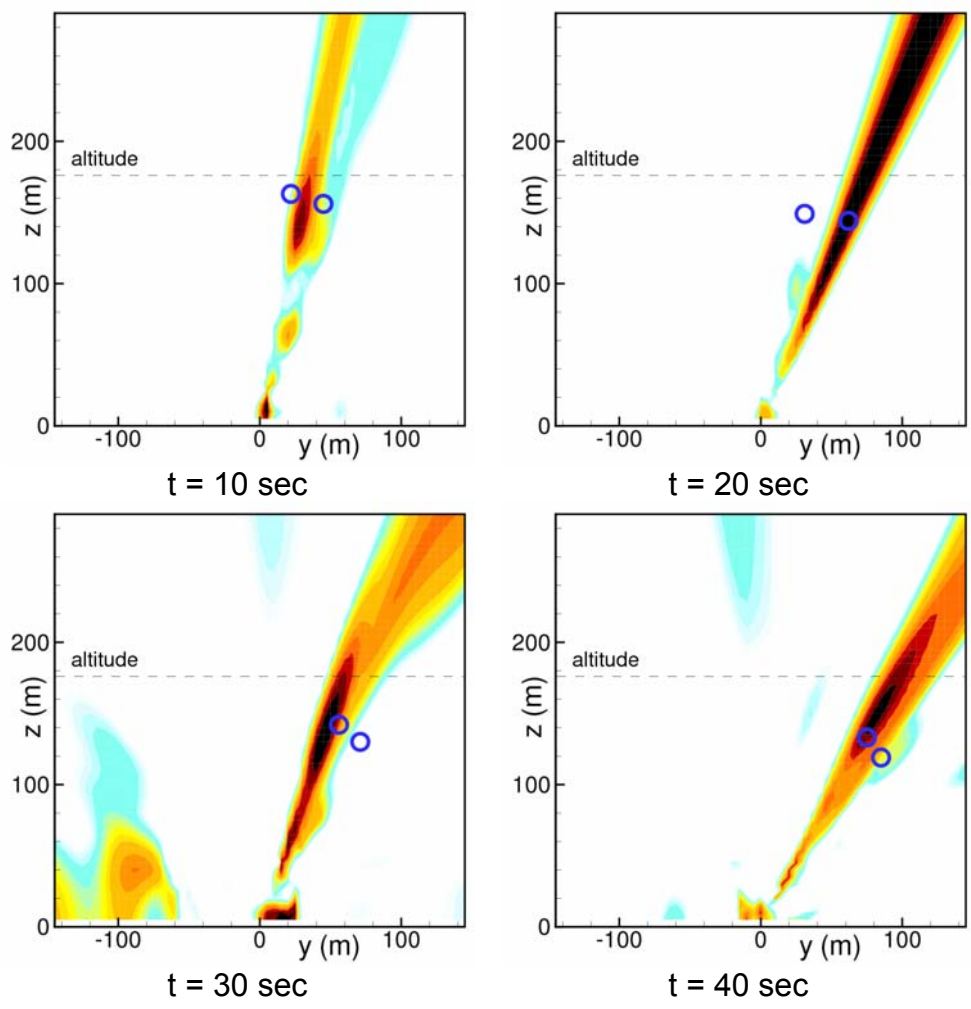

FIG 8: Source distribution in the y-z plane in the 1/3-octave band f = 200 Hz of a wake vortex behind an aircraft of type B733 at different times after fly-over

In some of the plots the maximal sound pressure level appears below and in others above the actual vortex position. The direction switches between left and right vortex. This switching can be avoided by an adopted averaging in space and time allowing both vortices to be tracked at the same time. It is believed that even a de-convolution algorithm would fail to detect the right vortex height. Larger microphone arrays provide better spatial resolution in vertical direction but also suffer from coherence loss between

largely spaced microphones. A more appropriate solution is seen in the application of two microphone arrays spaced a lateral distance similar to the aircraft height $\Delta y \approx z_{ac}$. The first microphone array would detect the wake vortices under an angle of $\varphi = 90°$ and the second of $\varphi = 45°$. Hence, the source altitude can be derived via triangulation.

It was mentioned above that the source distribution strongly depends on the averaging time used for the *beamforming*. Therefore, it is important that the source strength at each point of the plot is evaluated at its retarded time $t_r \approx t - |\vec{x} - \vec{y}| / c_0$. This is even more important when the source altitude is determined by means of the source positions in the x-y plane via triangulation.

5.3. Source distribution in the y-t plane

An important factor in terms of safety is the crosswind which transports the wake vortices out of the flight corridors. To observe the lateral transport of the wakes the source distribution scanned along a line perpendicular to the flight path and plotted as a function of time is very useful.

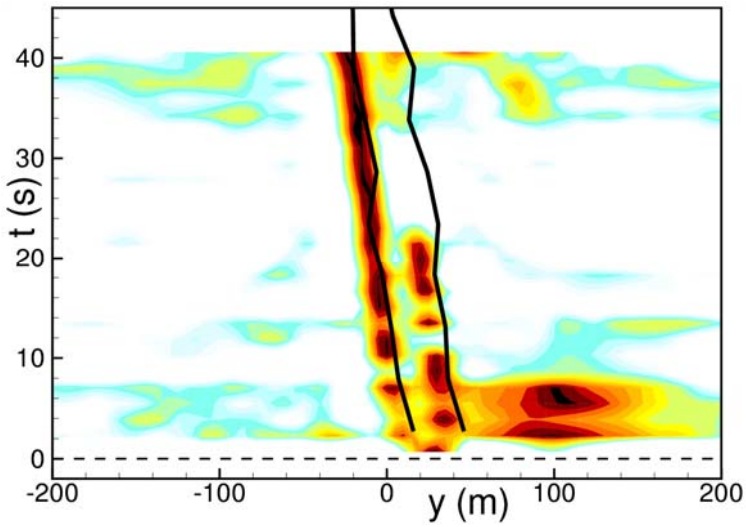

FIG 9: Source distribution in the y-t plane after a fly-over of an aircraft of type B733

In **FIG 9**, the lateral source distribution behind an aircraft of type B733 is plotted as a function of time. The aircraft crosses the microphone array centre at t = 0 sec which is indicated by a dotted line.

The vortex cores are recognized as non-continuous source distribution along two vertical lines. The source distribution is occasionally dominated by only one of the two vortices. If both vortices need to be tracked at the same, the dominance of only one vortex can be avoided by an adopted averaging in space and time. The black lines represent the vortex trajectories obtained by the LIDAR measurements. A slight offset between the LIDAR trajectories and the acoustic source distribution can be observed and was probably caused by an undocumented offset between the measurement systems.

5.4. Detection rate of the wake vortices

To evaluate the reliability of the sound emission of the wake vortices and its weather dependence the detection rates were determined. The source distributions in the y-t plane in all 1/3-octave bands between 40 Hz and 630 Hz of all flyovers were checked for clearly detectable wake vortices. For a graphical presentation in **FIG 10** the number of detected wakes is plotted as function of the flyover index number.

The detected wakes were counted at t = 10, 20, 30 and 40 sec after the flyover. The aircraft types were not distinguished. The test days are separated by vertical dashed lines. The graph shows that wake vortices were detected at t = 10 sec in about 85% of all flyovers. Only slightly less wake vortices were detected at t = 20 sec. The lines at t = 30 sec and t = 40 sec show a smaller gradient for the days D2 to D6 than for days D8 to D10. A correlation with the weather data revealed much higher wind speeds for the first period than for the second period.

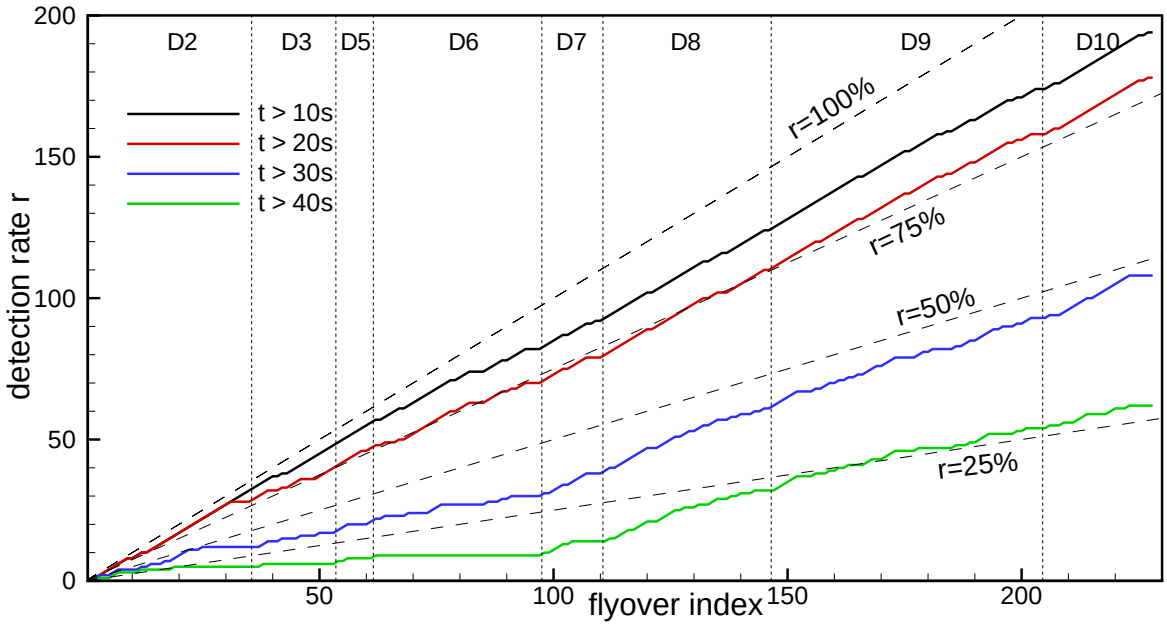

FIG 10: Number of detected wake vortices over the identification number of the measured flyovers

A correlation with the vortex trajectories obtained by LIDAR revealed that LIDAR detected vortices in nearly all flyovers. For some flyovers LIDAR was able to capture the vortices up to 20 sec longer that the phased microphone array. Despite the fact that LIDAR shows better detection capabilities, acoustic technologies are interesting as they are complimentary and still burry a huge potential for capability improvements.

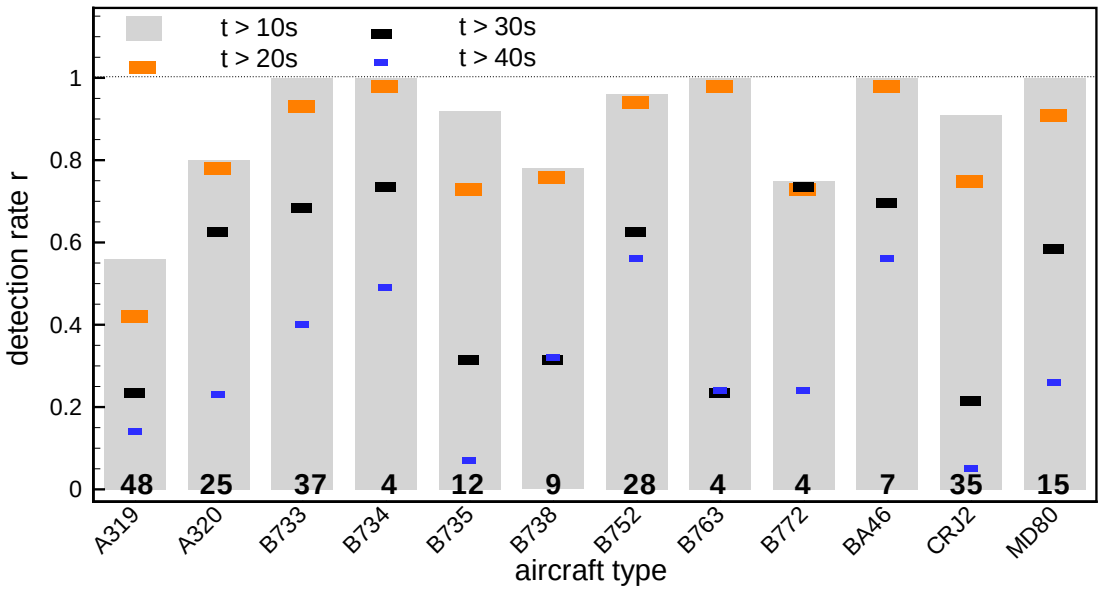

FIG 11: Wake vortex detection over aircraft type

FIG 11 shows the detection rate at four times after the aircraft flyover t = 10, 20, 30 and 40 sec for the different aircraft types. The detection rate is defined as the number of detected wakes divided by the total number of flyover of this type. The total number of flyovers of each type is plotted at the bottom of the graph.

It is interesting that the wake detection rate behind newer aircraft types such as A319, A320, B738 and B772 is obviously smaller than behind older types such as B733, B734, B763 and an MD80.

5.5. Normalized noise spectra

The narrow band spectrum of the wake vortex noise is expected to provide some characteristic spectral features such as the frequency at the peak level which are driven by flow parameters such as circulation and vortex core size.

The wake vortex noise spectra were obtained in two steps. First, the wake vortex tracks were derived from the *y-t* source distribution by means of a *Kalman* filter. Second, a spatial interval y = y0 $\pm$ Δy were defined for which i) the average power spectral density level PSD_a and ii) the highest peak level PSD_p was determined. A focused spectrum obtained by a *beamforming* method depends on the beam width of the microphone array. By normalizing the spectrum on the frequency *f* or wavelength λ, the array dimension *D*, source distance *r* and a characteristic array factor x_g this dependence can be eliminated. As the source distribution only extents in flight direction the spectra were normalised only on the array extension in flight direction.

$$\Delta L = -10\log(x_g \lambda r / D) \qquad (5)$$

The wake vortex noise spectra of 13 flyovers of the aircraft type B733 were compared at different times after flyover and found to be very similar in level and in its characteristics. **FIG 12** shows the normalised focused PSD_a (XA and TA) and PSD_p (XAM) spectra of the wake vortex noise for the aircraft type B733 at t = 10 sec and t = 25 sec. The spectra were obtained by averaging the PSD_a and PSD_p spectra of 13 flyovers. The

standard deviations added to the mean values are plotted as dashed lines. The frequency range f < 220 Hz is covered by the X-array (XA) and f > 220 Hz by the T-array (TA). The prefect match between the PSD_a-spectra of the XA and TA at f = 220 Hz proves the suitability of the normalisation. The PSD_p spectra were plotted as they stronger pronounce the level maxima. The PSD_p spectra of the XA and TA do not match at the f = 220 Hz as the peak levels depend on the array beam width even if the normalisation is applied.

The measured wake vortex noise spectra have two characteristic maxima: a weaker one around $f_1 \approx 12$ Hz and a stronger one around $f_2 \approx 100$ Hz. The source of the second has been clearly identified in the source distribution of the corresponding 1/3 octave band of all 13 flyovers to be the wake vortices. The hump moves towards lower frequencies as the wake ages. The origin of the first maximum has not been identified. Unfortunately, the XA is too small to allow localising the sound source in this frequency range. A much larger microphone array would be required for a reliable source localisation. The levels at all frequencies decrease with time. The narrow peaks at f = 30, 60, 120, 180 Hz are caused by the electric power supply.

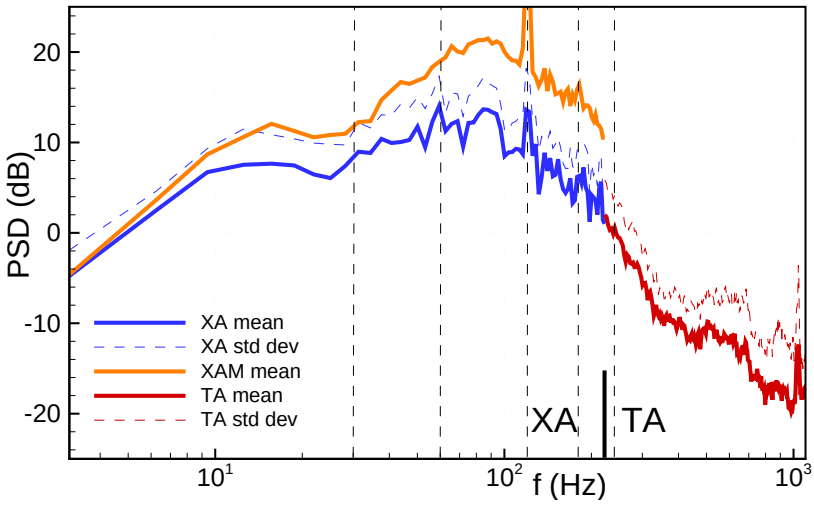

t = 10 sec

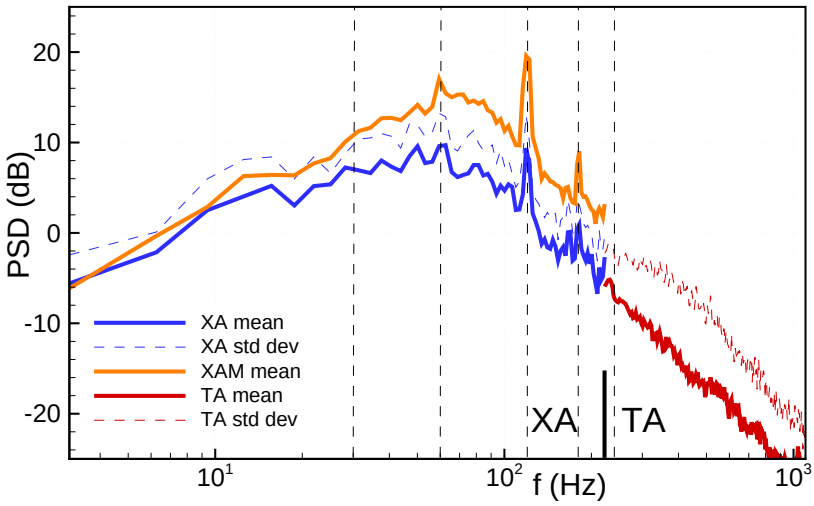

t = 25 sec

FIG 12: Average PSD of wake vortex noise of 13 flyovers of aircraft type B733 at 10 sec and 25 sec after flyover. The vertical, dashed lines indicate harmonics and sub-harmonics of the electric power supply frequency causing the narrow peaks.

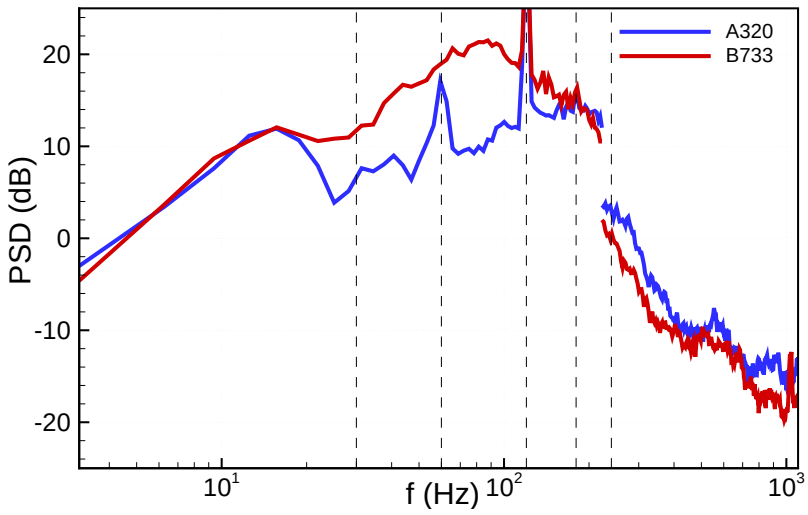

t = 10 sec

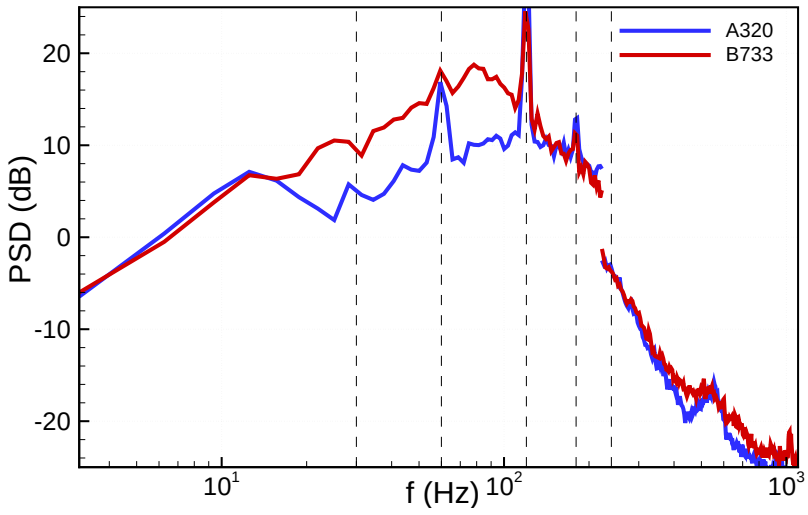

t = 20 sec

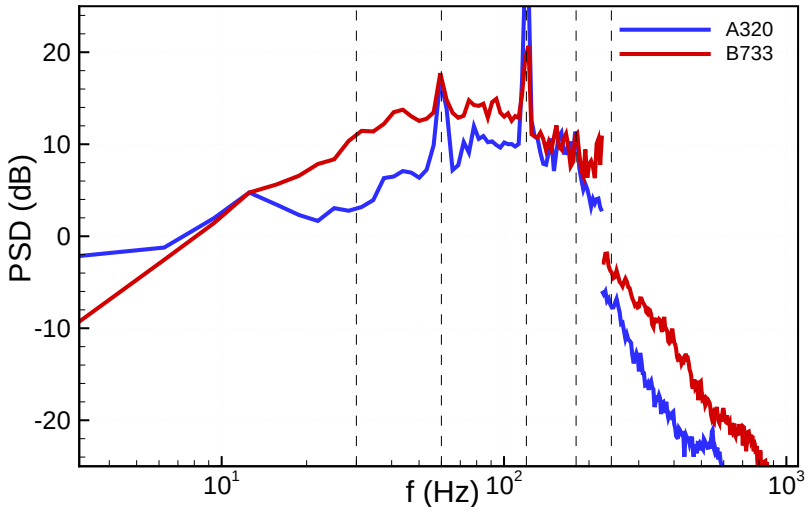

t = 30 sec

FIG 13: Comparison of the averaged wake vortex noise PSD_p behind the aircraft types A320 and B733 at different time after fly-over

FIG 13 shows the PSD_p -spectra for both of the types A320 and B733 at t = 10, 20, and 30 sec after flyover. The spectra were obtained by averaging the focused spectra of 12 A320 and 13 B733 flyovers. The frequency range f < 220 Hz is covered by the XA and f > 220 Hz by the TA. The spectra have similar levels below f < 12 Hz and above f > 220 Hz. The levels in the frequency range between differ significantly. The wake vortices of the B733 aircrafts are up to 10dB louder than the wakes of the A320 which is in agreement with the personal impression made in field test.

By comparing the averaged PSD_p of all aircraft types it was found the wake vortex noise spectra are either similar to the spectra of the A320 or to the B733. Two groups of aircraft with similar spectral vortex noise characteristics have been defined. The first class includes the types A319, A320, BA46, and CRJ200 and the second B733, B734, B735, B738, B752, and MD80. This surprising result needs to be confirmed by future measurements. The average wake vortex noise PSD_p at t = 20 sec of all aircraft types belonging to group 1 and 2 are plotted in **FIG 14** and **FIG 15** respectively.

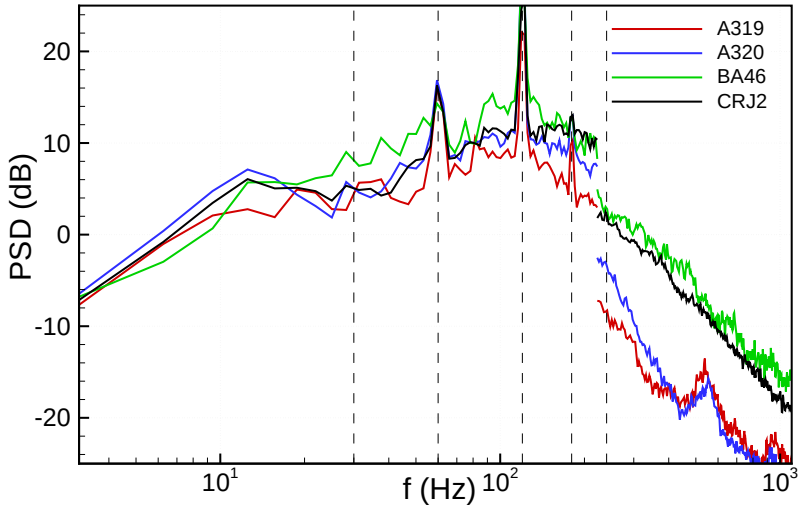

FIG 14: Averaged wake vortex noise PSD_p at t = 20 sec after flyover of group 1 aircraft types

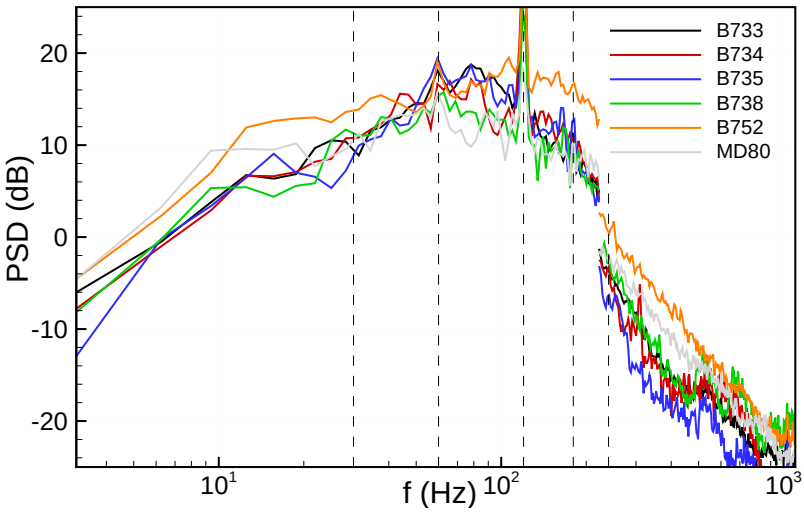

FIG 15: Averaged wake vortex noise PSD_p at t = 20 sec after flyover of group 2 aircraft types

The numerical study of the wake vortex noise suggested the relation $f_a \approx f_r = \Gamma / (2\pi r_c)^2$ between the vortex core rotation frequency f_r and the frequency of the peak level f_a in the noise spectra. According to this relation the rotation frequency is very sensitive to the estimated core radius.

TAB 1 summarizes the aircraft parameters and lists the resulting rotation frequencies of the core depending on its radius r_c = 0.06 B or r_c = 0.01 B which were reported in numerical and experimental wake vortex studies [16]. The range of the resulting frequencies estimated in **TAB 1** makes clear that both of the maxima found in the noise spectra can be related to the core rotation frequency by adjusting the core radius. The existing data base does not give sufficient evidence to draw a final conclusion about the components of the wake vortex noise spectra.

TAB 1: Aircraft and wake vortex parameters

a/c type	Wing span B m	Landing mass x10³ kg	Γ m²/s	f_r 6%B Hz	f_r 1%B Hz
A319	34.1	54.0	240.1	1.5	52.3
A320	34.1	57.4	255.2	1.6	55.6
B733	28.9	47.2	247.9	2.1	75.3
B734	28.9	50.6	265.6	2.2	80.7
B735	28.9	44.1	231.7	2.0	70.4
B738	34.3	59.3	262.1	1.6	56.4
B752	38.1	77.7	309.5	1.5	54.1
B763	47.6	110.7	352.6	1.1	39.5
B772	60.9	173.4	431.3	0.8	29.4
BA46	26.3	32.4	186.6	1.9	68.3
CRJ2	21.2	19.1	136.6	2.1	76.9
MD80	32.9	54.2	250.1	1.6	58.6

The core rotation frequency is expected to decrease as wake vortex ages. This is due to the decaying circulation and the increasing core size caused by diffusion. If the frequency at the peak level in the wake vortex noise spectra is a function of the core rotation frequency as found in the numerical study, the peak level should move towards lower frequencies as the wake vortex ages. Assuming the core growth is negligible, the frequency shift becomes only a function of time weighted by the circulation decay as stated in equation (6). The average circulation decay was derived from LIDAR results for each aircraft type.

$$f = (\Gamma_0 + \dot{\Gamma} t) / (2\pi r_c)^2 \qquad (6)$$

FIG 16 compares the expected frequency shift f_2 of the second peak level according to equation (6) (solid lines) with the shift observed in the averaged wake vortex noise PSD_p (dashed lines) behind the aircraft types A320, B733, B752 and CRJ2. The shifts measured for the aircraft types B733 and B752 match the model predictions but show an unexpected behaviour for the aircraft types A320 and CRJ2. The mismatch for the latter types might be caused by a wrong determination of the initial frequencies at t = 5 sec which seem to be too high for the types A320 and CRJ2.

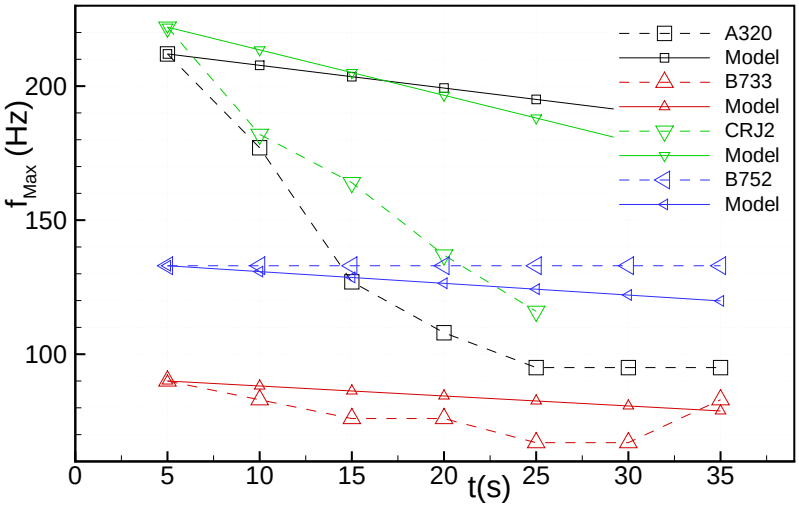

FIG 16: Predicted and measured frequency shift of the second maximum in wake vortex noise spectra for the aircraft types A320, CRJ200, B733 and B752

5.6. Single microphone data

During the field measurements sequences of audible sharp whipping noise events were regularly observed between t = 10 to 40 sec after the flyover. These acoustic events which were associated with bursting or linking of the vortices are also detectable in the recorded sound pressure time signals of single microphones. In **FIG 17** the time history of 1/3-octave band filtered sound pressure levels are plotted. In the frequency bands f = 250 Hz to f = 400 Hz a sudden level increase at about t = 20 sec happens which is followed by a fast level decrease. This event was clearly correlated with a whipping noise event by replaying the source track via loudspeakers.

Although these noise events are associated with vortex busting or linking they definitely do not provide a reliable indication of a final wake vortex break up. Moreover, a correlation between the sound pressure time histories and the sound source distributions revealed that the typical vortex noise signature in the localisation map disappeared after the noise event but reappeared only a few second later. This observation was confirmed by LIDAR data.

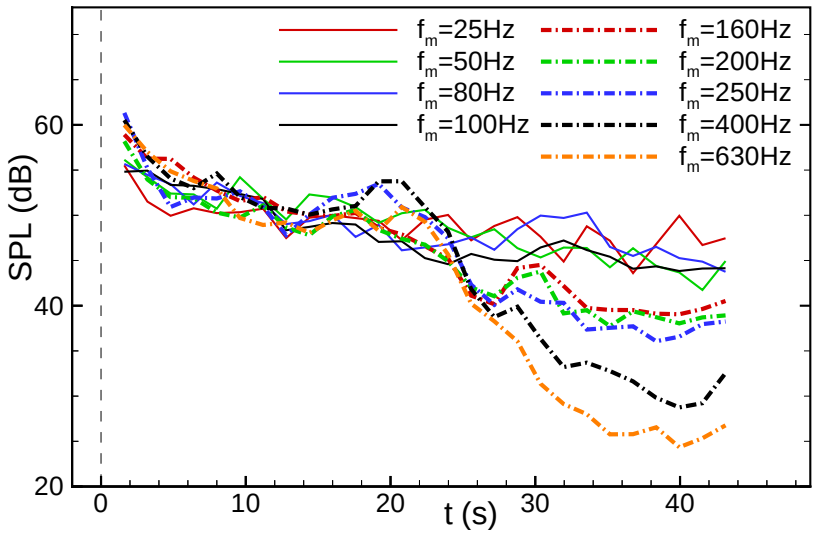

FIG 17: Time history of 1/3-octave filtered sound pressure signal of a single microphone after the flyover of a CRJ2 aircraft

6. CONCLUSIONS

The noise emission of aircraft wake vortices has been studied experimentally in several measurement campaigns at airports and investigated numerically using LES and an acoustic analogy method.

The numerical study of wake vortex noise suggests that:

1) The strongest sound sources are located close to vortex cores.
2) The frequency of peak level in noise spectra is related to the rotation frequency of vortex cores, $f_a \approx f_r = \Gamma / (2\pi r_c)^2$.

The experimental results showed that:

1) The sound sources of aircraft wake vortices are located close to or at the vortex cores.
2) The two vortices can be detected and tracked separately in the sound source localisation maps.
3) The source strength varies along vortex axes and is highly unsteady.
4) The focused wake vortex noise has probably two maxima: The origin of the first maximum at $f_1 \approx 10$ Hz has not been identified. The origin of second maximum at $f_2 \approx 100$ Hz are wake vortices.
5) The wake vortex noise spectra depend on the wake generating aircraft type: The aircraft could be categorized into two classes depending on the noise spectrum of the generated wake vortex.
6) A sudden noise event observed in the field tests is probably related to vortex bursting or linking but does not reliably indicate a final vortex break up.

Although, the wake vortex detection capability of LIDAR is superior, technologies based on the vortex noise emission remain interesting as they are complimentary and have the potential for further performance improvements.

Acknowledgments. Parts of the wake vortex simulation data used in this work have been obtained within the European research project AWIATOR (Contract G4RD-CT2002-00836).

REFERENCES

[1] International Civil Aviation Organisation: *Air Traffic Service Planning Manual II-5-3-2*, 1992.

[2] Gerz T., Holzäpfel F., Bryant W., Köpp F., Frech M., Tafferner A. and Winckelmans G.: Research towards a wake-vortex advisory system for optimal aircraft spacing, *Comptes Rendus Physique*, Académie des Sciences, Paris, **6**, No. 4-5, 501-523, 2005.

[3] Michel, U.; Böhning, P.: *Investigation of Aircraft Wake Vortices with Phased Microphone Arrays*, 8th AIAA/ CEAS Aeroacoustics Conf., AIAA 2002-2501, 2002.

[4] Böhning, P.; Michel U.: *Detektion von Wirbelschleppen mittels Mikrofon-Arrays*; DGLR 2004-015, 2004.

[5] Dougherty, R.; Wang, F.; Booth, E.; Watt M.; Fenichel, N.; D'Errico, R.: *Aircraft Wake Vortex Measurements at Denver International Airport*, 10th AIAA/CEAS Aeroacoustics Conf., AIAA 2004-2880, 2004.

[6] Booth, E.; Humphreys, W.: *Tracking and Characterization of Aircraft Wakes using Acoustic and Lidar Measurements*, 11th AIAA/CEAS Aeroacoustics Conf., AIAA Paper 2005-2964, 2005.

[7] Wang, F.; Wassaf, H.; Gulsrud, A.: *Acoustic Imaging of Aircraft Wake Vortex Dynamics*, 23th AIAA/CEAS Applied Aerodynamics Conf., AIAA 2005-4849, 2005.

[8] Fine, N., Kring, D.: *Opto-Acoustic Tracking of Aircraft Wake Vortices*, 11th AIAA/CEAS Aeroacoustics Conf., AIAA 2005-2965, 2005.
[9] Holzäpfel, F.: *Probabilistic Two-Phase Wake Vortex Decay and Transport Model*, J. Aircraft, **40** (2), 2003.
[10] Zheng, Z.; Wenhua L.; Wang F.; Wassaf H.: *Influence of Vortex Core on Wake Vortex Sound Emission*, 12th AIAA/CEAS Aeroacoustics Conf., AIAA 2006-2538, 2006.
[11] Holzäpfel, F.; Hofbauer; T.; Darracq; D., Moet; M.; Garnier, F.; Gago, C.: *Analysis of wake vortex decay mechanisms in atmosphere*, Aerospace Science and Technology, Vol. **7**, 2003.
[12] Rossow, V.: *Lift-generated vortex wakes of subsonic transport aircraft*, Progress in Aerospace Science **35**, 507-660, 1999.
[13] Donaldson, C., Bilanin, A.: *Vortex wakes of conventional aircraft*, AGARDograph 204, 1975.
[14] Holzäpfel F., Gerz T., Baumann R.: *The turbulent decay of trailing vortex pairs in stably stratified environments*, Aerospace Science Technology, vol. **5**, 95-108, 2001.
[15] Jeong, J., Hussain, F.: *On the identification of a vortex*, J. Fluid Mech., **285**, 69-94, 1995.
[16] Delisi, D.; Greene G.; Robins, R.; Vicroy, D.; Wang, F: *Aircraft Wake Vortex Core Size Measurements*, 21th AIAA/CEAS Applied Aerodynamics Conf., AIAA 2003-3811, 2003.
[17] Powell, A., *Theory of vortex sound*, Journal of the Acoustical Society of America, vol. **36**, 177-195, 1964.
[18] Howe M. S., *Theory of Vortex Sound*, Cambridge University Press, 2003.
[19] Möhring, W.: *On vortex sound at low Mach number*, J. Fluid Mech. **85**(4), 685-691, 1978.
[20] Elias, G.: *Source Localisation with a Two-Dimensional Focused Array: Optimal Signal Proces-sing for a Cross-Shaped Array*; Inter-Noise 95, 1995.
[21] Dougherty, R.: *Advanced Time-domain Beamforming Techniques*; 10th AIAA/CEAS Aeroacoustics Conf., AIAA- 2004-2955, 2004.
[22] The Airline Codes Web Site: *IATA Aircraft Type Codes*; http://www.airlinecodes.co.uk/acrtypes.htm

APPENDIX A

The ICAO aircraft type codes [22] are explained in TAB 2

TAB 2: IATA aircraft type codes

ICAO Code	Aircraft manufacture and type
A319	Airbus A319
A320	Airbus A320
B733	Boeing 737-300
B734	Boeing 737-400
B735	Boeing 737-500
B738	Boeing 737-800
B752	Boeing 757-200
B763	Boeing 767-300
B772	Boeing 777-200
BA46	British Aerospace BAe 146
CRJ2	Canadair Regional Jet 200
MD80	McDonnell Douglas MD80

THE WAKE VORTEX PREDICTION AND MONITORING SYSTEM WSVBS PART I: DESIGN

F. Holzäpfel[a], T. Gerz[a], M. Frech[a], A. Tafferner[a], F. Köpp[a],
I. Smalikho[a], S. Rahm[a], K.-U. Hahn[b], C. Schwarz[b]

[a]Institut für Physik der Atmosphäre, DLR-Oberpfaffenhofen, 82234 Weßling, Germany
[b]Institut für Flugsystemtechnik, DLR-Braunschweig, 38108 Braunschweig, Germany

ABSTRACT

The design of the Wake Vortex Prediction and Monitoring System WSVBS is described with all its components and their interaction. The WSVBS has been developed to tactically increase airport capacity for approach and landing on closely-spaced parallel runways. It is thought to dynamically adjust aircraft separations dependent on weather conditions and the resulting wake vortex behaviour without compromising safety. Dedicated meteorological instrumentation and short-term numerical terminal weather prediction provide the input to the prediction of wake-vortex behaviour and respective safety areas. The prediction tools employ a number of conservative aircraft parameter combinations that represent the aircraft weight categories medium and heavy. The times when the approach corridors do no more or not yet overlap with all predicted safety areas determine aircraft separations for follower aircraft of categories medium and heavy. As a safety net a LIDAR monitors the correctness of WSVBS predictions in the most critical gates at low altitude.

ZUSAMMENFASSUNG

Das Manuskript beschreibt das Design des Wirbelschleppen Vorhersage- und Beobachtungssystems WSVBS mit seinen Komponenten und ihrem Zusammenspiel. Das WSVBS wurde zur dynamischen Reduzierung der Wirbelschleppenstaffelung im Landeanflug unter geeigneten meteorologischen Bedingung entwickelt. Dabei gilt stets die Maxime, dass Kapazitätssteigerungen nur bei mindestens gleich bleibender Sicherheit umgesetzt werden können. Daten meteorologischer Messinstrumente und aus der numerischen Kurzfrist-Wettervorhersage werden zusammen geführt, um das Verhalten der Wirbelschleppen mit den notwendigen Sicherheitszuschlägen vorherzusagen. Dabei werden die Flugzeug-Gewichtsklassen Medium und Heavy durch konservative Flugzeugparameter-Kombinationen repräsentiert. Der Zeitpunkt, an dem die prognostizierten Sicherheitszonen die Anflugkorridore nicht mehr oder noch nicht überlappen, legt die Abstände zwischen den Flugzeugen fest. Ein LIDAR überwacht die WSVBS Vorhersagen in den wichtigsten Kontrollebenen kurz vor dem Aufsetzen.

1. INTRODUCTION

Aircraft trailing vortices may pose a potential risk to following aircraft. The empirically motivated separation standards between consecutive aircraft which were introduced in the 1970s still apply. These aircraft separations limit the capacity of congested airports in a rapidly growing aeronautical environment. Capacity limitations are especially drastic and disagreeable at airports with two closely-spaced parallel runways (CSPR) like Frankfurt Airport (Germany) where the potential transport of wakes from one runway to the adjacent one by crosswinds impedes an independent use of both runways.

The most rapid growth scenario within a Eurocontrol study [1] indicates that in the year 2025 sixty European airports could be congested and as a results 3.7 million flights per year could not be met. This is opposed by an estimate of annual savings of US $ 15 million per year and airport that could be achieved by the introduction of a wake-vortex advisory system [11]. This estimation accounts only for cost avoidance based on reductions in arrival delays. Savings due to reduced departure delays, value of passenger time, additional airline revenue, avoidance of runway or airport construction and airline relocation are not considered. A survey on wake-vortex advisory systems and modifications of procedures that are meant to increase airport capacity is available in [21].

DLR has developed the Wake Vortex Prediction and Monitoring System (WirbelSchleppen-Vorhersage- und -BeobachtungsSystem WSVBS [8]) to tactically increase airport capacity for approach and landing. The WSVBS is thought to dynamically adjust aircraft separations dependent on weather conditions and the resulting wake vortex behaviour without compromising safety. The system is particularly adapted to the closely spaced parallel runway system of Frankfurt airport. For this purpose it predicts wake vortex transport and decay and the resulting safety areas along the glide slope from final approach fix to threshold. The manuscript describes the design of the WSVBS with all its components and their interaction. The elements of the WSVBS are generic and can well be adjusted to other runway systems and airport locations. The integration of the WSVBS into air traffic control and its promising performance during a three-month measurement campaign at Frankfurt Airport are described in Part II of this manuscript. Precursor versions of these papers have been presented at the CEAS Conference 2007 [9], [17].

2. SYSTEM OVERVIEW

FIG 1 delineates the components of the WSVBS and their interplay. The bottleneck of runway systems prevails in ground proximity because there stalling or rebounding wake vortices may not descend below the flight corridor. Therefore in that domain the best wake prediction skill is required which here is achieved based on measurements of meteorological conditions with a SODAR/RASS system and an ultra sonic anemometer (USA). Because it is not possible to cover the whole glide slope with such instrumentation, the meteorological conditions in the remaining area are predicted with a numerical weather prediction system (NOWVIV) leading to wake predictions with increased uncertainty bounds. Based on glide path adherence statistics (FLIP) the

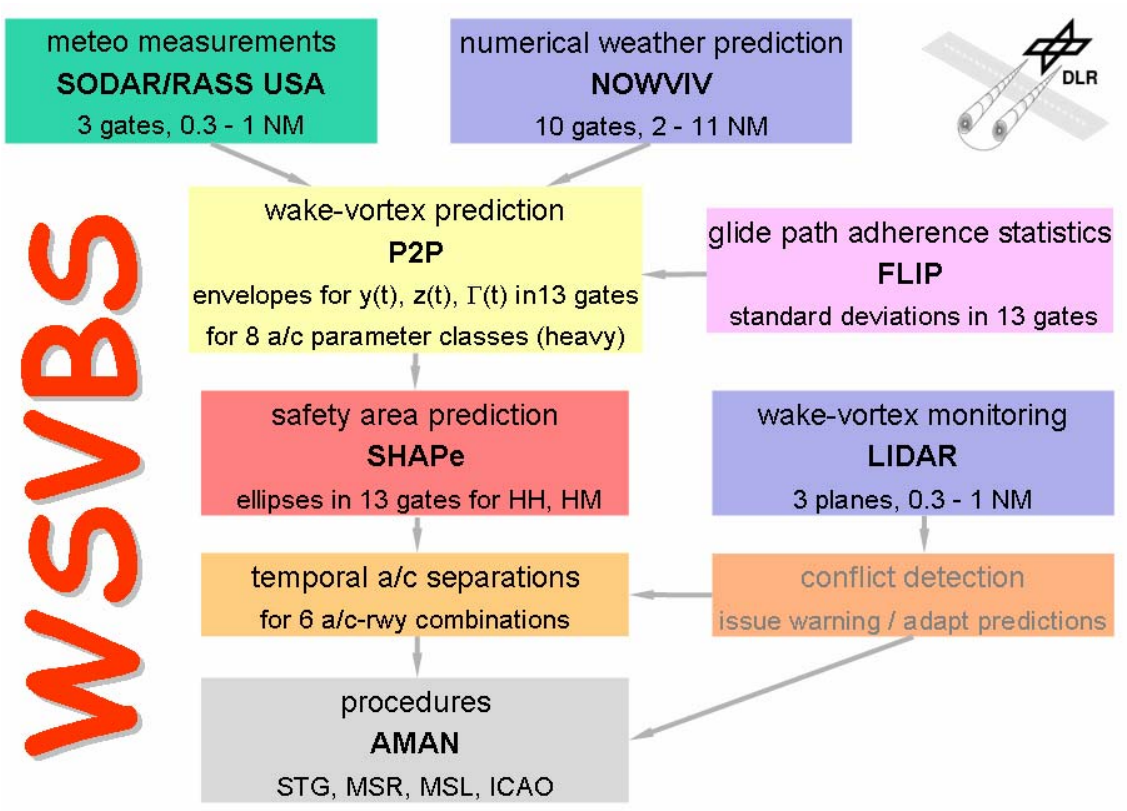

FIG 1.Flowchart of the WSVBS.

probabilistic wake vortex model P2P predicts upper and lower bounds for position and strength of vortices generated by heavy aircraft. These bounds are expanded by the safety area around a vortex that must be avoided by follower aircraft for safe and undisturbed flight (SHAPe). The instant when these safety areas do not overlap with the flight corridor define temporal aircraft separations that are translated into established procedures by the arrival manager (AMAN). As a safety net the LIDAR monitors the correctness of WSVBS predictions in the most critical gates at low altitude. The components of the WSVBS are described in detail in section 4.

3. TOPOLOGY

The WSBVS requires that all aircraft are established on the glide slope at the final approach fix (FAF) which is situated 11 NM before touchdown. For each runway wake-vortex evolution is predicted within 13 gates along the final approach. In ground proximity the gate separation of 1 NM is reduced to 1/3 NM to properly resolve the interaction of wake vortices with the ground. TAB 1 lists the gates' altitudes and distances from the touchdown zone (TDZ). FIG 2 delineates the parallel runway system with the employed geodetic coordinate system and a few gates next to the ground. The parallel runways and consequently also the gate centres are laterally spaced by 518 m and axially displaced by 226.5 m.

gate No	x_{gate} [NM]	x_{gate} [m]	z_{gate} [m]
1	-11	-20372	-1077
2	-10	-18520	-979
3	-9	-16668	-880
4	-8	-14816	-781
5	-7	-12964	-683
6	-6	-11112	-584
7	-5	-9260	-486
8	-4	-7408	-387
9	-3	-5556	-289
10	-2	-3704	-191
11	-1	-1852	-94
12	-2/3	-1235	-61
13	-1/3	-617	-29

TAB 1.Gate centre positions along glide path in geodetic coordinates.

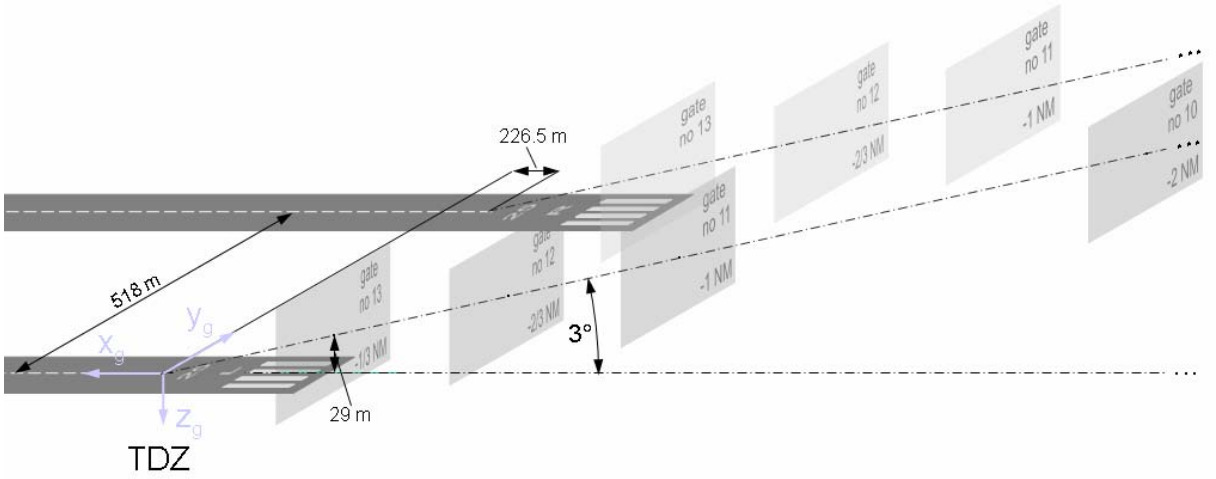

FIG 2.Zoom on gate topology for Frankfurt's closely-spaced parallel runway system.

4. SYSTEM COMPONENTS

It is planned to adjust the different system components to consistent probability levels such that the WSVBS will meet accepted risk probabilities as a whole. Since a comprehensive risk assessment of the WSVBS is still pending, we currently employ 95.4% probabilities (two standard deviations, 2σ, for Gaussian distributions) as a basis for the probabilistic components of the WSVBS. The following sections describe the components delineated in the flowchart in FIG 1 in detail.

4.1. Meteorological Data

For prediction of wake-vortex behaviour along the final approach path meteorological conditions with good accuracy must be provided for the complete considered airspace

with a forecast horizon of 1 hour. A combination of measurements (employing the persistence assumption) and numerical weather predictions accounts for the required temporal and spatial coverage.

4.1.1. Instrumentation

For the three lowest gates at 1/3, 2/3, and 1 NM from the TDZ a METEK Sodar with a RASS extension provides 10-minute averages of vertical profiles of the three wind components, vertical fluctuation velocity, and virtual temperature with a vertical resolution of 20 m. The Sodar/RASS system is complemented by an ultrasonic anemometer (USA) mounted on a 10 m mast. Eddy dissipation rate (EDR) profiles are derived from vertical fluctuation velocity and the vertical wind gradient employing a simplified budget equation [5]. A spectral analysis of the longitudinal velocity measured by the sonic is used to estimate EDR by fitting the -5/3 slope in the inertial subrange of the velocity frequency spectrum.

4.1.2. Numerical Weather Prediction

The non-hydrostatic mesoscale weather forecast model system NOWVIV (NOwcasting Wake Vortex Impact Variables) is used to predict meteorological parameters in the area which is not covered by measurements (the more remote 10 gates from 2 to 11 NM). NOWVIV has been successfully employed for predictions of wake vortex environmental parameters in the field campaigns WakeOP 2001 [14] and WakeTOUL 2002 [15] of projects Wirbelschleppe and C-Wake, in the first flight test campaign 2003 of AWIATOR [15], and in the measurement campaign at Frankfurt airport accomplished in fall 2004 [6], [16]. Detailed descriptions of NOWVIV and its nowcasting skill are available in [7], [8].

Within the forecast system NOWVIV, the mesoscale model MM5 [10] predicts the meteorological conditions for the Frankfurt terminal area in two nested domains with sizes of about 250 x 250 km² and about 90 x 90 km² centred on Frankfurt airport with grid distances of 6.3 km and 2.1 km, respectively. 60 vertical levels are employed such that in the altitude range of interest ($z < 1100$ m above ground) 26 levels yield a vertical resolution varying between 8 m and 50 m.

Initial and boundary data are taken from the operational weather prediction model LM (Local Model, [3]) of DWD (German Weather Service). These data represent the best possible forcing of NOWVIV since actual observations (radio soundings, AMDAR (Aircraft Meteorological Data Relay), satellite data, surface observations, etc.) are used to analyse the state of the atmosphere. Detailed topography, land use and soil type data for the Frankfurt area are employed.

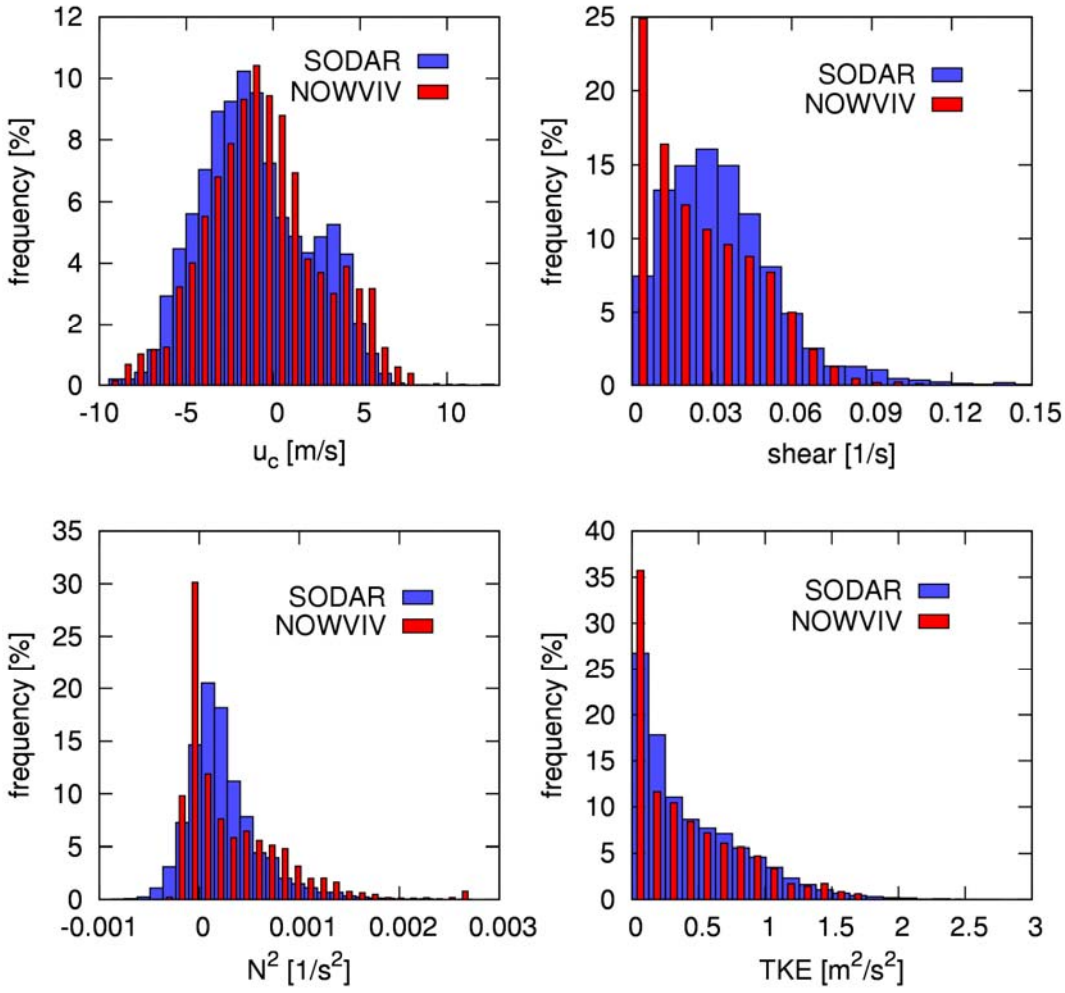

FIG 3. Histograms of measured and predicted crosswind, wind shear, temperature stratification, and turbulent kinetic energy at a height of 100 m above ground for a 40-day measurement campaign at Frankfurt airport [7].

NOWVIV runs twice a day (at 00 and 12 UTC) on a dedicated LINUX cluster at University of Stuttgart. Profiles of meteorological data are extracted at gates 1 through 10 with an output frequency of 10 minutes. The meteorological quantities comprise the three wind components, air density, virtual potential temperature, turbulent kinetic energy, eddy dissipation rate (EDR), and pressure.

FIG 3 shows the favourable comparison of measured and predicted key meteorological quantities for wake vortex prediction collected during a 40 days measurement campaign conducted at Frankfurt airport in 2004 [7].

4.1.3. Integration of Meteorological Data

For approaches the largest probability to encounter wake vortices prevails at altitudes below 300 ft [2], [18], [21]. There stalling or rebounding vortices may not clear the flight corridor vertically and weak crosswinds may be compensated by vortex-induced lateral transport which may prevent the vortices to quit laterally. Since vortex decay close to the ground is almost not sensible to meteorological conditions [16] the only remaining

mechanism that may allow for reduced aircraft separations is lateral transport of wake vortices by crosswind.

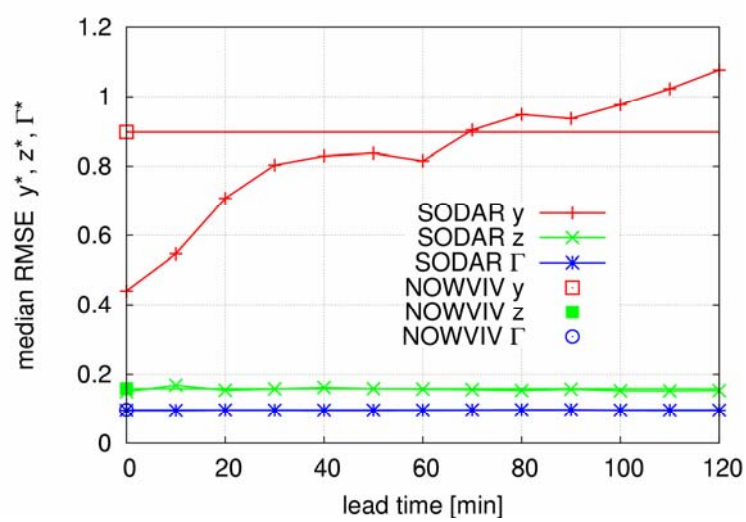

FIG 4. Median of normalized root-mean square deviations between measured and predicted lateral position, y*, vertical position, z*, and circulation, Γ^*, as a function of the source of meteorological data and lead time.

FIG 4 evidences that the best wake-vortex prediction skill of lateral transport is achieved employing SODAR wind measurement data. Only if it is assumed that the measured wind would persist for over 70 min (lead time), the lateral vortex transport predicted with NOWVIV input yields superior results. In ground proximity vertical transport and vortex decay is largely independent from meteorological conditions. Consequently, it is also almost independent from the source of the meteorological input data and the lead time.

Because it is not feasible to cover the complete final approach path with instrumentation we employ SODAR/RASS data for wake prediction in the bottleneck at low altitudes (gates 11 – 13) whereas for the less critical area aloft we use NOWVIV data which yields minor wake prediction skill.

4.2. Approach Corridor Dimensions

For the definition of approach corridor dimensions we employ the glide path adherence statistics of the FLIP study [4], an investigation of the navigational performance of ILS (Instrument Landing System) approaches at Frankfurt airport. FLIP provides statistics of 35,691 tracks of precision approaches on Frankfurt ILS of runways 25L/R. It does not differentiate between manual and automatic approaches. The study indicates that the measured flight path deviations are much smaller than specified by ICAO localiser and glide slope tolerances. The employed corridor dimensions decrease monotonically when approaching the runways and are kept constant within a distance of 2 NM from TDZ.

The approach corridors in the different gates consist of ellipses (see green ellipses in FIG 8). Vertical and horizontal semi axes of these ellipses correspond to two standard deviations derived from glide path adherence statistics, respectively. For Gaussian

distributions two standard deviations (2σ) correspond to a probability of 95.4% that an aircraft does not leave the corridor in one dimension (either laterally or vertically). For ellipsoidal corridors this probability reduces to 86.5% assuming statistical independence of lateral and vertical positions.

4.3. Representation of Aircraft Weight Classes

In principle, the WSVBS could predict conservative separations for individual aircraft pairings provided that the approaching aircraft types are known. However, in order to keep the system as simple as possible and, thus, to minimize additional workload for controllers, the WSVBS only considers aircraft weight class combinations. For Frankfurt airport the relevant combinations are heavy followed by heavy (HH) and heavy followed by medium (HM).

To conservatively represent generator aircraft parameters of the heavy weight category at first fits are established which bound a representative compilation of parameters of existing aircraft as function of the maximum take-off weight (see green lines in FIG 5). For the individual aircraft the circulation of the generated wake vortices is calculated according to

(1) $$\Gamma_0 = \frac{M \cdot g}{\rho \pi / 4 B V}$$

where M is the maximum landing weight, ρ is air density of the standard atmosphere at sea level, $\pi/4\,B$ is the vortex separation for an elliptically loaded wing, and V the final approach speed.

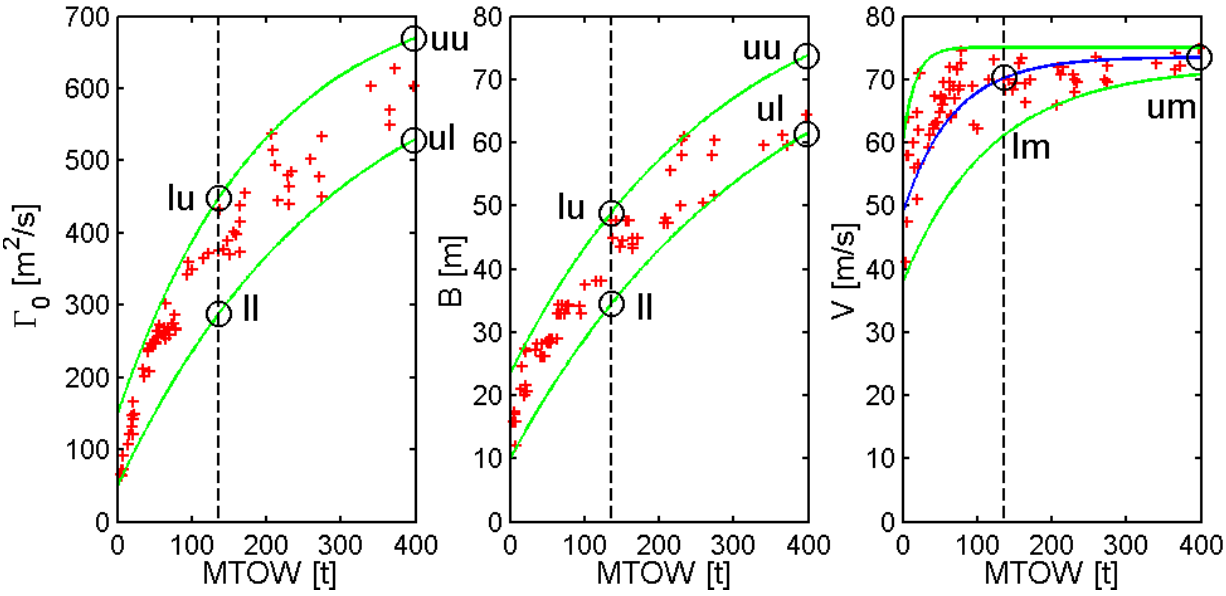

FIG 5. Initial circulation, Γ_0, wing span, B, and flight speed, V, for final approach as function of maximum take-off weight, MTOW, for 73 aircraft types. Green lines border aircraft parameters, circles denote the parameters which are combined to represent the aircraft weight class heavy.

FIG 5 and TAB 2 illustrate the way initial circulations, wing spans, and approach speeds are combined at the weight class boundaries. The B747-400 with a MTOW of 397 t is

chosen as upper limit of the heavy weight category. TAB 2 lists the 8 resulting parameter combinations which conservatively represent all possible generator aircraft within the heavy weight category. In FIG 5 and TAB 2 the first u (l) denotes the upper (lower) bound of the weight class and the second u (l) upper (lower) fits at a weight class boundary. The resulting wide variations of initial vortex descent speed and wake vortex time scales (variations by almost a factor of four) which are employed for any approaching aircraft indicate one of the conservative margins of the WSVBS.

parameter comb.	Γ_0 [m²/s]	b_0 [m]	V [m/s]	char. time scale t_0 [s]	desc. speed w_0 [m/s]
Γ_{0uu} b_{0uu}	669.2	57.9	73.5	31.5	1.84
Γ_{0uu} b_{0ul}	669.2	48.2	73.5	21.8	2.21
Γ_{0ul} b_{0uu}	528.5	57.9	73.5	**39.9**	1.45
Γ_{0ul} b_{0ul}	528.5	48.2	73.5	27.6	1.75
Γ_{0lu} b_{0lu}	448.1	38.4	70.3	20.7	1.86
Γ_{0lu} b_{0ll}	448.1	27.1	70.3	**10.3**	**2.63**
Γ_{0ll} b_{0lu}	288.2	38.4	70.3	32.1	**1.19**
Γ_{0ll} b_{0ll}	288.2	27.1	70.3	16.0	1.69

TAB 2. Aircraft parameter combinations for initial circulation, Γ_0, vortex separation, b_0, and flight speed, V, which represent the aircraft weight class heavy and resulting characteristic time scales and initial descent speeds (maxima and minima in bold).

4.4. Wake-Vortex Prediction

Wake-vortex prediction is conducted with the Probabilistic Two-Phase wake-vortex decay model (P2P) which is described in detail in [13]. Applications, assessments and further developments are reported in [6], [14], [15], and [16]. P2P considers all effects of the leading order impact parameters: aircraft configuration (span, weight, velocity, and trajectory), wind (cross and head components), wind shear, turbulence, temperature stratification, and ground proximity. P2P has been validated against data of over 1,300 cases gathered in two US and five European measurement campaigns.

Precise deterministic wake vortex predictions are not feasible operationally. Primarily, it is the nature of turbulence that deforms and transports the vortices in a stochastic way and leads to considerable spatiotemporal variations of vortex position and strength. Moreover, the variability of environmental conditions must be taken into account. Therefore, the output of P2P consists of confidence intervals for vortex position and strength (see FIG 6). FIG 6 illustrates asymmetric vortex rebound characteristics caused by crosswind in ground proximity.

For the time being, the confidence intervals for y, z, and Γ_0 are adjusted to 2σ-probabilities. The respective uncertainty allowances are achieved by a training procedure which employs statistics of measured and predicted wake vortex behaviour [15]. Note that the training procedure implicitly considers the quality of the meteorological input data. As a consequence, uncertainty allowances of wake-vortex

predictions based on the high-quality SODAR/RASS measurements in the lowest three gates are smaller than uncertainty allowances applied to wake-predictions at higher altitudes which are based on NOWVIV input.

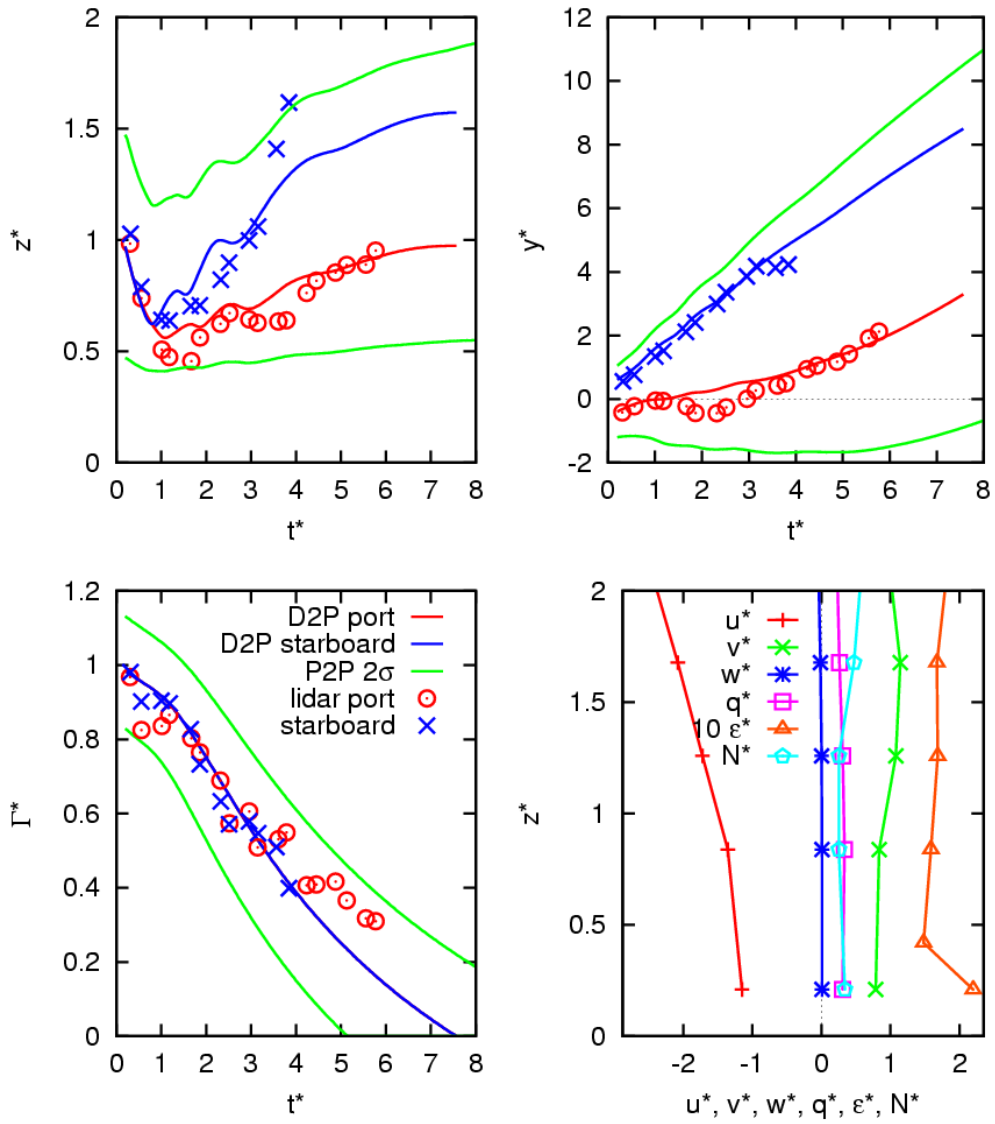

FIG 6. Evolution of normalized vertical and lateral positions and circulation in ground proximity. Measurements by lidar (symbols) and predictions with P2P wake vortex model (lines). Red and blue lines denote deterministic behaviour, green lines are probabilistic envelopes (95.4%). Right below vertical profiles of measured meteorological parameters. Normalizations based on initial values of vortex spacing, circulation, and time needed to descend one vortex spacing.

4.5. Safety-Area Prediction

Once the potential positions of the wake vortices at each gate are known, safe distances between wake vortex core positions and the follower aircraft need to be assigned. The Simplified Hazard Area (SHA) concept [11], [20] predicts distances which guarantee safe and undisturbed operations.

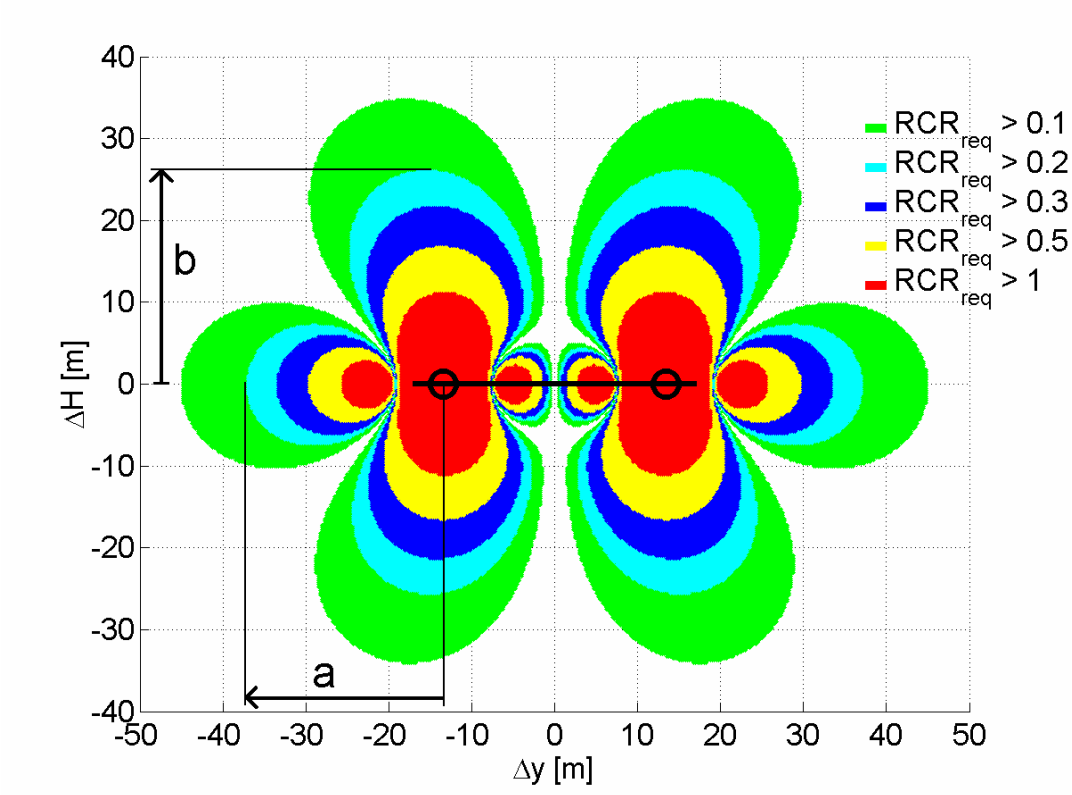

FIG 7. Roll control power required to compensate wake-vortex induced rolling moments. Horizontal and vertical allowances a and b for $RCR_{req} < 0.2$.

The SHA-concept assumes that for encounters during approach and landing the vortex induced rolling moment constitutes the dominant effect and can be used to define a safety area representing the entire aircraft reaction. Then encounter severity can be characterized by a single parameter, the required Roll Control Ratio RCR_{req} which relates the roll control input that is required to compensate the exerted rolling moment to the maximum available roll control power.

In FIG 7 the red areas with $RCR_{req} > 1$ denote regions where the roll capability of the follower aircraft is exceeded. Full flight simulator investigations yield acceptable results for manual control for a value of $RCR_{req} = 0.2$ [20]. Results from real flight tests using DLR's fly-by-wire in-flight simulator ATTAS support this conclusion [19]. In FIG 8 the lines a and b denote the resulting distances between vortex centres and follower aircraft for $RCR_{req} < 0.2$ which are added to the wake vortex envelopes.

As for wake vortex prediction no individual wake vortex and follower aircraft pairings are considered for the WSVBS (although that would be possible) but wake vortex envelopes which represent the heavy category are combined with the follower categories medium

or heavy. In order to represent the follower aircraft weight classes heavy and medium all relevant aircraft parameters (wing span, wing area, airspeed, lift gradient, maximum roll control power, and taper ratio) are conservatively combined to mimic the worst case scenarios. The values of the worst case parameter combinations are again derived from envelopes of aircraft parameters as function of MTOW, similarly as it was described in section 4.3 for wake vortex prediction. This method of using MTOW based aircraft parameters for the determination of simplified hazard areas is called SHAPe (Simplified Hazard Area Prediction) [11].

5. SYSTEMS INTEGRATION

This section describes how the above introduced components are combined for the prediction of adapted aircraft separations. Section 5.1 considers components within a single gate, section 5.2 then explains how the minimum temporal aircraft separations are derived from the predictions within all the gates. Finally, section 5.3 sketches the temporal prediction cycle which defines parameters like update rate and prediction horizon.

5.1. Components in Single Gate

FIG 8 illustrates the process seen in flight direction in control gate 11 for the leader aircraft parameter combination Γ_{0uu}, b_{0uu} and a vortex age of 100 s. The different ellipses are defined by the respective sums of vertical and horizontal probabilistic allowances of the components approach corridor, vortex area prediction, and safety area prediction. Note that horizontal and vertical dimensions in FIG 8 are in scale.

The dark blue corridor of possible vortex positions indicates that superimposed to vortex descent a southerly cross-wind advects the wake from runway 25L to 25R. Because the lateral vortex position can only be predicted less precise (uncertainty and variability of crosswind) than vertical position (cf. FIG 4), the aspect ratio of the vortex area ellipse exceeds a value of eight. Out of ground effect this aspect ratio is much smaller because there uncertainties regarding vortex descent are increased [16]. Safety area margins for aircraft pairings HH and HM are added to the vortex corridors, resulting in overall safety areas to be avoided.

One important aspect is that the safety corridors are not static but move depending on wake transport. Further, they grow due to vortex spreading and shrink according to wake decay.

For aircraft pairings on approach to a single runway, the time interval between the passage of the generator aircraft through a gate and the time when a safety area does no longer overlap with the approach corridor (gate obstruction time) determines the minimum temporal separation for that gate. For the parallel runway system, the question is whether the safety areas reach the neighbouring runway within the prediction horizons. The prediction horizons of 100 s for HH and of 125 s for HM are derived from the temporal equivalents to ICAO separations used by the DLR Arrival Manager (AMAN).

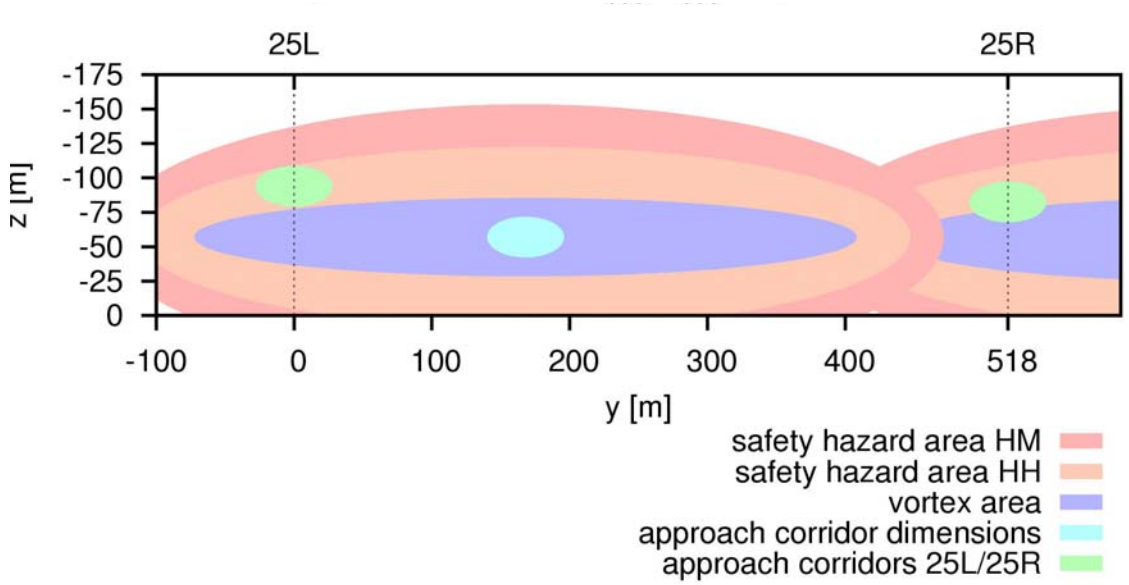

FIG 8. Ellipses denoting approach corridor dimensions, vortex areas, and safety areas in gate 11 for a vortex age of 100 s.

Our example in FIG 8 illustrates that after 100 s the vortex area has just left the approach corridor of runway 25L, yet the gate is blocked as both safety corridors still overlap with the approach corridor. On the other hand, after 100 s the safety envelopes for HH and HM have not reached glide path corridor 25R. However, at 125 s the HM envelope obviously will reach the glide path 25R, so that this runway can be used independently from 25L only by heavy aircraft. Safety areas from 25R in turn will not reach the corridor 25L, so 25L can be used independently from 25R for both follower weight categories.

5.2. Complete Domain

One prediction sequence comprises 13 gates for each runway, 8 generator aircraft parameter combinations, 3 runway combinations (generator and follower on single runway (25L25L or 25R25R), generator on 25L and follower on 25R (25L25R), and vice versa), and 2 follower weight classes. So in total 1248 cases are considered. From the 1248 cases for each of the 3 runway combinations and 2 follower weight classes the cases with maximum vortex ages with conflicts are identified. These maximum gate obstruction times define minimum aircraft separation times MST. The output of the WSVBS consequently consists of the following matrix.

rwy comb.	MST HH [s]	MST HM [s]
25L25L	100	125
25L25R	0	125
25R25L	0	0
25R25R	100	125

TAB 3. Minimum separation times for different runway and weight category combinations.

Note that the MST in TAB 3 are consistent with the situation displayed in FIG 8. In TAB 3 a MST = 0 s means that no aircraft separation with regard to wake vortices is needed, i.e. vortices do not reach the adjacent runway. In practise the aircraft separations can then be reduced to radar separation (for example 70 s). The translation of the separation matrix into procedures and displays which are suitable for air traffic control (ATC) is described in part II of the paper.

The idea is that all corridors used in the process and shown in FIG 8 should be based on identical probability levels, currently, twice the standard deviations (2σ) of respective data. However, the safety area prediction concept on one hand is not probabilistic, i.e. the predicted safety areas are safe without any exception for the investigations conducted so far, and on the other hand it assumes that the wake vortices are situated along the envelopes of the vortex area. A reduction of vortex area allowances to 1.7σ (91.1%) causes that the safety areas are only added to 95.4% of the potential wake vortex positions and herewith implicitly confers a 2σ-confidence level to the safety area module.

Unfortunately, the very question: “Which overall safety is actually achieved by the combination of the various conservative elements of the WSVBS?” can not be answered easily. It is planned to adjust all components to consistent confidence levels once the methodology of a comprehensive risk analysis is established.

5.3. Prediction Cycle

Every 10 minutes new Sodar/RASS and NOWVIV data are available. Then the WSVBS predicts MST matrices for a 60 min horizon with 10 min-increments. For planning purposes this guarantees availability of predictions for at least 45 min in advance. The last 10 min of the predictions are not touched to ensure the stability of the system.

6. WAKE-VORTEX MONITORING

Wake-vortex monitoring is used to identify potential erroneous predictions of the WSVBS. For this purpose DLR’s 2 µm pulsed Doppler LIDAR is operated in vertical scan mode with elevations between 0° to 6° to detect and track the vortices alternately in the three lowest and most critical gates of runway 25R (see part II of this manuscript). Once the real-time capability of vortex monitoring is established it is foreseen to integrate a conflict detection module which may issue warnings and/or may adapt the WSVBS predictions (see FIG 1).

7. CONCLUSIONS

The manuscript describes the design of the Wake Vortex Prediction and Monitoring System WSVBS with all its components and their interaction. The WSVBS consists of components that consider meteorological conditions, aircraft glide path adherence, aircraft parameter combinations representing aircraft weight categories, the resulting wake-vortex behaviour, the surrounding safety areas, and wake vortex monitoring. The elements of the WSVBS are generic and can well be adjusted to other runway systems and airport locations.

A specific feature of the WSVBS is the usage of both measured and predicted meteorological quantities as input to wake vortex prediction. In ground proximity where the probability to encounter wake vortices is highest, the wake predictor employs measured environmental parameters that yield superior prediction results. For the less critical part aloft, which can not be monitored completely by instrumentation, the meteorological parameters are taken from dedicated numerical terminal weather predictions. The wake vortex model predicts envelopes for vortex position and strength which implicitly consider the quality of the meteorological input data. This feature is achieved by a training procedure which employs statistics of measured and predicted meteorological parameters and the resulting wake vortex behaviour.

The WSVBS combines various conservative elements that presumably lead to a very high overall safety level of the WSVBS. a) Wake vortex prediction as well as safety area prediction employs worst case combinations of aircraft parameters that represent complete aircraft weight categories. b) The wake vortex model assumes that the aircraft are situated on the envelopes of the approach corridors. (The probability that this assumption actually occurs is extremely small.) Likewise, the safety area model assumes that the wake vortices are situated along the wake vortex envelopes. As a consequence the probability to actually encounter wake vortices at the edges of the safety areas is outermost small. c) The most critical within 1248 investigated parameter combinations determines the possible aircraft separations. d) A safety net consisting of a LIDAR that scans the most critical gates at low altitude monitors the correctness of suggested aircraft separations. The combination of these conservative measures certainly leads to a very high but currently unknown overall safety. Once the methodology of a comprehensive risk analysis will be established, it is planned to adjust all components to appropriate and consistent confidence levels.

ACKNOWLEDGEMENTS

The work presented here was funded by the DLR project *Wirbelschleppe* and benefited from the EU projects *ATC-Wake* (IST-2001-34729), *FAR-Wake* (AST4-CT-2005-012238), *FLYSAFE* (AIP4-CT-2005-516 167), and the European Thematic Network *WakeNet2-Europe* (G4RT-CT-2002-05115). We greatly appreciate the excellent support of the teams from DFS Deutsche Flugsicherung GmbH, DWD Deutscher Wetterdienst, Fraport AG, and METEK GmbH.

REFERENCES

[1] Challenges to Growth 2004 Report, Eurocontrol, Brussels, 2004.
[2] J.B. Critchley, P.B. Foot, UK CAA Wake Vortex Database: Analysis of Incidents Reported Between 1982 and 1990, Civil Aviation Authority, CAA Paper 91015, 1991.
[3] G. Doms, U. Schaettler, The nonhydrostatic Limited Area Model LM (Lokal Modell) of DWD. Part I: Scientific Documentation, Deutscher Wetterdienst, Offenbach, 1999.
[4] H. Frauenkron, M. Maiss, P. Nalpanis, FLIP - Flight Performance using Frankfurt ILS, DFS German Air Navigation Services, Air Traffic Management Division, Version 2.0, 2001.
[5] M. Frech, A simple method to estimate the eddy dissipation rate from SODAR/RASS measurements, 16th Symposium on Boundary Layers and Turbulence, AMS, Portland, Paper 6.13, 2004, p. 4.

[6] M. Frech, F. Holzäpfel, Skill of an aircraft wake-vortex transport and decay model using short-term weather prediction and observation, 12th Conference on Aviation, Range, and Aerospace Meteorology, Atlanta, Paper 6.9, 2006, p. 10 (to be published in J. Aircraft).
[7] M. Frech, F. Holzäpfel, A. Tafferner, T. Gerz, High-Resolution Weather Data Base for the Terminal Area of Frankfurt Airport, J. Appl. Meteor. Climat. 46 (2007) 1913-1932.
[8] T. Gerz, F. Holzäpfel, W. Bryant, F. Köpp, M. Frech, A. Tafferner, G. Winckelmans, Research towards a wake-vortex advisory system for optimal aircraft spacing, Comptes Rendus Physique +6 (2005) 501-523.
[9] T. Gerz, F. Holzäpfel, W. Gerling, A. Scharnweber, M. Frech, A. Wiegele, K. Kober, K. Dengler, S. Rahm, The Wake Vortex Prediction and Monitoring System WSVBS - Part II: Performance and ATC Integration at Frankfurt Airport, 1st European Air and Space Conference (CEAS 2007) / Deutscher Luft- und Raumfahrtkongress 2007, CEAS-2007-178, 10-13 September 2007, Berlin, Germany, pp. 3391-3399.
[10] G.A. Grell, S. Emeis, W.R. Stockwell., T. Schoenemeyer, T. Forkel, J. Michalakes, R. Knoche, W. Seidl, Application of a multiscale, coupled MM5/chemistry model to the complex terrain of the VOTALP valley campaign, Atmosph. Environ. 34 (2000) 1435-1453.
[11] K.-U. Hahn, C. Schwarz, H. Friehmelt, A Simplified Hazard Area Prediction (SHAPe) Model for Wake Vortex Encounter Avoidance, 24th International Congress of Aeronautical Sciences, Yokohama (Japan), 29 August - 3 September 2004, ICAS, 24th International Congress of Aeronautical Sciences Proceedings, 2004
[12] R. Hemm, G. Shapiro, D.A. Lee, J. Gribko, B. Glaser, Benefit Estimates of Terminal Area Productivity Program Technologies. NASA/CR-1999-208989, 1999, p. 144.
[13] F. Holzäpfel, Probabilistic Two-Phase Wake Vortex Decay and Transport Model, J. Aircraft 40 (2003) 323-331.
[14] F. Holzäpfel F., R.E. Robins, Probabilistic Two-Phase Aircraft Wake-Vortex Model: Application and Assessment, J. Aircraft 41 (2004) 1117-1126.
[15] F. Holzäpfel, Probabilistic Two-Phase Aircraft Wake-Vortex Model: Further Development and Assessment, J. Aircraft 43 (2006) 700-708.
[16] F. Holzäpfel, M. Steen, Aircraft Wake-Vortex Evolution in Ground Proximity: Analysis and Parameterization, AIAA J. 45 (2007) 218-227.
[17] F. Holzäpfel, T. Gerz, M. Frech, A. Tafferner, F. Köpp, I. Smalikho, S. Rahm, K.-U. Hahn, C. Schwarz, The Wake Vortex Prediction and Monitoring System WSVBS - Part I: Design, 1st European Air and Space Conference (CEAS 2007) / Deutscher Luft- und Raumfahrtkongress 2007, CEAS-2007-177, 10-13 September 2007, Berlin, Germany, pp. 3383-3390.
[18] F. Holzäpfel, M. Frech, T. Gerz, A. Tafferner, K.-U. Hahn, C. Schwarz, H.-D. Joos, B. Korn, H. Lenz, R. Luckner, G. Höhne, Aircraft Wake Vortex Scenarios Simulation Package - WakeScene, ICAS 2006, 25th International Congress of the Aeronautical Sciences, Hamburg, ICAS 2006-8.6.3, 2006, pp. 12 (Aerosp. Sci. Technol., in print).
[19] C. Schwarz, K.-U. Hahn, Simplified Hazard Area for Wake Vortex Encounter Avoidance, AIAA Paper 2005-5903, AIAA Atmospheric Flight Mechanics Conference, San Francisco, CA, August 2005, pp. 5903.1 -5903.9.
[20] C.W. Schwarz, K.-U. Hahn, Full-flight simulator study for wake vortex hazard area investigation, Aerosp. Sci. Technol. 10 (2006) 136-143.
[21] Wake Vortex Research Needs for ``Improved Wake Vortex Separation Ruling" and ``Reduced Wake Signatures", Final Report of the Thematic Network 'WakeNet2-Europe', 6th Framework Programme, National Aerospace Laboratory, NLR-CR-2006-171, Amsterdam, 2006.

THE WAKE VORTEX PREDICTION & MONITORING SYSTEM WSVBS

PART II: PERFORMANCE AND ATC INTEGRATION AT FRANKFURT AIRPORT

T. Gerz[1], F. Holzäpfel[1], W. Gerling[2], A. Scharnweber[2],
M. Frech[1], A. Wiegele[1], K. Kober[1], K. Dengler[1], S. Rahm[1]
[1] Institut für Physik der Atmosphäre
Deutsches Zentrum für Luft- und Raumfahrt (DLR),
Oberpfaffenhofen, D-82234 Wessling, Germany
[2] Institut für Flugführung
Deutsches Zentrum für Luft- und Raumfahrt (DLR),
Lilienthalplatz 7, D-38108 Braunschweig, Germany

OVERVIEW

The performance and ATC integration of DLR's wake vortex advisory system "WSVBS" (*Wirbelschleppen-Vorhersage- und -Beobachtungssystem*) for the dependent parallel runway system 25L and 25R at Frankfurt Airport are described. WSVBS has components to forecast and monitor the local weather and to predict and monitor wake transport and decay along the glide paths. It is integrated in the arrival manager AMAN of DLR. Each 10 minutes it delivers minimum safe aircraft separation times for the next hour to air traffic control. These times are translated into operational modes for runways 25L/R aiming at improving the capacity. From 66 days of a performance test at Frankfurt it was found that the system ran stable and the predicted minimum separation times were safe. The capacity improving concepts of operation could have been used in 75% of the time and continuously applied for at least several tens of minutes. From fast-time simulations the eventual capacity gain for Frankfurt was estimated to be 3% taking into account the real traffic mix and operational constraints in the period of one month.

1. INTRODUCTION

Aircraft trailing vortices may pose a potential risk to following aircraft. The empirically motivated separation standards between consecutive aircraft which were introduced in the 1970s still apply. These aircraft separations limit the capacity of congested airports in a rapidly growing aeronautical environment. Capacity limitations are especially drastic and excruciating at airports like in Frankfurt (Germany) with two closely spaced parallel runways (CSPR) where the possible transport of wakes from one runway to the adjacent one by cross-winds impedes an independent use of both runways.

To increase airport capacity for landing aircraft, DLR has developed a wake vortex advisory system named WSVBS, German for Wake Vortex Prediction and Monitoring System [5]. The WSVBS is intended to dynamically adjust aircraft separations dependent on weather conditions and the resulting wake vortex behaviour without compromising safety. The system is particularly designed for the closely spaced parallel runway system of Frankfurt Airport (Fig. 1) but can be adapted to any other airport. It predicts wake vortex transport and decay and the resulting safety areas along the glide slope from final approach fix to threshold. The design of the WSVBS is described in Part I [13]. Here we particularise its performance at Frankfurt Airport and indicate possible gains in capacity if the WSVBS should be installed at Frankfurt and used by air traffic control (ATC) authorities.

Fig. 1. Frankfurt Airport with the two parallel runways 25L and 25R, spaced by 1727 feet (518 m).

2. INSTALLATION AT FRANKFURT AIRPORT

The WSVBS with its components (*tools*)

- weather forecast (*NOWVIV*),
- wake vortex predictor (*P2P*),
- safety area predictor (*SHAPe*),
- weather profiler (*SODAR/RASS/SONIC*), and
- wake detector (*LIDAR*) as a safety net

has been employed at Frankfurt Airport in the period of December 2006 until February 2007. The system used forecasted and measured meteorological parameters along the glide path to predict temporal separations of aircraft landing on the parallel runway system 25L/R and translated the required separation between two aircraft into approach procedures. At the same time, the transport of the wake vortices was monitored by the wake detector component (LIDAR) in different control gates. All components of the WSVBS are described in detail in [13]. Here we summarise some specific features of the set-up at Frankfurt Airport.

Fig. 2 sketches the instrumentation layout at Frankfurt Airport. It depicts runways 25L and 25 R with the locations of the employed sensors and the local operation centre (LOC) which is situated in the observer house of the German weather service (DWD). Close to the LOC midway between the glide paths a METEK SODAR with a RASS extension provides 10-minute averages of vertical profiles of the three wind components, vertical fluctuation velocity, and virtual temperature with a vertical resolution of 20 m and up to 300 m AGL. The SODAR/RASS system is complemented by an ultrasonic ane-

mometer (USA) mounted on a 10 m mast which measured wind and temperature with a frequency of 20 Hz. Eddy dissipation rate (EDR) profiles are derived from vertical fluctuation velocity and the vertical wind gradient employing a simplified budget equation [2]. A spectral analysis of the longitudinal velocity measured by the sonic is used to estimate EDR by fitting the -5/3 slope in the inertial subrange of the velocity frequency spectrum. Due to the position of the SODAR/RASS/SONIC between the extended centrelines of both runways these data are considered representative for the area where aircraft and vortices are in ground proximity. In the LOC a Linux-PC is installed which is connected via ethernet to the SODAR/RASS/USA system and via UMTS to the computers at DLR and to the LIDAR container. This PC serves as a front-end for the weather and wake forecasts and observations.

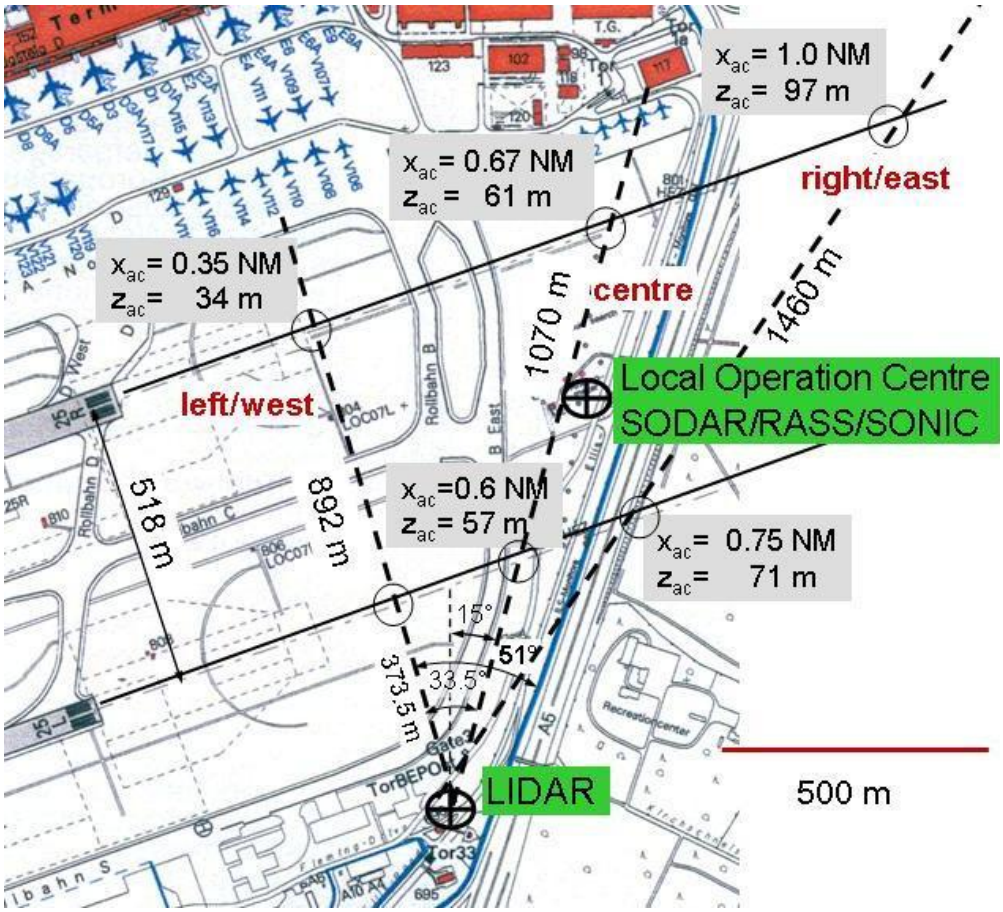

Fig. 2. The instrumentation layout at Frankfurt Airport; x_{ac}, z_{ac} denote the distance to touch-down zone and the height of landing aircraft in the three vertical scan planes of the LIDAR (dashed lines); LOC and the meteorological profiler were situated between both extended runway centrelines. Map reprinted by courtesy of Fraport AG.

The weather forecast model NOWVIV [3, 4, 5] ran twice a day on a massively parallel LINUX cluster at University Stuttgart where it predicted the meteorological conditions for the Frankfurt Airport Terminal Area. The forecast output was sent via UMTS to a LINUX-PC in the Local Operation Centre (LOC) (situated in the observer house of DWD) to be used by the real-time wake predictor P2P (Fig. 3).

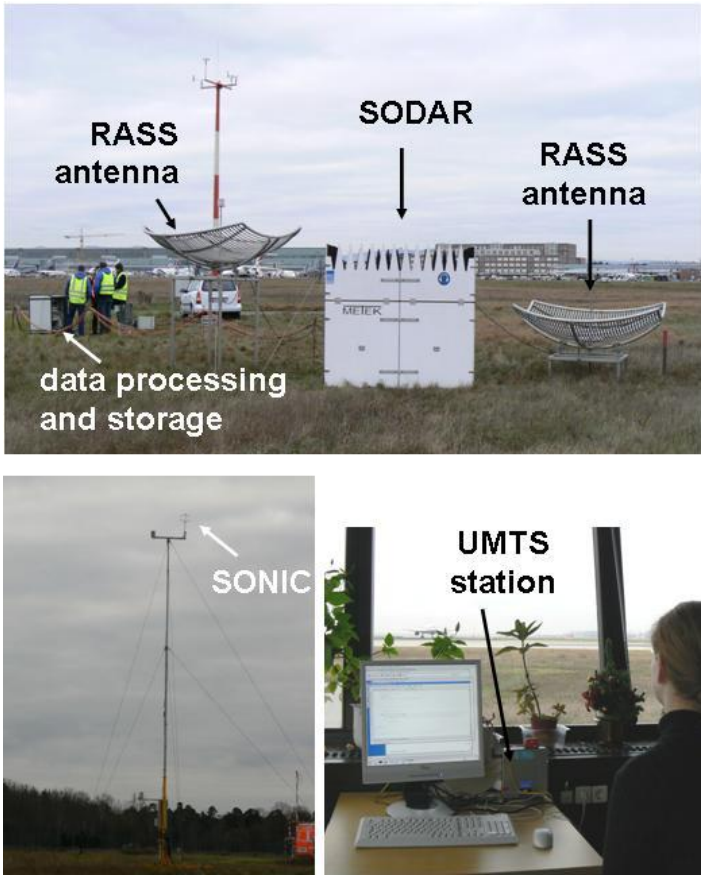

Fig. 3. Meteorological instruments at Frankfurt Airport. Top & lower left: SODAR/RASS and SONIC by Fa. Metek; lower right: the LOC with LINUX-PC & UMTS station in the DWD observer house.

Fig. 4 shows two examples of diurnal variations of horizontal wind profiles, a weak wind condition on 15th of January and a stronger wind case on the following day. The height range covered by the SODAR/RASS measurements depends on the backscatter properties and ambient noise level in the boundary layer which vary during the day. The NOWVIV forecasts are only plotted in the range where observations were available. Also indicated are the differences between observed and predicted cross-wind u_c. On the calm day the deviation between observation and prediction was about ±1.5 m/s on average but considerably larger in the early morning hours between 2 and 5 UTC. This was due to a south-westerly low level jet which developed and vanished earlier than anticipated by the forecast yielding to the blue and red u_c-deviation dipole. So, the phenomenon – the low level jet – was predicted but with a delay of about 2 hours. A similar phenomenon was observed on the next morning but now the jet developed later than predicted. The generally higher winds on the 16th of January also indicate that the weather was dominated by advection processes (large scale weather patterns) where initial and boundary conditions for NOWVIV have a larger impact than on the 15th where the weather was driven by local orographic and land-use features.

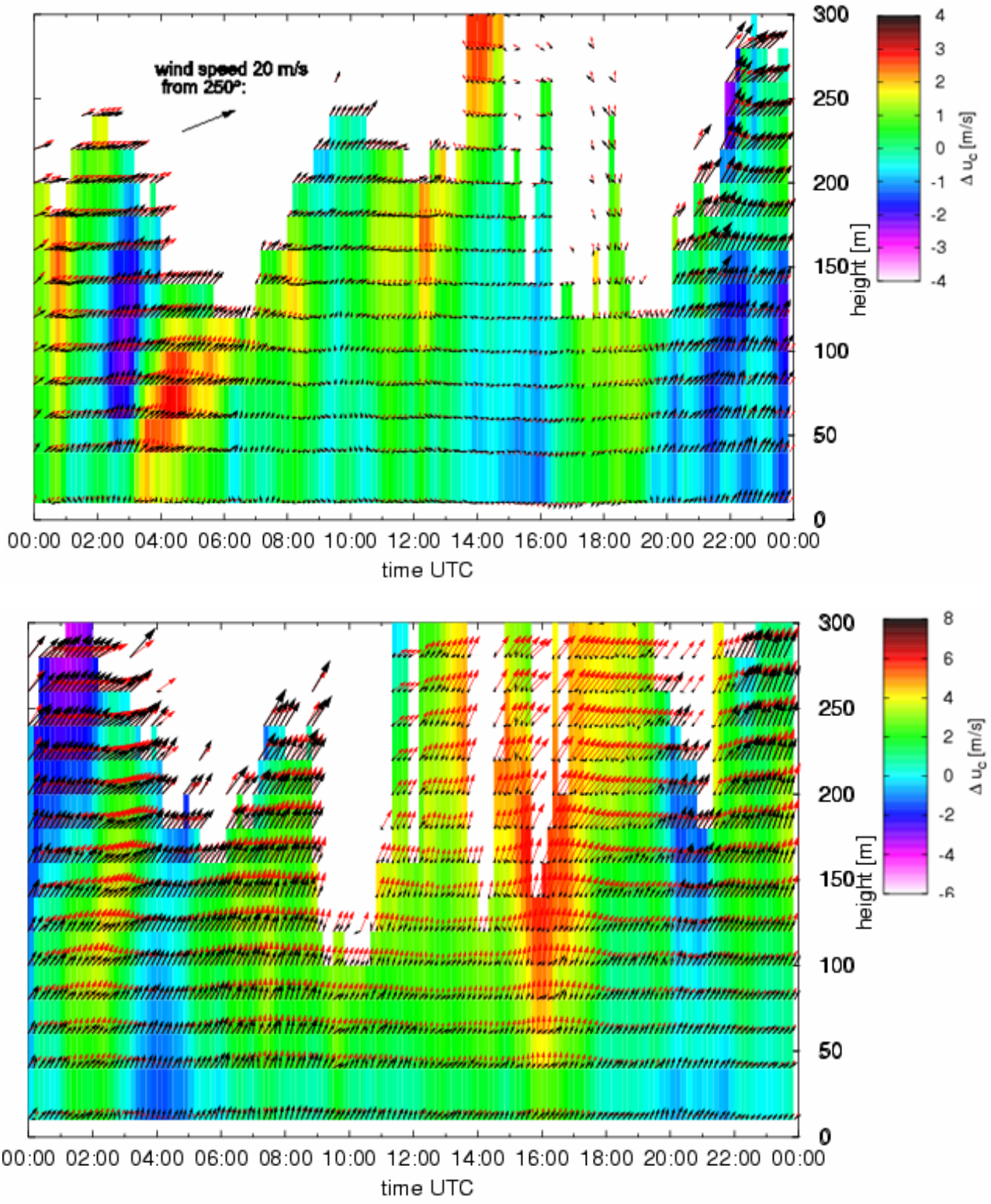

Fig. 4. Diurnal variations of the wind velocity profile measured by SODAR/RASS (black) and predicted by NOWVIV (red) on 15.01.07 (top) and 16.01.07 (bottom). Deviations in cross-wind u_c between observation and prediction are colour coded.

The real-time probabilistic two-phase wake vortex decay and transport model P2P [3, 8, 9, 10, 11, 13] was fed by the measured and forecast meteorological profiles and computed envelopes of the behaviour and location of wake vortices of aircraft from class HEAVY (H) in 13 gates along the glide path to runways 25L/R at the PC in the LOC. The Simplified Hazard Area Prediction (SHAPe) model [7, 13, 14, 15] then computed safety zones around the area contaminated by the vortices.

DLR's 2 µm pulsed Doppler LIDAR was used as the safety net within the WSVBS concept at Frankfurt Airport. It operated in vertical scan-plane mode with elevations between 0° to 6° to detect and track the vortices alternately in the three lowest and most critical planes (Fig. 2). The LOS velocity in a scanned plane is immediately visible in the so-called "quick-look". These quick-looks were transmitted via UMTS to the LOC computer and were also accessible via internet. Fig. 5 shows a quick-look result from 16. January 2007 at 04:17 UTC in the "centre" vertical scan plane.

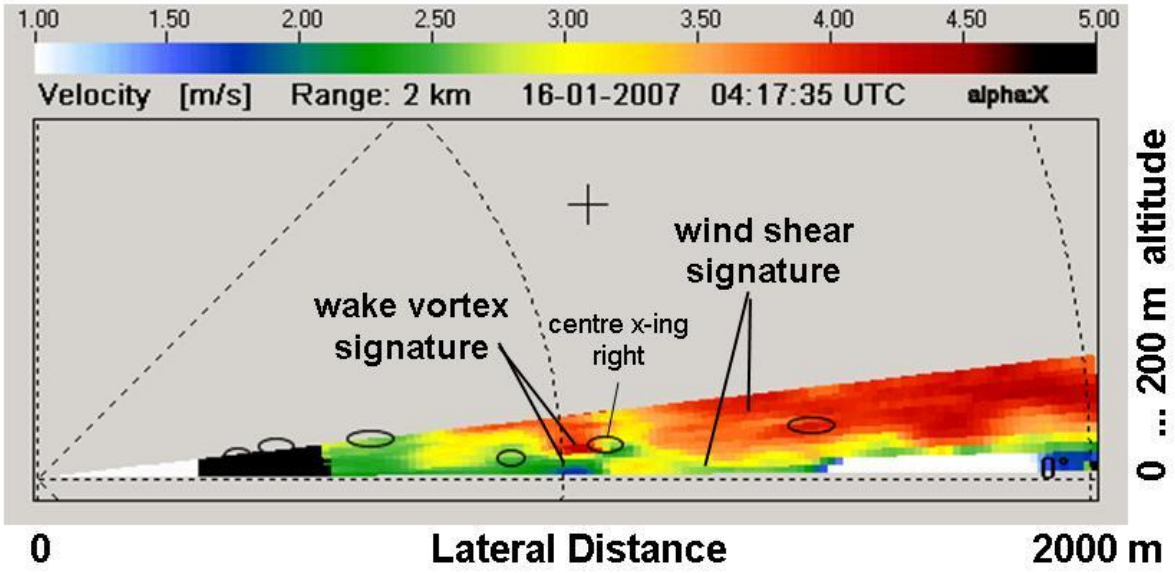

Fig. 5. LOS velocity as measured by LIDAR (quick-look after one scan, positive values indicate velocities away from the instrument) with signatures of wind shear and a wake vortex pair. The crossings of the laser beam with the glide paths are indicated by small ellipses; "centre x-ing right" identifies the approximate intersection of the beam in scan plane "centre" with runway 25R at 1070 m distance.

At that time most heavy aircraft landed on runway 25R (the northern runway). The colour-coded area shows the line-of-sight (LOS) wind component. Patterns of wind shear and of a wake vortex pair can be distinguished. The quick-look also indicates roughly the position of the two flight corridors for landing aircraft in the scan plane. Thus, it is possible to check if the predicted minimum separation times are correct: the vortices visible in the LIDAR quick-look should not reside within the flight corridors when the forecast system allows the next aircraft to enter the control gate. The quick-look, however, only allows for a rough estimate of the vortex location. After signal and image (post-) processing, the spatial resolution of the LOS velocity is 3 m and the wake vortex position (and strength) can be deduced with high accuracy, see Section 4.

3. INTEGRATION INTO ATC PROCEDURES

3.1. The concepts of operation

The German Air Safety Provider DFS has established four modes or concepts of operation for aircraft separation to be applied for the dependent parallel runway system at Frankfurt Airport under instrumented meteorological conditions (IMC), see Fig. 6 & [6]:

- "ICAO" – standard procedure under IMC with 4 NM for a HH aircraft pair and 5 NM for a HM pair across both runways;

- “Staggered” (STG) – procedure where both runways can be used independently from each other but obeying the radar (minimum) separation of 2.5 NM;
- “Modified Staggered Left” (MSL) – aircraft on right (windward) runway keep 2.5 NM separated from aircraft of left (lee) runway;
- “Modified Staggered Right” (MSR) – aircraft on left (windward) runway keep 2.5 NM separated from aircraft of right (lee) runway.

Note that in all modes, the aircraft in-trail (approaching the same runway) remain separated according to ICAO standards. The modes STG, MSL, MSR can only be applied on favorable weather conditions (esp. favorable cross-wind) and require the use of a wake vortex advisory system as DLR’s WSVBS or DFS’ wake vortex warning system, WSWS [6]. These modes are not used operationally today.

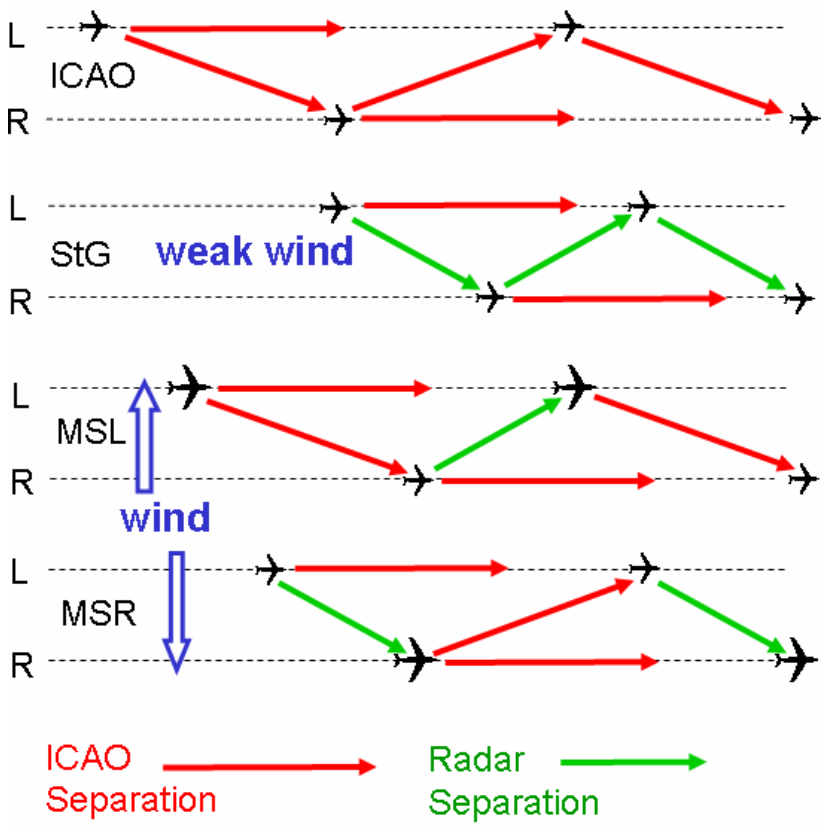

Fig. 6. The concepts of operation under IMC for the dependent parallel runway system at Frankfurt Airport.

Tab. 1 translates the operationally applied separation distances for HH, HM and radar separation into separation times which must be followed in each concept of operation and for each runway combination. For 5 and 4 NM separation we applied an approach speed of 74 m/s (144 knots) to all aircraft. For the minimum (radar) separation we took conservative 70 s (instead of 62.5 s).

ICAO	H-H	H-M	STG	H-H	H-M
LL	100 s	125 s	LL	100 s	125 s
LR	100 s	125 s	LR	70 s	70 s
RL	100 s	125 s	RL	70 s	70 s
RR	100 s	125 s	RR	100 s	125 s

MSR	H-H	H-M	MSL	H-H	H-M
LL	100 s	125 s	LL	100 s	125 s
LR	100 s	125 s	LR	70 s	70 s
RL	70 s	70 s	RL	100 s	125 s
RR	100 s	125 s	RR	100 s	125 s

Tab. 1. Aircraft separation times for the four DFS concepts of operation ICAO, STG, MSL, MSR and the four runway combinations of leader and follower aircraft (e.g., RL = leader on 25R, follower on 25L runway).

3.2. The prediction cycle

The installation of the WSVBS at Frankfurt Airport was accomplished on 19th of December 2006. It then delivered data on 66 days until 28/02/07. The chain started with the forecast of the local weather twice a day at 0 and 12 UTC. The SODAR/RASS/SONIC ran continuously 24 hours a day and delivered measured weather profiles each 10 min. With these weather data the areas of possible vortex locations and the surrounding safety areas were computed by P2P and SHAPe. This forecast was made each 10 min for both runways at all 13 gates with a forecast horizon of 60 min (controllers require at least 45 min). The *minimum separation time MST* between two aircraft landing on the same or the adjacent parallel runway is determined by the maximum time, computed in all gates for the respective aircraft weight class combinations.

Based on the MST, landing procedures were eventually recommended and displayed on the PC in the Local Operation Centre as shown in Fig. 7 and Fig. 8 and also accessible remotely via Internet. Fig. 7 is updated each ten minutes and adjusted to the progressing time each minute. The figure shows that for most of the forecast time the operational procedure MSL can be used with a short period where the (northerly) wind is so weak that the runways can be used independently (STG). After 50 minutes the system anticipates a change which requires a return to the standard separations (ICAO).

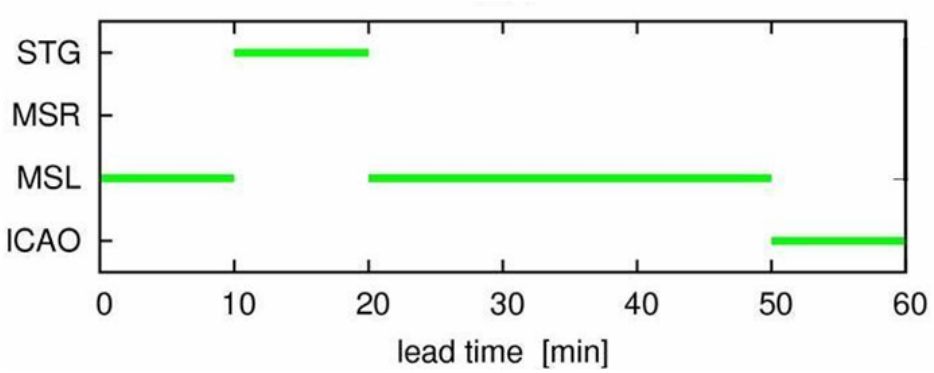

Fig. 7. Indicated use of DFS approach procedures within the next hour.

Fig. 8 displays the full MST information as it is available in the WSVBS. In addition to the four procedures which were defined by DFS, such a display allows also to survey possible reduced separations for aircraft flying in-trail and it further distinguishes HH and HM aircraft pairs. The sketched example reads that not only the DFS procedure MSL can be used (no wake-vortex separation required for runway combination 25L25R but full ICAO separation for 25R25L), but that also aircraft which follow each other on the same runway (in-trail) can be radar-separated. The meteorological reason for that case is a strong northerly crosswind that clears both runways quickly from vortices of the leading aircraft.

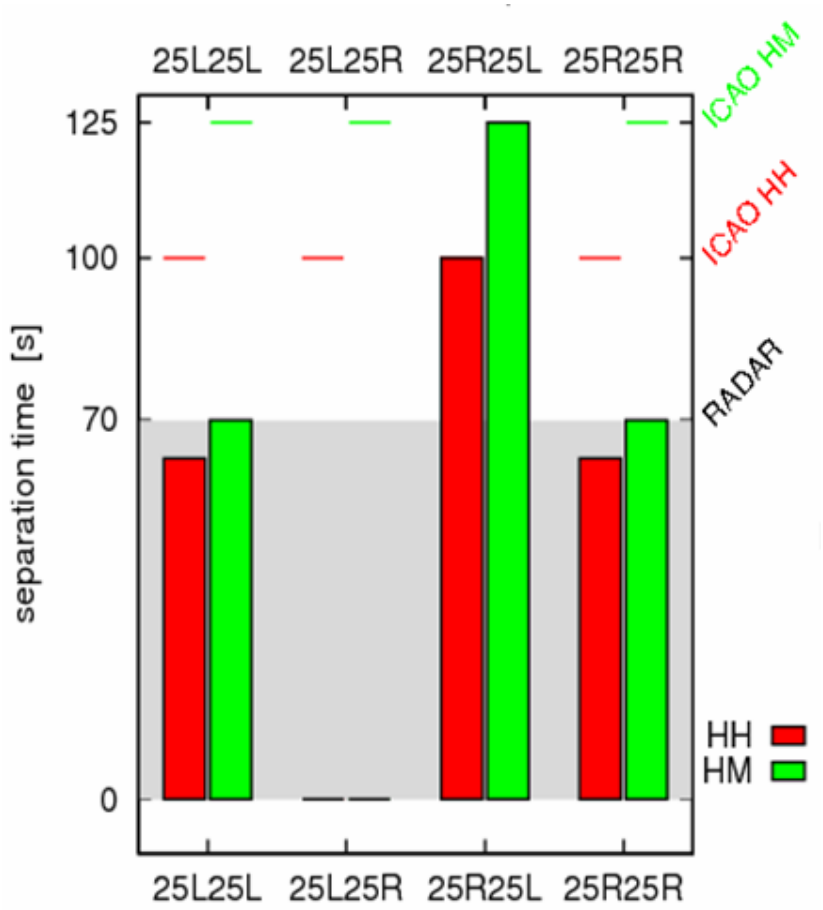

Fig. 8. Display of full MST information and derived arrival procedures for Frankfurt Airport on 2007-Jan-25 at 15:10 UTC.

3.3. The Human-machine interfaces

The proposed operational procedures for up to one hour were also displayed on controller screens for the real-time simulations. The layout has been developed with and accepted by controllers. Fig. 9 shows two green bars along the dynamic time scale indicating mode MSL for the period 07:06 until 07:29 and mode STG afterwards. Upon request from controllers also the wind direction and speed at heights FL 70 and 4000 feet and on ground were displayed. The green bars along the final approach paths on the radar display in Fig. 10 show another situation where mode STG can be used with a change towards mode MSL.

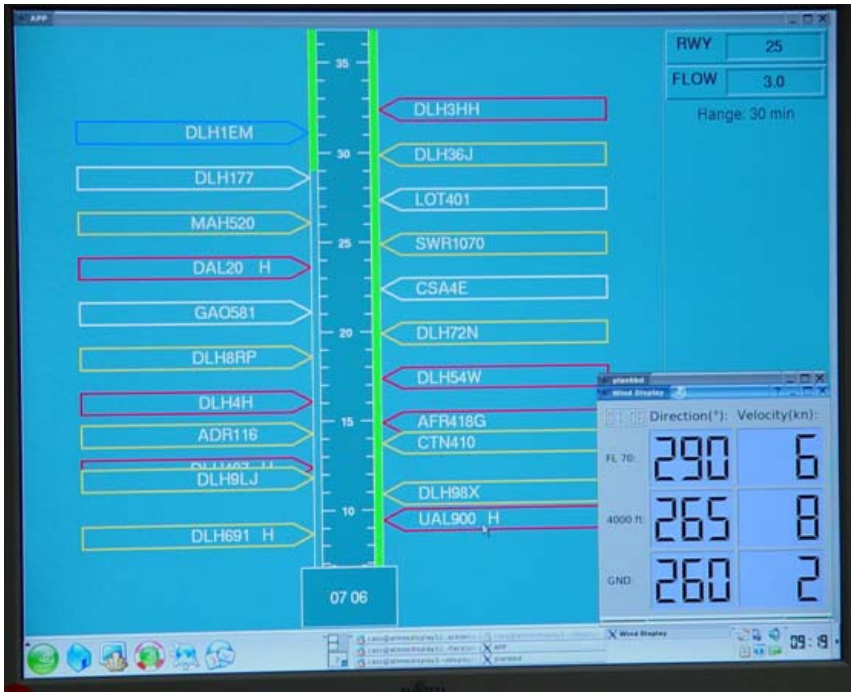

Fig. 9. Controller's planning screen with dynamic time scale and wind information.

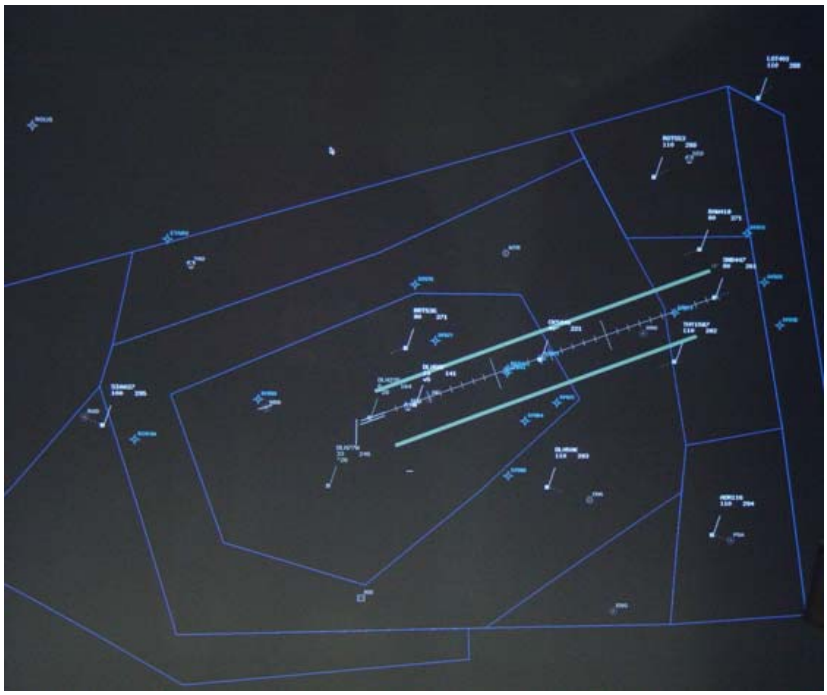

Fig. 10. Controller's radar screen.

4. PERFORMANCE AND IMPROVED CAPACITY

To check if the WSVBS products and the proposed features on the displays fulfil ATC requirements, are well designed and easy to use, and will eventually improve capacity at Frankfurt Airport, we performed real-time and fast-time simulations using the Air Traffic Management and Operations Simulator (ATMOS II) and the SIMMOD tool of DLR Institute of Flight Guidance at DLR Braunschweig, respectively.

During a period of one week real-time simulations were carried out at the simulator ATMOS II under the assistance of five air traffic controllers from DFS. The investigations aimed at evaluating the behaviour and efficiency of the WSVBS on a real time controller working position and to inquire the controller's judgement of the system.

By means of a systematic questionnaire the controllers from DFS were interviewed with respect to aspects as

- acceptance of the simulation environment,
- acceptance of the WSVBS,
- procedural regulations and human interface,
- operational appliance.

The participating controllers generally agreed with the WSVBS system and procedures. In particular, the system does not interfere with their normal working procedures.

We also performed fast-time simulations to obtain capacity figures for the different concepts of operation utilised by WSVBS under real world conditions. To establish a baseline, the simulations were initially performed using ICAO separations. The simulations were then matched with separations derived from WSVBS and re-run (Fig. 11). The simulations included flight plans with realistic distributions of wake vortex categories, demand peaks throughout the day, weather data, and the WSVBS proposals for a period of one month.

Fig. 11 shows traffic demand and traffic flow for a "heavily loaded" day at Frankfurt with 721 arrivals. Using the WSVBS predictions, MSR separations could be used for 76.4% of the day, with intermittent use of ICAO separations in the morning hours. The peak demand exceeds capacity in both scenarios. However, the WSVBS flow closely follows the demand flow whereas the ICAO flow is unable to cope with the demand and accumulates delayed flights which can only be served in the late evening hours.

Improved capacity at an airport offers a variety of options for future aircraft operations (Fig. 12) which range from an entirely tactical scenario (increase punctuality of flights while keeping number of landings constant) to an entirely strategic scenario (increase the average traffic flow at the expense of higher average delays). Fig. 13 shows the theoretical capacity gain for the different concepts of operation. A SIMMOD model of the parallel runways at Frankfurt Airport was fed with a constant flow of arrivals assuming a traffic mix of 27, 67 and 6% of heavy, medium and light aircraft, respectively. For each number of arrivals per hour the computed flight plans were randomised over ten iterations. The figure reveals that 2 (5) more aircraft can land per hour when changing from ICAO mode to MSL/R (STG) mode, respectively, and accepting an average delay of 4 minutes. Or, vice versa, the average delay of 4 minutes (ICAO) would drop down to a bit more than 2 minutes (STG) when keeping the arrival rate at almost 33 aircraft per hour. The figure also points out that a further increase of capacity beyond 39 arrivals per hour for mode STG would rapidly increase delays, since the system runs into its saturation. When taking into account the real traffic mix and operational constraints in that period of one month we received a net capacity gain of slightly larger 3%.

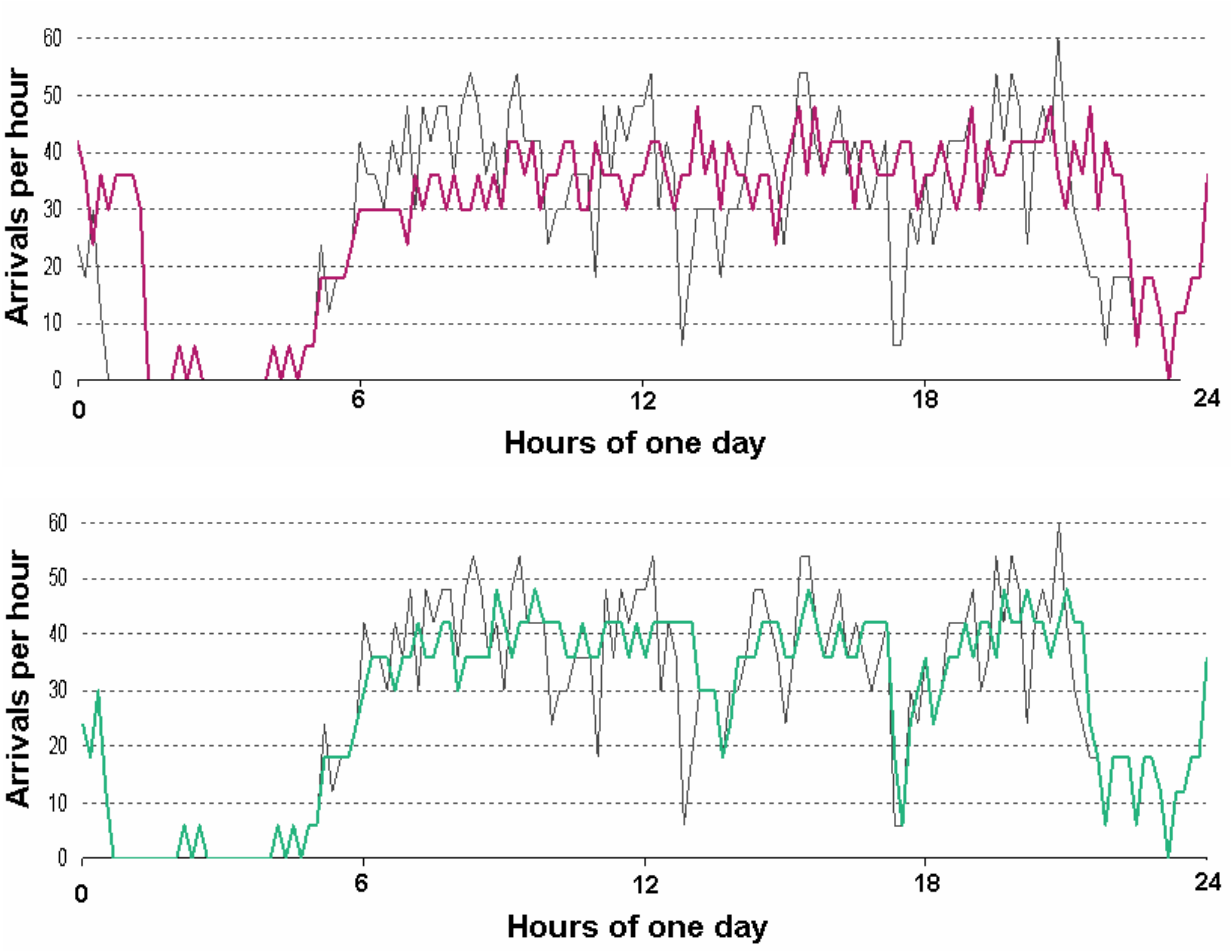

Fig. 11. Traffic flow (arrivals per hour) during a day at Frankfurt Airport. Top: demand (grey) vs. ICAO standards (red); bottom: demand vs. WSVBS utilisation (green).

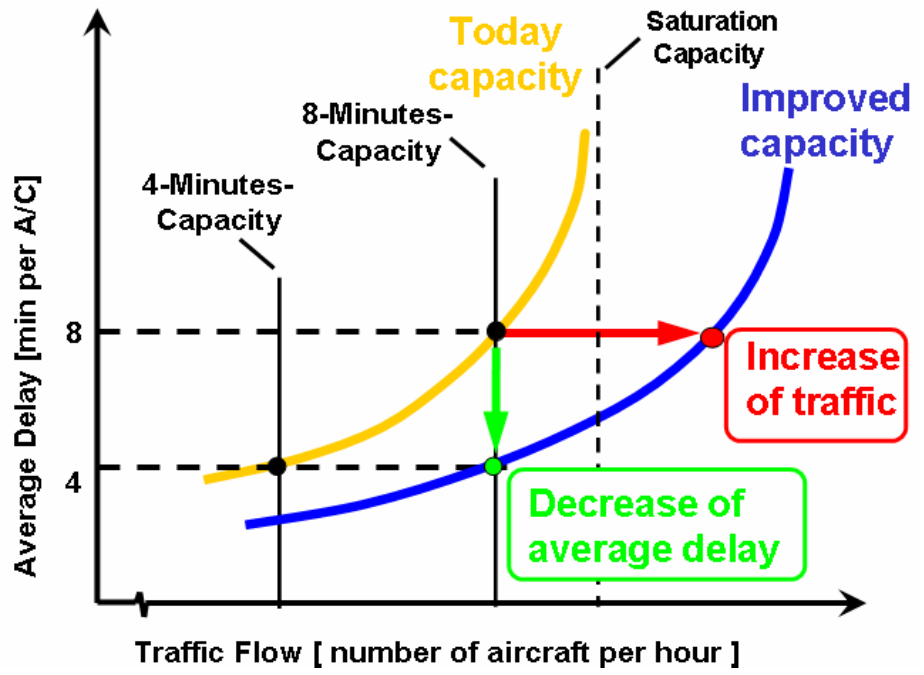

Fig. 12. Principle relation between average delay versus traffic flow (demand).

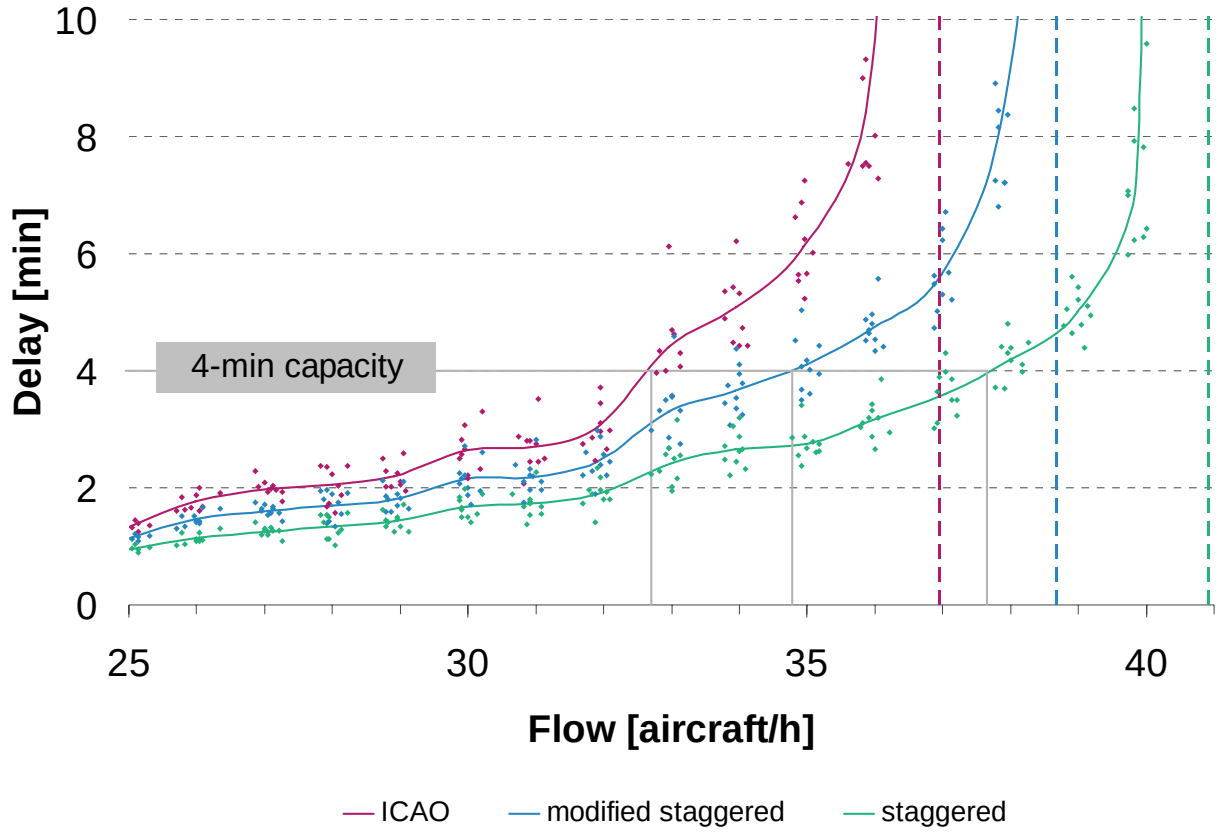

Fig. 13. Average delay versus traffic flow (for a mix of H/M/L aircraft of 27/67/6%) for the concepts of operation ICAO (red), MSL/R (blue), and STG (green) from fast-time simulations; the “4-min delay” capacity is indicated by grey vertical lines.

Fig. 14 summarises the history of DFS operation modes as proposed by WSVBS during the 66 days of performance at the airport (not considering any traffic mix). It is evident that in the majority of time those modes could have been deployed which allow improving capacity or punctuality of landing aircraft. The focus on five days indicates that each mode can be deployed throughout a significant fraction of time (see also Fig. 15).

Tab. 2 lists the use of all operation modes as predicted by WSVBS during the 66 days for the fraction of time in which radar separation of 2.5 NM (70 s) was suggested. Thus, the table also includes reduced in-trail separation and differentiates between HH and HM aircraft pairs (cf. Fig. 8). Hence, from the meteorological conditions which prevailed during that winter period, heavy aircraft could have landed behind heavy aircraft in-trail on R or L runway in 2.6 % of the time with an average MST of 60 s (but *de facto* separated by 70 s). Another example: in 47.9% of the time a medium aircraft could have landed 2.5 NM behind the preceding heavy aircraft landing on R. The cases where DFS-mode STG could have been used for HH (HM) pairings summed up to 10% (3.6%). For the DFS operation modes, the ICAO separation mode was required in only 25% of the time.

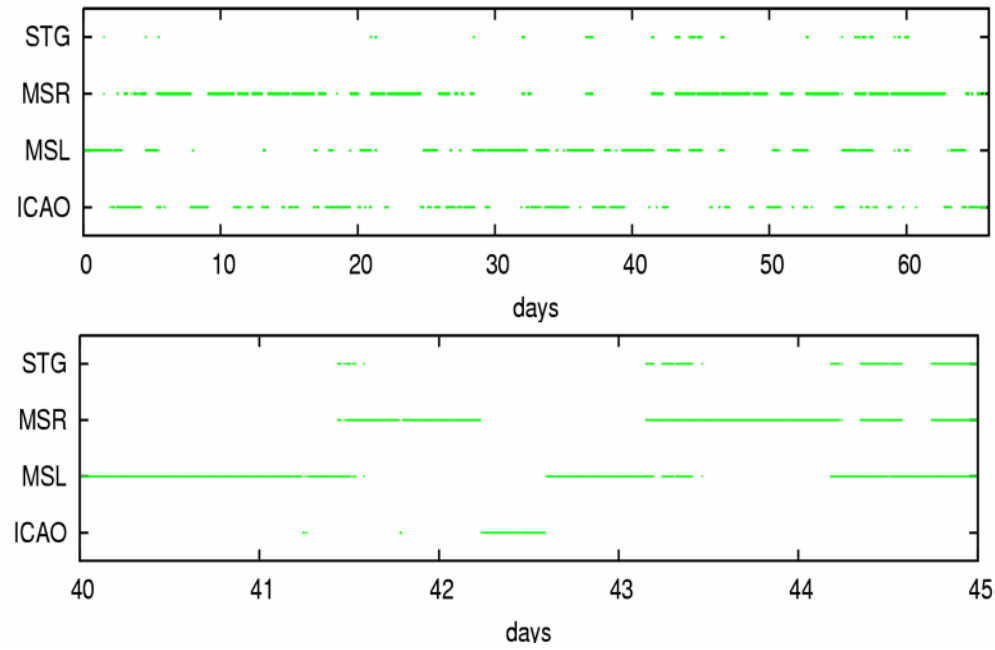

Fig. 14. History of usage of the 4 DFS operation modes during the 66 days of the campaign at Frankfurt. Top: full period; bottom: zoom on five days.

Landing procedure	Average MST [s]	Frequency of use [%]
LL HH	60.0	2.6
LL HM	61.9	1.5
LR HH	0	40.3
LR HM	0	30.7
RL HH	0	54.3
RL HM	0	47.9
RR HH	60.0	2.6
RR HM	61.9	1.5
STG HH	0	10.0
STG HM	0	3.6
ICAO		25.0

Tab. 2. Average minimum separation time and frequency for HH and HM aircraft pairs landing in-trail (LL, RR) or across (LR, RL) for the fraction of time in which radar separation was suggested.

Landing procedure	Average MST [s]	Frequency of use [%]
LL HH	75.7	6.6
LL HM	93.5	9,0
LR HH	0.1	40.3
LR HM	1.2	31.0
RL HH	0.5	54.6
RL HM	1.6	48.6
RR HH	75.7	6.6
RR HM	93.5	9.0

Tab. 3. As for TAB 3 but all separation times between 70 and 100/125 s are used.

Tab. 3 displays the same information as Tab. 2 but now assuming that all separation times between 0 and 100 s (125 s) for HH (HM) pairs could be used. In particular the use of reduced in-trail separations increases strongly by factors 2.5 (6) although at the expense of larger average MST. The staggered procedures are almost unchanged compared to the values in Tab. 2 as these depend predominantly on the question if a vortex reaches the parallel runway or not.

The question how long the DFS ConOps MSL, MSR, STG or no one of them (ICAO) could continuously be used and how often this happened during the campaign is answered in Fig. 15 for pairs of Heavy/Medium aircraft. In the 66 days the procedures MSL/MSR/STG could have been used 36/7/14 times for 10 minutes only. However, a continuous use of these ConOps for 1 hour would have been possible 16/13/10 times, respectively. Even a usage as long as 8 hours would have been feasible still 2/2/1 times. Somewhat higher numbers hold for the aircraft pairing HH and somewhat reduced numbers for single runway approaches (not shown). Due to the strong wind conditions in January it would even have been possible to use MSR for HH pairings once throughout almost 4 days (93 hours).

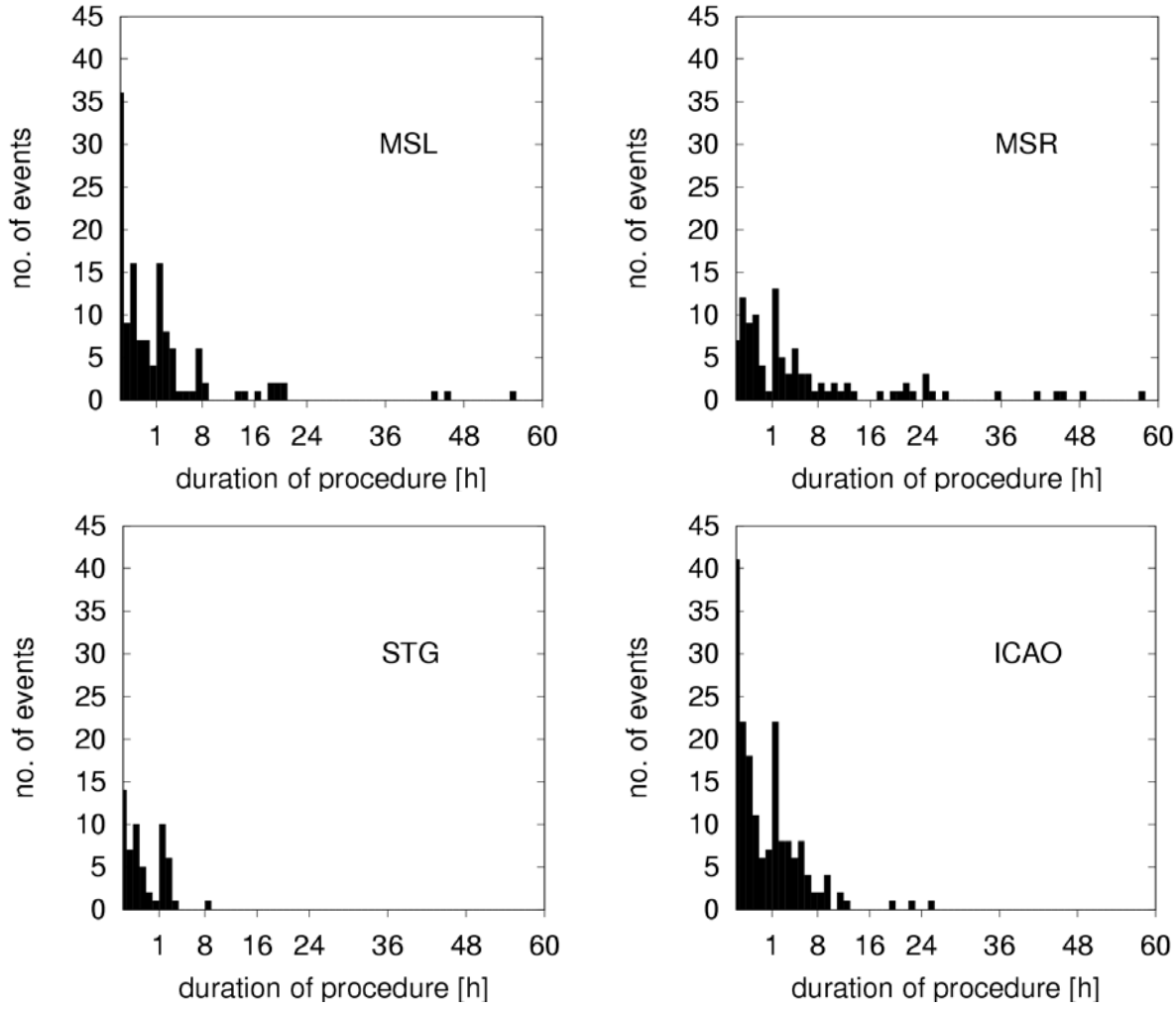

Fig. 15. Number of events versus duration of DFS procedures in hours for HM aircraft pairs; a 10 min interval is used in the 1st hour, the interval is 1 hour afterwards.

For the interested reader it is further analysed which gates impede reduced aircraft separations. This analysis reveals that gate 13 (the one closest to the runway threshold where aircraft fly at 29 m above ground) hinders WSVBS operations for single runway approaches in 51% out of 6042 cases, which is another evidence for the bottleneck

close to the ground. Interestingly though, also gate 1 (the far-out gate at 1077 m height) blocks reduced separations in almost 31% of the cases which is attributed to the fact that the first approach corridor features the largest dimensions. For staggered and modified staggered approaches, gate 13 is no longer an issue but gate 10 with 26 to 48%. At this gate two effects appear decisive. First, it is the lowest gate employing numerical cross-wind predictions which lead to larger uncertainty allowances of vortex position compared to the wind measurements. Second, the aircraft vortices are shed at 190 m height where ground effect still contributes to the lateral wake vortex transport for the aircraft parameter combinations with the largest wing spans (see [13]). Similar as for the single runway approaches, the first gate with the largest approach corridor dimensions blocks reduced separations for approaches towards the parallel runway system in 10 to 45% of the cases.

Fig. 16 shows two examples of traces of the port and starboard vortices of heavy aircraft landing on runway 25R as measured by the safety net LIDAR in the three scan planes shown in Fig. 2. For the 18th of January, the WSVBS predicted the modes MSR followed by reduced in-trail separation. The plot, which shows vortex positions of 8 landing heavy aircraft, corroborates both scenarios as the southerly cross-wind hindered the vortices to reach runway 25L (hence, MSR) and the wind became obviously so strong later[1] that also a reduced separation in-trail could have been operated. For the 8th of February, WSVBS recommended to use operations STG followed by MSR. Again, the LIDAR data, now from 32 landing heavy aircraft, confirm the predictions; the wind is very weak and does not transport the vortices to the adjacent runway.

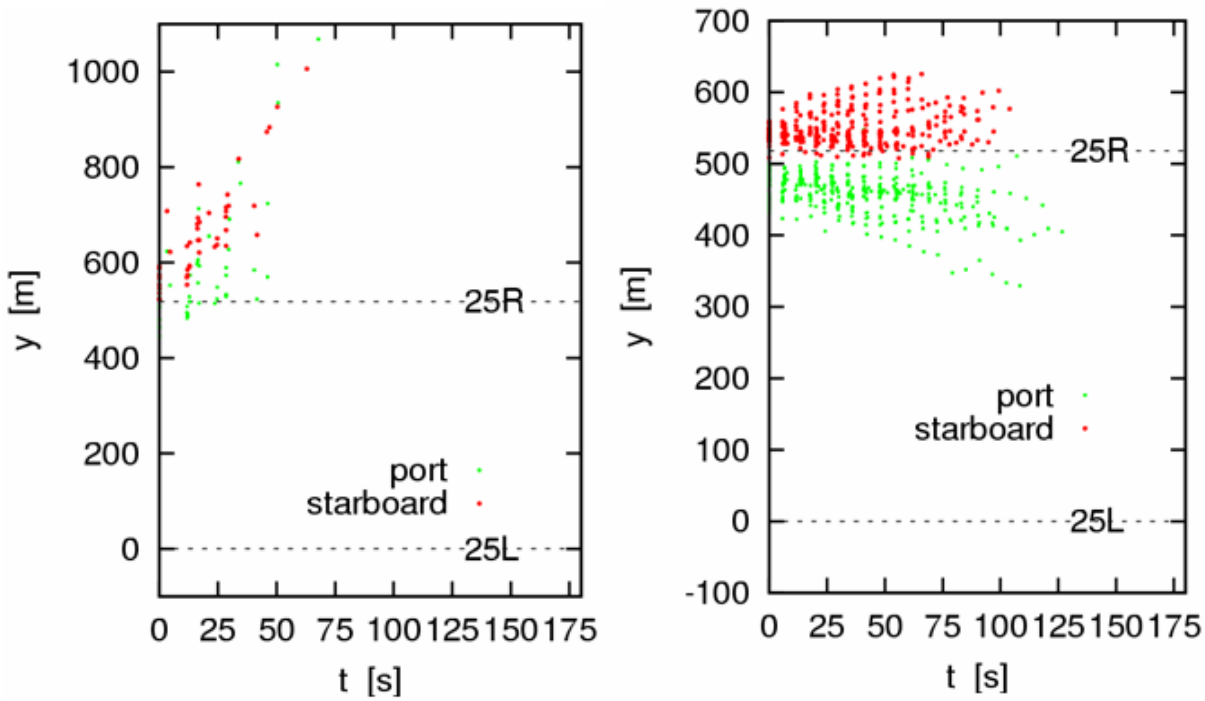

Fig. 16. Lateral positions of wake vortices vs. vortex age from 8, 32 heavy aircraft landing on 25 R on 18th Jan. (left) and 8th Feb. (right) 2007, respectively, as traced by the LIDAR in the three scan planes.

The (manned) LIDAR did not measure continuously throughout the campaign. It was operated on 16 days where it traced the wake vortices of about 1100 landing heavy aircraft in the three most critical control gates (Fig. 2). In all these cases it was found that

[1] The LIDAR stopped operation early that day because of storm *Kyrill* which passed Germany on the 18th of January.

the recommended operation mode was well predicted – no vortices were detected in the flight corridor after the predicted minimum separation time.

5. CONCLUSIONS

DLR has developed a wake vortex advisory system for airports and air traffic control, the *Wirbelschleppen-Vorhersage- und -Beobachtungssystem*, named WSVBS. It has the components SODAR, RASS, SONIC and NOWVIV for monitoring and forecasting the local weather around the airport in Frankfurt (or any other airport), the components P2P and SHAPe for predicting wake transport and decay and required safety areas, and the LIDAR as the safety net to survey the lower most critical heights along the glide path for wake vortices. WSVBS is integrated in the arrival manager AMAN of DLR. The prediction horizon is larger than 45 min (as required by air traffic controllers) and updated every 10 minutes. It predicts the concepts of operations and procedures established by DFS and it further predicts additional temporal separations for in-trail traffic.

The WSVBS has demonstrated its functionality at Frankfurt airport during 66 days in the period from 18/12/06 until 28/02/07. It covers the glide paths of runways 25L and R from the final approach fix to the threshold (11 NM). It combines measured & forecasted meteorological data for wake prediction. From the 66 days of performance test at Frankfurt we found that

- the system ran stable - no forecast breakdowns occurred,
- aircraft separations could have been reduced in 75% of the time compared to ICAO standards,
- reduced separation procedures could have been continuously applied for at least several tens of minutes and up to several hours occasionally,
- the predictions were correct as for about 1100 landings observed during 16 days no warnings occurred from the LIDAR.

Fast-time simulations revealed that the concepts of operation, which were introduced by DFS (i.e. MSL, MSR, STG and keeping 2.5 NM or 70 s as the minimum separation) and utilised by WSVBS for Frankfurt Airport, yield significant reductions in delay and/or an increase in capacity to 3% taking into account the real traffic mix and operational constraints in the period of one month. Relaxing the DFS constraints and allowing more operation modes would further increase capacity.

We consider these capacity gains as tactical. “Tactical” means that the system aims at increasing the punctuality of flight operations as of today by avoiding holding patterns. After experience has gained over some years of application (including diurnal and seasonal statistics of meteorological quantities along the glide path) the system may also allow increasing the number of flight operations at the airport, i.e. gain capacity “strategically” probably depending on the time of the day or the season of the year.

Before the WSVBS can be handed over for final adaptations to become a customized fully operational system some further steps are planned. DLR will expand the system to include landings on runways 07/L/R. The LIDAR shall be operated automatically and the traced vortex positions shall be used on-line to check for forecast errors and warn the operators in case of an increased risk. Finally, also a risk analysis needs to be pursued to convince all stakeholders of the usefulness and capabilities of our system.

ACKNOWLEDGEMENTS

We highly acknowledge the support and help from the Fraport AG, Frankfurt, in setting up and running the field trial at their airport. We also thank the German Weather Ser-

vice, Offenbach, for offering their observer house as the Local Operation Centre and supplying the model output data of their routine weather forecasts. The German air traffic safety provider DFS, Langen, is acknowledged for their support. We finally thank Fa. Metek, Elmshorn, for renting their very reliable and robust meteorological profiler system to us. The work presented here was funded by the DLR project *Wirbelschleppe* and did benefit from the EU projects *ATC-Wake* (IST-2001-34729), *FAR-Wake* (FP6–012238), *FLYSAFE* (AIP4-CT-2005-516 167), and the European Thematic Network *WakeNet2-Europe* (G4RT-CT-2002-05115).

REFERENCES

[1] de Bruin A., Speijker L., Moet H., Krag B., Luckner R., Mason S. 2003: S-Wake – Assessment of wake vortex safety. NLR-TP-2003-234, 77 pp.

[2] Frech M. 2007: Estimating the turbulent energy dissipation rate in an airport environment. *Boundary-layer Meterol.* **123**, 385-393.

[3] Frech M., Holzäpfel F. 2008: Skill of an Aircraft Wake-Vortex Model Using Weather Prediction and Observation. *J. Aircraft* **45**, 461-470.

[4] Frech M., Holzäpfel F., Tafferner A., Gerz T. 2007: High-Resolution Weather Data base for the Terminal Area of Frankfurt Airport. *J. Appl. Meteor. Climat.* **46**, 1913-1932.

[5] Gerz T., Holzäpfel F., Bryant W., Köpp F., Frech M., Tafferner A., Winckelmans G. 2005: Research towards a wake-vortex advisory system for optimal aircraft spacing, *Comptes Rendus Physique*, Académie des Sciences, Paris, **6**, No. 4-5, 501-523.

[6] Gurke T., Lafferton H. 1997: The development of the wake vortex warning system for Frankfurt Airport: Theory and implementation, *Air Traffic Control Quarterly* **5**, 3-29.

[7] Hahn K.-U., Schwarz C., Friehmelt H. 2004: A simplified hazard area prediction (SHAPe) model for wake vortex encounter avoidance, in: Proc. 24th International Congress of Aeronautical Sciences, Yokohama, Japan.

[8] Holzäpfel F. 2003: Probabilistic two-phase wake vortex decay and transport model, *Journal of Aircraft* **40**, No. 2, 323-331.

[9] Holzäpfel F., Robins R.E. 2004: Probabilistic two-phase aircraft wake-vortex model: application and assessment, *Journal of Aircraft* **41**, No. 5, 1117-1126.

[10] Holzäpfel F. 2006: Two-Phase Aircraft Wake Vortex Model: Further development and Assessment, *J. Aircraft* **43**, 3, 700-708.

[11] Holzäpfel F., Steen M. 2007: Aircraft wake-vortex evolution in ground proximity: Analysis and parameterization. *AIAA J.* **45**, No.1, 218-227.

[12] Holzäpfel F., Frech M., Gerz T., Tafferner A., Hahn K.U., Schwarz C., Joos H.-D., Korn B., Lenz H., Luckner R., Höhne G. 2006: Aircraft Wake Vortex Scenarios Simulation Package – WakeScene. Proc. 25th International Congress of the Aeronautical Sciences (ICAS), Hamburg, pp 1-12.

[13] Holzäpfel F., Gerz T., Frech M., Tafferner A., Köpp F., Smalikho I., Rahm S., Hahn K.-U. & Schwarz C. 2008: The wake vortex prediction and mointoring system WSVBS. Part I: Design. See this issue.

[14] Schwarz C., Hahn K.-U. 2005: Simplified hazard areas for wake vortex encounter avoidance. AIAA Atmospheric Flight Mechanics Conference and Exhibits, San Francisco, California, USA.

[15] Schwarz C., Hahn K.-U. 2006: Full-flight simulator study for wake vortex hazard area investigation, *Aerospace Science and Technology* **10**, 136–143.

AUTOMATED PILOT ASSISTANCE FOR WAKE VORTEX ENCOUNTERS

C. Schwarz , K.-U. Hahn
Institut für Flugsystemtechnik, Deutsches Zentrum für Luft- und Raumfahrt
Lilienthalplatz 7, 38108 Braunschweig, Germany

OVERVIEW

Wake vortices pose a possible hazard for encountering aircraft in all phases of flight. Hence wake vortex encounters are to be avoided. In case of an unintended wake vortex encounter special aircraft controllers can act as a safety net. Such an active wake vortex control system is being developed by the DLR Institute of Flight Systems based on feed-forward disturbance compensation. The control system has been tested with offline and pilot-in-the-loop investigations as well as with flight tests. It can be shown that the aircraft response can be improved significantly if a specific wake vortex controller is active. For the subjective assessment of the wake vortex encounters a dedicated pilot rating scale has been developed. The results show a clear tendency that the wake vortex controller improves the situation.

ZUSAMMENFASSUNG

Wirbelschleppen stellen in allen Flugphasen eine mögliche Gefährdung für einfliegende Flugzeuge dar. Daher sind Wirbelschleppeneinflüge zu vermeiden. Für den Fall unbeabsichtigter Wirbelschleppeneinflüge können spezielle Flugregler die Sicherheit erhöhen. Solch ein aktives Wirbelschleppensteuerungssystem, das auf einer Vorsteuerung zur Störungskompensation basiert, wird am DLR Institut für Flugsystemtechnik entwickelt. Das Steuerungssystem wurde mit offline und pilot-in-the-loop Simulationen, sowie mit Flugversuchen untersucht. Es kann gezeigt werden, dass die Flugzeugreaktion mit einer spezifischen Wirbelschleppensteuerung deutlich verbessert werden kann. Für die subjektive Bewertung von Wirbelschleppeneinflügen wurde eine spezielle Bewertungsskala entwickelt. Die Ergebnisse zeigen eine klare Tendenz, dass die aktive Wirbelschleppensteuerung die Situation verbessert.

1. INTRODUCTION

Active aircraft controllers specifically designed to cope with (unintended) wake vortex encounters can handle the vortex imposed forces and moments in order to alleviate the induced aircraft reaction [25]. Based on the availability of forward looking sensors an active wake vortex control system can be established with feed-forward disturbance compensation. This approach has been investigated with offline and pilot-in-the-loop simulations as well as with flight tests.

These flight tests have been conducted with DLR's fly-by-wire test aircraft ATTAS (Advanced Technologies Testing Aircraft System, FIG 1) using in-flight simulation. ATTAS is particularly designed for this task. During the in-flight simulation the computers onboard the real test aircraft simulate a wake vortex encounter and the real aircraft acts accordingly, i.e. it is flying through a 'simulated vortex.'

FIG 1. DLR test aircraft ATTAS (Advanced Technologies Testing Aircraft System)

2. ROLL CONTROL RATIO FOR ASSESSMENT OF WAKE VORTEX ENCOUNTER SEVERITY

Especially for approach and landing wake vortex encounters are typically nearly parallel to the wake vortex axes. In that case the dominating effect is the rolling moment induced by the wake vortex [2]. This is particularly true for the outer regions of the wake vortex, where the aircraft reaction can possibly be alleviated, as the stronger effects of the core region cannot be completely compensated. For that reason the definition of a roll control ratio (RCR) based on the wake vortex induced rolling moment taking into account the controllability of the encountering aircraft is a viable measure to assess the severity of the wake vortex encounter [22], [23], [24]. The magnitude of wake vortex induced rolling moment $C_{l,WV}$ is related to the maximum possible roll control power $C_l(\delta_{a,max})$ [4], [21]:

$$(1)\quad RCR = \frac{C_{l,WV}}{C_l(\delta_{a,\max})}$$

The worst case is the quasi stationary flight parallel to the vortex axis, because here the wake vortex is permanently acting on the aircraft.

3. CONTROLLER CONCEPT

3.1. Principles

The commonly accepted policy regarding wake vortices is that no planned wake vortex penetration is permitted [1]. However, unintended wake vortex encounters may occur, not necessarily being unacceptable [15], [20]. For those encounters special wake vortex controllers could assist the human pilot. The pilot will stay in the control loop and has guidance authority while the vortex controller is active. However the vortex controller has the authority to use up to 100% of the available control power.

It is desirable that the vortex controller system does not change the aircraft handling. This is the case for feed-forward controllers.

For approach and landing parallel-like encounters are typical, which can also occur in other flight phases. Especially for these encounter situations the wake vortex induced rolling moment is the dominating effect [2], [3].

The idea is to measure the wake vortex flow field and feed this information into the vortex controller to create appropriate counteracting control commands. It is assumed that the flow field can be determined in spanwise direction of the wake encountering aircraft. In principle this can be done with flow probes mounted on the encounter aircraft or by scanning the flow field upstream. The latter has the advantage that system time delays can be accounted for. A disadvantage can be that the flight path of the aircraft does not exactly match the measured positions of the flow field and the control commands are not based on the actual vortex flow field.

In principle forward measurement can be achieved with LIDAR technology (light detection and ranging), laser measurements based on the Doppler effect (like RADAR). Wake vortex measurements have been successfully performed with ground based LIDARs, also in axial direction [16], [17], [18]. Airborne LIDAR wake vortex measurements have also been demonstrated successfully for smoke-seeded vortices [19].

3.2. Feed forward concept

The aircraft reaction during wake vortex penetration can be improved by a pilot assistance system based on a feed forward control concept. This principle of disturbance compensation has the advantage that the aircraft handling characteristics remain unchanged. The control system is only active if an external disturbance is detected. For this concept (FIG 2 and FIG 5) it is assumed that the airflow in front of the aircraft can be measured by a forward looking sensor [4].

The feed forward concept reacts based on the predicted wake vortex velocity flow field V_{WV}, which is determined with the measured vectors of airspeed V and the flight path velocity V_K. The mean wind speed vector V_W has to be determined shortly before the wake vortex encounter and is assumed to be constant throughout.

(2) $V_{WV} = V_K - V - V_W$

The velocity field is fed into an aerodynamic interaction model which calculates the wake vortex induced forces and moments. As aerodynamic interaction model the strip method is used, where the lift generating surfaces are subdivided into sections for which the vortex influence is determined. This method was deemed feasible in [5], verified against windtunnel tests in [6] and validated with flight test data in [7] and [8]. The moments are then used with an inverted aerodynamic model to command appropriate control inputs to compensate the aircraft response due to the vortex.

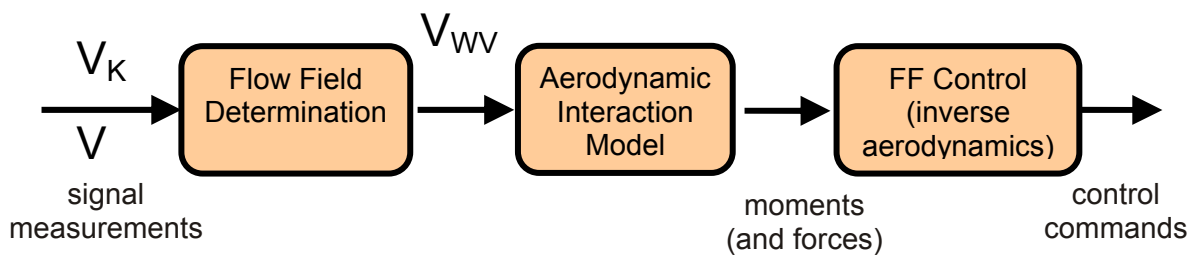

FIG 2. Feed forward concept overview

3.3. Combination with autopilot

The feed forward concept in combination with an autopilot is analysed with an offline simulation. It comprises the description of the vortex generation and aging [26], the representation of the wake vortex induced velocity distribution and the modelling of the encounter aircraft reaction with the aerodynamic interaction model. The 6 degree of freedom simulation of wake vortex encounters is described in more detail in [4] and [9]. In order to maintain the required flight path a regular autopilot/auto-throttle system [4] (based on a model following controller concept) is applied.

The simulated aircraft is a Do 128 aircraft (ICAO class 'light', MTOW = 4.4 t). The sensors are modelled ideally so that the exact disturbance is known to the assistance system. FIG 3 shows an example flight passing vertically through a wake vortex flow field, with autopilot only in blue and with a combination of autopilot and wake vortex controller in red. The vortex generating aircraft is a category 'medium' aircraft (MTOW = 94 t) with a vortex age of t = 50 s (with a circulation of 252 m²/s for the selected example case). The side view and the top view show the flight path with the wake vortex encounter scenario. The reference flight path (green dashed line) is inclined with 3° to represent an approach situation and the wake vortex (black dashed line) is aligned horizontally. The time histories show the bank angle and the aileron command normalized with the maximum deflection.

While the autopilot is able to cope with the wake vortex to a certain degree, the pilot assistance system improves the situation significantly, for example with respect to flight path deviations and bank angle.

FIG 4 shows a wake vortex flow field penetration with the same scenario as above but for a reference flight path closer to the wake vortex and hence higher forces and moments imposed on the encountering aircraft. The aircraft reaction is stronger (bank angle up to 15° with and significantly worse without assistance system, the latter case not shown in FIG 4), but still well acceptable due to the assistance system. The components of the aileron commands are shown for the feed forward command due to the vortex disturbance (‘FF’, green dashed line), the autopilot due to flight path and state deviations (‘AP’, blue dotted line) and the resulting overall command (‘com’, black solid line). The actual aileron deflection considering actuator dynamics and limitations are shown in red (‘defl’, dashdotted). The feed forward and overall commands exceed 100% for a few seconds and are consequently limited during that time. Despite the strong disturbance the resulting aircraft reaction is very satisfactory.

The results of the offline simulations with autopilot for different encounter scenarios, vortex generators and strengths generally suggest that the concept of the assistance system is appropriate for wake vortex hazard alleviation.

4. ACTUATOR DYNAMICS

Investigations with offline simulations showed that no extra demands for actuator dynamics compared to existing systems result from the wake vortex controller [12]. The overall system delays must not be too large ($\Delta t < 0.25$ s) which holds for present systems. In any case the dominating factor is the limited available roll control power rather than actuator dynamics.

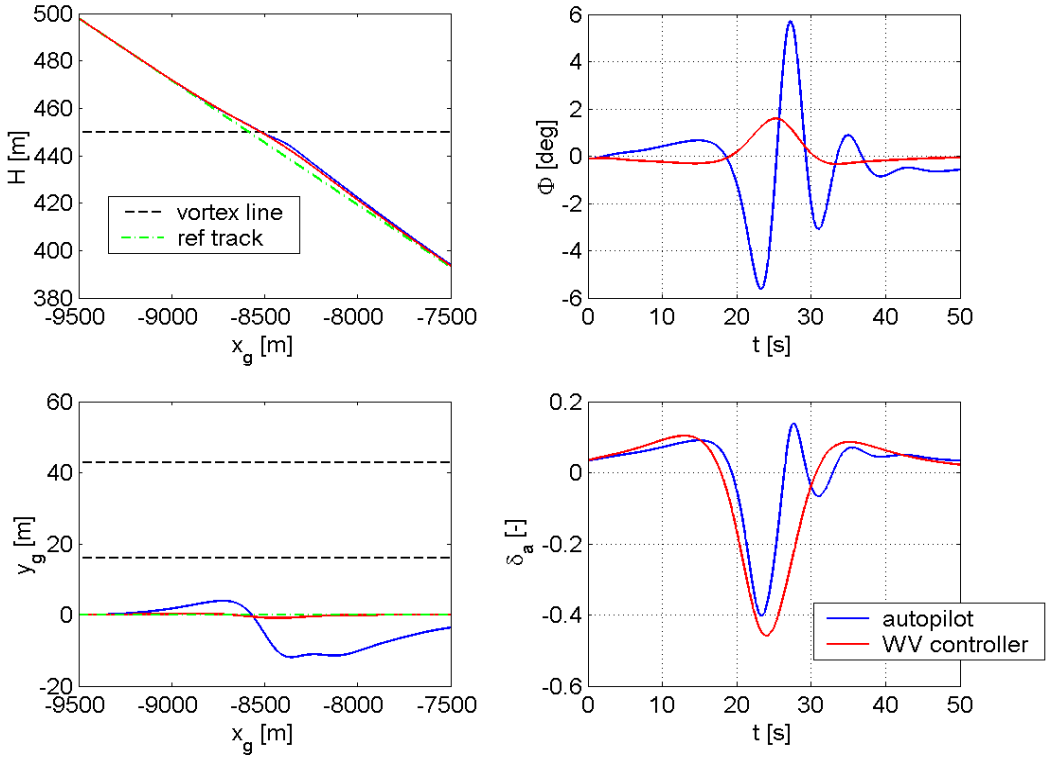

FIG 3. Flight track and parameter time histories of a flight through wake vortex flow field: side view and top view, bank angel and aileron command (offline simulation with regular autopilot and combination autopilot wake vortex controller)

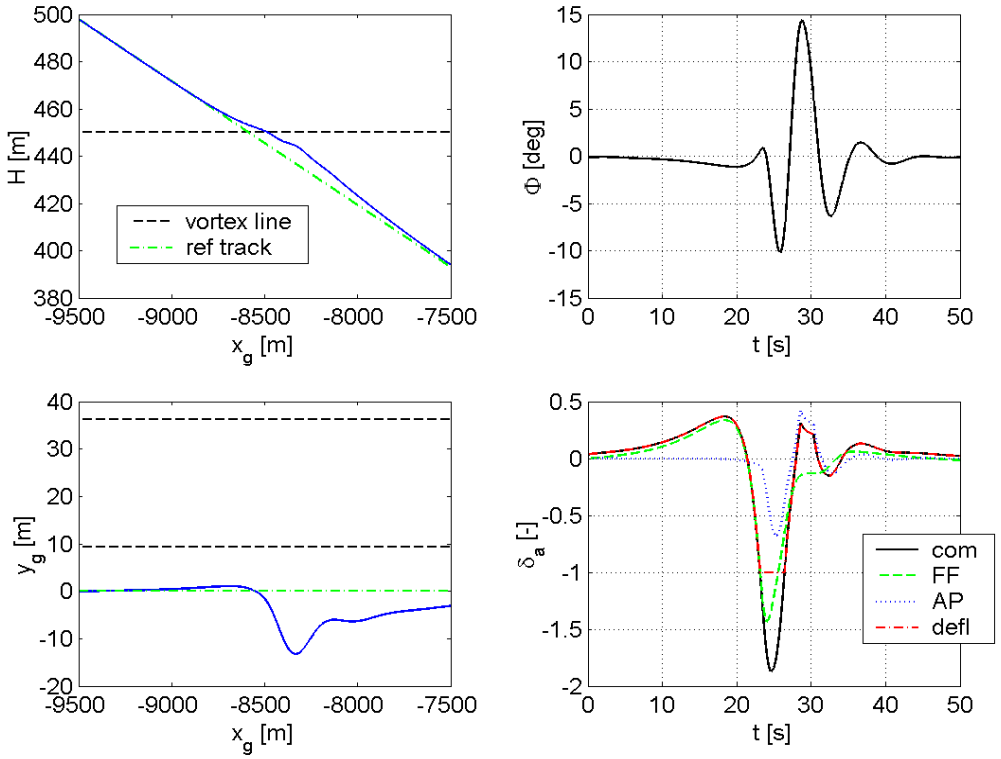

FIG 4. Flight track and parameter time histories of a flight through wake vortex flow field: side view and top view, bank angel and aileron command components and actual deflection (offline simulation with autopilot plus wake vortex controller)

5. SENSOR MEASUREMENT CONCEPT

Different forward looking measurement strategies were investigated with offline simulations [13]. Various concepts for the measurement direction and dimension in combination with data processing concepts have been developed (TAB 1).

concept	measurement		data
	direction	dimension	interpolation
1	airframe fixed	1D (line)	no
2	air path fixed	1D (line)	no
3	air path fixed	1D (line)	wing span direction
4	air path fixed	2D (plane)	wing span and vertical direction

TAB 1.Forward looking measurement strategies

The first approach is to measure the air flow in an airframe fixed direction at positions along a line in wing span direction (concept 1). Here it is assumed that the measured wake vortex velocities apply delayed at the aircraft wing. To enhance the flight path prediction quality the measurement direction is chosen along the current flight path (concept 2). For concept 3 the actual wing position is interpolated within the measurement points. To account for vertical flight path deviations a two dimensional pattern is scanned in front of the aircraft and the wing position is interpolated (concept 4)(FIG 5).

A comparison between the four sensor measurement concepts is shown in FIG 6. The absolute value of the maximum bank angle, which occurred during a wake vortex penetration is plotted against the measurement distance.

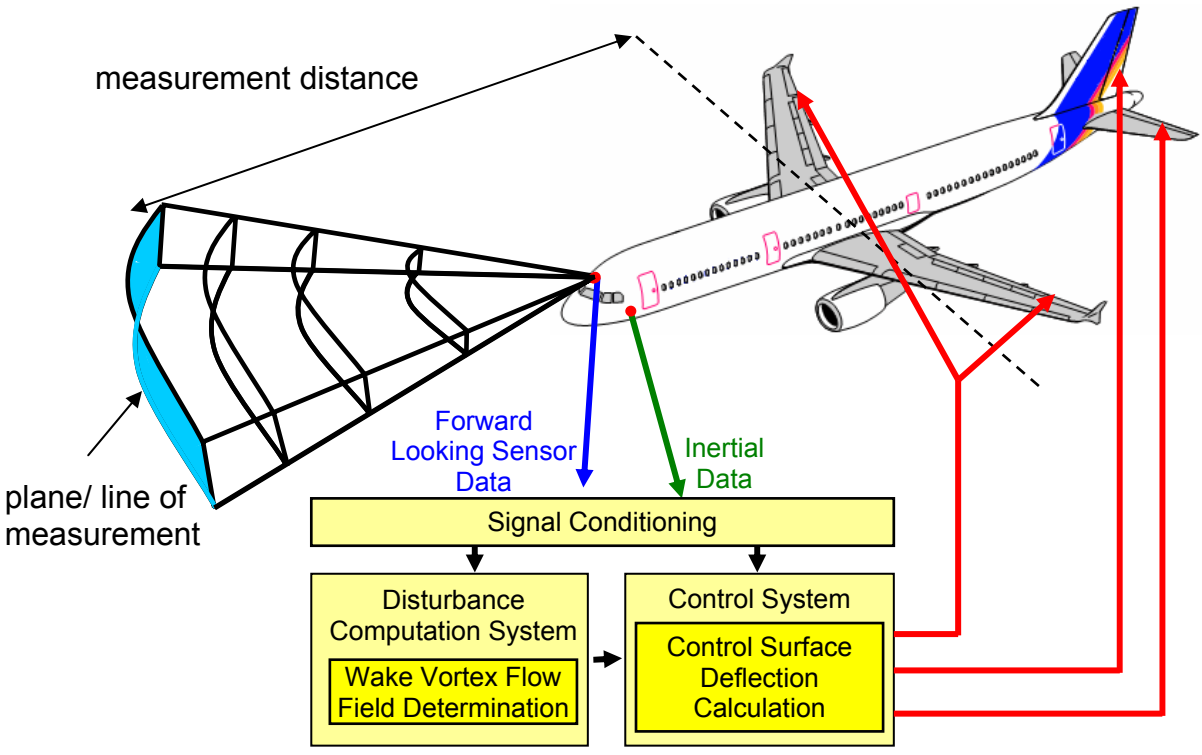

FIG 5. Forward Looking Sensor

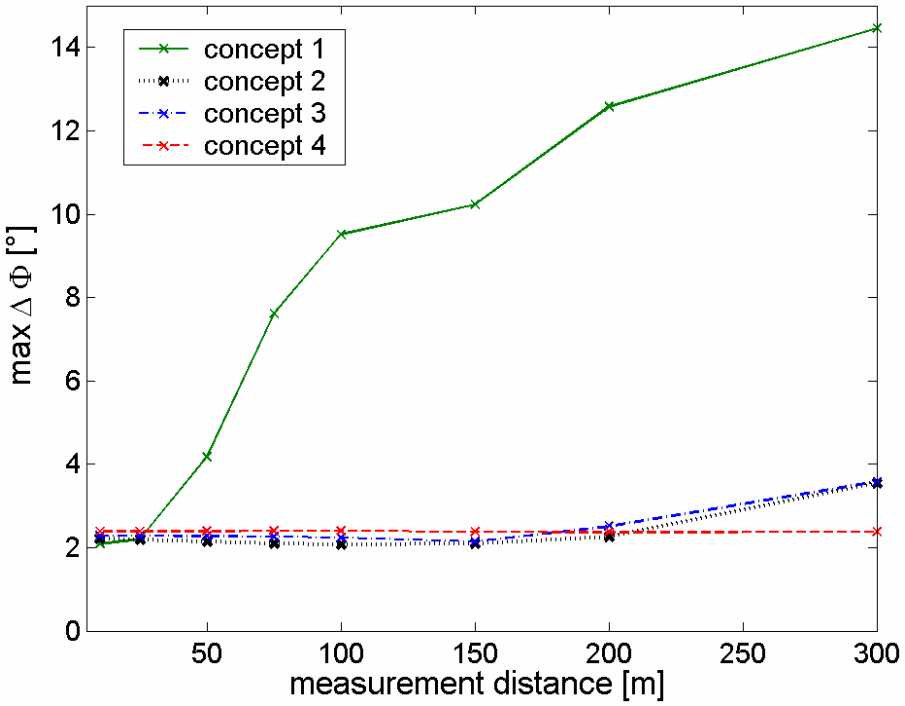

FIG 6. Effect of measurement distance on bank angle

It is obvious that the flow field has to be scanned in air path direction. Otherwise the aircraft is not flying in the direction of the measurement and hence not flying through the measurement volume. In the investigated scenario landing approach the difference between measurement direction and flight path for concept 1 was several degrees. The best results were achieved with the two dimensional measurement and interpolation of concept 4. Further investigations yielded a required sampling rate of $f > 3$Hz. The horizontal resolution of the measurements should be less than 10% of the encounter aircraft wing span. The horizontal size of the measurement plane should be at least 2.5 times the wing span and vertically at least 100% of the span.

6. PILOTED WAKE VORTEX ENCOUNTERS

Experiments in real flight offer the most realistic simulation environment. This is achieved by means of in-flight simulation. The DLR testing aircraft ATTAS (Advanced Technologies Testing Aircraft System, FIG 1) is specifically designed for this task. The real aircraft acts like the simulated aircraft (in this case the same aircraft type as the real aircraft), which encounters the wake vortex. The experimental pilot is flying the simulated aircraft using real controls. The pilot inputs are fed into the onboard computers stimulating the model aircraft which reacts on the inputs and on the effects of the virtual wake vortex flow. The resulting model aircraft states are fed into the model following control system. The model following controller generates the control surface deflections of the (real) host aircraft which are necessary to make the host aircraft behave like the simulated aircraft. So the flight states of the host aircraft experienced by the experimental pilot are matching the flight states of the simulated aircraft. The feasibility of wake vortex in-flight simulations was already demonstrated [14], exhibiting a good simulation fidelity for an RCR at least up to 50%.

Manually controlled wake vortex encounters in an authentic environment including air traffic control and other traffic permit a subjective pilot evaluation in addition to the objective data analysis.

The encountering aircraft (ATTAS) type is a VFW614 (ICAO class 'medium', MTOW = 21 t). The vortex generating aircraft is a category 'medium' aircraft (MTOW = 94 t) with a vortex age of t = 50 s (same wake vortex scenario as in section 3.3 but different encounter aircraft). The experiment scenario begins 6 nm before runway threshold and consists of an ILS approach and the landing (FIG 7).

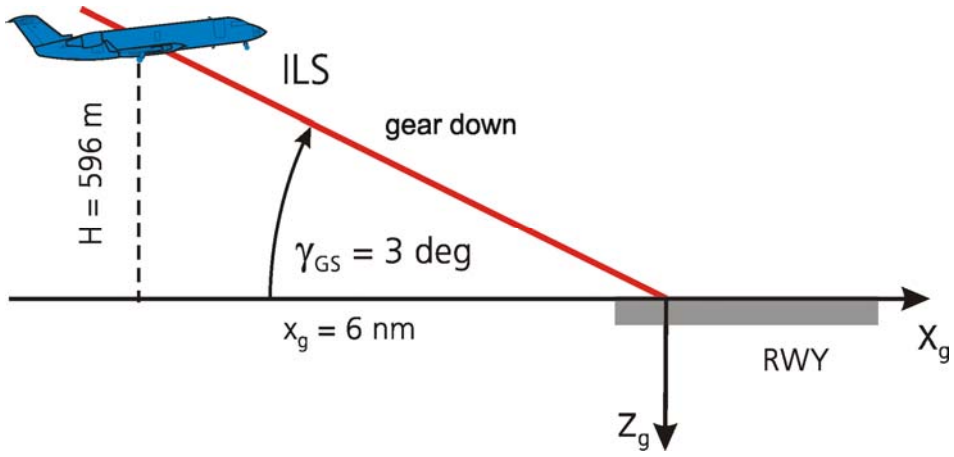

FIG 7. Approach scenario (side view)

The pilot ratings for each approach comprise four categories: aircraft control, demands on the pilot, aircraft excursions from flight state and path and overall hazard. The rating scale is graduated into four levels, with a rating of 1 denoting an uncritical case and a 4 denoting an unacceptable one (FIG 8). Ratings of 1-3 are considered acceptable.

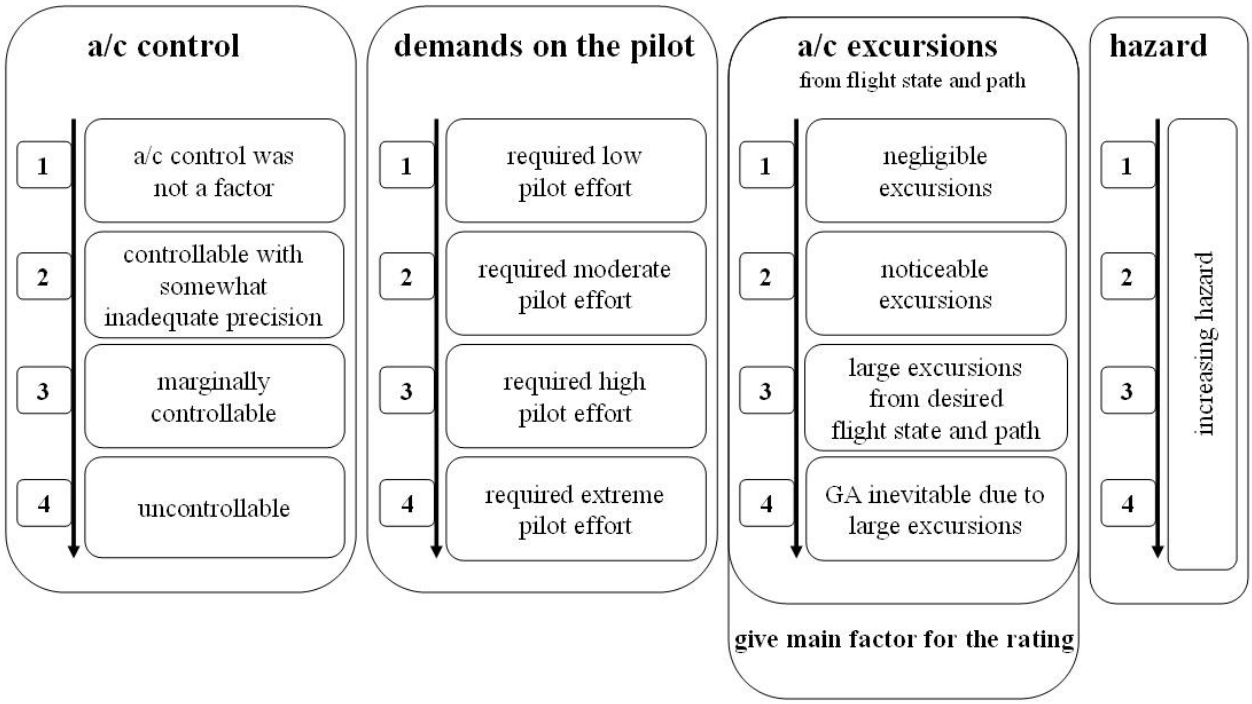

FIG 8. Pilot rating scale [10], [11]

FIG 9 shows the effect of the pilot assistance system on the pilot average ratings. The results come from three in-flight simulation (IFS) flight tests with time fixed wake vortex disturbances featuring a maximum required roll control ratio of RCR = 0.5. The sensors are modelled ideally so that the exact disturbance is known to the assistance system. Altogether 9 approaches were conducted in fine weather, 7 approaches were executed in IMC conditions and 4 in light turbulence. Although the diagram is based on only 20

approaches (12 approaches with assistance system, 8 without) the tendency of improved rating can clearly be seen when the automatic controller is engaged.

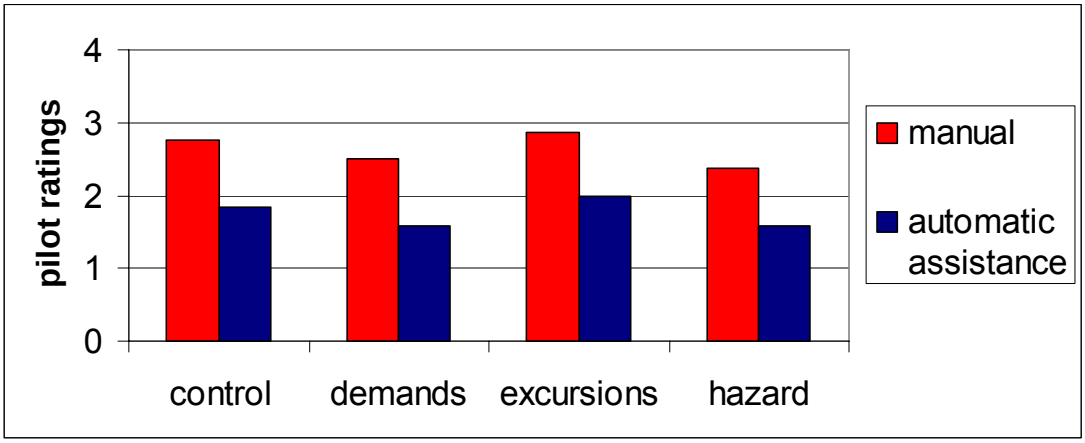

FIG 9. Average pilot ratings for wake vortex encounters

7. CONCLUSION

Automatic control systems can improve the aircraft behaviour during (unintended) wake penetrations by supporting the pilot's control task. This was shown by offline simulations and piloted simulations in real flight (in-flight simulations).

Wake vortex specific pilot assistance increases safety since more severe encounter situations can be handled in an acceptable way. With regard to the implementation of larger aircraft types and the worldwide attempt to revise (and decrease) wake vortex separation distances dedicated automatic control systems can play a major role concerning safety by providing a safety net.

ACKNOWLEDGEMENT

The presented work was mainly performed within the DLR project "Wirbelschleppe II". The authors would like to thank the whole project team for their fruitful discussions and contributions, and especially the DLR colleagues from the flight test department and from the simulator branch for their support.

REFERENCES

[1] IFALPA Wake Vortex Policy, International Federation of Air Line Pilots' Associations, July 1998
[2] Bruin, A. de, S-Wake Assessment of Wake Vortex Safety - Publishable Summary Report, NLR-TP-2003-243, 2003
[3] Hallock, J.N., Eberle, W.R., Aircraft Wake Vortices: A State-of-the-Art Review of the United States R&D Program, U.S. Department of Transportation (DOT), Federal Aviation Administration (FAA), Report No. FAA-RD-77-23, February 1977
[4] Hahn, K.-U., Coping with Wake Vortex, 23rd International Congress of Aeronautical Sciences (ICAS), Toronto (Canada), 8-13 September 2002
[5] Barrows, T.M., Simplified Methods of Predicting Aircraft Rolling Moments due to Vortex Encounters, AIAA 76-61, AIAA 14th Aerospace Sciences Meeting, Washington, DC, Jan. 1976
[6] Bruin, A. de, WAVENC, Wake Vortex Evolution and Wake Vortex Encounter, Publishable Synthesis Report, National Aerospace Lab., NLR-TR-2000-079, Amsterdam, 2000
[7] Fischenberg, D., Results of Flight Test Data Analysis, SWAKE-TN-222_1, 2002

[8] Jategaonkar, R., Fischenberg, D, Gruenhagen, W. v., Aerodynamic Modeling and System Identification from Flight Data – Recent Applications at DLR, Journal of Aircraft, Vol. 41, No. 4, July – August 2004, p. 687, 2004
[9] Schwarz, C., Hahn, K.-U., Gefährdung beim Einfliegen in Wirbelschleppen, German Aerospace Congress, Munich, 17.-20. Nov. 2003, DGLR-JT2003-242
[10] Hahn, K.-U., Schwarz, C., Kloidt, S., Full-Flight Simulatorstudie zur Verifizierung von Wirbelschleppen-Gefährdungsraumgrenzen, DLR IB 111-2004/42, DLR Institute of Flight Systems, Braunschweig, 2004
[11] Hahn, K.-U., Schwarz, C., Friehmelt, H., A Simplified Hazard Area Prediction (SHAPe) Model for Wake Vortex Encounter Avoidance, 24th International Congress of Aeronautical Sciences (ICAS), Yokohama (Japan), 29 August - 3 September 2004
[12] Kirchhoff, B.; Carl, U.; Schwarz, C.; Hahn, K.-U.; Auswirkungen realer Systemeigenschaften auf den geregelten Wirbelschleppeneinflug (Effects of Real System Characteristics on the Controlled Wake Vortex Encounter), DLR report IB 111-2004/36, Deutsches Zentrum für Luft- und Raumfahrt, Braunschweig, Germany, 2004
[13] Fock, H.; Hahn, K.-U.; Schwarz, C.; Verwendung von vorausschauenden Strömungssensoren in Pilotenassistenzsystemen für den Wirbelschleppeneinflug (Application of forward looking flow sensors for pilot assistance systems for wake vortex encounters), DLR report IB 111-2006/12, Deutsches Zentrum für Luft- und Raumfahrt, Braunschweig, Germany, 2006
[14] Reinke, A., Leißling, D., and Bauschat, J.-M., Simulation des Einflugs in Wirbelschleppen mit dem ATTAS Flugsimulator (Simulation of wake vortex encounters with ATTAS flight simulator), German Aerospace Congress, Munich, 17.-20. November 2003, DGLR-JT2003-245
[15] Critchley, JB, Foot, PB, UK CAA Wake Vortex Database: Analysis of incidents reported between 1982 and 1990, CAA paper 91015, 1991
[16] Harris, M., Young, R. I.; Köpp, F., Dolfi, A., Cariou, J.-P., Wake vortex detection and monitoring, Aerospace Science and Technology 6 (2002)
[17] Keane, M., Buckton, D., Redfern, M., Bollig, C., Wedekind, C., Köpp, F., Berni, F., Axial Detection of Aircraft Wake Vortices Using Doppler Lidar, Journal of Aircraft, Vol. 39, No 5. 2002
[18] Köpp, F., Rahm, S., Smalikho, I., Characterization of Aircraft Wake Vortices by 2-µm Pulsed Doppler Lidar, Journal of Atmospheric and Oceanic Technology Vol. 21 (2004), Nr. 2
[19] Rahm, S., Smalikho, I., Köpp, F., Characterization of Aircraft Wake Vortices by Airborne Coherent Doppler Lidar, Journal of Aircraft, Vol. 44, No 3. 2007
[20] Wake Turbulence Encounters, Aviation Safety Reporting System (ASRS) Database Report set, Update 11, January 23, 2007.
[21] Schwarz, C., Hahn, K.-U., Gefährdungsräume zur Vermeidung von Wirbelschleppeneinflügen, German Aerospace Congress, Dresden, 20.-23.September 2004, DGLR-JT2004-014
[22] Schwarz, C., Hahn, K.-U., Full-flight simulator study for wake vortex hazard area investigation, AST – Aerospace Science and Technology, 10 (2), Elsevier, p. 136 – 143, DOI 10.1016/j.ast.2005.09.005, March 2006
[23] Schwarz, C., Hahn, K.-U., Simplified Hazard Areas for Wake Vortex Encounter Avoidance, AIAA Atmospheric Flight Mechanics Conference and Exhibit, San Francisco, 15.-18.8.2005
[24] Hahn, K.-U., Schwarz, C., Safe Limits for Wake Vortex Penetration, AIAA Guidance, Navigation and Control Conference and Exhibit, Hilton Head, South Carolina, 20.-23.8.2007

[25] Hahn, K.-U., Höhne, G., Schwarz, C., WakeNet2-Europe - Wake Vortex Research Needs for 'Improved Wake Vortex Separation Ruling' and 'Reduced Wake Signatures' Part II Section 5: Wake Vortex Encounter Assessment, 2006
[26] Holzäpfel, F., Probabilistic Two-Phase Wake Vortex Decay and Transport Model, Journal of Aircraft, Vol. 40, No. 2, March - April 2003, 2003

Publications emerging from the project

Agnew, P., Lunnon, B., Hoad, D., Frech, M., Gerz, T., Carriere, J.M., Bruin, A. de (2001): Wake Vortex Alleviation Strategies Focus on Influence of Weather on Vortex Behaviour. *ICAO Journal* **56**, No. 7, 8-10.

Bao F., Vollmers H. 2003: Untersuchungen an Wirbelschleppen im Hinblick auf den Endeffekt in einem Wasserschleppkanal, STAB 2003, DLR, Göttingen , 4-6 Nov. 2003, 26 - 27 pp.

Bao F., Vollmers H., Mattner H.: 2003. Experimental study on controlling wake vortex in water towing tank. Proc. of ICIASF'03, Göttingen, 25-29 Aug. 2003.

Bao F., Vollmers H. 2004: Experimental investigation of wake vortices with respect to wake vortices with respect to „end-effect" in a water effect" in a water-towing towing-tank. In: DGLR [eds.]:, DGLR-Fach-Symposium der STAB, Bremen, Germany, 16-18 Nov. 2004, 14 pp.

Bao F., Vollmers H. 2004: Wake Vortex Investigation in WSG without / with End-effect, DLR/ONERA [eds.], Proceedings of Annex II Meeting, DLR, Cologne, 6-7 April 2004.

Bao F., Vollmers H., Schröder A. 2004: Experimental Study on the Alleviation of Wake Vortices. In: INSEAN [eds.]: Proceedings of Workshop on Applications of Particle Image Velocimetry to Naval and Industrial Hydrodynamics, Rome, I, 5-6 May 2004, 1-19 pp.

Bao F., Vollmers, H. 2005: Alleviation of end-effect in facilities for far wake investigations. 43rd AIAA Aerospace Sciences Meeting and Exhibit, Reno, NV, AIAA 2005–0907.

Baumann R., Gerz T. 2002: Large-eddy simulations of two disturbed counter-rotating vortex pairs. Proceedings of the EUROMECH Colloquium No 443 Dynamics of Trailing Vortices at RWTH Aachen, 21.-22. 3. 2002.

Carmer C.F.v., Konrath R. 2006: Vortex characterization in multiple-vortex systems of wing model wakes., Proceedings of DGLR-Fach-Symposium der STAB, Darmstadt, 29 Nov. – 1 Dec. 2006, STAB-Mitteilung, Jahresbericht 2006, 31-32 pp.

Carmer C.F.v., Konrath R. 2006: Influence of Reynolds number on generation and decay of aircraft wakes: experimental investigation using generic models, F13 and F13X. Tech. Rep. DLR-IB 224-2006 A 29, German Aerospace Center, Bunsentr. 10, Göttingen.

Carmer C.F.v., Konrath R.; Schröder A., Monnier J.-C. 2006: Identification and visualization of parallel vortex pairs in aircraft wakes from PIV data. In: I. Grant, Optimage Ltd., Edinburgh (UK) [ed.]:, Proceedings of 12th International Symposium of Flow Visualization (ISFV12), Göttingen, 10-14 Sept. 2006, ISBN 0-9533991-8-4, CD ROM, 12 pp.

Carmer C.F.v., Heider A., Schröder A., Konrath R., Agocs J., Gilliot A., Monnier J.-C. 2007: Evaluation of large-scale wing vortex wakes from multi-camera PIV measurements in free-flight laboratory. In: Schröder A, Willert CE (eds) Particle Image Velocimetry: New Developments and Recent Applications, Topics in Applied Physics 112, Springer, Berlin, 379–396.

Carmer C.F.v., Konrath R., Schröder A., Monnier J.-C. 2008: Identification of vortex pairs in aircraft wakes from sectional velocity data, *Experiments in Fluids* **44**, 367-380.

Combe H., Köpp F., Keane M. 2000: On-board wake-vortex detection: Definition, ground experimentation and first results in the MFLAME EC Program, Proceedings of the 3rd WakeNet Workshop, May 20-23, 2000, DERA, Malvern, UK.

Coustols E., Gerz T. 2000: “Minimized Wake”. A collaborative research programme on aircraft wake vortices. Implemented in Annex 3 “Large Aircraft” of the ONERA-DLR Cooperation Agreement. 8 pp.

Coustols E., Stumpf E., Jacquin L., Moens F., Vollmers H., Gerz T. 2003: Minimised wake: A collaborative research programme on aircraft wake vortices, AIAA Paper 2003-0938.

Dörnbrack A., Stumpf E., Prusa J.M., Smolarkiewicz P.K. 2002: Two and three dimensional vortex decay simulated by non oscillatory forward-in-time schemes, Proceedings of EuroMech Colloquium 433, Aachen.

Elsenaar B., van der Geest P., Speijker L., de Bruin A., Wolf S., Braun N., Gerz T., Holzäpfel F., Hahn K.-U., Schwarz C., Frech M., Köpp F., Mutuel L., Bourrez A., Barny H., Barbaresco F., Konopka J., Winckelmans G., Desenfans O., Pugh C., Davies H., Galpin D., Nicolaon J.-P., Vidal A., Harvey A., Wennerberg A., Schumacher J., Luckner R., Höhne G., Fuhrmann M., Laporte F., Hinsinger R., Schrauf G., Turp D., Agnew P., Hill C., Young R., Coustols E., Dolfi A., Jacquin L. 2006: Wake Vortex Research Needs for "Improved Wake Vortex Separation Ruling" and "Reduced Wake Signatures", Part I, Summary & Recommendations, Final Report of the Thematic Network "WakeNet2-Europe", 6th Framework Programme, 51 pp.

Elsenaar B., van der Geest P., Speijker L., de Bruin A., Wolf S., Braun N., Gerz T., Holzäpfel F., Hahn K.-U., Schwarz C., Frech M., Köpp F., Mutuel L., Bourrez A., Barny H., Barbaresco F., Konopka J., Winckelmans G., Desenfans O., Pugh C., Davies H., Galpin D., Nicolaon J.-P., Vidal A., Harvey A., Wennerberg A., Schumacher J., Luckner R., Höhne G., Fuhrmann M., Laporte F., Hinsinger R., Schrauf G., Turp D., Agnew P., Hill C., Young R., Coustols E., Dolfi A., Jacquin L. 2006: Wake Vortex Research Needs for "Improved Wake Vortex Separation Ruling" and "Reduced Wake Signatures", Part II, Specialists's Reports, Final Report of the Thematic Network "WakeNet2-Europe", 6th Framework Programme, 114 pp.

Fischenberg D. 2002: Bestimmung der Wirbelschleppen-Charakteristik aus Flugmessdaten. Deutscher Luft- und Raumfahrtkongress, Stuttgart, 2002.

Fischenberg D. 2002: Results of Flight Test Data Analysis. IB 111-2002/11, DLR, Institute of Flight Systems, Braunschweig.

Frech M., Holzäpfel F., Gerz T. 1999: Entwicklungsarbeiten zum Wirbelschleppen-Warnsystem am Flughafen Frankfurt, Abschlussbericht.

Frech, M. 2001: VORTEX-TDM. A Parameterized Wake Vortex Transport and Decay Model and its Meteorological Input Data Base. DFS German Air Navigation Services, 57 pp.

Frech M., Tafferner A., Gerz T. 2001: The performance of the model system NOWVIV to forecast the horizontal awind over an Airport. ATCA 46th Annual Meeting on Improving Capacity and Efficiency, Washington, DC, USA November 4-8, 2001.

Frech M., Holzäpfel F. 2002: A probabilistic prediction scheme for wake vortex evolution in a convective boundary layer. *Air Traffic Control Quarterly* **10**, 23-42.

Frech M., Tafferner A. 2002: The performance of the model system NOWVIV to forecast the horizontal wind over an airport. 10th Conference on Aviation, Range and Aerospace Meteorology 13-16 May 2002, Portland, Oregon, USA, 216-219.

Frech M., Holzäpfel F., Gerz T., Konopka J. 2002: Short-term prediction of the horizontal wind vector within a wake vortex warning system. *Meteorological Applications* **9**, 9-20.

Frech M. 2004: A simple method to estimate the eddy dissipation rate from SODAR/RASS measurements. 16th Symposium on Boundary Layers and Turbulence, AMS, Portland, Paper 6.13, 2004, 4 pp.

Frech M., Zinner T. 2004: Wake vortex behaviour classes and their initial validation. *Journal of Aircraft* **41**, No. 3, 564-570.

Frech M., Holzäpfel F. 2006: Skill of an aircraft wake-vortex transport and decay model using short-term weather prediction and observation. 12th Conference on Aviation, Range, and Aerospace Meteorology, Atlanta, Paper 6.9, 10 pp.

Frech M., 2007: Estimating the turbulent energy dissipation rate in an airport environment. *Boundary-Layer Meteorology* **123**, 385-393, DOI 10.1007/s10546-006-9149-2.

Frech M., Holzäpfel F., Tafferner A., Gerz T. 2007: High resolution data base for the terminal area of Frankfurt Airport, *Journal of Applied Meteorology* **46**, No. 11, 1913-1932.

Frech M., Holzäpfel F. 2008: Skill of an Aircraft Wake-Vortex Model Using Weather Prediction and Observation, *Journal of Aircraft* **45**, No. 2, 461-470.

Friedrich K., Hagen M. 2004: Evaluation of wind vectors measured by a bistatic Doppler radar network, *Journal of Atmospheric and Oceanic Technology* **21**, 1840-1854.

Gerling W., Schick F.F., Klostermann E., Keck B., Ehr, H. 2007: Echtzeitsimulationen mit Wirbelschleppenvorhersage, DLR-IB 112-2007/18.

Gerz T., Holzäpfel F. 1998: Wingtip Vortices, Turbulence, and the Distribution of Emissions, 2nd AIAA Theoretical Fluid Mechanics Meeting, Albuquerque, NM, AIAA Paper 98-2856, 11 pp.

Gerz T., Dürbeck T., Konopka P. 1998: Transport and effective diffusion of aircraft emissions, *Journal of Geophysical Research* **103**, 25905-25913.

Gerz T., Frech M., Holzäpfel F. 1998: Analyse des Wirbelschleppen-Warnsystems am Flughafen Frankfurt. Abschlußbericht für DFS Deutsche Flugsicherung GmbH vom 16.6.98, 26 pp.

Gerz T., Holzäpfel F. 1999: Wingtip vortices, turbulence, and the distribution of emissions, *AIAA Journal* **37**, No. 10, 1270-1276.

Gerz T., Holzäpfel F., Hofbauer T., Frech M. 1999: Wake vortices in the atmospheric boundary layer: Decay, bouncing and encounter risk. In: The Large Aircraft Operational Challenge, (G. Laruelle, J. Szodruch, eds.), AAAF-DGLR Symposium Notes.

Gerz T., Holzäpfel F., Hofbauer T., Dörnbrack A., Frech M. 1999: Aircraft wake vortices in the atmosphere. In: Industrial and Environmental Applications of Direct and Large Eddy Simulations, (S. Biringen, H. Ors, A. Tezel, J.H. Ferziger, eds.), Lecture Notes in Physics, Springer Berlin, 83-92.

Gerz T. 2000: Wirbelschleppen bremsen den Luftverkehr. *DLR-Nachrichten* **97**, Juni 2000, 60-63.

Gerz T., Holzäpfel F. 2000: Near-field to far-field simulations of A3XX wakes, Technical Report on the Numerical Studies in the joint ONERA-DLR Research Programme on A3XX Wake Vortices for Airbus Industrie, and DLR-IB 553-1/2000, 33 pp.

Gerz T., Holzäpfel F., Hofbauer T. 2000: Two-dimensional and three-dimensional numerical simulations. Chap. 6 in: A3XX - Wake Vortex Investigations, Final Report for ONERA/DLR contract with Airbus Industries, 6-1- 6-12.

Gerz T. 2001: Wake vortex prediction and observation: Towards an operational system. Proceedings of 3rd ONERA-DLR Aerospace Symposium, Paris, France, June 20-22 2002, S1-3, 10 pp.

Gerz T., Holzäpfel F., Darracq D. 2001: Aircraft wake vortices. A position paper, Available from http://www.pa.op.dlr.de/wirbelschleppe, 43 pp.

Gerz T. 2002: Wirbel im Schlepp – Erforschung des aerodynamischen Phänomens kann den Luftverkehr effektiver machen. Helmholtz-Jahresheft 2002.

Gerz T. 2002: Trailing Wake Vortices in the Atmosphere. Proceedings of the EUROMECH Colloquium No 443 Dynamics of Trailing Vortices at RWTH Aachen, 21.-22. 3. 2002.

Gerz T., Holzäpfel F., Darracq D. 2002: Commercial aircraft wake vortices. *Progress in Aerospace Sciences* **38**, 181-208.

Gerz T., Frech M., Hahn K.-U., Holzäpfel F., Köpp F., Schwarz C., Smalikho I., Tafferner A. 2004: Atmospheric Impact on Wake Vortex Development. European Congress on Computational Methods in Applied Sciences and Engineering, ECCOMAS, Jyväskylä, Finnland.

Gerz T., Holzäpfel F., Bryant W., Köpp F., Frech M., Tafferner A., Winckelmans G. 2005: Research towards a wake-vortex advisory system for optimal aircraft spacing. *Comptes Rendus Physique* **6**, No 4-5, 501-523.

Gerz T., Baumann R. 2006: Decay characteristics of single and double wake-vortex pairs in different atmospheric flow realisations. Proc. 25th International Congress of the Aeronautical Sciences (ICAS), Hamburg, 12 pp.

Gerz T., Tafferner A., Rosczyk S., Mirza A., Turp D., Le Bot Ch. 2006: Improved Weather Information for Cockpit and Tower. Proc. 25th International Congress of the Aeronautical Sciences (ICAS), Hamburg, 13 pp.

Gerz T., Holzäpfel F. 2007: Gutachten zum Gefährdungspotential durch Wirbelschleppen an der 3. Start- und Landebahn des Flughafens München, Planfeststellungsverfahren 3. Start- und Landebahn, Flughafen München, 36 pp.

Gerz T., Holzäpfel F., Gerling W., Scharnweber A., Frech M., Wiegele A., Kober K., Dengler K., Rahm S. 2007: The wake vortex prediction and mointoring system WSVBS. Part II: Performance and ATC integration at Frankfurt Airport. 1st CEAS European Air and Space Conference, Berlin, CEAS-2007-178, 3391 - 3399.

Hahn K.-U. 2002: Coping with Wake Vortex. Proceedings of the 23rd Congress of the International Council of the Aeronautical Sciences, Toronto, Canada.

Hahn K.-U., Schwarz C.: 2005: Einfluss einer individuellen und dynamischen Wirbelschleppenstaffelung auf die Anflugkapazität eines Flughafens. Deutscher Luft- und Raumfahrtkongress, DGLR Jahrestagung, DGLR-2004-071, Friedrichshafen.

Hahn K.-U.; Schwarz C.W. 2006: Einfluss einer individuellen und dynamischen Wirbelschleppenstaffelung auf die Anflugkapazität eines Flughafens. In: Deutsche

Gesellschaft für Luft- und Raumfahrt - Lilienthal-Oberth e.v. (DGLR) [Hrsg.]: Luft- und Raumfahrtkongress Jahrbuch 2005 Band III, Deutscher Luft- und Raumfahrtkongress 2005, Friedrichshafen, 2005-09-26 - 2005-09-29, ISSN ISSN 1438-1648.

Hahn K.-U., Schwarz C. 2006: Wake Vortex Avoidance versus Landing Capacity. In: AIAA - American Institute of Aeronautics and Astronautics [Hrsg.]: 2006 AIAA Guidance, Navigation, and Control Conference, 2006 AIAA Guidance, Navigation, and Control Conference and Exhibit, Keystone, CO (USA), 2006-08-21 - 2006-08-24.

Hahn K.-U., Schwarz C. 2007: Safe Limits for Wake Vortex Penetration. In: 2007 AIAA Guidance, Navigation and Control Conference and Exhibit Proceedings, AIAA 2007 Guidance, Navigation and Control Conference and Exhibit, Hilton Head, South Carolina (USA), 2007-08-20 - 2007-08-23.

Hahn K.-U., Schwarz C., Friehmelt H. 2004: A Simplified Hazard Area Prediction (SHAPe) Model for Wake Vorttex Encounter Avoidance. Proceedings of the 24th Congress of the International Council of the Aeronautical Sciences, Yokohama, Japan.

Hahn K.-U., Schwarz C., Kloidt S. 2004: Full-Flight Simulatorstudie zur Verifizierung von Wirbelschleppen-Gefährdungsraumgrenzen, DLR-IB 111-2004/42.

Harris M., Young R.I., Köpp F., Dolfi A., Cariou J.-P. 2002: Wake vortex detection and monitoring, *Aerospace Science and Technology* **6**, 325-331.

Hauf T., Sasse M., Frech M., Gerz T., Holzäpfel F. 2001: Konzept für die Erweiterung des WSWS auf den Gleitpfad, 5. Februar, DFS, Langen, 15 pp.

Hennemann I., Holzäpfel F. 2007: Aircraft Wake Vortex Deformation in Turbulent Atmosphere, 5th Int. Symposium on Turbulence and Shear Flow Phenomena, Vol. 2, TU Munich, 597-602.

Hofbauer T., Gerz T. 1999: Effects of shear layers and thermal stratification on the dynamics of a counter-rotating vortex pair. Proc. 1st International Symposium for Turbulence and Shear Flow Phenomena, 12-15 September 1999 in Santa Barbara, USA.

Hofbauer T., Gerz T. 2000: Shear-layer effects on the dynamics of a counter-rotating vortex pair. AIAA Paper 2000-0758, 7 pp.

Hofbauer T: 2003: Numerische Untersuchungen zum Einfluss von Windscherung und Turbulenz auf Flugzeugwirbelschleppen. DLR-FB 2003-01, 111 pp.

Hofbauer T., Holzäpfel F. 2003: Behavior of aircraft wake vortices subjected to wind shear. AIAA Paper 2003-3813.

Holzäpfel F., Gerz T. 1998: Two-Dimensional Wake Vortex Simulations in the Stably Stratified Atmosphere, 2nd AIAA Theoretical Fluid Mechanics Meeting, Albuquerque, NM, AIAA Paper 98-2857, 9 pp.

Holzäpfel F., Gerz T. 1999: Two-dimensional wake vortex physics in the stably stratified atmosphere. *Aerospace Science and Technology* **3**, 261-270.

Holzäpfel F., Gerz T., Frech M., Dörnbrack A. 1999: The Decay of Wake Vortices in the Convective Boundary Layer, AIAA Paper 99-0984, 37th Aerospace Sciences Meeting and Exhibit, Reno, NV, 10 pp.

Holzäpfel F., Schumann U. 2000: How to Model Aircraft Wake Vortices in the Atmosphere -Methodologies, Benefits and Limitations, EUROMECH Colloquium 412, Munich University of Technology, 32-34 pp.

Holzäpfel F., Gerz, T., Baumann R. 2000: The Turbulent Decay of Wake Vortices in the Stably Stratified Atmosphere, AIAA Paper 2000-0754, 38th Aerospace Sciences Meeting and Exhibit, January 10-13, Reno, NV.

Holzäpfel F., Gerz T., Frech M., Dörnbrack A. 2000: Wake vortices in a convective boundary layer and their influence on following aircraft. *Journal of Aircraft* **37**, 1001-1007.

Holzäpfel F., Gerz T., Baumann R. 2001: The turbulent decay of trailing vortex pairs in stably stratified Environments, *Aerospace Science and Technology* **5**, 95-108.

Holzäpfel F., Hofbauer T., Darracq D., Moet H., Garnier F., Ferreira Gago C. 2001: Wake vortex evolution and decay mechanisms in the atmosphere, Proceedings of 3rd ONERA-DLR Aerospace Symposium, Paris, France, S3-2, 10 pp.

Holzäpfel F., Hofbauer T., Gerz T., Schumann U. 2002: Aircraft Wake Vortex Evolution and Decay in Idealized and Real Environments: Methodologies, Benefits and Limitations, Fluid Mechanics and its Applications 65, Advances in LES of Complex Flows, edited by R. Friedrich, W. Rodi, Kluwer Academic Publishers, Dordrecht, 293-309.

Holzäpfel F. 2003: Probabilistic Two-Phase Wake Vortex Decay and Transport Model. *Journal of Aircraft* **40**, No. 2, 323-331.

Holzäpfel F., Robins R.E. 2003: Probabilistic Wake Vortex Decay Model Predictions Compared with Observations, AIAA Paper 2003-3809***,*** 21st AIAA Applied Aerodynamics Conference, Orlando, FL.

Holzäpfel F., Gerz T., Köpp F., Stumpf E., Harris M., Young R.I., Dolfi-Bouteyre A. 2003: Strategies for circulation evaluation of aircraft wake vortices measured by lidar, *Journal of Atmospheric and Oceanic Technology* **20**, No. 8, 1183-1195.

Holzäpfel F., Hofbauer T., Darracq D., Moet H., Garnier F., Ferreira Gago C. 2003: Analysis of wake vortex decay mechanisms in the atmosphere. *Aerospace Science and Technology* **7**, 263-275.

Holzäpfel F. 2004: Adjustment of subgrid-scale parametrizations to strong streamline curvature. *AIAA Journal* **42**, 7, 1369 – 1377.

Holzäpfel F., Robins R.E. 2004: Probabilistic Two-Phase Aircraft Wake Vortex Model: Application and Assessment, *Journal of Aircraft* **41**, 5, 1117-1126.

Holzäpfel F., Gerz T., Schumann U. 2004: Aircraft wake vortex evolution in the stably stratified atmospheric boundary layer. Conference for Turbulence and Waves in Stably Stratified Atmospheric Shear Flows, Lighthill Institute for Mathematical Sciences, University College London, 13-15 September 2004.

Holzäpfel, F., Frech, M., Hahn, K.-U., Schwarz, C., Joos, H.-D., Ringel, G., Korn, B. 2004: Development of a Concept for the Assessment of A380 Wake Vortices, DLR-IB 553-1/2004, DLR Oberpfaffenhofen, 72 pp.

Holzäpfel F. 2005: Aircraft Wake Vortex Evolution and Prediction, Habilitationsschrift, Technical University Munich, October 2005, 132 pp.

Holzäpfel F., Frech M., Tafferner A., Hahn K.-U., Schwarz C., Joos H.-D., Korn B., Lenz H. 2005: Wake Vortex Scenarios Simulation Package 2, DLR-IB 553-2/2005, DLR Oberpfaffenhofen, 87 pp.

Holzäpfel F. 2006: Two-Phase Aircraft Wake Vortex Model: Further development and Assessment, *Journal of Aircraft* **43**, 3, 700-708.

Holzäpfel F. 2006: Wirbelschleppen - Forschung zur Optimierung von Flugzeugstaffelungen, Mitteilungen DMG 01 / 2006, ISSN 0177-8501, 3 - 6.

Holzäpfel F., Steen M. 2006: Aircraft Wake-Vortex Evolution in Ground Proximity: Analysis and Para-meterization, AIAA Paper 2006-1077, 44th AIAA Aerospace Sciences Meeting and Exhibit, Reno, NV.

Holzäpfel F., Frech M., Gerz T., Tafferner A., Hahn K.-U-, Schwarz C., Joos H.-D., Korn B., Lenz H., Luckner R., Höhne G. 2006: Aircraft Wake Vortex Scenarios Simulation Package - WakeScene, ICAS 2006, 25th International Congress of the Aeronautical Sciences, Hamburg, ICAS 2006-8.6.3, 12 pp.

Holzäpfel F., Frech M., Gerz T., Tafferner A., Hahn K.U., Schwarz C., Joos H.-D., Korn B., Lenz H., Luckner R., Höhne G. 2006: Aircraft Wake Vortex Scenarios Simulation Package – WakeScene. Proc. 25th International Congress of the Aeronautical Sciences (ICAS), Hamburg, 12 pp.

Holzäpfel F., Steen M. 2007: Aircraft wake-vortex evolution in ground proximity: Analysis and parameterization. *AIAA Journal* **45**, No.1, 218-227.

Holzäpfel F., Gerz T., Baumann R. 2007: Aircraft Wake Vortices - Prediction and Mitigation, 6th International Congress on Industrial and Applied Mathematics, IC/MP4402/105, Zürich, Switzerland, 16-20 July 2007, 2 pp.

Holzäpfel F., Gerz T., Frech M., Tafferner A., Köpp F., Smalikho I., Rahm S., Hahn K.-U., Schwarz C. 2007: The wake vortex prediction and mointoring system WSVBS. Part I: Design. 1st CEAS European Air and Space Conference, Berlin, CEAS-2007-177, 3383 - 3390.

Holzäpfel F., Frech M., Gerz T., Tafferner A., Hahn K.U., Schwarz C., Joos H.-D., Korn B., Lenz H., Luckner R., Höhne G. 2008: Aircraft Wake Vortex Scenarios Simulation Package – WakeScene. *Aerospace Science and Technology*, doi:10.1016/j.ast.2007.09.008.

Jacquin L., Fabre D., Sipp D., Theofilis V., Vollmers H. 2003: Instability and unsteadiness of aircraft wake vortices. *Aerospace Science and Technology* ***7***, 577–593.

Keane M., Buckton D., Redfern M., Bollig C., Wedekind C., Köpp F., Berni F. 2002: Axial detection of aircraft wake vortices using Doppler lidar. *Journal of Aircraft* **39**, 850-862.

Kirchhoff B., Carl U. Schwarz C., Hahn K.-U. 2004: Auswirkungen realer Systemeigenschaften auf den geregelten Wirbelschleppeneinflug. IB 111-2004/36, Deutsches Zentrum für Luft- und Raumfahrt, Braunschweig.

Köpp F. 1999: Wake-vortex characteristics of military-type aircraft measured at Airport Oberpfaffenhofen using the DLR Laser Doppler Anemometer. *Aerospace Science and Technology* **4**, 191-199.

Köpp F., Smalikho I., Rahm S., Dolfi A., Cariou J.-P., Harris M., Young R.I., Weekes K., Gordon N. 2003: Characterisation of aircraft wake vortices by multiple-lidar triangulation, *AIAA Journal* **41**, 1081-1088.

Köpp F., Rahm S., Smalikho I. 2004: Characterisation of aircraft wake vortices by 2µm pulsed Doppler lidar, *Journal of Atmospheric and Oceanic Technology* **21,** No. 2, 194-206.

Köpp F., Rahm S., Smalikho I., Dolfi A., Cariou J.-P., Harris M., Young R.I. 2005: Comparison of wake-vortex parameters measured by pulsed and continuous-wave lidars, *Journal of Aircraft* **42**, No.4, 916-923.

Krag B. 2001: S-WAKE Flight Test Report. Technical Note SWAKE-D-221_2_1, IB 111-2001/40, DLR Institute of Flight Research, Braunschweig.

Krag B. 2003: Final Report for Work Package 2 of S-wake Aerodynamic Models for Wake Vortex Encounter. IB 111-2003/13, DLR, Institute of Flight Research, Braunschweig.

Labbé O., Stumpf E., Sagaut P., Rudnik R. 2001: Near- to Midfield Wake: Numerical Prediction, Proceedings of ODAS 2001, Paris.

Langhans S., Stumpf E., Gollnick V., Hepperle M. 2008: A holistic approach to evaluate the air transportation system, paper accepted for ICAS 2008, Anchorage.

Melber-Wilkending S., Stumpf E., Wild J., Rudnik J.R. 2003: Overview about the HLRS Project "Numerical High Lift Research II" (NHLRes II), IB 124-2003/17, 23 pp.

Melber-Wilkending S., Stumpf E., Wild J., Rudnik R. 2003: Numerical High Lift Research II - NHLRes II, High Performance Computing in Science and Engineering '03, Springer-Verlag, 315 – 330.

Melber-Wilkending S., Stumpf E., Stürmer A., Wild J., Rudnik R. 2004: Numerical High Lift Research II/III, High Performance Computing in Science and Engineering '0*4*, Springer-Verlag, 237 – 259.

Meleshko V.V., Gurzhi A.A., Dörnbrack A., Gerz T., Holzäpfel F., Hofbauer T. 2001: Interaction of two-dimensional trailing vortex pair with a shear layer. *International Applied Mechanics* **37**, No. 7, 948-957. (Russisches Original: *Prikladnaya Mekhanika* **37**, No. 7, 128-136.)

Monnier J.C., Gillot A., Vollmers H., Schröder A., Lozier J.L. 2002: Caractérisation de Sillage d'Avion de Transport par Vélocimétrie par Images de Particules (PIV). In: 8ème Congrès Francophone de Vélocimétrie Laser, Proceedings of 8ème Congrès Francophone de Vélocimétrie Laser, Orsay, France, 17-10 Sept. 2002, 219-220.

Reinke A., Fischenberg D. 2003: Validation of Aerodynamic Models for Wake Encounter Response with Flight Test Data. IB 111-2003/14, DLR, Institute of Flight Systems, Braunschweig.

Schwarz C., Fischenberg D. 2006: Analysis of two 2005 Wake Vortex Encounter Incidents, DLR-IB 111-2006/32.

Schwarz C., Hahn K.-U. 2003: Gefährdung beim Einfliegen in Wirbelschleppen. Deutscher Luft- und Raumfahrtkongress, DGLR Jahrestagung, Jahrbuch 2003, DGLR-JT2003-242, München.

Schwarz C., Hahn K.-U. 2004: Gefährdungsräume zur Vermeidung von Wirbelschleppeneinflügen. Deutscher Luft- und Raumfahrtkongress, DGLR Jahrestagung, Jahrbuch 2004, DGLR-JT2004-014, Dresden.

Schwarz C., Hahn K.-U. 2005: Simplified Hazard Areas for Wake Vortex Encounter Avoidance. AIAA Atmospheric Flight Mechanics Conference and Exhibits, San Francisco, California, USA.

Schwarz C., Hahn K.-U. 2006: Full-flight simulator study for wake vortex hazard area investigation, *Aerospace Science and Technology* **10**, 136–143.

Schwarz C., Hahn K.-U. 2006: Impact of individual and dynamic wake vortex

separations on airport capacity. Proc. 25th International Congress of the Aeronautical Sciences (ICAS), Hamburg, 1-9.

Schwarz C., Hahn K.-U. 2007: Automated Pilot Assistance for Wake Vortex Encounters. In: CEAS 2007 Proceedings, First CEAS European Air and Space Conference, Berlin, 2007-09-10 - 2007-09-13, ISSN 0700-4083Frech, Michael (2007): Estimating the turbulent energy dissipation rate in an airport environment. *Boundary-Layer Meteorology* **123**, 385 - 393, DOI 10.1007/s10546-006-9149.

Speijker L., Vidal A., Barbaresco F., Frech M., Barny H., Winckelmans G., 2007: ATC-Wake: Integrated Wake Vortex Safety and Capacity System. Air Traffic Control Association; [Hrsg.]: *Journal of Air Traffic Control* **49**, No. 1, 17-32.

Smalikho I., Köpp F., Rahm S. 2006: Measurement of atmospheric turbulence by 2-µm Doppler lidar, *Journal of Atmospheric and Oceanic Technology* **22**, 1733 -1747.

Stuff R., Dieterle L., Horstmann K.-H., Pailhas G., Coton P., Lozier J.-F. 2001: Near-to Midfield-Wake: Experimental Characterisation. In: ONERA, DLR [eds.], Proceedings of 3rd ONERA-DLR Aerospace Symposium ODAS 2001, Paris, 20-22 June, 2-1 – 5-1, ISBN 2-7257-006-X.

Stumpf E. 2000: Vortex Wake of an A/C in High-Lift Configuration, Proceedings of EGS - Geophysical Research Abstracts, Vol. 2, Nice.

Stumpf E. 2000: Effect of Flap Strakes with regard to Vortex Wake Alleviation, Proceedings of ECCOMAS, Barcelona.

Stumpf E., Rudnik R., Ronzheimer A. 2000: Euler computation of the nearfield wake vortex of an aircraft in take-off configuration, *Aerospace Science and Technology* **4**, 535-543.

Stumpf E. 2002: Numerical Investigation of the Effect of the High-Lift Configuration of a Transport Aircraft on its Vortex Wake, Notes on Numerical Fluid Mechanics 77, 50-58.

Stumpf E. 2002: Numerical Study of 4-Vortex Aircraft Wakes, Proceedings of EuroMech Colloquium 433, Aachen.

Stumpf E., Darracq D., Meese E.A., Elphick G., Galpin S. 2002: Benchmark Test for Euler Calculations of a High Lift Configuration Vortex Wake, AIAA 2002-0554, Reno.

Stumpf E., Rakowitz M., Lekemark L. 2003: Numerical Investigation of Flow Separation on an Isolated A400M Landing Gear Door, IB 124-2003/32.

Stumpf E. 2004: Numerical Study of 4-Vortex Aircraft Wakes, Springer, Notes on Numerical Fluid Mechanics 87, 10-17.

Stumpf E. 2004: Untersuchung von 4-Wirbelsystemen zur Minimierung von Wirbelschleppen und ihre Realisierung an Transportflugzeugen. DLR-FB 2004-03, Dissertation an RWTH Aachen, 133 pp.

Stumpf E. 2004: Numerical Study of Four-Vortex Aircraft Wakes and Layout of corresponding High-Lift Configurations, AIAA 2004-1067, Reno, (and as invited talk in proceedings of RAeS Aerodynamics Conference, London.)

Stumpf E., Dafa'Alla A., Meese E. 2004: Numerical Simulations of the wake vortex near field of high lift configurations, Proceedings of ECCOMAS 2004, Jyväskylä, Finnland.

Stumpf E. 2005: Numerical Study of Four-Vortex Aircraft Wakes and Layout of corresponding High-Lift Configurations, *Journal of Aircraft* **42**, 722- 730.

Stumpf E., Vollmers H., Bao F., C-Wake Report DLR-F11 Tests in DNW-NWB and DNW-LLF 5-Hole Probe PIV Results, 224-2003 C 20, 21 pp.

Tinapp F., Stumpf E., Nitsche W. 1997: Active separation control on a high-lift configuration, Proceedings of EuroMech Colloquium 316, Berlin.

Tafferner A., Birke L., Frech M., Friedrich K., Hagen M. 2003: Weather forecast and monitoring during wake vortex campaigns WakeOP an WakeTOUL. In: Final Colloquium of the DLR project “Wirbelschleppe I”, 28.-29. 01.2003, DLR Oberpfaffenhofen, 14 presentations on CD (Gerz T., ed.) .

Vollmers H. 2001: Detection of vortices and quantitative evaluation of their main parameters from experimental velocity data. *Measurement Science and Technology* **12**, 1199–1207.

Vollmers H., Bao F., Castagno G., Mattner H. 2002: Measurement on interaction and stability of four vortex wakes. In: Institute for Fluid Mechanics and Aerodynamics, Wüllener Str. 5, 52062 Aachen, Germany [eds.] (CD), Proceedings of the EUROMECH Colloquium No 443, Dynamics of Trailing Vortices, RWTH Aachen, Aachen 1-22 March 2002.

Vollmers H., Schröder A., Gilliot A., Monnier J.-C., Lozier J.-F. 2003: Erfassung des Geschwindigkeitsfeldes im Nachlauf frei fliegender Modelle mit PIV., 11th STAB Workshop, DLR, Göttingen, 4-6 Nov. 2003, 198 -199.

Vollmers H., Puffert-Meissner W., Schröder A. 2004: Analysis of PIV Flow Field Measurements behind the ALVAST-Model in High-Lift Configuration., Proceedings of 14th DGLR-Fach-Symposium der STAB, Bremen, 16-18 Nov. 2004,1-8.

Voß G., Stumpf E. 2005: Wake Alleviation by Configuration Modifications at DLR, Proceedings of WakeNetII-Europe Workshop, Toulouse.

Voß G., v. Carmer C.F., Konrath R., Stumpf E., Krückeberg C.-P., Meyer H.-H., Mattner H. 2007: Wake vortex alleviation by differential and oscillating flap setting: A comparative numerical and experimental study, Proceedings of 1st CEAS European Air and Space Conference, Berlin.

Winckelmans G., Desenfans O., Barbaresco F., Deltour J.-C., Pham K., Frech M., Gerz T., Holzäpfel F., van Baren G., Spejker L., Verhoogt T., Vidal A., 2005: The ATC-Wake Predictor system and its potential use to increase the capacity at airports., Joint International Symposium on Sensors and Systems for Airport Surveillance, Paris (F), 2005-06-20 - 2005-06-21, 1-10.

Wirbelschleppen – Faszination eines unsichtbaren Phänomens, Wake Vortices – Fascination of an Invisible Phenomenon 2006, DVD VIDEO, DLR, 15’30’’.